General Disclaimer

One or more of the Following Statements may affect this Document
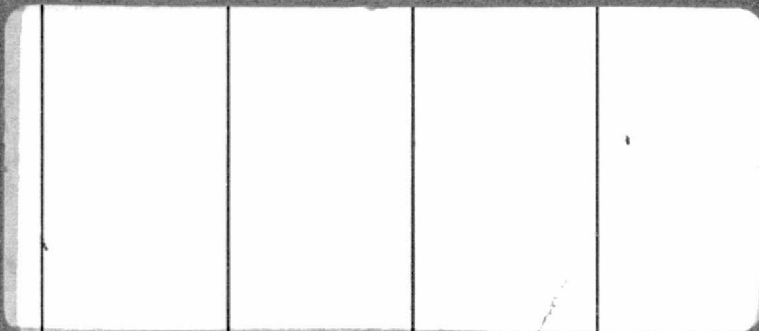
- This document has been reproduced from the best copy furnished by the organizational source. It is being released in the interest of making available as much information as possible.

- This document may contain data, which exceeds the sheet parameters. It was furnished in this condition by the organizational source and is the best copy available.

- This document may contain tone-on-tone or color graphs, charts and/or pictures, which have been reproduced in black and white.

- This document is paginated as submitted by the original source.

- Portions of this document are not fully legible due to the historical nature of some of the material. However, it is the best reproduction available from the original submission.

JET PROPULSION LABORATORY
CALIFORNIA INSTITUTE OF TECHNOLOGY
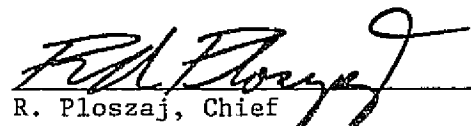PASADENA, CALIFORNIA

VFT-022

VIKING ORBITER SYSTEM
PRIMARY MISSION PERFORMANCE REPORT
(August 20, 1975 – November 15, 1976)
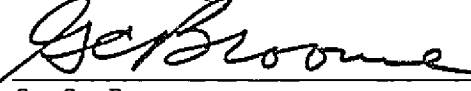
June 15, 1977

Prepared by
J. R. Goudy, Deputy Chief
Orbiter Performance Analysis Group, VEM

Approved:

R. Ploszaj, Chief
Orbiter Performance Analysis Group

H. W. Norris
Orbiter Manager

G. C. Broome
Viking Project Manager, VEM

ACKNOWLEDGMENT

PART I

SYSTEM PERFORMANCE

CONTENTS

CONTENTS (Continued)

Figures

Tables

PART II

CONTENTS

CONTENTS (Continued)

CONTENTS (Continued)

CONTENTS   (Continued)

CONTENTS (Continued)

CONTENTS (Continued)

CONTENTS (Continued)

CONTENTS (Continued)

CONTENTS (Continued)

Figures

Figures

Figures

Figures

Tables

Tables

GLOSSARY

ABD	adjacent bit disturb
ACE	attitude control electronics
ACQ	acquisition
ACS	Attitude Control Subsystem
ADC	analog-to-digital converter
AGC	automatic gain control
AMC	approach midcourse
A/PW	analog to pulse width
ARTC	Articulation Control Subsystem
ARTC-E	articulation control electronics
BOT	beginning of tape
BPA	Bioshield Power Assembly
B/R	booster regulator
CC	coded command
CCS	Computer Command Subsystem
CDU	Command Detector Unit
CELREF	Celestial Reference Program
CM	center-of-mass
CR	cruise
CRS	celestial reference set
CT	Canopus tracker
CW	continuous wave
D/A	digital-to-analog
DC	discrete command
DN	data number

GLOSSARY (Continued)

DOD	depth of discharge
DSE	DTR electronics
DSN	Deep Space Network
DSS	Data Storage Subsystem, Deep Space Station
DST	nine-track tape transport (DTR)
DTR	digital tape recorder
EMF	electromotive force
EOT	end of tape
EU	engineering unit
EV	engine valve
FB	feedback
FB/S	flyback and sweep
FDS	Flight Data Subsystem
FOV	field of view
FPAG	Flight Path Analysis Group
FSK	frequency-shift-keyed
GA	gimbal actuator
GSA	Gas Share Assembly
HGA	High-Gain Antenna (S/X-band)
HPM	high-pressure module
IC	integrated circuit
IF	intermediate frequency
IFOV	instantaneous field of view
IRS	infrared science
IRTM	Infrared Thermal Mapper

GLOSSARY (Continued)

IRU	inertial reference unit
ITC	interplanetary trajectory correction
LGA	Low-Gain Antenna (S-band)
LIP	Limb Interference Program
LO	local oscillator
LPM	low-pressure module
MAWD	Mars Atmospheric Water Detector
MC	midcourse correction
MDS	Modulation Demodulation Subsystem
MOI	Mars orbit insertion
MOT	Mars orbit trim
MTC	Mission and Test Computer
NAT	Network Analysis Team
NEI	noise equivalent irradiance
NPM	non-propulsive maneuver
NRZ	non-return to zero
OPAG	Orbiter Performance Analysis Group (at JPL)
OSG	Orbiter Science Group
OU	output unit
PAS	pyrotechnic arming switches
PAU	Propulsion Actuation Unit
PCA	Pressurant Control Assembly
PCM	pitch control module, pulse-code modulation
PIA	Propellant Isolation Assembly
POT	potentiometer

GLOSSARY (Continued)

PPL	phase lock loop
PROP	Propulsion Subsystem
PSOP	propulsion system mathematical model
PSPA	Power Subsystem Performance Analysis
PSU	Pyrotechnic Switching Unit
PTA	Pressurant Tank Assembly
PTO	Proof-Test Orbiter
PWR	Power Subsystem
PYRO	Pyrotechnic Subsystem
QSS	quasi-sum-of-the-squares
RA	Radio Assembly (S-band)(also known as RFS)
RAS	Relay Antenna Subsystem
RCA	reaction control assembly
REA	Rocket Engine Assembly
RF	radio frequency
RFI	radio frequency interference
RFS	Radio Frequency Subsystem
RRL	(see Canopus Tracker)
RRS	Relay Radio Subsystem (UHF-FSK)
RTS	Relay Telemetry Subsystem
RYCM	roll/yaw control module
S/A	solar array
S/C	spacecraft
SCANOPS	Scan Platform Operations Program Set
SDA	Subcarrier Demodulator Assembly

GLOSSARY (Continued)

SEC	Solar Energy Controller
SG	sun gate
S/N	serial number
SNORE	signal-to-noise ratio estimator
SNR	signal-to-noise ratio
SPE	static phase error
S/S	sun sensor
STEP	Star Tracker Evaluation Program
SXA	S/X-Band Antenna
THEM	Transport Mounted Electronics Module
TIC	tape increment count
TIP	Tracker Interference Program
TMU	Telemetry Modulation Unit
TSF	track synthesizer frequency
TVC	thrust vector control
TWTA	traveling-wave tube amplifier
TWT	traveling-wave tube
UHF	ultra-high frequency
VCO	voltage-controlled oscillator
VIS	Visual Imaging Subsystem
VL	Viking Lander
VLC	Viking Lander Capsule
VO	Viking Orbiter
XTX	X-Band Transmitter

SECTION I

SYSTEM PERFORMANCE

A.   INTRODUCTION

The Viking Orbiters were divided by function into 21 subsystems which, when combined, comprised the Viking Orbiter System. Inflight performances of these subsystems are described in Part II of this report.

Viking was an adaptive mission, as was demonstrated several times, e.g., a prolonged search for landing sites; developing a work-around for the VO-1 helium leakage problem; utilizing the availability of programmable telemetry to replace IRU-1 measurements with those of IRU-2 when IRU-1 was lost on VO-2.

Adherence to, and compliance with, the Orbiter Design Criteria "--- functional or alternate mode redundance should be employed such that no single failure mode of any component (electronic, mechanical, pyrotechnic, electromechanical, or structural) could cause a catastrophic effect on the mission" was instrumental in the success of the Viking Mission.

Performance of all VO-1 and VO-2 subsystems, both individually and as an integrated system, was "as designed" throughout the Primary Mission. "Configuration of the orbiter is shown in Figure I-1 and I-2."

B.   PURPOSE

The purpose of this document is to provide an overview of Viking Orbiter (VO) system and subsystem performances during the primary mission. In-depth descriptions of system and subsystem parameters are contained in Volumes I and II of the Orbiter Design Book, 612-2, and the Spacecraft Operations Handbook, HB-3720311. Brief descriptions, key design requirements, pertinent historical information, unique applications or situations, and predicted versus actual performances are included herein. Subsequent pages of this report are predicated on engineering information only. Scientific results/conclusions are not included nor were they intended to be.

For purposes of this report, the primary mission is defined as the time period from VO-1 launch on (Day 232) August 20, 1975, through (Day 320) November 15, 1976. <u>All times are UTC (which replaced GMT) Earth received.</u>
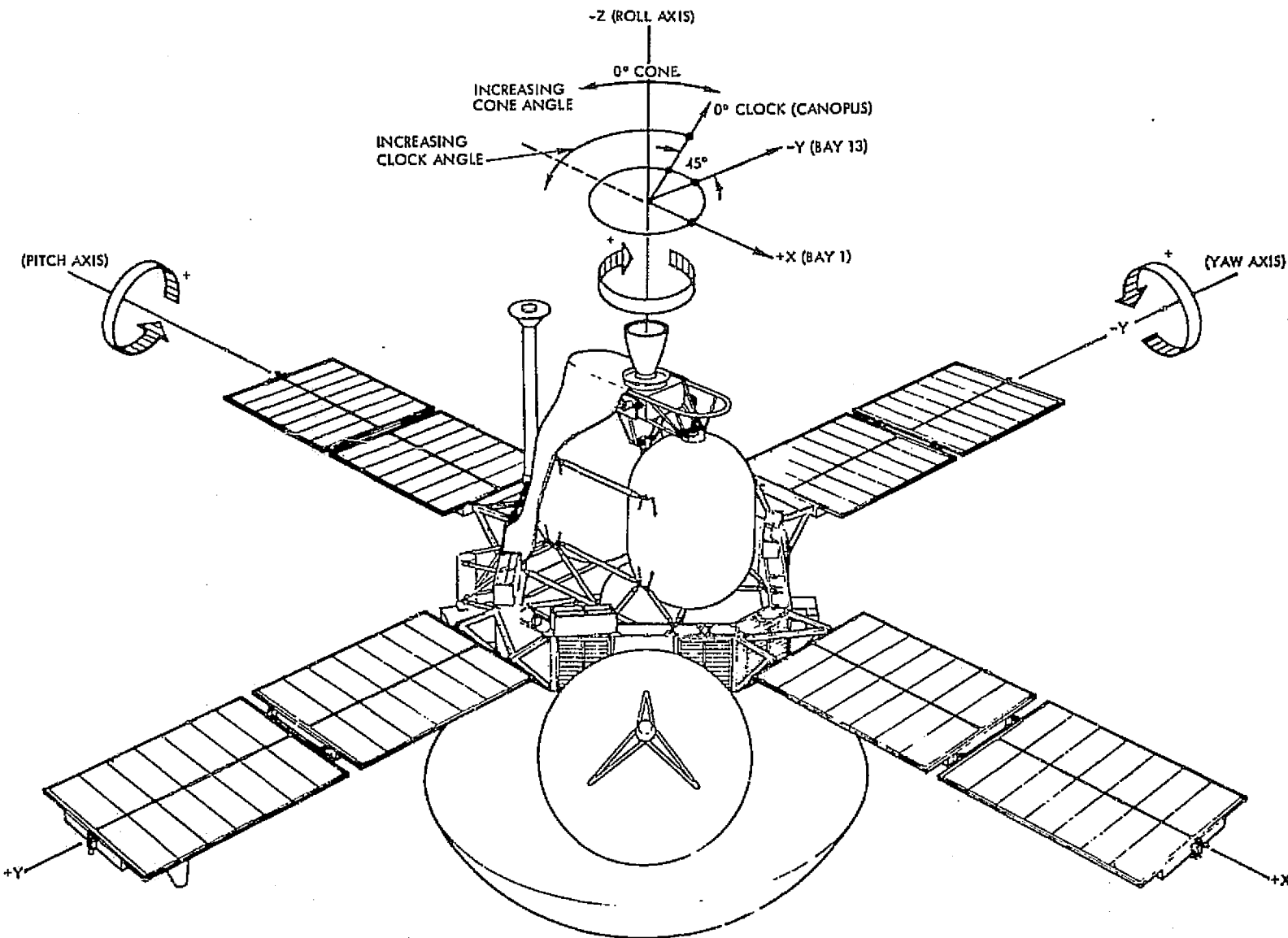
Figure I-1. Viking Orbiter Configuration

RF ABSORBER

PAYLOAD ELECTR
INTERFACE PANEL
(LOCATED ON TRA
ADAPTER)

PRESSURANT TANK
25.2 DIA

O'CLOCK

HINGE RATE LIMITER ASSY (4 PLACES)

310° MAX PLATFORM CLOCK ANGLE

MAWD DIFFUSER PLATE
VIEW POSITION 90° CLOCK

BAY

BAY 12

BAY 13

BAY 14

SOLAR PANEL DEPLOY/DAMPER/LATCH ASSY (4 PLACES)

BPA ENVELOPE

BA

LANDER/ORBITER UMBILICAL CONNECTOR 3 PLACES

SEPARATION SPRING AND
RELEASE NUT ASSY (4 PLACES)
LANDER ADAPTER/ORBITER SEPARATION

A

—Y

353.90

-X

RF ABSORBER

PAYLOAD ELECTRICAL
INTERFACE PANEL (2)
(LOCATED ON TRANSITION
ADAPTER)

PRESSURANT TANK
3.2 DIA

CLOCK

BAY 9

BAY 10

BAY 11

BAY 12

BAY 13

BAY 14

ENVELOPE

UMBILICAL CONNECTOR 3 PLACES

SEPARATION SPRING AND
RELEASE NUT ASSY (4 PLACES)
UNDER ADAPTER/ORBITER SEPARATION

BAY 15

BAY 16

BAY 1

30° TYP

BAY 8

BAY 7

BAY 6

BAY 5

BAY 4

BAY 3

BAY 2

VIS CAMERA "A"

MARS ATMOSPHERIC
WATER DETECTOR

60 MIN PLATFORM CLOCK ANGLE

PLATFORM LOOK VECTOR

VIS HOOD ASSYS

0.69° TYP

INFRARED THERMAL MAPPER

SCAN PLATFORM THERMAL
BLANKET NOT SHOWN FOR CLARITY

VIS CAMERA "B"

PLATFORM LOUVER ASSY (2)

SCAN PLATFORM SUN SHADE

ACCELEROMETER AMPLIFIERS (4)
(LOCATED ON TRANSITION ADAPTER)

+Y

+Z

CABLE TROUGH

HGA SNUBBER ASSY (2)

HGA PIN PULLER

HIGH GAIN ANTENNA OUTRIGGER

X-BAND TRANSMITTER

A

+X

-X

156.00

150.00 DIA PAYLOAD ENVELOPE

VLC ADAPTER

LGA DAMPER (2)

75.00 R

+ Z

VIKING LANDER
CAPSULE (REF)

BFA ENVELOPE

THERMAL BLANKET

SEPARATION SPRING AND
RELEASE NUT ASSY (4 PLACES)

SOLAR PANEL TIP LATCH

RELAY ANTENNA

LANDER CAPSULE FIELD JOINT
V S/C STA 200.00
C/S STA 2541.50
Z = 53.00

130° CONE
720° CLOCK

Z = 0.00
LV-V S/C ADAPTER SEPARATION
V S/C STA 147.00

LANDER ADAPTER
SEPARATION JOINT
V S/C STA 165.50

+ X
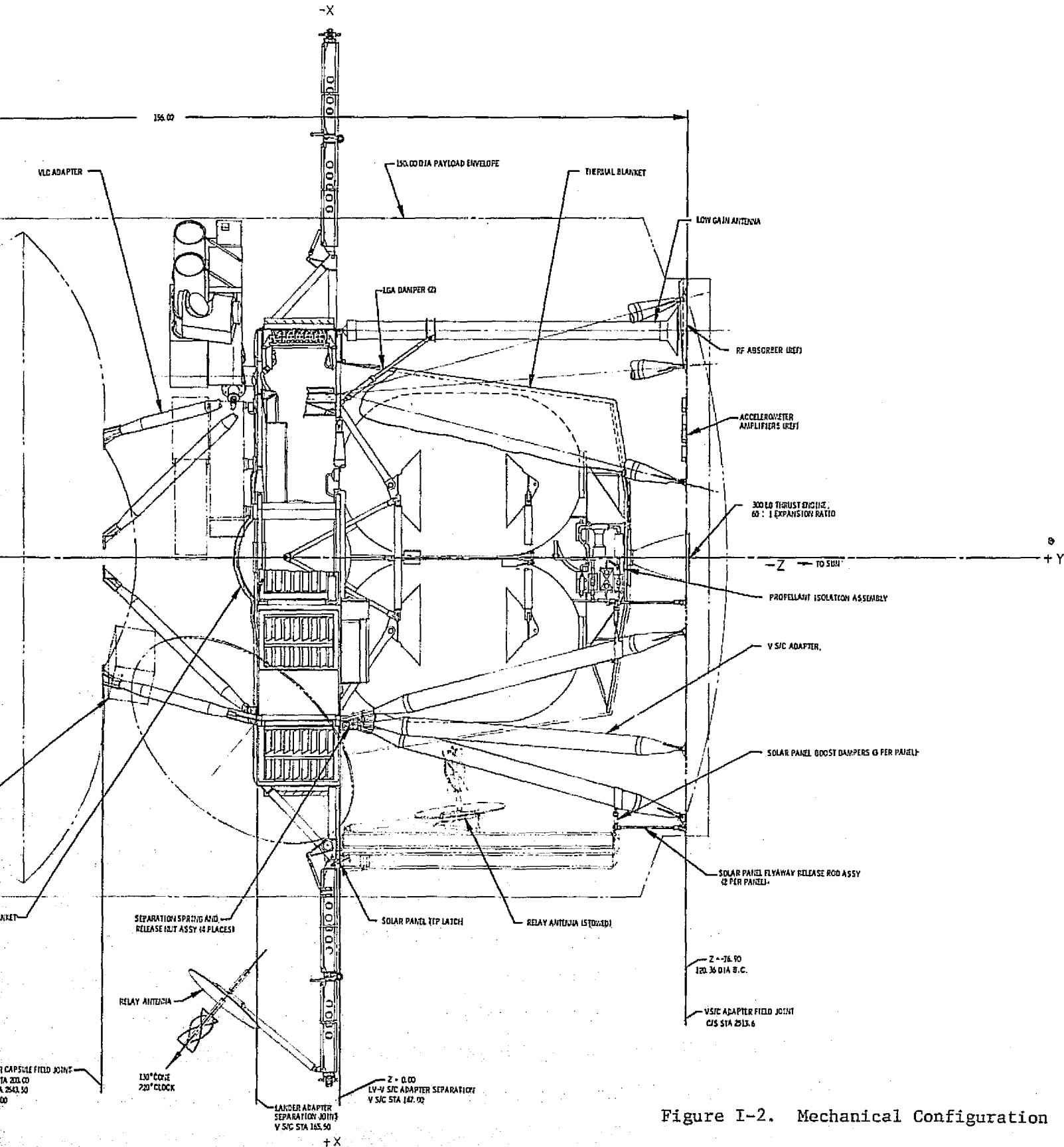
Figure I-2. Mechanical Configuration

C.   LAUNCH AND CRUISE

VO-1 was successfully launched on August 20, 1975 at 21:22:00.6. Spacecraft separation was achieved at 21:56:31 and the solar panels were deployed and latched with full sun acquisition occurring at 22:05:30. The high-gain antenna (HGA) was unlatched approximately one hour after launch, responding to its first slew position command at 22:38:40. Separation of the bioshield cap from the Viking Lander Capsule (VLC) was confirmed at 23:28:50.

VO-2 launch was successfully achieved on September 9, 1975 at 18:38:59.9, with separation of the spacecraft from the Centaur occurring at 19:16:13. Following deployment and latching of the solar panels, the sun was acquired at 19:30:13. The HGA slewed to its commanded position, after being unlatched at 19:55:30, and VLC bioshield cap separation occurred at 20:45:57. Events from launch through 18 hours after launch are shown for VO-1 and VO-2 in Tables I-1 and I-2 respectively.

1.   Canopus Acquisition

A Canopus acquisition strategy was developed because, at the time of Canopus Tracker (CT) turn-on for both VO-1 and VO-2, either the Earth or the Moon could have been acquired. Pre-launch analysis of spacecraft (S/C) attitude during S/C - Centaur separation, sun acquisition and roll rate control indicated that roll attitude at CT turn-on could not be predicted. The on-board (stored) programmed sequence strategy of CT turn-on followed by a roll search to Canopus acquisition could have led to some highly undesirable S/C conditions. Rather than relying on a CCS stored sequence, a new strategy employing ground commands was designed, and implemented, to fit within the established constraints and contingency plans.

Shortly after a successful sun acquisition was confirmed the roll reference loss routine was disabled, the S/C was placed in roll inertial and started a negative roll turn. The next event was a normal — pre-programmed — CT turn-on at launch plus 2 hr 22 min 42 s. At this time CT intensity readings during the commanded roll provided star map information leading to identification of roll attitude.

Table I-1. VO-1 Launch Events

UTC (HR:MIN:SEC)	Event	TLM Verification
August 20, 1975 232/21:56:31	S/C SEPARATION (Unlatch PAS; Solar Panels, RAS deployed; ACS launch mode disabled)	CAPACITOR BANKS CHARGED. ACS and LAUNCH STATUS WORDS
232/22:03:55	EXIT EARTH SHADOW	
232/22:05:30	SUN ACQUISITION	SOLAR PANEL CURRENT and UNREGULATED DC V INCREASE
232/22:13:02	CCS HOUR PULSE	CHECKSUMS
232/22:14:46	RFS — 2-WAY	RECEIVER AGC < 127 DN
232/22:14:56	CC7D1221 — LAUNCH MODE DISABLE (BACKUP)	ACS STATUS WORD
232/22:17:10	DC8X1 — PYRO COMMAND ENABLE	
232/22:18:57	DC8BR — BIOSHIELD SEP DISABLE	
232/22:20:45	DC75X3 — VLC COMMAND ENABLE	
232/22:22:59	DC15D — HGA UNLATCH	MANEUVER STATUS WORD
232/22:24:47	DC8CR — ORBITER PYRO DISABLE	CAPACITOR BANKS DISCHARGED
232/22:27:01	DC8X1R — PYRO COMMAND DISABLE	
232/22:28:48	DC15A — ARTC 1 POWER ON	2.4 kHz OUTPUT CURRENT $\Delta = +1$ DN
232/22:31:03	CC15W — ARTC HR SLEW	
232/22:32:50	CC15J0514 — HGA AZ SLEW	HGA AZ COARSE = 64 DN HGA AZ FINE = 79 DN

Table I-1. VO-1 Launch Events (Contd)

UTC (HR:MIN:SEC)	Event	TLM Verification
232/22:35:59	CC15L0093 - HGA EL SLEW	HGA EL COARSE = 11 DN HGA EL FINE = 107 DN
232/23:13:03 Start cmds 232/23:28:50 Separation 232/23:36:48 End cmds	(Block 6.4, Bio-Cap Sep) 13 VLC COMMANDS WITH PULSED ENABLES ON 2 min CENTERS	FROM VLC
232/23:39:09	CC7C2221 - ROLL INERTIAL	ACS STATUS WORD
232/23:40:32	ENABLE SUN ACQ ROUTINE	
232/23:40:56	CC7A2122 - NEGATIVE ROLL TURN (2000 Sec/Rev)	ROLL GYRO RATE = 55 DN
232/23:44:58	CC7D1122 - CT POWER ON	CT CONE ANGLE = 127 DN
233/00:02:53	DC16AR - DTR-A OFF	2.4 kHz OUTPUT CURRENT Δ = -4 DN
233/00:05:08	DC16BR - DTR-B OFF	2.4 kHz OUTPUT CURRENT Δ = -4 DN
233/00:20:15	CC7C2222 - FIRST GROUND COMMAND	ACS STATUS WORD
233/00:42:04	CANOPUS ACQUISITION	STAR INTENSITY = 86 DN
233/00:54:52	CC6B03 - CRUISE TLM FMT	FDS STATUS-WORD
233/00:58:55	DC2A - RANGING CH ON	RFS STATUS WORD

Table I-1.   VO-1 Launch Events (Contd)

UTC (HR:MIN:SEC)	Event	TLM Verification
233/01:00:56	DC4N – REPL HTR's ON	REG HTR CURRENT = 70 DN
233/01:01:50	CC15N36 – SEC 4 SLEW	SEC 4 POSITION = 71 DN
233/01:02:57	CC15Q39 – SEC 6 SLEW	SEC 6 POSITION = 78 DN
233/01:03:51	CC15S36 – SEC 12 SLEW	SEC 12 POSITION = 72 DN
233/01:04:58	CC15U36 – SEC 14 SLEW	SEC 14 POSITION = 71 DN
233/01:05:52	DC15AR – ARTC 1 OFF	2.4 kHz OUTPUT CURRENT Δ = –1 DN
233/01:07:53	(BLOCK 1.1, BAT CHG) DC4G – CHRG A TO BAT 1 AND CHRG B TO BAT 2	
233/01:05:54	DC4CR – CHRG A HR (IF 4BR)	
233/01:05:55	DC4BR – CHRG A MR/HR	BAT 1 CHARGE CURRENT = 77 DN
233/03:00:00	DC4B – CHRG A LR	BAT 1 CHARGE CURRENT = 20 DN
233/03:00:01	DC4FR – CHRG B HR (IF 4ER)	
233/03:00:02	DC4ER – CHRG B MR/HR	BAT 2 CHARGE CURRENT = 77 DN
August 21, 1975 233/08:30:00	DC4E – CHRG B LR	BAT 2 CHARGE CURRENT = 20 DN

Table I-2. VO-2 Launch Events

UTC (HR:MIN:SEC)	Event	TLM Verification
September 9, 1975 252/19:16:13	S/C SEPARATION (Unlatch PAS; Solar Panels, RAS deployed; ACS LM disable)	CAP BANKS CHARGED. ACS and LAUNCH STATUS WORDS
252/19:29:07	EXIT EARTH SHADOW	
252/19:29:50	CCS HOUR PULSE	CHECKSUMS
252/19:30:13	SUN ACQUISITION	SOLAR PANEL CURRENT AND UNREGULATED DC V INCREASE
252/19:31:50	CC7D1221 – LAUNCH MODE DISABLE (BACKUP)	ACS STATUS WORD
252/19:32:20	RFS – 2-WAY	RECEIVER AGC < 127 DN
252/19:33:50	DC8X1 PYRO COMMAND ENABLE	
252/19:36:04	DC8BR – BUISHLD SEP DISABLE	
252/19:37:51	DC75X3 0 VKC CINNABD EBABKE	
252/19:40:06	DC15D – HGA UNLATCH	MANEUVER STATUS WORD
252/19:41:53	DC8CR – ORBITER PYRO DISABLE	CAPACITOR BANKS DISCHARGED
252/19:44:08	DC8X1R – PYRO COMMAND DISABLE	
252/19:45:55	DC15A – ARTC 1 POWER ON	2.4 kHz OUTPUT CURRENT Δ = +1 DN
252/19:48:10	CC15W – ARTC HR SLEW	
252/19:49:57	CC15J0514 – HGA AZ SLEW	HGA AZ COARSE = 64 DN HGA AZ FINE = 80 DN

Table I-2. VO-2 Launch Events (Contd)

UTC (HR:MIN:SEC)	Event	TLM Verification
252/19:53:05	CC15L0093 – HGA EL SLEW	HGA EL COARSE = 11 DN HGA EL FINE = 106 DN
252/20:29:50 Start cmds 252/20:45:57 Separation 252/20:54:28 End cmds	(Block 6.4, Bio-Cap Sep) 13 VLC COMMANDS WITH PULSED ENABLES ON 2 min CENTERS	FROM VLC
252/20:55.49	CC7C2221 – ROLL INERTIAL	ACS STATUS WORD
252/20:57:39	ENABLE SUN ACQ ROUTINE	
252/20:58:03	CC7A2122 – NEGATIVE ROLL TURN (2000 Sec/Rev)	ROLL GYRO RATE = 55 DN
252/21:02:05	CC7D1122 – CT POWER ON	CT CONE ANGLE = 96 DN
252/21:20:00	DC16AR – DTR-A OFF	2.4 kHz OUT CURRENT Δ = -4 DN
252/21:21:48	DC16BR – DTR-B OFF	2.4 kHz OUT CURRENT Δ = -4 DN
252/21:46:29	CC7C2222 – FIRST GROUND COMMAND	ACS STATUS WORD
252/22:00:38	CANOPUS ACQUISITION	STAR INTENSITY = 86 DN
252/22:11:53	CC6B03 – CRUISE TLM FMT	FDS STATUS WORD
252/22:15:55	DC2A – RANGING CH ON	RFS STATUS WORD

Table I-2. VO-2 Launch Events (Contd)

UTC (HR:MIN:SEC)	Event	TLM Verification
252/22:17:56	DC4N – REPL HTR's ON	REG HTR CURRENT = 70 DN
252/22:18:50	CC15N36 – SEC 4 SLEW	SEC 4 POSITION = 71 DN
252/22:19:43	CC15Q39 – SEC 6 SLEW	SEC 6 POSITION = 78 DN
252/22:20:51	CC15S36 – SEC 12 SLEW	SEC 12 POSITION = 72 DN
252/22:21:44	CC15U36 – SEC 14 SLEW	SEC 14 POSITION = 71 DN
252/22:22:52	DC15AR – ARTC 1 OFF	2.4 kHz OUTPUT CURRENT Δ = –1 DN
252/22:24:53	(BLOCK 1.1, BAT CHG) DC4G – CHRG A TO BAT 1 and CHRG B TO BAT 2	
252/22:24:54	DC4CR – CHRG A HR (IF 4BR)	
252/22:24:55	DC4BR – CHRG A MR/HR	BAT 1 CHARGE CURRENT = 77 DN
September 10, 1975 252/00:26:00	DC4B – CHRG A LR	BAT 1 CHARGE CURRENT = 20 DN
253/05:24:58	DC4FR – CHRG B HR (IF 4ER)	
253/05:24:59	DC4ER – CHRG B MR/HR	BAT 2 CHARGE CURRENT = 77 DN
253/05:37:31	DC4E – CHRG B LR	BAT 2 CHARGE CURRENT – 20 DN

This sequence continued until Canopus was observed <u>following</u> passage through the Earth. (This was done because a bright source like the Earth can temporarily desensitize the CT, making the Canopus acquisition in Brightness Gate (BG) 1 impossible for a time. By rolling through Canopus, it was possible to determine whether or not the BG had to be stepped to a lower (more sensitive) gate before attempting to acquire Canopus. The length of the roll turn (38 min to 66 min) was dependent upon roll attitude at CT turn on.

The on-board commanded roll turn continued past Earth, Canopus, and finally Earth again. By the time Canopus was first encountered, roll attitude was well known and analysts calculated the time to command the S/C to roll-rate mode. This was done at 160 deg clock, just after Earth had been passed the second time. The first ground command was then transmitted and a roll search of 200 deg, culminating in Canopus acquisition, followed. Time of Canopus acquisition for VO-1 and VO-2 is shown in Tables I-1 and I-2 respectively.

Two more sets of commands followed to back up the sequence. The first set provided a back up roll turn stop and roll inertial. If the previous command (to roll search mode) was not executed, these commands were timed to stop the commanded turn nominally on Canopus. If the S/C did go to roll search but failed to acquire, these commands would have stopped it at 56 deg clock, a known region of command capability. If Canopus was acquired as expected, these commands would turn the gyros on and put the S/C in roll inertial, a desired state at this time because of the uncertain particle environment.

Following time to evaluate S/C state, limit cycle behavior, and the particle environment, the second set of commands were sent. This set had the effect of returning the S/C to the celestial cruise mode and enabling the roll reference loss routine.

2.   Earth Departure Maneuvers

Preparation for each Orbiter maneuver involved various events. Propellant lines were vented, pyrotechnic isolation valves in the fuel and oxidizer lines were opened and the propellant was pressurized by opening the first (P1) of five squib actuated valves in the pressurant control system. After the maneuver the event sequence was reversed, i.e., pressurant was isolated by firing the second valve (P2) in the pressurant control system followed a day later by closure of the fuel and oxidizer solenoid isolation valves.

a.   **VO-1 Earth Departure Maneuver (MC-1) Parameters.** VO-1 vented its propellant lines on August 21, 1975. Propellant tank pressurization commenced on August 26, 1975, followed by the maneuver one day later. Initial pre-burn conditions of all subsystems had been previously established and were checked/ verified seven hours prior to ignition. Checksums of both Computer Command Subsystem (CCS) processors, resulting from the command load for the burn, were verified as correct. Pre-aim positions of the pitch and yaw gimbals were veri- fied by the Attitude Control Subsystem (ACS). The thrust vector direction was properly oriented via two programmed turns by the ACS. First a negative roll turn of 226.7 deg was performed, followed by a negative yaw turn of 79.5 deg.

Motor burn ignition was on August 27, 1975 at 18:30:11 and lasted 12.07 sec, imparting a velocity change (ΔV) of 4.68 mps to the S/C. Approxi- mately 6 minutes after the burn, the programmed unwind turns commenced. A positive yaw turn of 79.48 deg followed by a roll turn of 226.79 deg were per- formed, and Canopus was reacquired. Roll reference and command loss routines were re-enabled, after which a normal celestial cruise-mode was attained. The pressurant was isolated on September 16, 1975.

b.   **VO-2 Earth Departure Maneuver (MC-1) Parameters.** VO-2 vented its propellant lines on September 10, 1975 and propellant pressurization commenced on September 17, 1975. It followed the same sequence up to the programmed turns as VO-1. Direction of the first roll turn was positive, for 102.71 deg, followed by a negative yaw turn of 53.22 deg. Ignition occurred September 19, 1975 at 16:30:12 and had a duration of 21.30 sec, imparting a ΔV of 8.11 mps to the S/C. Approximately 6 min after motor burn the programmed unwind turns, first a positive yaw turn of 53.25 deg followed by a negative roll turn of 102.67 deg, started. The pressurant was isolated on October 7, 1975.

3.   Viking Lander Capsule, Checkout and Test Support

Throughout the primary mission each VO supported numerous VLC activities such as: VLC updates — to the Viking Lander (VL) Guidance Control and Sequencing Computer (GCSC); tape recorder maintenance; battery conditioning and charging; Gas Chromatograph Mass Spectrometer (GCMS) venting, oven bakeouts and charac- terizations, evaluation tests, and ion-pump evaluations; cruise checkouts and updates; meteorology checkouts; relay communications equipment (RCE) checkouts;

planetary updates; relay links and playbacks; and pre-separation checkouts. The chronology shown in Table I-3 is not all inclusive but merely a listing of some of the more significant events involving VO participation.

4.   Science Instrument Checkout

Non-propulsive roll maneuvers were performed, and the scan platform slewed in clock and cone, as part of the science instrument checkout on both VOs. Six pictures and infrared (IR) data taken during the checkout were recorded on the digital tape recorders and played back during the two days following the instrument checkout.

The purpose of these activities was to demonstrate that the Orbiter Science Instruments had survived the launch environment and were in good working order. All engineering, housekeeping and status data were closely monitored and compared with pre-launch data. Real-time telemetry was correct and as expected in all instances.

a.   Infrared Thermal Mapper (IRTM). IRTM power was turned on for the first time October 16, 1975 on VO-2 and October 20, 1975 on VO-1. Correct response to all commands was observed, verifying that both VO-1 and VO-2 IRTM instruments were operating properly.

b.   Mars Atmospheric Water Detector (MAWD). Power was turned on for the first time on the same days for each VO as that of IRTM. The MAWD cruise checkout(s) consisted of intensity, wavelength, gain-state and raster step calibrations. Intensity calibration consisted of 10 intensity calibrations followed by a wavelength calibration, and then 10 additional intensity calibrations. Data received measured detector responsivity and offsets. Mechanical action of the shutter in a zero-gravity field was also analyzed for the first time by performing these 10 consecutive calibrations.

The wavelength calibration checked the wavelength scan servo and its auto-lock capability. In the wavelength lock mode, the wavelength null position was monitored for drift versus MAWD head temperature. MAWD science checkouts were repeated every 30 days during cruise and were known then as lambda calibrations. Responsivity of the lead sulfide detectors was found to be low, but stable at the low value.

Table I-3. VO/VLC Activities

VO/VL No.	Date(s)	VL Activity Supported
1	September 4, 1975	Tape Recorder Maintenance.
2	September 24, 1975	Tape Recorder Maintenance.
2	October 6, 1975	Tape Recorder Maintenance.
1	October 8, 1975	Tape Recorder Maintenance.
1	October 14, 1975 through October 19, 1975	Battery Conditioning.
1	October 30, 1975	GCMS vent.
2	October 31, 1975 through November 6, 1975	Battery conditioning: switch of VL-2 battery charger A to charger B due to VL anomaly.
2	November 10, 1975	VLC update and tape recorder maintenance.
1	November 13, 1975	VLC update and cruise checkout.
1	November 17, 1975	GCMS ion pump evaluation.
2	November 21, 1975	VLC update and cruise checkout.
2	November 25, 1975	GCMS vent.
2	December 3, 1975	GCMS oven bakeout.
2	December 4, 1975	Tape recorder maintenance and meteorology checkout.
1	December 10, 1975	GCMS evaluation test.
1	December 15, 1975	GCMS evaluation test.
2	December 19, 1975	GCMS oven characteristics test.
2	January 5, 1976	Tape recorder maintenance and meteorology checkout.
1	January 7, 1976	Tape recorder maintenance and meteorology checkout.

Table I-3. VO/VLC Activities (Contd)

VO/VL No.	Date(s)	VL Activity Supported
1	January 8, 1976 through January 9, 1976	GCMS oven bakeout, and battery conditioning.
2	January 13, 1976	GCMS oven characteristics test and VLC update.
1	January 14, 1976	GCMS oven bakeout and VLC update.
2	January 20, 1976	GCMS oven characteristics test and RCE checkout.
1	February 2, 1976	GCMS oven characteristics test.
2	February 3, 1976	Tape recorder maintenance and meteorology checkout.
2	February 6, 1976	GCMS vent and VLC update.
1	February 7, 1976	GCMS oven bakeout, RCE test and VLC update.
2	February 10, 1976	Power conditioning (all four VL batteries charged and discharged, one battery (B) left on low-rate charge.
1	February 12, 1976	GCMS oven bakeout, RCE tests and VLC update.
1	February 17, 1976	GCMS vent and VLC update.
1	February 19, 1976	Power conditioning (same as VO/VL-2 on February 10).
1	March 10, 1976	Tape recorder maintenance and meteorology checkout.
2	March 11, 1976	Tape recorder maintenance and meteorology checkout.
2	April 16, 1976	Tape recorder maintenance and meteorology checkout.

Table I-3. VO/VLC Activities (Contd)

VO/VL No.	Date(s)	VL Activity Supported
1	April 17, 1976	Tape recorder maintenance, meteorology checkout, stop low-rate charge on battery B.
1	April 23, 1976 through April 26, 1976	Battery conditioning and GCSC-A turned on.
1	May 5, 1976 through May 8, 1976	Battery operations.
2	May 9, 1976	Tape recorder maintenance, meteorology checkout, stop low-rate charge on battery B.
1	May 13, 1976 through May 14, 1976	Battery operations, GCSC-A turned on.
2	May 16, 1976 through May 18, 1976	Battery operations, GCSC-A turned on.
1	May 18, 1976 through May 21, 1976	Battery operations, GCSC-B turned on.
2	May 23, 1976 through May 26, 1976	Battery operations, GCSC-B turned on.
1	May 25, 1976	Tape recorder maintenance.
2	June 4, 1976 through June 5, 1976	Battery operations, GCSC-A turned on.
2	June 10, 1976 through June 13, 1976	Battery operations, GCSC-B turned on.
2	June 15, 1976	Tape recorder maintenance.

Table I-3. VO/VLC Activities (Contd)

VO/VL No.	Date(s)	VL Activity Supported
1	June 24, 1976	Planetary update, GCSC-A and GCSC-B turned on.
1	July 18, 1976	Pre-separation checkout.
1	July 20, 1976	Separation through touchdown, first relay link playback.
1	July 21, 1976	Start of post-touchdown relay links and playbacks.
2	July 25, 1976	Tape recorder maintenance.
2	August 23, 1976	VLC checkout.
2	September 2, 1976	Pre-separation checkout.
2	September 3, 1976	Separation through touchdown.
2	September 4, 1976	Playback of data from separation through touchdown and first landed pictures. First post-touchdown relay link and playback.

c.   Visual Imaging Subsystem (VIS). Prior to a complete check of the
VIS, a star/star picture sequence was taken by the cameras of both orbiters.
Two pictures, one from each camera taken 4.48 sec apart, contained the
expected stars. The sequence, which lasted 4 hr 10 min and 35 s, was clocked
out by VO-2 on October 9, 1975 and VO-1 on October 13, 1975. Seven days after
the star/star sequence an Earth/star sequence was performed by each VO. In the
latter sequence, two pictures were taken by each camera to image both Earth and
a star field in their field of view. One of the pictures, however, failed to
contain the Earth due to a pointing error.

5.   Calibrations

a.   Science Instruments. Through observation of engineering and house-
keeping data, VO science instruments were monitored for changes to maintain an

accurate accounting of their performance. Any deviation was noted and closely followed to ascertain if a trend developed, or a change had occurred, which might offset their calibration.

1)   IRTM. The IRTM has six wavelength channels. The five longest channels were calibrated using a serrated reference surface whose temperature was separately monitored by thermistor circuitry. Stability of the shortest wavelength channel was calibrated using a reference filamentary lamp. All four cassegrain telescopes in each VO IRTM were simultaneously calibrated with MAWD on the days indicated for MAWD.

2)   MAWD. Each VO conducted a series of tests known as MAWD Lambda Calibrations, see Table I-4. These calibrations monitored drift trends of all MAWD parameters including radiation cooling.

3)   VIS. A series of three sequences known as photometric calibrations were performed by VO-1 and VO-2, during which a total of 75 pictures were exposed by both cameras on each VO. VO-1 sequences were clocked out on March 23, May 1 and May 8, 1976. VO-2 sequences were clocked out on March 16, May 21 and May 25, 1976. Calibration data for VIS was also obtained during calibration of the scan platform and is described in paragraph f.

Table I-4.   Lambda (λ) Calibrations

No.	VO-1	VO-2
1	November 25, 1975	November 26, 1975
2	January 5, 1976	January 5, 1976
3	February 4, 1976	February 11, 1976
4	March 1, 1976	March 11, 1976
5	April 12, 1976	April 15, 1976
6	--	May 12, 1976

b.   Canopus Tracker. Calibration of the Canopus trackers was accomplished during, and as part of, the Science Instrument Checkout Sequences on October 20, 1975 for VO-1 and on October 16, 1975 VO-2. A Canopus Tracker (CT) calibration consisted of monitoring the CT engineering telemetry channel while the non-propulsive maneuver was being executed. Each of the above sequences included specification of a commanded turn about the roll axis (magnitude and direction), CT cone angle setting, and CT acquisition gate setting for CT calibration. The resultant star map (CT intensity versus time) was compared with an apriori star map predict (Canopus ratio stimulus versus turn angle) generated by the Celestial Reference (CELREF) computer program. Final product of this calibration was an updated CT response model (Canopus ratio stimulus versus CT voltage output) that was incorporated into the CELREF program.

Whenever a roll turn was performed by either Orbiter the CT was closely monitored. Any deviations from star map predictions for intensity were noted, as were trends which developed, and subsequently incorporated in CELREF. A check on CT calibration was thus maintained, as well as a current star intensity map, even though the actual calibration occurred only once on each Orbiter.

c.   High-Gain Antenna. The HGA on each Orbiter was periodically calibrated to improve pointing knowledge, and accuracy of its pointing, toward Earth. Pre-launch analysis had indicated a gradual increase in pointing uncertainty with time. However, the anticipated offsets in pointing knowledge were less than predicted. Calibration consisted of slewing the HGA in a box scan sequence which changed its position in both azimuth and elevation. Slews were separated by eight minutes and the average downlink X-band AGC recorded for each position. The final position, regardless of slew quantities in the sequence, was always that of the original position. VO-1 calibrated its HGA seven times during the primary mission and VO-2 six times shown in Table I-5. Comparison of actual versus predicted values verified design objectives had been met, assuring that the HGA would correctly — and accurately — respond to commanded positions.

d.   Gyro Drift. Gyro drift calibrations provided information about gyro drift magnitude and stability. Data obtained during these calibrations was used in the design of maneuvers to increase execution accuracy and also to assure satisfactory control of the Orbiters during periods of inertial operation.

Table I-5. HGA Calibrations

No.	VO-1	VO-2
1	January 6, 1976	January 9, 1976
2	February 2, 1976	February 7, 1976
3	February 18, 1976*	March 3, 1976*
4	March 10, 1976	March 18, 1976*
5	March 27, 1976	April 29, 1976
6	April 17, 1976*	October 21, 1976
7	September 17, 1976	—

*Calibration sequence clocked out but resultant data either partial or non-existent due to DSN antenna/equipment problems.

In-flight calibration of gyro drift was required to be completed during the cruise phase of the primary mission, i.e., prior to Mars orbit insertion. Combined gyro and integrator drift rates were calibrated in the pitch, yaw and roll axes three times on each VO. The inertial reference unit (IRU) of the ACS was placed in its all-axes-inertial mode for these calibrations, remaining therein approximately eight hours. Changes to celestial sensor outputs were recorded during the aforementioned time period and subsequently plotted. Gyro drift rates were established (calculated) from slopes of the individual plots. VO-1 gyro drift was calibrated from data obtained on October 30, 1975, March 18 and May 25, 1976. Calibration data for VO-2 was taken on October 23, 1975, March 15 and May 12, 1976. In all cases, drift rates were less than those which had been established as allowable.

e. Accelerometer Bias. In order to meet mission requirements on ΔV magnitude accuracy, accelerometer bias calibrations of sufficient accuracy to guarantee 150 µg total uncertainty had to be accomplished prior to attempting orbital trims.

Data received on earth was input to a special computer program which generated the accelerometer bias value. Calibrated values were used in the design and analysis of subsequent propulsive maneuvers. Calibrations were performed simultaneously with the gyro drift calibrations. Each calibration was conducted during two hours of the gyro calibration periods. All values were well within specified tolerances, meeting mission requirements.

f.   Scan Platform. The intent of the scan platform calibrations was to determine the absolute pointing knowledge of the scan platform in the presence of S/C attitude control motion and to quantify any errors or offsets detected. To accomplish this, the VIS cameras were used to image selected star-fields throughout the available con/clock space. Additional information on camera-to-camera alignment and raster twist was obtained from the results.

VO-1 calibrated its scan platform on February 9 and April 12, 1976, taking a total of 45 pictures with Camera A and 16 with Camera B. Calibration of the VO-2 scan platform was performed on February 13 and April 15, 1976, with the same numbers of pictures. Results of the calibrations were input to a SCANOPS computer program; thereby, (1) enhancing the pointing control accuracy of the scan platform and (2) improving knowledge of the FOV for platform mounted science instruments.

D.   MARS ORBIT INSERTION

Prior to the actual propulsive maneuvers which placed VO-1 and VO-2 into orbit around Mars, various events were deemed essential in preparing the individual parameters necessary to accomplish a precise orbit whose periapsis was over a specific area. The objectives were met by both VO-1 and VO-2.

In addition to the major events delineated in the following paragraphs, 1. through 4., other items of importance transpired in preparation for Mars Orbit Insertion (MOI). For example: maneuver and cruise telemetry formats were updated in the Flight Data Subsystem (FDS); a region in the CCS memory reserved for flight software and MOI tables was checked; calibrations of the cameras, accelerometers and gyros were made; and checkout of the thrust vector control was accomplished.

1.   Optical Navigation

Optical navigation sequences during the Mars approach phase were carried out in support of the approach midcourse and MOI maneuvers. Approach midcourse maneuver support consisted of a series of star-Mars-star 3-frame swath sequences a few days prior to, and a few days after, the maneuver execution. The pre-maneuver observations were in support of the orbit determination and final maneuver design processes. Post maneuver observations supported orbit determination activities to verify the satisfactory execution of the maneuver and the resulting possible elimination of the necessity for an additional approach midcourse maneuver. Because of a pressure regulator problem on VO-1 and the resulting necessity to execute a second propulsive maneuver prior to MOI, the post observations were of value for design of this second propulsive maneuver.

MOI maneuver support consisted of a series of Deimos/star background single frame observations a few days prior to the insertion. These observations were used for orbit determination processes prior to final design of the maneuver.

VO-1 and VO-2 each took a total of 172 and 168 pictures respectively, for the purpose of optical navigation as shown in Table I-6.

Table I-6. VO-1/VO-2 Optical Navigation Sequences

Series No.	VO-1		VO-2	
	From – To	(PICS)	From – To	(PICS)
1	May 17 – May 20, 1976	(61)	July 7 – July 9, 1976	(36)
2	June 3 – June 6, 1976	(61)	July 16 – July 18, 1976	(36)
3	June 10 – June 13, 1976	(26)	July 22 – July 24, 1976	(36)
4	June 16 – June 18, 1976	(26)	July 28 – July 31, 1976	(36)
5	–		August 2 – August 6, 1976	(24)

2.   Approach Midcourse Correction Maneuvers

Preparation of the propulsion (PROP) module on both VOs commenced with opening the solenoid operated propellant isolation valves. These valves had isolated propellants from the rocket engines during the long cruise period following the midcourse maneuvers previously described. VO-1 latch valves had been closed for 261 days prior to their reopening on June 4, 1976, whereas VO-2 valves were reopened on July 26, 1976, after 293 days.

VO-1 second pressurization occurred on June 7, 1976 with the firing of P3, the third of five squib actuated valves. A leaktight seal was not effected by the helium pressure regulator in the pressurant system, resulting in continued helium flow into the propellant tanks and producing higher than normal tank pressures. This caused a delay of one day in the previously planned Approach Midcourse Maneuver (AMC), revision of parameters contained in AMC-1 and implementation of an option in the approach plan, i.e., AMC-2. The combined approach maneuvers produced a significantly greater reduction in trajectory velocity than was originally planned. However, this was partially recovered by the MOI maneuver. AMC-1 was conducted on June 10, 1976 and AMC-2 on June 15, 1976. A total ΔV of 110.5 mps was imparted to VO-1 by these maneuvers, 50.5 mps by AMC-1 and 60.0 by AMC-2. VO-2, unlike VO-1, had only one AMC and it was conducted in the "blowdown mode," i.e., with the pressurant regulation system inactive (P3 was not actuated). On July 28, 1976, VO-2 AMC-1 was performed and imparted 9.2 mps of ΔV as planned.

3. Approach Science

Approach science conducted by each VO was essentially the same, being conducted in conjunction with their last series of optical navigations. VIS approach science provided complete longitudinal and color coverage of Mars, including the primary and secondary landing sites. VO-1 took 67 photographs for this purpose whereas VO-2 took 101.

Between approximately MOI-120 hr and MOI-48 hr MAWD acquired 12 min of IR data, centered on Mars lighted crescent, in the wavelength calibration mode at 12 hr intervals. Between approximately MOI-48 hr and MOI-20 hr it acquired data every 4 hr. The last observation and the one before it were extended to receive 16 min of data. All MAWD observations began immediately after adjacent VIS sequences, acquiring 176 min of data in this fashion. These observations served to characterize, in a very general sense, the planet-wide distribution of water vapor.

IRTM acquired approach data as headers prior to each VIS sequence between MOI-72 hr to approximately MOI-18 hr. On VO-1, a header was acquired every 2 hr during the period from MOI-71 hr to MOI-19 hr. VO-2 acquired a header every 2 hr between MOI-72 hr and MOI-60 hr, one every 4 hr during the period MOI-60 hr to MOI-24 hr, and one every 2 hr from MOI-24 hr to MOI-18 hr. Sufficient longitudinal variation was achieved to provide full global coverage. Also, IRTM coverage of the entire Mars disc was provided as close to MOI as possible.

a. First Color Photograph of Mars. The first color picture of Mars (actually a mosaic) was made from three frames (pictures), shuttered nine sec apart, by VO-1 on June 17, 1976. Each of the three pictures was taken through a different filter — red, green and violet. The large impact basin Argyre, the south pole, and the "Grand Canyon" of Mars, called Vallis Marineris, are visible in the total mosaic.

4. Orbit Insertion

Eight days after the CCS MOI region was checked on each VO, the initial MOI command load was transmitted. These loads were subsequently updated three days before, and tweaked just hours prior to, the actual MOI. Table I-7 is a chronology of these pre-MOI events.

Table I-7. Pre-MOI Events

Event	VO-1	VO-2
CCS MOI Region Check	May 14, 1976	July 13, 1976
MOI Load Transmitted	May 22, 1976	July 21, 1976
MOI Load Updated	June 16, 1976	August 4, 1976
MOI Load Tweaked	June 19, 1976	August 6, 1976

Updates and tweaks of the MOI loads contained the latest available information on the position of each S/C (as applicable) relative to Mars. Data obtained from optical navigation, approach science, S/X-band ranging and doppler residuals was analyzed, combined and input to these loads. The sequence of events needed to prepare each S/C for orbit insertion, as well as the engine burns themselves, was executed flawlessly — as reflected in the accuracy of initial orbits achieved by both VOs. Sequences commenced approximately 13 hr 47 min prior to start of the first roll turn and ended approximately 12 hr 6 min after it; i.e., a total length of almost 26 hr. Positioning before and after the motor burn was identical in sequence and direction, but not magnitude, for both VO-1 and VO-2 as follows:

	VO-1 6/19/76	VO-2 8/7/76
Positive Roll Turn	+101.8 deg.	+136.3 deg.
HGA Slew (Elevation)	29.4 deg.	160.3 deg.
(Azimuth)	108.8 deg.	55.3 deg.
Negative Yaw Turn	-96.8 deg.	-111.0 deg.
Positive Roll Turn	+158.0 deg.	+142.8 deg.
Motor Burn	--	--
Negative Roll Turn	-157.8 deg.	-142.4 deg.
Positive Yaw Turn	+96.6 deg.	+110.8 deg.
HGA Slew (Azimuth)	108.8 deg.	55.0 deg.
(Elevation)	29.2 deg.	160.5 deg.
Negative Roll Turn	-101.4 deg.	-135.4 deg.

The HGA was repositioned so that a communication link would be assured during the engine burn. These maneuvers produced a short but predicted blackout period prior to engine burn but the link was regained 7 min before ignition as expected.

VO-1 motor burn start was delayed approximately 6 hr 40 min from its original schedule due to reduction in its speed from the two AMC's previously described. Motor burn start for VO-2 was on time. Pin-point accuracy of navigation and VO performance preciseness is shown in Table I-8.

These were two of the longest engine burns every accomplished in deep space. For comparison, the Mariner 9 engine burned for 15 min when placed in orbit about Mars in 1971.

a. <u>Orbit Trims</u>. The orbit of VO-1 was successfully trimmed on June 21, 1976, by a propulsive maneuver lasting 2 min 10.6 s. Ignition of the rocket engine occurred at 17:43:55, imparting a ΔV of 80.5 mps. Referred to as Mars Orbit Trim (MOT)-1, the maneuver lowered apoapsis from an insertion altitude of 50,300 km to 32,800 km without changing the periapsis altitude of 1514 km.

Table I-8. MOI Significant Events and Parameters

Event/Parameter	VO-1	VO-2
Date of MOI	June 19, 1976	August 7, 1976
Engine Burn Start	22:38:11	11:49:35
Engine Burn Duration	37 min 36.3 s	39 min 22.7 s
Total ΔV	1097.27 mps	1100.8 mps
Periapsis:		
Planned	1500 km	1500 km
Achieved	1514 km	1519 km
Orbit Duration:		
Planned	42.6 hr	27.4 hr
Achieved	42.4 hr	27.6 hr

Once MOT-1 was completed, VO-1 was in a 24.6 hr orbit — compared to the insertion orbit of 42.6 hr — that positioned it over the prime landing site of Chryse. (Note: A Martian day is 24 hr 39 min 35 s, approximately 24.6 earth hr). Accuracy of MOT-1 and preciseness of all orbital parameters precluded the necessity of performing three other scheduled (planned) maneuvers, i.e., MOT-2 through MOT-4, on VO-1.

VO-2 executed its MOT-1 on August 9, 1976. Rocket engine burn duration was 7.08 s, starting at 17:35:47, and imparted a ΔV of 4.07 mps as planned. The orbit was reduced from 27.4 hr to 27.3 hr. A second propulsive maneuver, MOT-2, was performed on August 14, 1976, and further refined the orbit of VO-2. Ignition was at 08:51:11 and lasted 3.06 s for a ΔV of 1.77 mps.

The orbit of VO-2 was deliberately not synchronized over a precise or specific point on the Martian surface as was the VO-1 orbit. VO-2 was left out of sync so that its periapsis "walked" around the planets longitude in 40 deg steps each day at a band between 40 and 50 deg north latitude. A complete "walk" took nine days, permitting examination of two proposed landing sites, Alba Patera and Utopia.

E.   SITE CERTIFICATION

Certification of the first landing site consumed more time than allocated in the mission design. Photographic coverage was initiated by VO-1 on June 22, 1976 as it was approaching periapsis 3. Exceptional resolution from VIS stereo pictures, coupled with IR data, caused concern about a safe touchdown at the prime site for the first VL in Chryse. The unexpected variety of terrain features at the pre-selected landing site extended the site certification process to add information from other pre-selected and proposed landing sites. Photographic reconnaissance from VO-1 was also an aid in final selection of landing sites for the second Lander.

Once acceptable landing sites had been located and certified, both VO-1 and VO-2 performed two propulsive maneuvers. The first repositioned them over the selected site and the second synchronized their new orbits. Table I-9 summarizes these propulsive events.

Table I-9. Site Certification Maneuvers

VO/Event	Date	Duration	ΔV	Engine Ignition
VO-1/MOT-5	July 8, 1976	41.1 sec	25.7 mps	00:58:28
VO-1/MOT-6	July 14, 1976	4.4 sec	2.7 mps	07:30:44
VO-2/MOT-3	August 25, 1976	72.7 sec	42.7 mps	18:08:46
VO-2/MOT-4	August 27, 1976	19.2 sec	11.3 mps	20:45:58

F. PRESEPARATION CHECKOUT THROUGH AFT-BIOSHIELD SEPARATION

1. Preseparation Checkout

Starting at separation (S) minus 30 hr, each VO issued commands which put them in the Orbit II telemetry format and placed their telemetry modulation unit (TMU) in the VLC checkout mode. Commands from the VO were sent to the VLC which turned on power control and distribution assemblies and initiated a pre-programmed VLC pre-separation sequence. The VO Relay Radio Subsystem (RRS) and Relay Telemetry Subsystem (RTS) were turned on to verify VLC relay transmitter power changes and also VLC data-rate changes. These were all recorded by a Digital Tape Recorder (DTR) in the VO. Current drain by the VLC on VO power was monitored throughout as were all communication links. Approximately 25 min prior to ending the five hour preseparation checkout sequence, the VLC Descent telemetry format was selected by the FDS. Performance of all VO subsystems on both VO-1 and VO-2 was nominal throughout the sequence and there were no flight hardware anomalies.

2. Separation

Prior to commencing separation activities, VO-1 and VO-2 performed a CT straylight sequence, participated in the VLC S-9.5 hr update load and updated their own separation load. At S-5 hr the final VLC separation activity commenced with a check of all VO subsystems for compliance with established parameters. All events contained in a long and complicated sequence were executed flawlessly by both VO-1 and VO-2 up to separation. Ground (contingency backup) commands, to ensure recording of VL data by both VO DTRs when the VL switched to 16 kbps, were planned for both Orbiters. These commands were transmitted at approximately 2 hr 18 min after separation. Commands to VO-1 became redundant when the on-board sequence switched DTR-A and DTR-B on schedule. The planned commands to VO-2 became a necessity when the on-board sequence was stopped by the CCS — as designed — due to an anomaly at VL separation. VO-2 successfully executed these commands, as was later evidenced when the 16 kbps data was played back.

VO-1 and VLC-1 were separated on July 20, 1976 at 08:51:52. A small disturbance was observed on roll gyro telemetry. Disturbances noted in the pitch and yaw axes (caused by fuel slosh in the PROP module) exhibited normal performance in the first twenty minutes after separation, indicating a smooth separation. The RRS maintained contact with VL-1 throughout its descent phase, confirming touchdown with receipt of a 16 kbps signal at a level of -105.1 dBm. Touchdown of VL-1 occurred on July 20, 1976 at 12:12:07.

VO-2 and VL-2 separated on September 3, 1976 at 19:39:58. From this time on there was no similarity to VO-1/VL-1 events. At 19:40:24 (26 seconds after separation) 400 Hz current to IRU-1 was lost, leading to rundown of the primary gyros approximately 200 seconds later. (Note: IRU-2 power was turned off one min after separation, as it was on VO-1, as part of the normal sequence of events.) Without rate damping provided by the gyro error signal, VO-2 pitch and yaw limit cycles went into rapid, expanding oscillations. ACS gas-jet activity had increased to something on the order of an 80 percent duty cycle when the attitude control electronics (ACE) spin-up inhibit detector exceeded its threshold. This caused an ACE changeover interrupt signal to be sent automatically to CCS. The CCS response was normal and correct, including selection of the low-gain antenna (LGA) which caused the downlink signal level to drop approximately 20 db. At 19:47:44 the low-rate data stream was out-of-lock, followed by loss of the S-band downlink at 19:47:52. Inability to lock onto the low-rate data stream was caused by the on-board — automatic — selection of the LGA and the resultant drop of signal strength.

In addition to selecting the LGA, CCS response to the ACE changeover was to 1) terminate the programmed sequence, 2) switch power from ACE-1 to ACE-2, and 3) condition the new ACE, including having it select IRU-1. Since the non-operative IRU was re-selected, the pitch and yaw oscillations continued until the ACE-2 spin-up inhibit detector exceeded its threshold. Because there is no ACE changeover interrupt between ACE-2 and CCS, the only response this time was internal to ACE-2 and that was to select IRU-2. With the selection of IRU-2, pitch and yaw oscillations were damped out, and attitude control essentially returned to normal. Roll orientation was inertially held, although roll attitude was unknown since VO-2 was not celestially acquired. Relay communications

between VO-2 and VL-2 was maintained throughout the Orbiter anomaly and remained solid throughout the remainder of the descent of VL-2. The communication black-out condition persisted until three ground commands turned off the high-rate sub-carrier and lowered the engineering data rate from 33-1/3 to 8-1/3 bps. The three commands (DC2ER, DC3A and CC6B10) were transmitted on 15 sec intervals starting at 20:08:34. The low-rate data stream was back in lock at 20:53:02. Total loss of real-time data was 01 hr 05 min and 18 s.

A decision was made to take no further immediate corrective action, i.e., leave VO-2 attitude in its sun-acquired roll inertial state and continue with the original timeline. This action was based on the following rationale: 1) the relay link was nominal and all relay data was being recorded by VO-2; 2) any attempt to establish/correct the attitude ran the risk of degrading the relay link and possibly losing it; and 3) a new playback sequence could be programmed into the CCS after the post-touchdown relay link was over. Touchdown of VL-2 occurred at 22:58:20.

Subsequently, about four hours after touchdown, the Orbit II telemetry format was modified by replacing IRU-1 data with that of IRU-2, and CCS error and ACE power responses were altered. This was followed by transmission of a pre-prepared contingency command file, a first for either VO. Star intensity measurements were temporarily placed into three locations of the maneuver format to aid in star map data acquisition. The maneuver format itself was then selected and VO-2 was placed in a 360 deg roll turn via transmission of a second contingency command file.

Analysis of the resultant star map disclosed that the guide star Vega was 22.3 deg out of the FOV of the Canopus tracker. A positive roll turn was sub-sequently commanded by transmission of a third contingency file, and VO-2 regained celestial lock on Vega approximately 8 hr after VL-2 touchdown. The HGA was then energized, followed one minute later by a command selecting the Orbit II format and a data rate of 33-1/3 bps. Playback of the first landed pictures taken by VL-2 was then accomplished, some nine hours after touchdown, when VO-2 was essentially in a normal cruise mode. The preferred combination of ACE-1 and IRU-2 was successfully achieved on September 10, 1976, placing ACE-2 in a backup mode. Reaction of the various subsystems in responding to this anomaly was excellent and "as designed."

3.   Recording of Data

During the period from preseparation checkout to aft-bioshield
separation, the sequence of data recorded by VO-1 and VO-2 DTRs was identical.
Data recorded was always played back but not necessarily in the same sequence
as it was recorded. For example, the first landed data (two pictures) was
played back prior to playback of descent data.

At VO-VL separation minus 28 hr 20 min, VL pre-separation 4 and 16 kbps
data was recorded. Two min prior to separation, DTR-A starting recording VL
4 kbps data which included separation, deorbit burn and descent information
received by RRS/RTS. At touchdown minus 3 min, DTR-B commenced recording VL
16 kbps data, followed one min later by DTR-A. This contained terminal descent,
touchdown and landed data. Both DTRs were placed in their ready mode (non-
record) approximately 21 min after touchdown.

Recording after touchdown primarily consisted of IRTM, MAWD, VIS and VL
relay data on almost a daily basis. The sequence of recording was predicated
on periapsis time for VO-1 or VO-2 as applicable.

4.   First Pictures from Martian Surface

DTR-B on VO-1 started playback of the first pictures taken on the surface
of Mars on July 20, 1976, at 12:38:02, 26 min after VL-1 touchdown. The
panoramic picture spanned approximately 300 deg around VL-1 and its quality
exceeded expectations. (Note: July 20, was the same calendar day that
man first set foot on the Moon in 1969.)

5.   Aft-Bioshield Separation

The VO-1 aft-bioshield was separated on July 22, 1976, at 02:19:05.
Included in the separation was the VO-VLC Adapter. Separation was accomplished
by firing the four pyrotechnic release devices — spring-loaded shear bolts —
which attached the VLC Adapter to the VO. The event was smooth and successful.

VO-2 aft-bioshield separation has not occurred. This decision was made
shortly after loss of IRU-1 on the basis that it could possibly cause the
remaining IRU to fail and be catastrophic to the remaining VO-2 mission.

G. ORBITAL OPERATIONS

1. Orbital Science

For each orbital revolution, the length of the VL relay, the number of VIS frames and infrared science events were specified. Low altitude multiple frame coverage, as well as high altitude pentads, was provided by VIS. IRTM and MAWD obtained both global and wide area observational data of diurnal activities and monitored specific areas of interest.

Orbital scientific objectives, listed here, were accomplished by VO-1 and VO-2.

(1) Obtain image, thermal and water vapor information to be used in landing site selection for the VLs.

(2) Obtain repeated image, thermal, and water vapor coverage of landing sites during lifetime of VLs on the surface.

(3) Obtain image, thermal, and water vapor information to be used in the selection of landing sites for future missions.

(4) Obtain image, thermal, and water vapor information to be used in the study of the dynamic and physical characteristics of the planet and its atmosphere.

(5) Conduct scientific investigations using the VO radio system.

2. VL Relay Record and Playback

VL 16 kbps data was received by a VO and played back to Earth at 4 kbps. Due to uncertainty in start time resulting from VL and VO geometry, the VO commenced recording approxomately one min prior to VL transmitter turn on and stopped recording one min after it was turned off. Recording of VL data was limited to that portion of the VO orbit in the vicinity of periapsis.

Each VO could record data from either VL, provided their periapsis was over a landing site. This capability was successfully demonstrated on September 26, 1976 when VO-1 recorded VL-2 data. In keeping with the Mission Rule, VL data received by the VO was played back as soon as practical, usually within an hour after it was recorded. On those occasions, when VL data was

designated to be critical, the data was played back two times, one time each over two different DSN stations. VO-1 participated in 81 relay links during the primary mission, 67 with VL-1 and 14 with VL-2, VO-2 participated in 27 links, all with VL-2.

3. Maneuvers

During orbital operations, propulsive maneuvers were identified by one of two names, Mars Orbit Trim (MOT) or Station Keeping (SK). Long range planning included many propulsive maneuvers which were subsequently scrubbed due to precision performance of the Orbiters in preceding maneuvers. Only those maneuvers actually performed have been included herein.

Two of the more significant propulsive maneuvers occurring after VL-2 landing were the VO-1/MOT-7 and VO-2/MOT-5B. The VO-1 maneuver was an orbit period change maneuver initiating an "orbiter walk" around the planet, providing near periapsis observations at various longitudes. The VO-2 maneuver was a combination orbit plane change and orbit period change maneuver. The orbit inclination was increased from 55 deg to 75 deg to improve the polar region viewing conditions and an "orbit walk" was initiated providing near periapsis observations at various longitudes.

Table I-10, Orbital Operation Maneuvers, chronologically lists all propulsive maneuvers performed after site certifications through end of the primary mission.

Table I-10. Orbital Operation Maneuvers

VO/Event	Date	Duration	ΔV	Engine Burn Start
VO-1/SK-2	August 2, 1976	1.73 s	2.23 mps	03:19:13
VO-1/MOT-7	September 11, 1976	16.26 s	21.33 mps	19:24:34
VO-1/MOT-8	September 20, 1976	2.84 s	3.71 mps	22:36:18
VO-1/MOT-9	September 24, 1976	17.40 s	22.93 mps	15:30:52
VO-2/MOT-5A	September 28, 1976	4.58 s	4.0 mps	04:54:15
VO-2/MOT-5B	September 30, 1976	4 m 58.82 s	342.55 mps	21:38:34

The VO-2/MOT-5A engine burn was a test burn (not required for navigation) to verify ACS operational integrity, after the separation anomaly, before committing to the lengthy MOT-5B propulsive maneuver.

4.   Solar Occultations

During the primary mission, because of orbital geometry, only VO-1 was subjected to solar occultations. Predicted times for entry and exit were quite accurate when compared to actual times observed. Actual times were affected by the low data-rate — 8-1/3 bps — which sampled the engineering measurements used for these observations, i.e., unregulated dc voltage and solar panel current. Unregulated dc voltage was sampled once every 26.88 s, whereas solar panel current was sampled only once in 3 min 35 s. Criteria for solar occultation times was as follows:

(1)   Enter penumbra, first drop in unregulated dc voltage;

(2)   Enter umbra, solar panel array current drop to zero;

(3)   Exit umbra, first indication of array current greater than zero;

(4)   Exit penumbra, increase of approximately 49 DN in unregulated dc voltage.

The first solar occultation was observed on September 18, 1976 and the last occurred on October 25, 1976. Commencing with October 6, 1976, entry of penumbra and umbra could not be observed due to earth occultation but exit was observed. Neither entry or exit was observable from October 23 through October 25, 1976 — the last day of solar occultation — for the same reason. The shortest occultation, 8 min 18 s, was on September 18 whereas the longest observed was on October 5, with a duration of 2 hr 21 min 34 s.

VO-1 was placed in an all-axis-inertial mode — gyros on — for each solar occultation. This was accomplished by inclusion in programmed sequences which commanded the IRU on 20 min prior to predicted start of occultation and turned it off 20 min after the predicted exit from penumbra.

5.   Earth Occultations

Earth occultations, as was the case with solar occultations, affected only VO-1. They commenced on September 30 and concluded on November 5, 1976. The radio-science-earth-occultation experiment required a certain telecommunication configuration, during a specific period before and after the occultation, as follows:

   (1)   S- and X-band transmitters on;

   (2)   Low-rate telemetry at either 33-1/3 or 8-1/3 bps;

   (3)   High-rate channel Off.

   (4)   Ranging channel Off.

VO-1 performance during both types of occultation was as expected.

Batteries on VO-1 were placed in high-rate charge, for pre-determined lengths of time, at the conclusion of solar occultations.

H.   SUPERIOR CONJUNCTION

VO-1 and VO-2 were placed in a powered-down unattended state for superior conjunction, such that only those subsystems required to provide communication and proper attitude were left on. Command loads transmitted on November 6 and November 7, 1976 for VO-1 and VO-2 respectively, controlled sequences for a 36 day execution period. The on-board sequences contained only events necessary to maintain lock on celestial references (Deneb and the Sun), provide straylight interference protection and update the HGA. Normally, all engineering data was transmitted at 8-1/3 bps via the HGA (all VO science was off) by both VO-1 and VO-2. An exception to this data rate was on November 11, when VO-1 was commanded to 2 kbps link rate (for a short period of time) when a memory test on Processor-B was conducted. VO-1 was also utilized for an S/X-band relativity experiment. Superior conjunction occurred on November 25, 1976.

Table I-11. Primary Mission PFR Summarized[*]

VO-1	
PFR No.	Description
35401	Incorrect Processor-B checksum at first "hours pulse" after launch.
35402	Replacement Heater and Rear-mount temperature measurements reversed in IRTM.
35405	Incorrect constants used during ground calibration of gain states zero through three resulted in two to six percent low readings on MAWD gain state telemetry.
35406	Responsivity of MAWD PbS detectors 30 percent lower than pre-launch values.
35408	Helium pressure-regulator failed to effect a leak-tight seal after second pressurization of the system.
35412	Processor-B transferred to error during Sun/Earth occultation.
35411	Uplink AGC approximately 3 db below predicts. (Written for documentation only since levels still within command specifications.)
VO-2	
35402	Replacement heater and rear-mount temperature measurements reversed in IRTM.
35403	Responsivity of MAWD PbS detectors 30 percent lower than pre-launch test levels.
35404	Incorrect constants used for calibration of gain states 0 through 3 resulted in a 2 to 6 percent low reading on MAWD.
35407	Scan platform envelope would not permit IRTM "D" telescope to fully view the diffuser plate.
35409	400 Hz inverter current to IRU-1 went to zero at VL separation plus 26 seconds.
35410	When operating in the normal mode the IRTM scan mirror stepped past the space position 12 times when it should have stayed there for 3.36 s.
35413	During VIS playback DTR-B ran to sync speed, causing ccs to issue early track changes resulting in playback stop 17 min 21 s too soon.

[*]Refer to applicable subsystem in Section II for in-depth descriptions of these problem/failure reports (PFR).

I.   TELECOMMUNICATIONS

1.   Introduction

Orbiter telecommunications requires the proper functioning of both Orbiter and ground equipment. For this reason, it is included under "Systems," and thus some of the functions of the ground elements of the telecommunications system are discussed in this section. Figure I-3 is a conceptual block diagram of the important elements of the Orbiter S-band telecommunications system. The Orbiter receives S-band uplink from, and transmits an S-band downlink to, the Deep Space Stations. It also transmits an X-band downlink to 64-meter stations in the Deep Space Network (DSN).

Figure I-4 is a block diagram, at the subsystem level, of the Orbiter element of the telecommunication system. Each of these subsystems is discussed in detail, including description and performance during flight operations, in Part II of this report.

2.   Descriptions

a.   Telemetry and Command System. Beginning with the Deep Space Station (DSS), the DSS has either a 26-meter or a 64-meter antenna. The 64-meter antenna
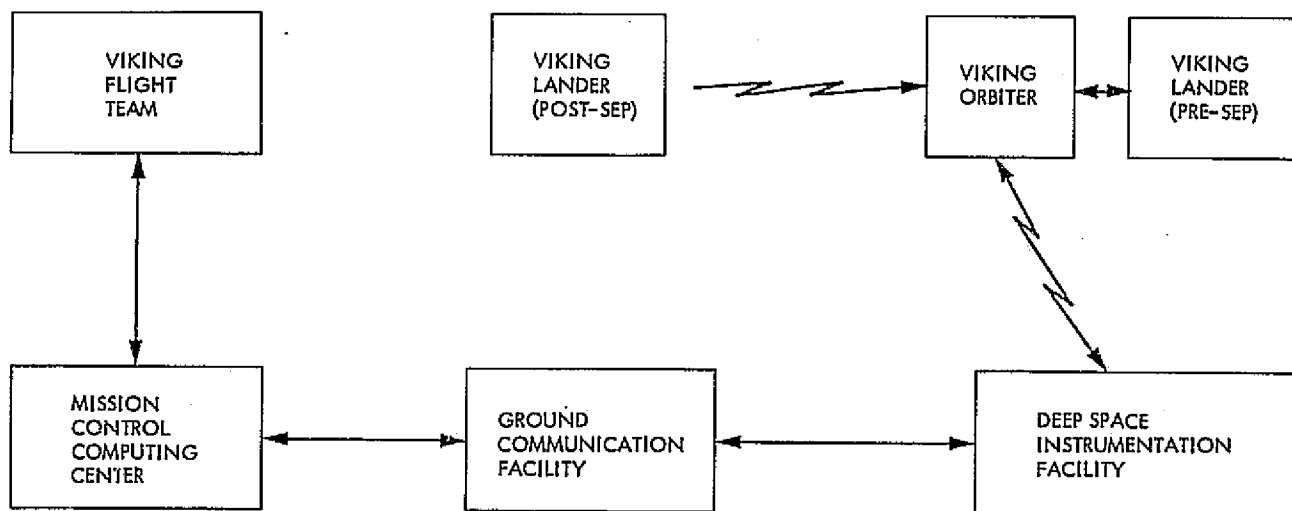
Figure I-3. S/X-Band Telecommunications System Overall Block Diagram
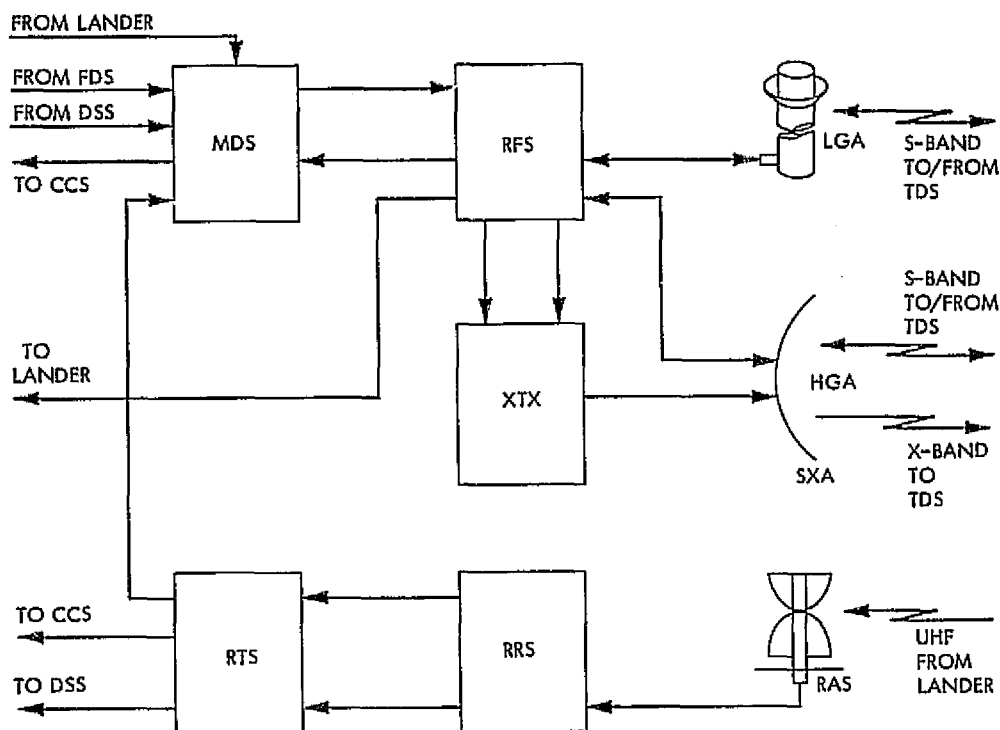
Figure I-4.   Viking Orbiter Telecommunications Subsystems

offers about 8.5 dB more gain for the S-band uplink or downlink than does a
26-meter antenna.   It, together with the lower system noise temperature associ-
ated with a 64-meter station, results in 10 dB greater performance.   During
cruise, the 26-meter stations were used extensively for telemetry, but also sig-
nificant 64-meter radiometric data was obtained.   During planetary operations,
the 64-meter stations were used for all downlinks, although some uplinks were
transmitted from 26-meter antennas.   This so-called "three-way" operation was
required because, while a 64-meter station could receive the downlinks from
both Orbiters (and a Lander) simultaneously, it could transmit only one uplink
at a time.

The 64-meter stations have both S-band (primary and secondary) and X-band
masers.   The secondary S-band maser has a higher system noise temperature which
results in about 1 dB degradation to the downlink when it is in use.   This

differerce in performance was accounted for in planning downlink data rates during planetary operations. The 26-meter stations do not have X-band receive capability. Figure I-5 shows the elements involved in downlink telemetry data processing, starting at the DSS and ending with the System Data Record (SDR) used for engineering evaluation or science data interpretation.

Orbiter engineering data is processed for realtime and non-realtime display in the Mission and Test Computer (MTC). This machine accepts both "monitor" and "telemetry" high-speed data blocks from the Ground Communications Facility (GCF), extracting the essential parameters necessary to assess the Orbiter's telecommunications links. These parameters include the uplink Automatic Gain Control (AGC) telemetry from the RFS, the S-band and X-band downlink AGCs from the station receivers, and the low-rate and high-rate signal-to-noise ratio (SNRs) from the station's Telemetry and Command Processor (TCP), Symbol Synchronizer Assembly (SSA), or Block Decoder Assembly (BCD). Quantities are formatted into plots which show them as a function of time; they also are included in printer formats, for exact analysis of levels and times. The SNRs were used for direct assessment of telecommunication link quality. The AGCs could be used for confirmation; however, they were subject to station calibration errors. The SNR was not subject to calibration or human error, and was used both for assessment and planning. The SNR, expressed in dB, was a true measure of data quality, at least to the analog original Data Record (AODR) or Digital Original Data Record (DODR) level at the station.

b. <u>Radiometric System</u>. The S- and X-band carriers were also used for radiometric doppler measurements; that is, measurements of the frequency changes due to the relative velocity of VO with respect to the earth. In addition, ranging modulation was present on the uplink and downlink carriers. The delay of the ranging signal through the Orbiter RFS was calibrated prior to launch, with an accuracy better than 10 nanoseconds. With this delay subtracted from the total station-VO-station measurement, the Earth-to-Orbiter distance could be computed.
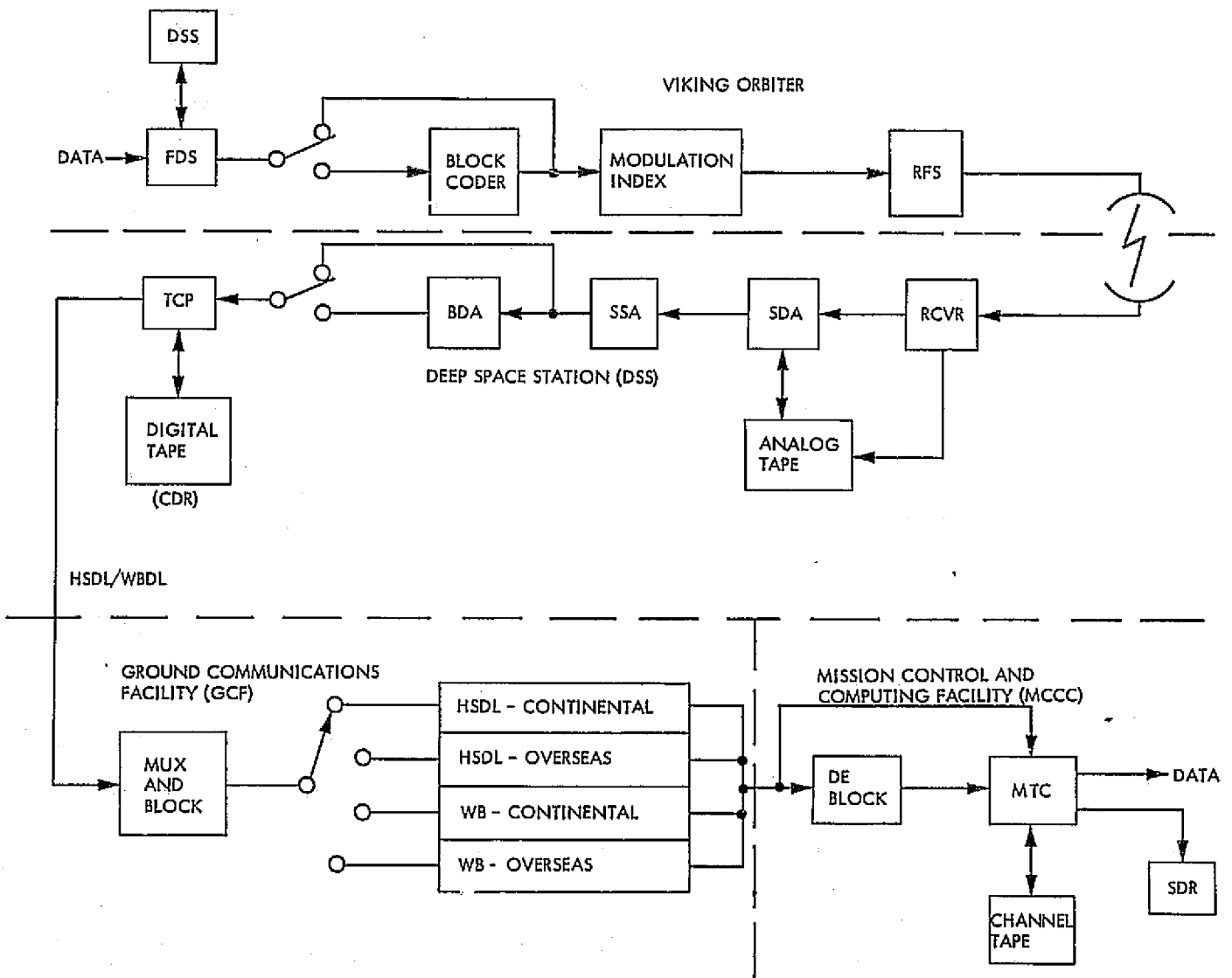
Figure I-5. Elements of the Downlink Telecommunications System

3.   Link Assessment

Link assessment is a matter of signal level vs. time. The signal levels
are predicted for each desired moment of time, as a function of power levels,
distance, antenna angles, system noise temperature, etc. The link quantities
measured at the station (AGC or SNR) and telemetered from the Orbiter (RRS
"Received Signal Strength" or RFS Uplink AGC) are compared with the pre-
dicted levels at the same moment. The difference, in decibels, between the
predicted level and the observed level is called a "residual." Accuracy of pre-
diction and measurement is indicated by the fact that the high-rate channel SNR
"residuals" were most often less than 0.5 dB. The most work went into reducing
these residuals, during flight operations. The AGC residuals were usually
within 1 dB for the S-band. At X-band, these were usually within 3 dB. Link
planning requires the prediction of the times for data rate switches, to ensure
continuous communications. This planning was an iterative process, with the
residuals observed at one time being factored into planning for a later time.

The Orbital Performance Analysis Group (OPAG) Telecom Analysts usually
assessed link performance for each Orbiter for each station pass (three station
passes per day per Orbiter). The link residuals were computed and then plotted
as a function of time, so that developing "trends" could be discerned. Figure I-6
for VO-1 and Figure I-7 for VO-2 display the S-band uplink and downlink AGC resi-
duals, each point representing the average for one month for that tracking station.
Each plot contains data for the period from January to September, 1976, thus includ-
ing the latter portion of interplanetary cruise and the majority of planetary
operations. The 64-meter stations at Goldstone, Australia and Madrid, respectively,
are DSS-14, DSS-43, and DSS-63. All other stations are 26-meter, with DSS-11 and
DSS-12 being at Goldstone, DSS-42 and DSS-44 at Australia and DSS-61 and DSS-62 at
Madrid.

One of the problems described in para 5.g., the so-called "second VO-1
uplink AGC anomaly", shows up clearly in Figure I-6. Between June and August,
all stations show a more negative uplink AGC residual. The other links are all
quite stable, although there are month-to-month variations at particular sta-
tions. It is possible that there is a slight downward trend in VO-1 downlink
AGC also; however, if there is, it was not reflected in the low-rate or high-
rate SNR, which remained stable throughout the primary mission. Similarly, there
may be a very slight downward trend in VO-2 downlink AGC; again, the signal-to-
noise ratios did not confirm this downward trend.
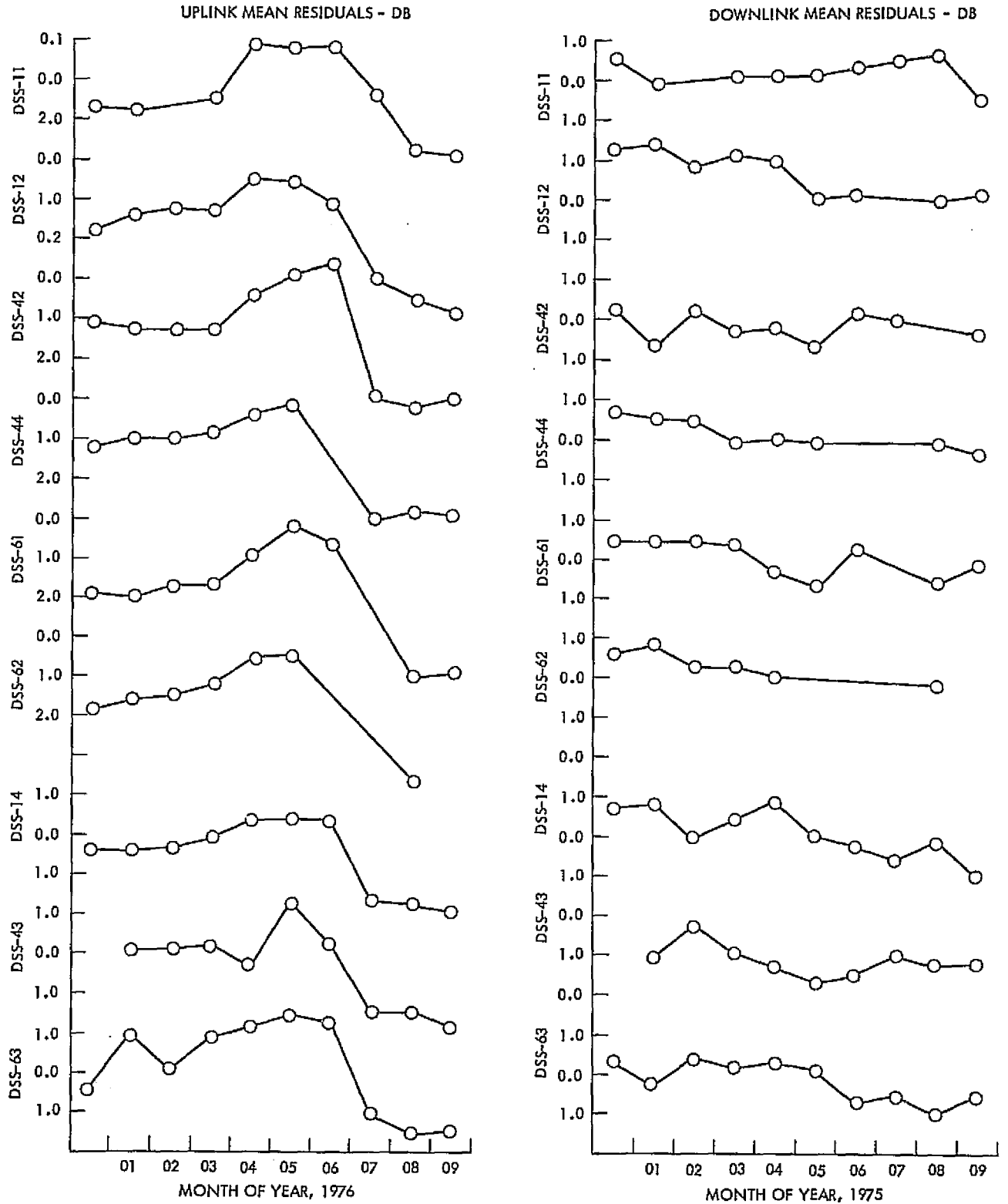
Figure I-6.   VO-1 Uplink and Downlink S-band AGC Residuals
(1/76 through 9/76)
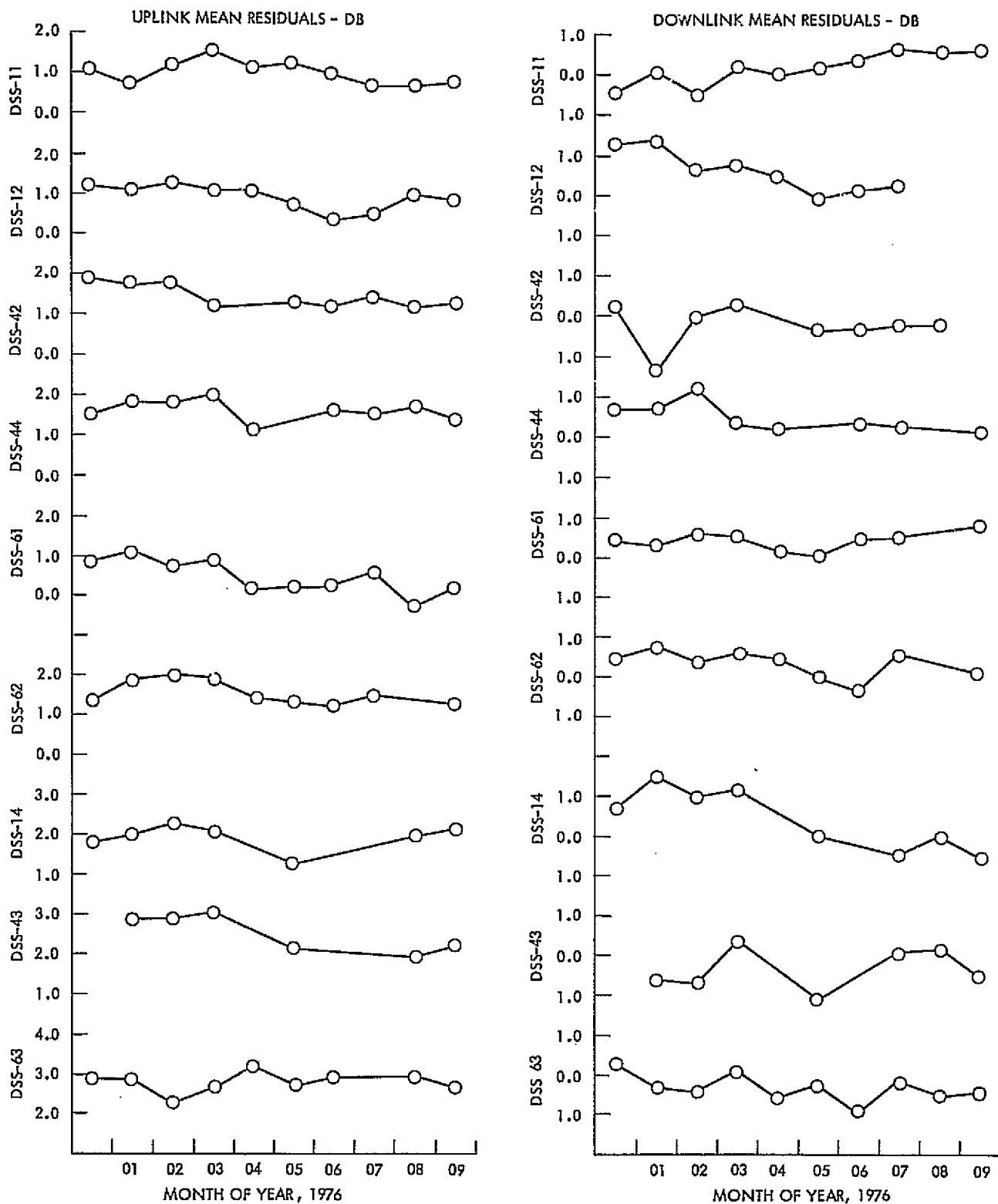
Figure I-7.   VO-2 Uplink and Downlink S-Band AGC Residuals
(1/76 through 9/76)

4.   Link Problems

a.   VO-1 Uplink AGC Anomaly No. 1 (Launch through March 2, 1976).
Beginning with the DSS-42 initial acquisition of VO-1 after launch, and con-
tinuing indefinitely, the uplink AGC telemetry showed signal levels lower than
predicted.   Shortly after launch, discrepancies as much as 6 dB were noted; the
residual later became about -1.5 dB average.   Uplink AGC residuals for VO-1 and
VO-2 are displayed in Figure I-8.   The changing residuals over the first month
after launch are believed to be caused by the large uncertainty of the LGA pat-
tern at high cone angles, including increased pattern effects of reflections.
These are present on both VO-1 and VO-2.   The remaining VO-1 residuals were
ascribed to AGC calibration shifts with vacuum.   The magnitude of vacuum
effects and their changes with time are not fully understood; however, it
is fairly certain that these effects occur.   RFS subsystem vacuum tests
showed an AGC indication of about 1 dB reduced level, with subsequent
recovery following vacuum.   The stabilized value appears shifted from pre-
launch by about -0.5 dB for VO-1 and + 0.5 dB for VO-2.   For flight operations,
the calibration curves for VO-1 and VO-2 were corrected and entered into the
MTC on March 2, 1976.

b.   Uplink AGC Variations Due to Ranging Modulation.   During several
ranging passes, for both VO-1 and VO-2, short-term decreases of 1 to 3 dB in the
indicated uplink AGC were seen.   On VO-1 these "AGC bumps" were significant,
because the average uplink AGC was close enough to command threshold that the
uplink level had to be considered as too low for commanding during the "AGC
bumps."   Telecom/Radiometric Analyst investigation showed that the cause of the
bumps was a fault in the Planetary Ranging Assemblies used at the stations.

c.   Unexpected CDU Bit Sync Lock or CCS Lock-Count Changes (Throughout
Mission).   A half-dozen times or more during the mission, with both VO-1 and
VO-2 and at various stations, the MDS CDU would indicate a momentary (i.e., one
telemetry sample) change from subcarrier lock to bit sync lock or the CCS would
show a change in its lock status count.   Occasionally both symptoms would be
present.   Most of these changes were correlated with the removal of command
modulation at the ground station, at an outgoing handover.
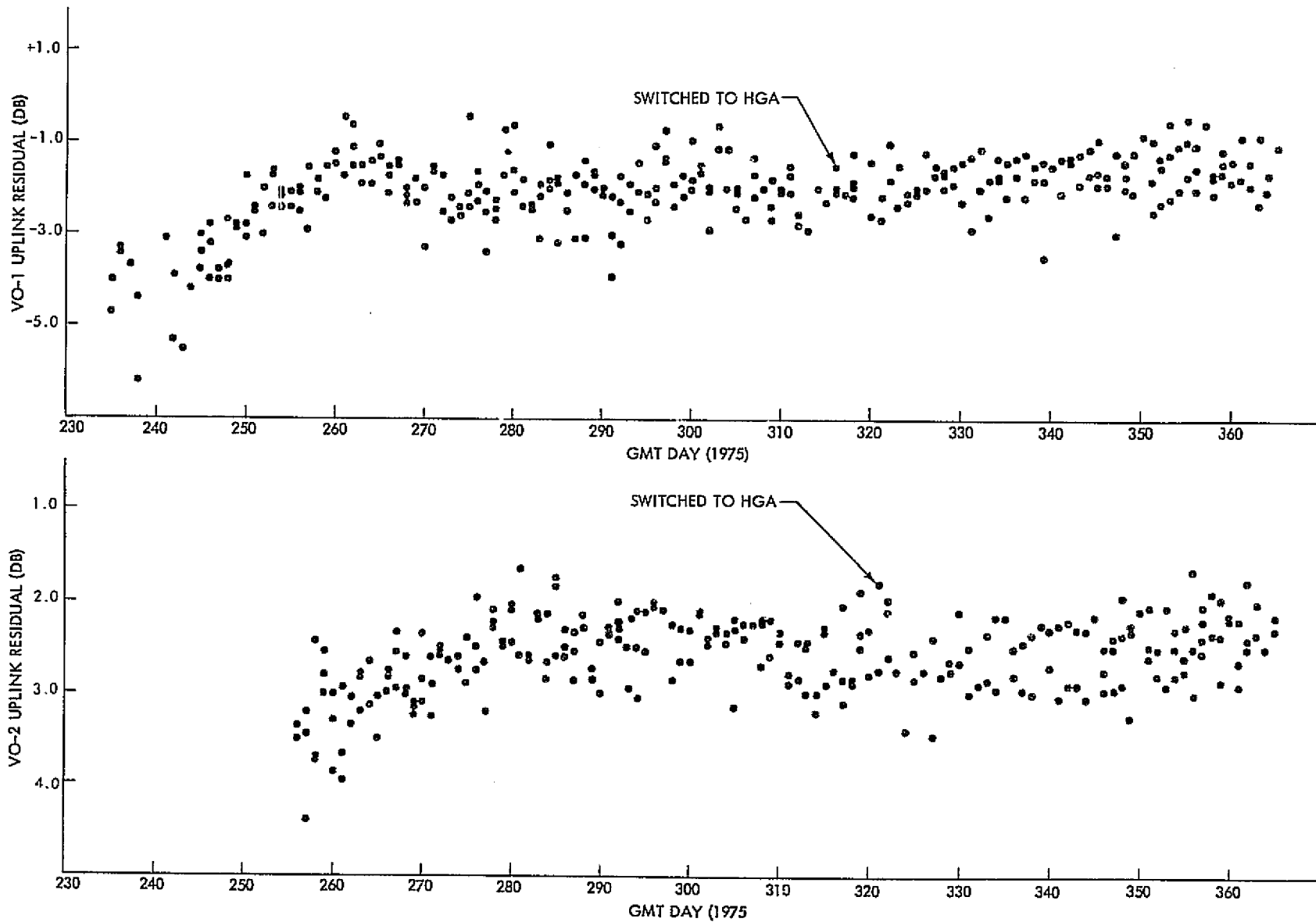
Figure I-8. Pass-Average "Uplink AGC Coarse" Residuals for VO-1 and VO-2 from Launch Through 12/75

d.   Static Phase Error Alarms. All Orbiter telemetry channels are "alarmed" with upper and lower limits, when feasible, so that incipient problems can be detected quickly. Two or three times during the primary mission, the RFS static phase error (SPE) channel alarmed. Unlike most other Orbiter telemetry channels, this one is a function of ground station activity as well. The cause for the alarms was found to be errors in frequency predictions (used for setting uplink transmitter frequency) or errors in setting the uplink frequency for a pass. In each case, it was necessary to review RFS data carefully to be sure that the problem was not in that subsystem.

e.   Interaction of High-Rate and Low-Rate Telemetry. With both VO-1 and VO-2, it was found that when the high-rate subcarrier was ON, and the bit rate was 8 kbps or 16 kbps, the low-rate channel SNR would be degraded by as much as 1 dB. Investigation of in-flight and pre-launch data revealed that this effect is caused by the particular bit pattern on the high-rate channel. it is not present for the 2 kbps or 4 kbps rates.

f.   VO-1 and VO-2 RFS Receiver VCO Rest Frequencies. In-flight frequencies measured by the DSN differed from those predicted from Viking telecom curves measured before launch. The condition did not represent a hazard to Orbiter health or operation; however, the cause was investigated in the event that the redundant receivers were needed later during the flight. The VO-1 frequency shift was ascertained to be due probably to a dc bias change. The VO-2 change appeared to be in the VCO itself. Frequencies in both radios were within the RFS specifications and stabilized during cruise. Both changes are believed to be due to ageing effects in a vacuum. Revised frequency curves were published by Telecom, for use in planetary operations and the extended mission. (The difference between measured and predicted frequencies were -38 Hz for VO-1 and -29 Hz for VO-2.) No further changes were observed during the primary mission.

g.   VO-1 Uplink AGC Anomaly No. 2 (June 30, 1976). Non-realtime link residual analysis showed that on this date, the VO-1 uplink AGC decreased by about -1.7 dB during a nonpropulsive maneuver. A CDU "SNORE" test was performed using DSS-11's transmitter at 10 kW, to determine the probable location of the AGC shift in the Orbiter communications subsystems. This test did not show a change in either the command ST/No or the Mean Value. Thus, it was concluded the shift had occurred as the result of a gain change of 1.7 dB in the 47 MHz IF or the 9.5 MHz IF of the RFS receiver. This gain shift is at the threshold

of measurement accuracy for the CDU SNORE test, so it could not conclusively rule out a change in the "RF head" (antenna cabling, switching circuitry) of the RFS. An RFS "bench test" was also performed, and the effect duplicated. Operationally, this AGC change resulted in a 2-dB "pad" being included in the uplink level for commanding VO-1 in critical situations, such as during maneuvers on the LGA, where signal levels might be low. There was no further shift in VO-1 uplink AGC through the end of the mission.

h.   Relay Link "glitches" (VL-2 to VO-2). On Viking 2 relay passes 8, 9, 10, 13, and 23, there were small unexplained steps in the VO-2 RTS SIG and and the RTS SNR telemetry (one step each relay pass, during "link rise"). The steps amounted to several tenths of a dB, much smaller than the tolerance on the link. Steps were not seen on any VL-1 to VO-1 relay links, or on subsequent VL-2 to VO-1 relay links. The cause of the "glitches", none of which affected the quality or quantity of relay link data return, remains unknown. It cannot be ascertained whether the cause lies in the Lander or the Orbiter. Operationally, the glitch was considered an idiosyncrasy, and no account was made of it in link planning.

i.   Radio Frequency Interference (RFI) (October 28, 1976). High-rate VIS playback at 8 kbps was disrupted at DSS-14 for 40 minutes, from both VO-1 and VO-2, on this date. It was later determined that the RFI came from an external source. Generally, coordination between RFI generators and the Viking Project/DSN was good during the primary mission. Planned RFI was coped with by rescheduling science playbacks to occur outside the time interval of the potential RFI. Similar planning will take place during the Viking extended mission, with regard to interference from an European Space Agency satellite over DSS-63 in Spain.

j.   Solar Interference (from October 6, 1976). The approaching superior conjunction at the end of the Viking primary mission degraded the low-rate SNR as early as the above date. Surprisingly, the bit error rate was not affected so severely as the indicated SNR. At a later time, the high-rate channel became quite noisy due to solar interference. In this case, which was the second week in November, 1976, the indicated SNR was well above threshold, 8 dB indicated for the block-coded 2 kbps data, but the bit error rate was well below threshold, at about 1/100 BER. The permitted high-rate data rate for Orbiter science playback was gradually reduced in October and November, to ensure that all data played back would be above threshold. In addition, the last permitted commanding of the

Orbiters was on November 10, when the sun-earth-probe angle had decreased to slightly less than five degrees. By the end of the primary mission, the solar effects were so severe at a three-degree sun-earth-probe angle, that the single-subcarrier cruise mode 8-1/3 bps data showed the same indicated SNR at both 64-meter and 26-meter stations.

PART II

SUBSYSTEM PERFORMANCE

VFT-022

SECTION I

COMMUNICATIONS

A. INTRODUCTION

Several elements provided the required Viking Orbiter (VO) radio communications links with Earth and Mars. The following subsystems and assemblies provided the necessary hardware:

(1) The S-Band Radio Assembly (RA), as seen in Figure II-1, provided the Earth to VO command link receiver and the VO to Earth data transmission link via the S/X-Band Antenna (SXA) Subsystem. Another important provision is that of the navigational S-band turn around ranging channel (see Figure II-1).

(2) The Modulation Demodulation Subsystem (MDS) consists of dual redundant Command Detector Units (CDUs) and dual Telemetry Modulation Units (TMUs) with only one CDU and one TMU powered continuously. The purpose of the CDU is to demodulate the Earth to VO uplink command signals. The purpose of the TMU is to generate composite telemetry signals for the modulation of the VO to Earth downlink.

(3) The Relay Telemetry Subsystem (RTS) is part of the VO Relay System which also includes the Relay Antenna Subsystem (RAS) and Relay Radio Subsystem (RRS). The RTS receives a noisy split-phase pulse-code modulation (PCM) waveform from the RRS and provides recorded PCM data, synchronization, lock detector status, and telemetry to the appropriate VO subsystems.

(4) The UHF-FSK Relay Radio Subsystem (RRS). Figure II-2 shows the receiver block diagram, from which it can be seen that the UHF input to the RRS is supplied via the RAS. The detected FSK signal is then routed to the RTS from either the 16 kbps or 4 kbps demodulator.

(5) The X-Band Transmitter (XTX) functional block diagram is shown in Figure II-3, the input signals are supplied by the S-band radio. The XTX multiplies the frequency to 8415 MHz and modulates this
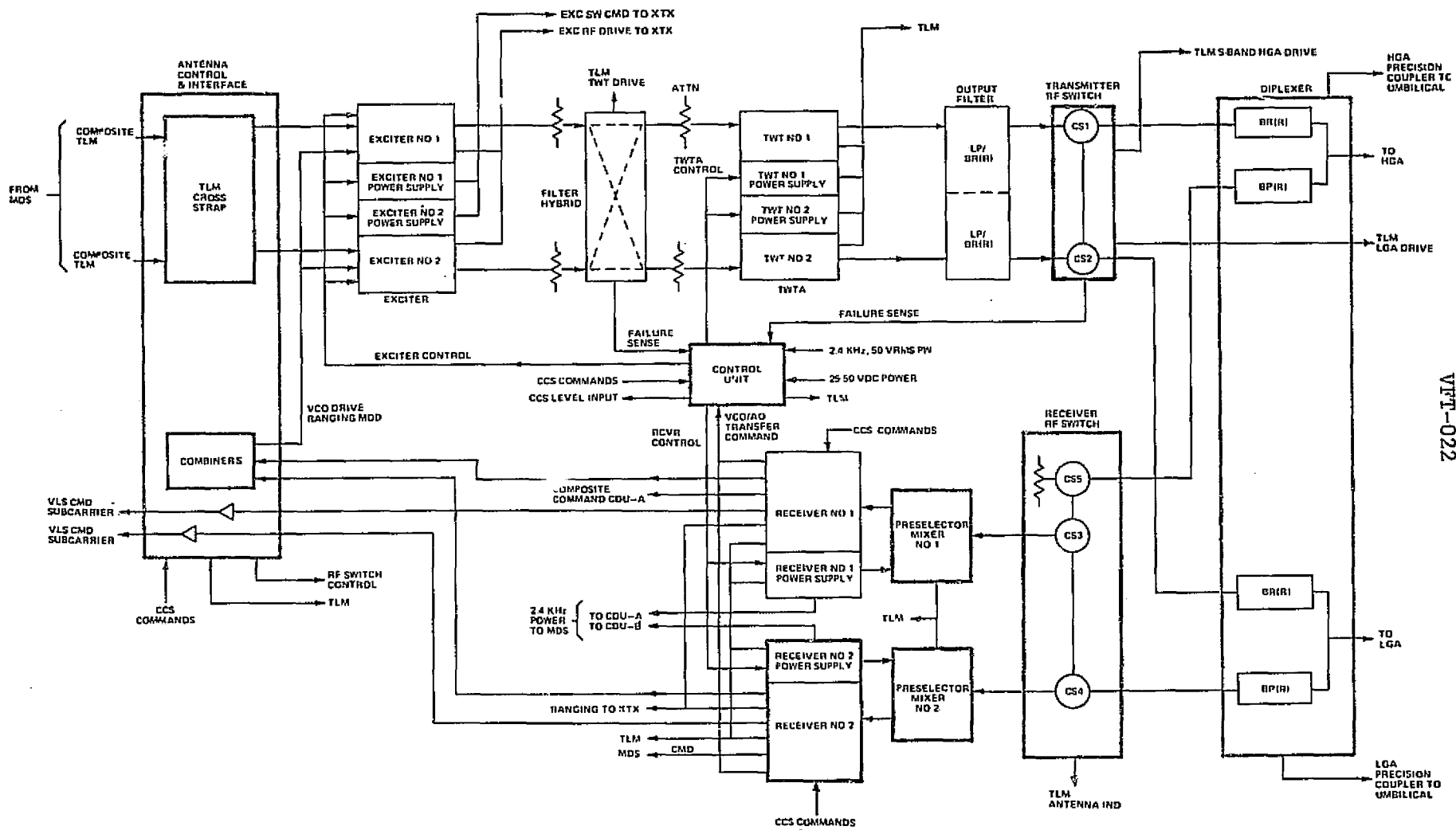
Figure II-1. S-Band Radio Assembly Block Diagram
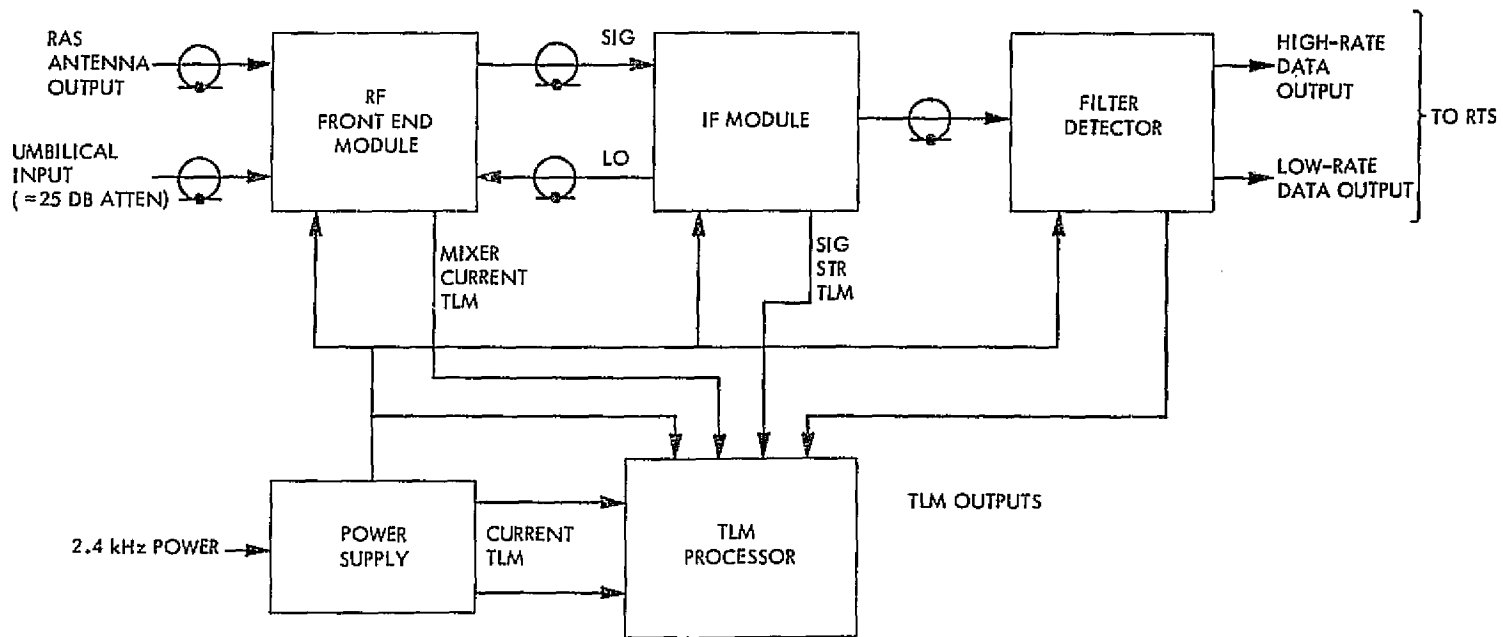
Figure II-2.   Relay Radio Subsystem Block Diagram
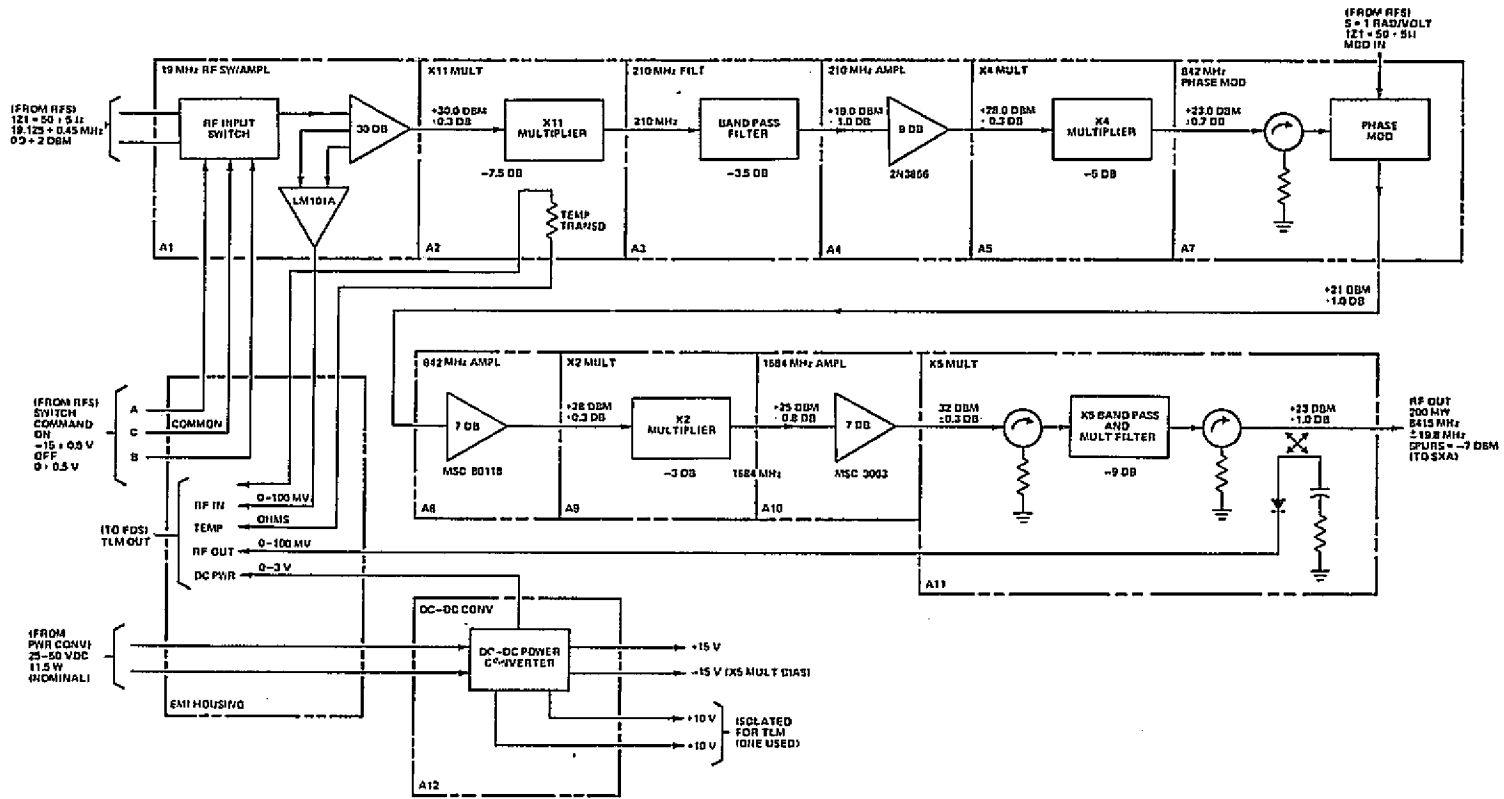
Figure II-3.   Transmitter Block Diagram and Internal Interfaces for X-Band

carrier frequency with the ranging code. This X-band signal is then fed to the X-Band High-Gain Antenna and thence radiated to earth.

(6)   The S- and X-Band High-Gain Antenna (HGA) and the S-Band Low-Gain Antenna (LGA) are associated with the RA. The combined antenna equipment is referred to as the SXA Subsystem. The VO input and output radio frequency (RF) signals are received and radiated by means of the SXA subsystem routing of these signals as shown in Figure II-4, which also shows the various cables, waveguides, and rotary joints. Figure II-5 is a sketch of the LGA giving the various dimensions.

(7)   Relay Antenna Subsystem (RAS) is connected to the RRS. It receives the Lander UHF signal which is then fed by cables to the RRS input.

The above mentioned hardware provides the required VO radio communications links, interconnected as shown in Figure II-6. This block diagram also shows the major VO spacecraft telecommunications system and associated interfaces.
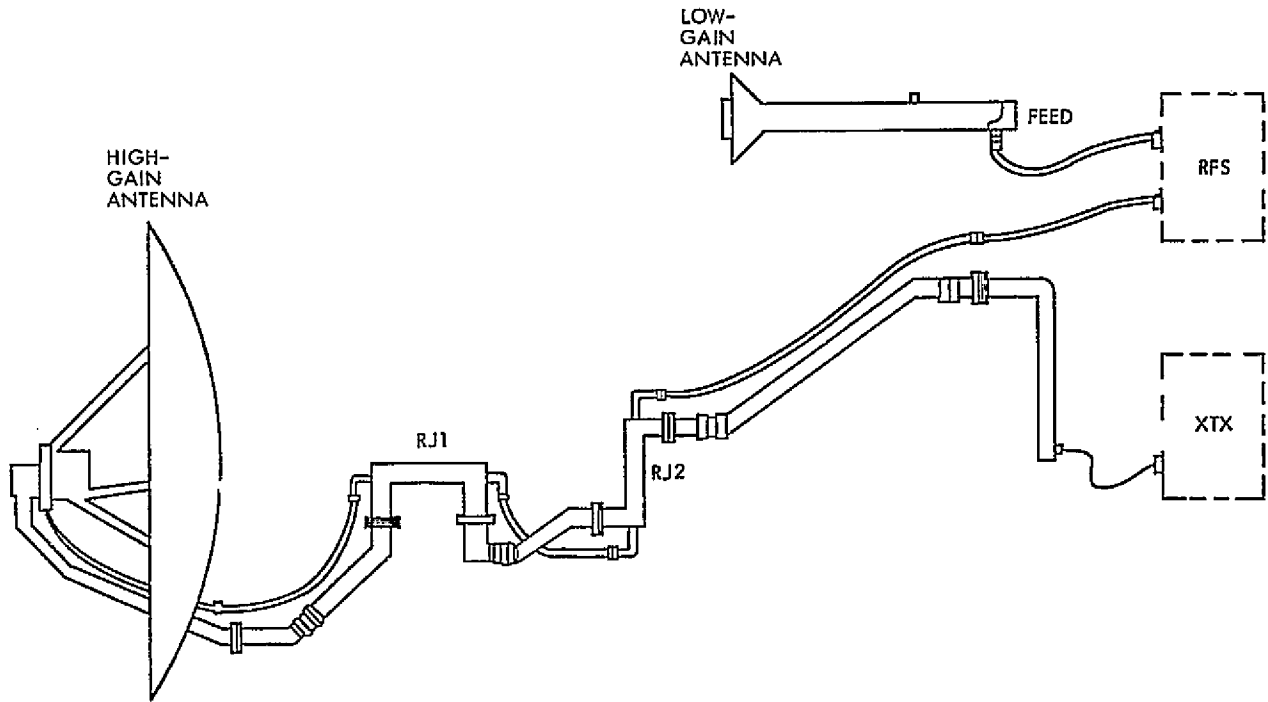
Figure II-4. SXA Antennas, Waveguides, and Cabling
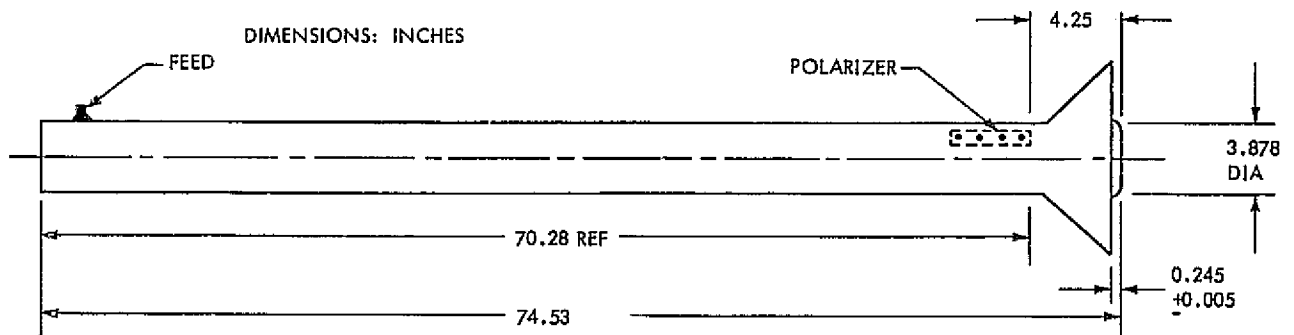
Figure II-5. Sketch of Low-Gain Antenna
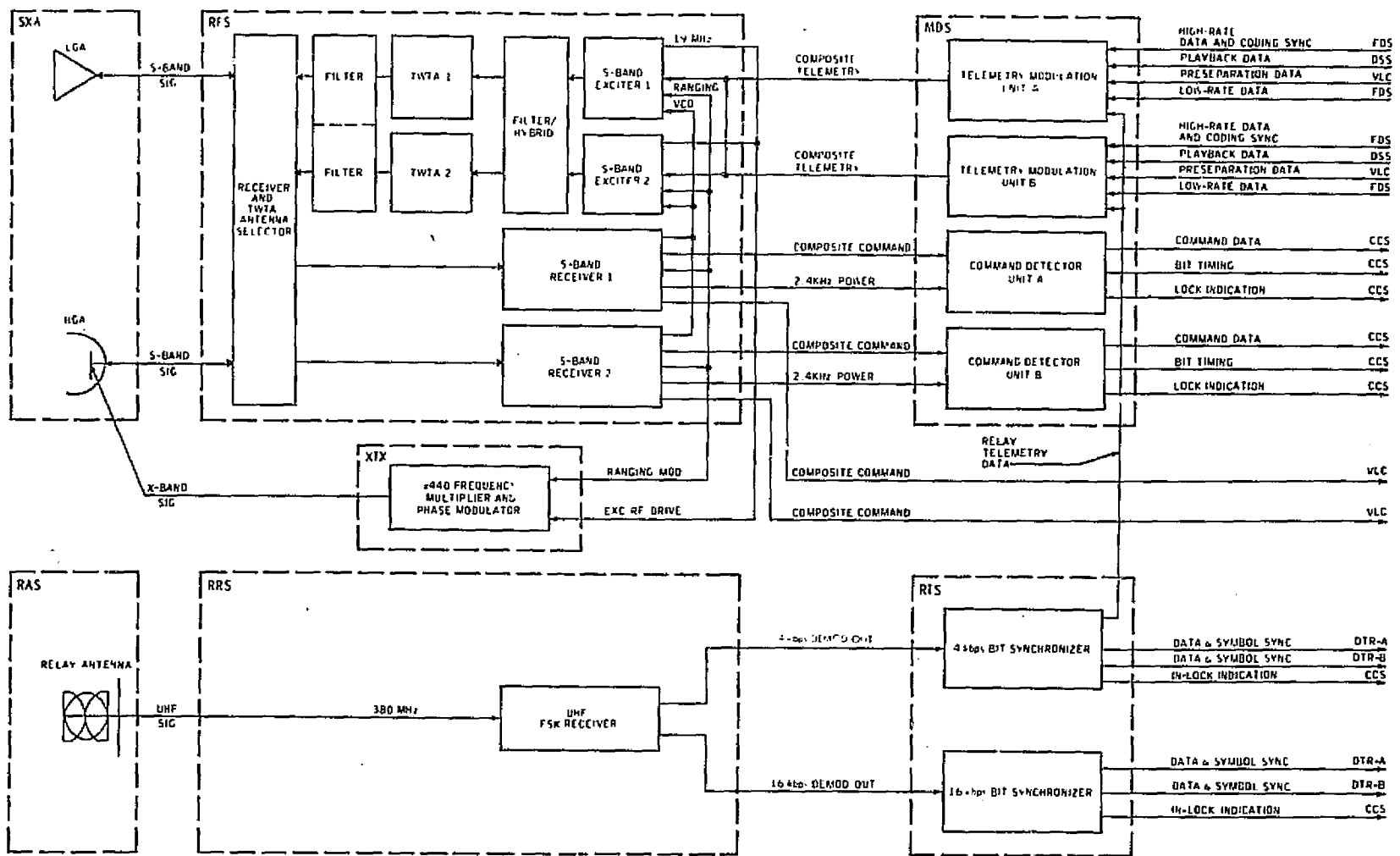
Figure II-6. Telecommunications Functional Block Diagram

B.   S-BAND RADIO ASSEMBLY

1.   Description

The RA, often referred to as the Radio Frequency Subsystem (RFS), is part of the VO Telecommunications System. It is designed to perform as: a command receiver, a phase-coherent ranging transponder, and a telemetry transmitter as shown in Figure II-1. The RA consists of double conversion, phase-coherent, redundant receivers and redundant continuous wave (CW) exciters, that can be connected to the receivers via switches to provide a two-way tracking transponder mode of operation. There is also a redundant traveling-wave tube amplifier (TWTA) together with microwave components that provide RF filtering and switching for connecting either transmitter to the HGA or LGA while either receiver is concurrently connected to the LGA or HGA antenna. The selection of the correct radio commands is provided by the control unit which selects the required redundant element and RF switches. The following are some of the major operating parameters of the RA:

(1)   A drop lock receiver threshold of approximately -152 dBm was found during in-flight testing, this sensitivity being a function of the receiver noise figure and the receiver phase loop noise bandwidth which was designed to be 18 Hz ($2B_{LO}$) at threshold.

(2)   When the receiver is locked to an input carrier frequency, the coherently translated transmitter frequency is precisely 240/221 times the received frequency.

(3)   Provide composite command signal output to MDS.

(4)   Provide a transmitter output power of approximately 20 watts (+43 dBm).

(5)   Transmit the VO composite telemetry signals back to earth.

(6)   Detect Earth-originated ranging signals and, after processing these signals, modulate the S-band transmitter with the ranging information.

(7)   Provide a coherent RF signal to the XTX, either via the voltage-controlled oscillator (VCO) or auxiliary oscillator.

(8)   Provide a ranging signal to the XTX.

(9)   When no ground originated uplink carrier is present, a non-coherent transmitted signal is derived from the auxiliary oscillator.

The RA is perhaps the final version of this type of mechanical package that has been developed over several past flight programs. The trouble-free mission may be due a great deal to this past evolution of the hardware. More redundancy was provided for in this version of the RA, for instance dual receivers, which provided for more complex interconnection with the MDS.

2.   Performance

Both VO-1 and VO-2 carried out similar major events during the primary mission which were separated by one or two weeks, the difference relating to the 20-day launch-day offset. This difference made VO-2 events a little easier to predict, but those of VO-1 were attended with bated breath and crossed fingers. The most significant parameter changes occurred about one hour after the launch of VO-1 in the following telemetry channels:

(1)   Receiver local oscillator (LO) drive from 40 DN to 44 DN which represented approximately −0.5 dB.

(2)   TWT helix current from 66 DN to 60 DN converting to a drop of less than 1 MA.

(3)   TWT drive from 105 DN to 102 DN representing a drop of some 0.2 dB.

These changes had been predicted prior to launch, being accounted for by the environmental changes of pressure and temperature. However, the change of the receiver LO drive was a little more than had been expected. Further pre-launch data research revealed that a change of the amount observed could be expected.

The only other area to produce any head scratching in the OPAG Radio/Telecommunications Unit was the VO-1 disparity between the telemetered value for the receiver automatic gain control (AGC) relative to the value predicted.

From the initial DSN two-way acquisition the uplink AGC telemetry was as much as 7 dB below the predicted value. Since it was known that at strong input signals the RA could have an error of up to 5 dB due to the non-linear characteristics of associated circuitry, little immediate concern for a major problem was held. Subsequently, as the distance from Earth increased, the signal level decreased, and the uplink AGC telemetered value converged toward the predicted level. This residual later tended to about a -1.5 dB average. No operational constraint was created by this discrepancy which was considered by all concerned to be more of a nuisance than a real problem. Additional correction to the residuals was also suggested from pre-launch radio vacuum test results, in which the telemetry circuits indicated 1 dB less than actual input signal. A receiver threshold verification test using VO-1 was conducted on Aug. 30, 1975. Results of this in-flight check established that the receiver threshold was unchanged since launch. Also, the calibration curve, from a input signal of -120 dBm to threshold was not significantly changed. Revised AGC calibration curves for both VO-1 and VO-2 were produced and submitted to the MTC on Feb. 3, 1976. It should be noted that this error was not as large in magnitude with VO-2 after its launch, being in the order of 1 to 2 dB. All other VO-2 radio parameters behaved as pre-launch predictions had indicated they would.

One other incident of pre-launch AGC calibration error was a difference in the respective signal level readings (engineering unit conversion) of the VO-1 AGC-coarse and AGC-Fine channels, with the Fine reading -0.5 dB relative to the Coarse reading. This difference was found to be due to a misinterpretation of the output signal from the Flight Data Subsystem (FDS) during pre-flight calibration testing. A correction was simple to remedy and the AGC-Fine calibration curves for VO-1 were resubmitted to the MTC.

VO-1 and VO-2 were switched to the HGA from the LGA on Nov. 11 and 18, 1975, respectively. For both, the transition produced the expected increase of uplink and downlink signals as determined from uplink receiver AGC changes. Late in the day on Nov. 21, 1975, X-band transmitters were turned on permanently for both VO-1 and VO-2. All telemetry readings produced values that were expected.

June 19, 1976 was the date of the Mars Orbit Insertion (MOI) for VO-1 and was performed as predicted for the radio subsystems. Several midcourse maneuvers prior to MOI were also executed without problems. During the MOI maneuver, the effect of transferring to internal (battery) power was observed by plotting variations of XTX input current versus unregulated dc voltage.

The month of June 1976 also produced the second VO-1 uplink AGC anomaly, which was also the only "Radio Mystery" of the primary mission. Non real-time analysis brought to light an offset of -1.7 dB in the uplink AGC during one of the many non-propulsive maneuvers. After a great amount of data research and a special in-flight test including a CDU SNORE test and comparison of telemetry channels AGC-Coarse and AGC-Fine it was concluded that the offset was indeed within the VO-1 S-Band receiver. The exact location was not easily determined from telemetry data. However, the main consensus of experts was that the shift was caused by a sudden change in gain within the early stages of the 47 MHz or 9.5 MHz IF amplifiers in the receiver. A continuous record of this shift was maintained in order to catch any failure trend. No further change was ever observed and the only problem caused was in operational evaluation of the command uplink in case command threshold (-145 dBm) were to be approached during critical maneuvers with the LGA.

On Aug. 7, 1976 VO-2 MOI was executed, and all radio communications performed as predicted. Many non-propulsive maneuvers were performed prior to the second Viking landing during September without any observed problems. The actual descent phase was carried out, almost without data due to the unfortunate loss of Sun/Star references, on Sept. 3, 1976. All descent data was obtained via the LGA at low-rate, so that the RRS received signal level was the only indicator of the Lander position. Playback of the first Lander pictures was delayed approximately nine hours until VO-2 was reconfigured to the required mode of operation. During the third week of September 1976 both the uplink and down-link began to fluctuate due to the onset of solar occultation, and this condition continued to worsen as the conditions for superior conjunction approached. Further interference to the up and downlinks occurred at the beginning of October 1976, due to the advent of Earth occultation.

a.   Operational Signatures. Several useful indications of RA mode changes were documented to aid analysis:

(1)   One-way/two-way acquisitions were readily found by observing the uplink receiver AGC. However, confirmation was provided by changes in the values of Exciter Input Current (increase of approximately 2 or 3 DN in two-way which indicated the increased current in the auxiliary oscillator circuits). A decrease of 1 or 2 DN in Receiver Input Current due to the transfer to the VCO and AGC control. The largest change was that of the XTX RF Drive with an increase of 7 to 8 DN in two-way, due to the difference of the drive levels from the VCO and Auxiliary Oscillator outputs.

(2)   In the event of the ranging channel being commanded on or off, it was found that the Receiver Input Current was about 2 DN less in the off state due to less video amplifier circuit current, added to which the TWT Helix Current was found to be 1 to 2 DN less with the ranging channel off. This is theorized as being due to a wide-band noise reduction of the ranging channel output, but this channel was extremely sensitive to many variations within the RA.

(3)   An increase of Receiver Input Current by 1 DN with application of command modulation.

(4)   The application of dual subcarrier modulation caused an increase of 1 to 2 DN in the TWT Helix current.

b.   Operational Cycles. During the primary mission a log of Radio Only commands was maintained for each VO, with the approximate totals as follows:

	DC Command	Function	Total
	DC2A	Ranging Channel ON	149
	DC2AR	Ranging Channel OFF	148
	DC2E	HGA Select	46
	DC2ER	LGA Select	47
VO-1	DC52A	RRS/RTS ON	8
	DC52AR	RRS/RTS OFF	7
	DC42A	XTX ON	2
	DC42AR	XTX OFF	1

	DC Command	Function	Total
	DC2A	Ranging Channel ON	125
	DC2AR	Ranging Channel OFF	124
	DC2E	HGA Select	53
VO-2	DC2ER	LGA Select	52
	DC52A	RRS/RTS ON	5
	DC52AR	RRS/RTS OFF	4
	DC42A	XTX ON	2
	DC42AR	XTX OFF	1

c.   Daily Trend Plots. All telemetry channels relative to radio commu-
nications equipment were plotted daily throughout the primary mission. The more
dynamic channels of uplink AGC and static phase error (SPE) could not be repre-
sented by a one-point-a-day plot and were treated separately by the telecommuni-
cations link analysts. An MTC plot from liftoff through launch plus ten hours
showed the major changes that occurred due to the environmental changes of space.
This, then, was the base reference from which the trends varied. From that time
on there were absolutely no adverse trends indicated by these daily plots. Most
changes, previously discussed, were due either to environmental conditions or
the expected changes due to idiosyncracies and signatures.

d.   Operating Hours. The RAs for both Orbiters were operating the same
elements for the duration of the primary mission. For VO-1 this time from Aug. 20,
1975 through Nov. 16, 1976 gives an approximate operating time of 10,920 hours. The
period for VO-2 is from Sept. 9, 1975 through Nov. 16, 1976 for a total of 10,440
hours. A situation that was a nice surprise for the OPAG radio analysts, was that,
for both orbiters, the S-band radio elements remained the same throughout. These
totals, of course, do not account for time variations of such operational mode
changes as: ranging channel ON/OFF or one-way/two-way tracking.

3.   Anomalies

a.   Anomalies Caused by Radio Communications Equipment. Several of the
anomalies have been already discussed at some length, i.e., those pertaining to
the VO-1 or VO-2 uplink AGC levels of the S-Band Radio Receivers. These
anomalies have also been discussed in Telecommunications, Part I, as "VO-1 uplink
anomaly #1" and "VO-1 uplink anomaly #2."

b.　　S-Band Receiver VCO Rest Frequencies.　After some six months of flight it became evident that the VCO rest frequencies for both VO-1 and VO-2 had changed from that frequency predicted from pre-launch data.　The reason for the offset of rest frequencies was not realized earlier because of (1) the relatively small changes and slow rate of change (VO-1 was -30 Hz and VO-2 was -26 Hz, relative to the predicted frequency) and (2) very little opportunity for rest frequency observation during two-way operation with doppler effects included. The VO VCO frequency is derived by calculation from knowledge of the DSN station track synthesizer frequency (TSF) and the one-way doppler frequency, neither of which were available within the OPAG area and had to be obtained via Network Analysis Team (NAT) track.　These changes were most likely caused by aging effects in the environment of deep space.　The individual mechanisms for VO-1 and VO-2 are considered to be different.　However, both frequencies have stabilized and have not shown any further changes.

For VO-1, a review of SPE and frequency data indicated that the shift in acquisition frequency (rest frequency) occurred shortly after launch. However, SPE voltage versus frequency had not changed when the receiver was in two-way phase lock with the uplink carrier.　This implies either a change in the phase detector output voltage level or the X10 operational amplifier offset had shifted.　Test results indicated a 24 mv shift in the phase detector output would produce a 29 Hz change in the rest frequency, well within the ±100 mv specification limit.　Data taken indicated that the shift took some four months after launch to stabilize.　For VO-2 the frequency shift appeared to be within the VCO itself.　The rest frequency value for SPE indicated no change had occurred from the predicted value.　Also, the slope of the telemetry curve of SPE versus frequency, as measured in flight for two-way operation, indicated no change had occurred in the gain of the VCO $\left(\partial \dfrac{Hz}{\partial \text{ Volts}} \right)$.

Data indicated that the shift began immediately after launch and progressed in an exponential manner toward its final value of -26 Hz, relative to the predicted frequency, well within the specification of ±440 Hz.

The recommended action to overcome these frequency offsets was to revise the predicted acquisition frequencies for both VO-1 and VO-2. Also, the telemetry curves of SPE Coarse and Fine versus frequency were revised to correct the frequency and were resubmitted to the MTC.

Continued monitoring of rest frequency versus SPE values for VO-1 and VO-2 indicated no further changes during the primary mission.

C. MODULATION DEMODULATION SUBSYSTEM

1. Description

a. Command Detector Unit. Each CDU is connected to one RFS receiver from which it receives the VO's uplink composite command signals. The composite command signal consists of a 512 Hz square-wave subcarrier, bi-phase modulated with command date at 4 bps and bit synchronization at 4 Hz. The CDU acquires subcarrier and bit synchronization, recovers the command data bits and delivers data bits, data bit timing, and lock status to the CCS and subcarrier/bit sync lock status to the FDS.

A block diagram of the CDU is shown in Figure II-7. The CDU establishes and maintains demodulation references, detects the command information, and generates the detector status signals. The detector establishes the subcarrier and bit synchronization references upon receipt of the command acquisition signal. The detector first establishes subcarrier synchronization by comparing the unmodulated subcarrier signal received from the RFS with internally gener- ated phase-shifted estimates of this signal. The estimate whose phase most closely agrees with that of the input signal is selected as the subcarrier demodulation reference. Subsequently, the detector establishes bit synchroni- zation by comparing the receiver output, which is now subcarrier modulated by bit synchronization, with internally generated, phase-shifted estimates of bit synchronization, each of which is half-added to the established subcarrier reference. The estimate whose phase most closely agrees with that of the bit synchronization signal received at the detector input is selected as the bit synchronization demodulation reference.

After having initially established the subcarrier and bit synchronization references, the detector enters the data mode and is ready to detect command information and provide it to the CCS.

The normal modes of CDU operation, observed in the MDS status word via telemetry, are out-of-lock, subcarrier lock, and bit-sync lock. These operat- ing modes are observed (in realtime or are recorded by the VO DSS and trans- mitted later) when an Earth to VO uplink exists and the uplink signal consists

LOCK INDICATION (CCS)

SUBCARRIER STATUS (FDS)

BIT SYNC STATUS (FDS)

REFERENCE
GENERATOR

MODE
SEQUENCE
LOGIC

ACTIVE UNIT INDICATOR (FDS)

SNR CLOCK (FDS)

SNR ALERT (FDS)

OSCILLATOR
&
TIMING

OSCILLATOR MONITOR (FDS)

BIT TIMING (CCS)

SUBCARRIER
& BIT SYNC
TRACKER

COMPOSITE
COMMAND

ANALOG-
TO-DIGITAL
CONVERTER

CORRELATOR

THRESHOLD
DETECTOR

SIGNAL
(RFS)

COMMAND DATA (CCS)

DETECTOR SNR (FDS)

Figure II-7.   Command Detector Unit Functional Block Diagram

of RF carrier only, subcarrier modulated carrier (IDLE 1) and subcarrier modulo-2 bit-sync modulated carrier (IDLE 2) respectively.

The DSN command acquisition sequence prior to commanding consists of IDLE-1 being transmitted for a time interval of at least 65 data bits (16.25s), followed by IDLE-2 for an interval of at least 25 data bits (6.25s).

b.   <u>Telemetry Modulation Unit.</u> The TMUs are cross-strapped to the RFS exciters, with the desired TMU selectable by CCS command. Each TMU generates squarewave subcarriers at 24 and 240 kHz. The 24 kHz subcarrier is bi-phase modulated with low-rate telemetry data supplied from the FDS at 8-1/3 or 33-1/3 bps. The 240 kHz subcarrier is bi-phase modulated with high-rate telemetry data supplied either from the FDS at 2 kbps, the VLC at 1 or 2 kbps, the RTS at 4 kbps or the Data Storage Subsystem (DSS) at 1, 2, 4, 8 or 16 kbps. The VLC signal was present only prior to Lander separation. The RTS signal was present only after Lander separation.

A block diagram of the TMU is shown in Figure II-8. The TMU is a two-channel telemetry system which allows VO low-rate data to be continuously transmitted to Earth, either separately or in a weighted sum with selected high-rate data. The TMU operating modes are determined by the presence and source of coded or uncoded high-rate data. These modes are summarized below.

(1)   Cruise Telemetry: Low-rate telemetry channel only.

(2)   VLC Checkout: dual channel telemetry with uncoded high-rate data supplied by the VLC.

(3)   Relay Telemetry: dual channel telemetry with the uncoded high-rate data supplied by the RTS.

(4)   Playback: dual channel telemetry with the coded high-rate data supplied by the DSS.

(5)   FDS High-rate: dual channel telemetry with the coded high-rate data supplied by the FDS.
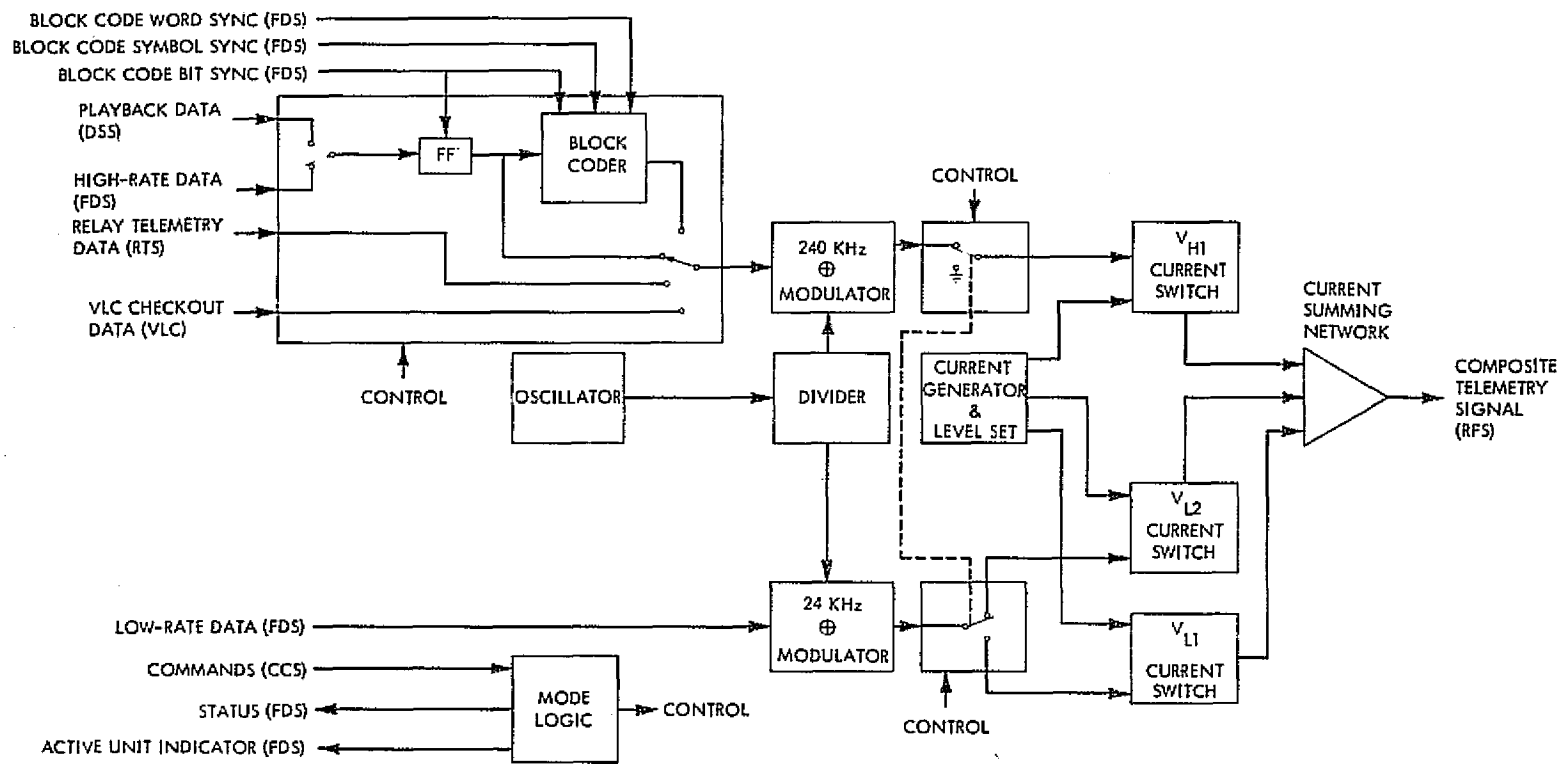
Figure II-8. TMU Functional Block Diagram

(6) Block Coder Bypass: dual channel telemetry with the uncoded high-rate data supplied by the FDS or DSS. Block coder bypass mode could be used in conjunction with Playback and FDS High-Rate modes. It was not used, however, during the primary mission.

The selection of high-rate data is determined by CCS command.

The TMU mode logic assures that the TMU is set to the cruise mode upon application of power.

The coded data is derived from the block coder which encodes six bits of high-rate data supplied from the DDS or FDS into a 32-symbol, bi-orthogonal, comma-free code.

2. Performance

The MDS (CDU and TMU) performance as deduced from the analysis of telemetry data (MDS status word and special in-flight tests) was normal throughout the entire primary mission. The back-up TMU and CDU were never required to be turned on for either VO-1 or VO-2.

The MDS status word was available from both Orbiters at all times during the primary mission. Special tests (CDU SNORE and TMU oscillator frequency) were conducted approximately every two weeks, whenever conditions were favorable during the cruise phase of the primary mission.

a. <u>Command Detector Unit.</u> The CDU performance was assessed by observing the CDU's response as a function of time to the application of command modulation (subcarrier and bit-sync) on Earth to the Orbiter uplink. In addition, CDU SNORE tests were conducted to detect any significant deviations between the predicted and measured uplink signal levels.

The CDU subcarrier and bit-sync lock status are indicated by the MDS status word.

The CDU SNORE test must be done with the VO in two-way. In addition, the CDU must be in bit-sync lock with no command bits being transmitted, i.e., data zero must be continuously transmitted during the SNR measurement process.

The quantity telemetered is the CDU SNR (a 20 binary-bit result of the integration of the command signal over one command-bit period) of which 500 samples are required to calculate a valid CDU input ST/N_o. The measured quantity is then compared with the predicted ST/N_o to determine if a change in performance has occurred. The CDU ST/N_o is computed from the following equation:

$$ST/N_o = 10 \log \left(\frac{\mu^2}{2\sigma^2} \right)$$

where: μ = the average of the CDU signal measurement

σ = the variance of the CDU signal measurements

There were eight usable SNORE tests conducted for VO-1 and ten for VO-2 during the primary mission. Results of these tests are tabulated in Tables II-1 and II-2, respectively. As can be seen from the tabulated ST/N_o residuals, deviations from predicted values were insignificant.

b. Telemetry Modulation Unit. The TMU's performance as observed from the TMU's response to commands and oscillator frequency test results was normal for both VO-1 and VO-2 throughout the primary mission.

The TMU operating mode is determined from the MDS status word. In all cases, the TMU responded to mode change commands as expected.

TMU oscillator frequency measurements were made six times on VO-1 and seven times on VO-2 to determine if the TMU oscillator frequency changed significantly from launch. These results are tabulated in Tables II-3 and II-4 respectively. It can be seen from the tabulated results that the TMU frequency had not changed from its pre-launch value on either VO.

The TMU oscillator frequency is determined by measuring the frequency of either the 24 or 240 kHz telemetry subcarrier at the tracking stations. The measurements were made using the backup Subcarrier Demodulator Assembly (SDA) to avoid disturbing the incoming VO data at the station. Approximately 15 minutes are required for each measurement. The downlink doppler at the time of the measurement was accounted for to correct the apparent subcarrier frequency measured.

Table II-1. VO-1 SNORE Measurement Summary

DATE	NO. OF SAMPLES	SNR (DN)* MEAN (μ)	SNR (DN) STD DEV(σ)	CALC. ST/N_o(dB)	PRED. ST/N_o(dBm)	PRED. P_c (dBm)	Δ (dB)** ST/N_o
2/20/76	509	41.17	1.965	40.6	39.4	−114.9	+1.2
3/3/76	526	42.10	2.075	40.1	39.1	−116.1	+1.0
3/24/76	526	34.71	2.368	38.8	38.7	−117.9	+0.1
4/6/76	505	37.33	2.457	38.5	37.8	−119.9	+0.7
4/22/76	526	36.45	2.547	38.2	37.8	−119.9	+0.4
5/11/76	549	102.4	5.509	29.4	29.3	−129.9	+0.1
8/14/76	518	30.33	3.48	35.3	35.3	−123.6	0.0
8/14/76	956	55.33	7.67	24.6	25.8	−132.6	−1.2

*DN (data number) = the telemetered number (word) between 0 and 127 that is equivalent to SNR value in dB.

**Residual difference between calculated and predicted ST/N_o.

Table II-2. VO-2 SNORE Measurement Summary

DATE	NO. OF SAMPLES	SNR (DN)* MEAN (μ)	SNR (DN) STD DEV(σ)	CALC. ST/N_0(dE)	PRED. ST/N_0(dBm)	PRED. P_c (dBm)	Δ (dB)** ST/N_0
2/16/76	544	19.36	1.813	40.6	41.2	−114.3	−0.6
3/5/76	524	13.43	1.868	40.2	40.3	−116.2	−0.1
3/24/76	557	10.49	2.143	38.9	39.4	−117.9	−0.5
4/6/76	526	13.17	2.266	38.5	38.9	−118.9	−0.4
4/22/76	527	8.49	2.561	37.3	37.4	−120.9	−0.1
5/11/76	509	5.87	2.609	37.2	37.3	−121.0	−0.1
5/25/76	527	4.25	2.520	37.3	36.8	−121.6	0.5
6/1/76	365	71.43	6.11	27.3	27.3	−130.8	0.0
8/2/76	384	49.39	6.75	25.4	25.4	−132.7	0.0
8/2/76	382	48.01	6.57	25.6	25.4	−132.7	+0.2

*DN (data number) = the telemetered number (word) between 0 and 127 that is equivalent to SNR in dB.

**Residual difference between calculated and predicted ST/N_0.

Table II-3.   VO-1 TMU Frequency Measurement Summary

DATE	VCO TEMP (°F)	TMU XTAL FREQ. (Hz)*	△ PARTS PER MILLION (PPM) FROM PRED. PRED = 2,879,976.0 Hz
2/20/76	69.4	2,879,976.0	0.00
3/3/76	69.4	2,879,975.7	+0.10
3/24/76	69.4	2,879,975.4	+0.21
4/6/76	68.4	2,879,977.2	−0.42
4/22/76	68.4	2,879,977.7	−0.59
5/11/76	68.5	2,879,980.4	−1.53

*The crystal frequency was calculated from measurements made on the SDA at the DSS.

Table II-4.   VO-2 TMU Frequency Measurement Summary

DATE	VCO TEMP (°F)	TMU XTAL FREQ. (Hz)*	△ PARTS PER MILLION (PPM) FROM PRED. PRED = 2,879,968.8 Hz
2/16/76	69.7	2,879,967.0	+0.63
3/5/76	70.7	2,879,970.0	−0.42
3/24/76	70.7	2,879,971.3	−0.87
4/6/76	69.7	2,879,974.1	−1.84
4/22/76	69.7	2,879,971.8	−1.04
5/11/76	69.7	2,879,970.24	−0.50
5/25/76	69.7	2,879,967.0	+0.63

*The crystal frequency was calculated from measurements made on the SDA at the DSS.

3.   Anomalies

There were six anomalies (total) for VO-1 and VO-2 observed in the CDU
performance which, after analysis, could not be explained. However, since at
all other times the CDU performance was normal and the consequence of the type
of anomaly observed was trivial, no corrective action was recommended.

Five of the anomalies were unexpected increments (indicating bit-sync
lock) in the CCS counter that keeps track of the CDU bit-sync lock status. The
incidents occurred when command modulation on the uplink went from IDLE 1
to OFF (no modulation). The CDU remained in bit-sync lock less than 5 seconds,
as there was no indication in telemetry of the locked condition in the MDS
status word.

The sixth anomaly was also an unexpected increment in the CCS counter.
However, the incident occurred immediately after an uplink station transfer.
It did not occur in response to any known modulation state change at the
station. Modulation had been turned off six minutes prior to the incident,
according to the DSN station log. It was suspected that the lock change was
caused by a spurious tone on the RF uplink near the command subcarrier
frequency.

D.   RELAY TELEMETRY SUBSYSTEM

1.   Description

The RTS consists of two independent, functionally-identical, bit synchronizers and their associated power supplies. One synchronizer operates at 4 kbps while the other synchronizer operates at 16 kbps. A block diagram of the RTS is shown in Figure II-9.

The functions of the RTS are synchronization, estimation, and decoding of the VL data stream from the RRS. Two synchronizers (for 16 kbps and 4 kbps data) synchronize the noisy, split-phase data stream. Bit values within the stream are estimated and the data is restored to non-return to zero (NRZ) form. The restored data stream and symbol sync, at 16 and 4 kbps, is sent to the DSS for recording. The 4 kbps output is also routed to the MDS for real-time transmission to Earth. In addition, the RTS estimates the SNR and signal component level of the data waveform from the RRS, and provides this informa-tion in the form of telemetry measurements to the FDS.

The RTS is either off or on: no other operating modes exist. Power is provided by the power subsystem under control of the CCS. The RRS and both RTS synchronizers are switched on and off together. The proper synchronizer will automatically acquire synchronization when the signal from the RRS (4 or 16 kbps) is above threshold.

2.   Performance

UHF elements on both the Lander and the Orbiter contributed to the quality of the relay link data recorded on the VO tape recorder during each relay pass. OPAG RRS and RTS Analysts had available three telemetry channels to monitor the quality of the relay data passed to the VO tape recorder, each sampled approximately every 5 seconds at the normal 33-1/3 bps rate. These channels are (1) RRS received signal strength, (2) RTS signal mean, and (3) RTS SNR. The RRS received signal strength measurement was an AGC quantity. The signal mean (either 16 kbps or 4 kbps) was a dc voltage, produced by the RTS signal mean estimator, proportional to the demodulated output from the RRS
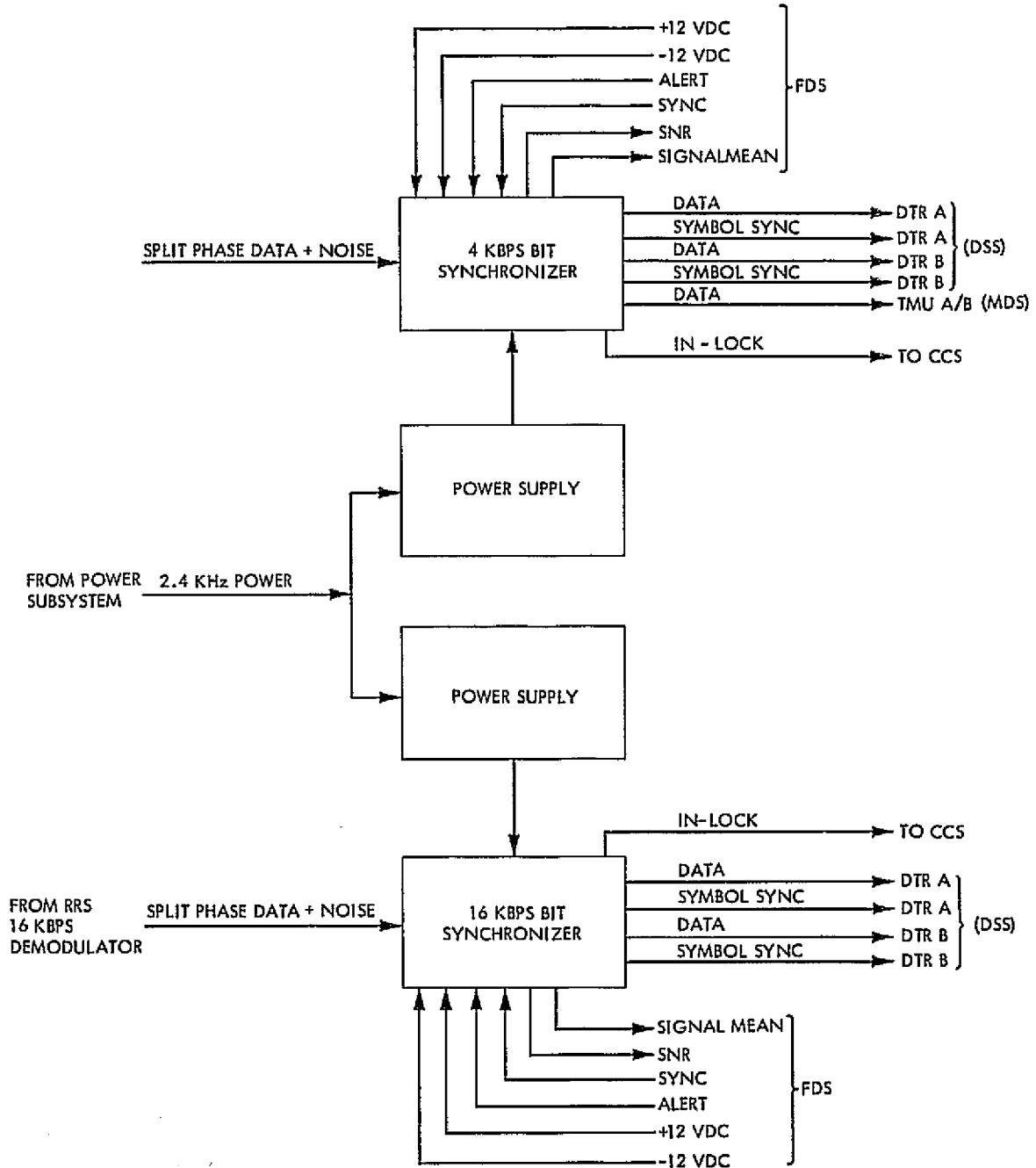
Figure II-9. Relay Telemetry Subsystem Block Diagram

to the RTS and thus at the input to the bit synchronizer. The SNR was a count of the number of symbol errors in 1024 symbol segments of the (16 kbps or 4 kbps) data stream received from the RRS. (This count is possible because each bit consisted of two split phase-L symbols, and disagreements between the two symbols were detected.)

Analysis of the VO Relay subsystems was accomplished by determining the relationship between these three measurement quantities for each relay pass, and comparing this relationship with that existing during pre-launch laboratory tests. In addition the OPAG analysts produced plots of the telemetry quantities versus time for each relay pass as well as a plot of the RTS SNR versus the RTS signal mean. The analysts also determined the times at which the relay link bit-error rate passed predetermined thresholds. All this data was given to the VL Relay analysts. In turn, they compared the RRS signal strength versus time plot with predicted signal levels versus time, as provided by the FPAG. The complete analysis of relay link performance is contained in the Lander Performance Report. The present discussion is confined to the performance of the VO Relay subsystems.

During the descent of each Lander, the relay data received by the VO Relay subsystems was placed directly on the Orbiter's S-band link, in the Relay feed-through mode. Figure II-10 shows the RRS received signal strength plotted from telemetered data during VL-1 descent. Similar data is not available during the second Lander's descent, because of the VO-2 "separation anomaly" discussed elsewhere.

The real-time DTV display provided plots of the three relay quantities for rapid assessment of each relay pass. Figure II-11 shows such a plot for a typical pass, VL-2 to VO-2 SOL 9, which took place on September 13, 1976. The quantities are expressed in data numbers (DN) which then need to be converted to the more familiar dBm (RRS signal strength) or db (RRS SNR). Qualitatively, it can be said that there are negligibly few bit-errors on the relay link when the RTS SNR is near or at zero DN and the RTS signal mean is saturated at 127 DN which is the maximum value.
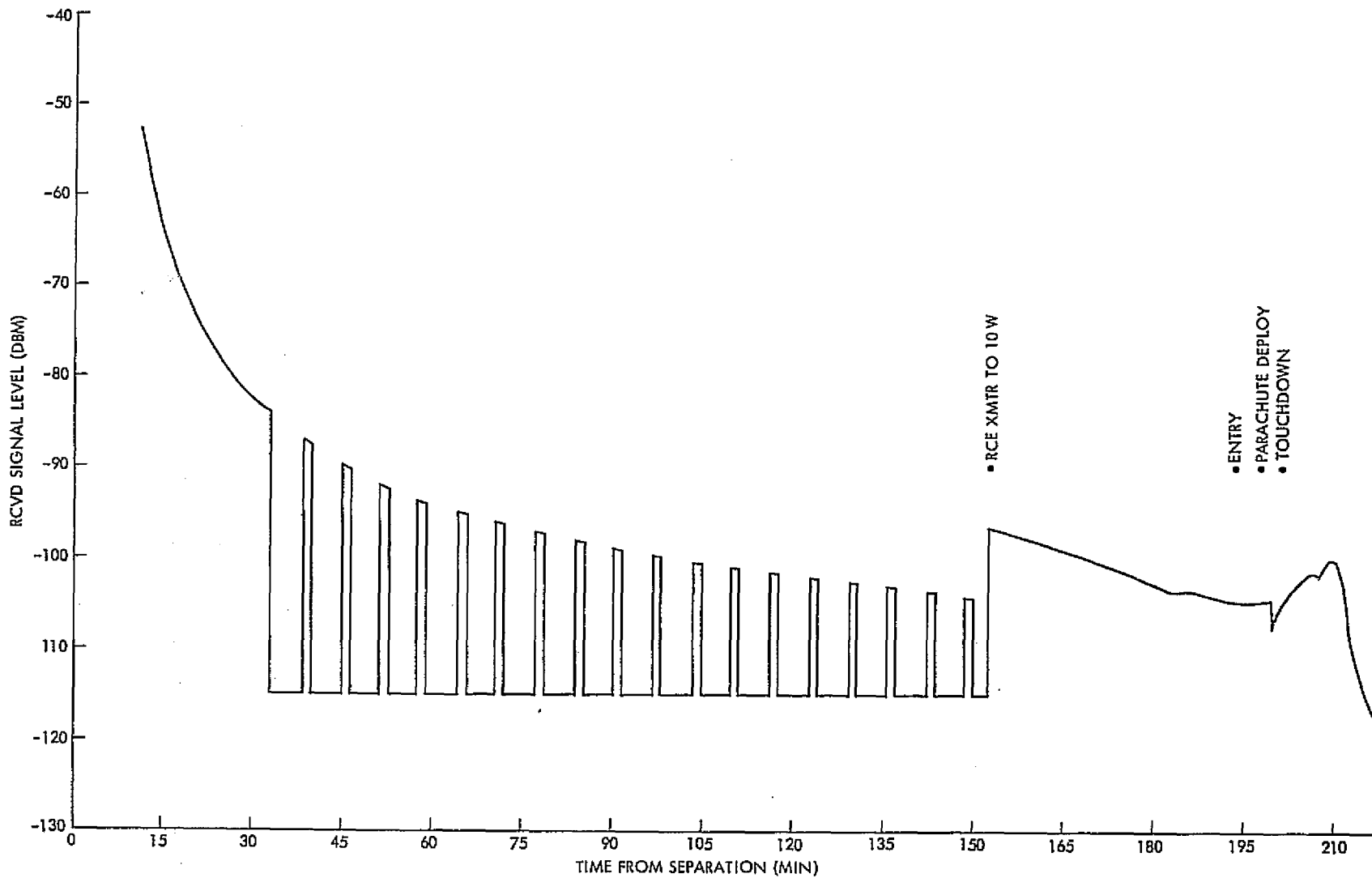
Figure II-10. Telemetered RRS Signal Strength During VL-1 Descent and Touchdown

VO-2

45

TLM CHANNEL
E-626

RRS RECEIVED
SIGNAL STRENGTH

30

15

287/0413

0   20   40   60   80
MINUTES

TLM CHANNEL
E-651

RTS 16 Kbps
SNR

100

50

0

287/0413

0   20   40   60   80
MINUTES

TLM CHANNEL
E-653

RTS 16 Kbps
SIGNAL MEAN

100

50

0

287/0413

0   20   40   60   80
MINUTES
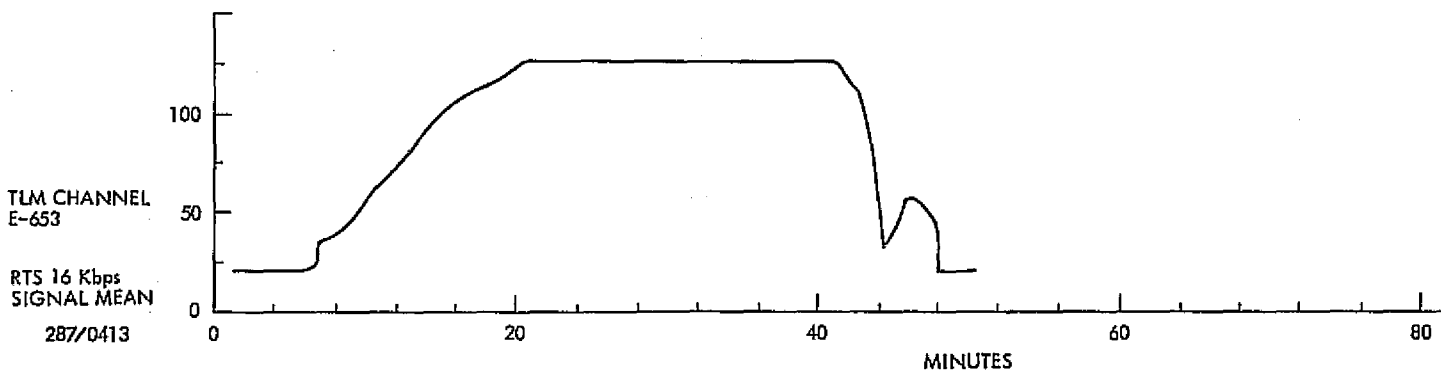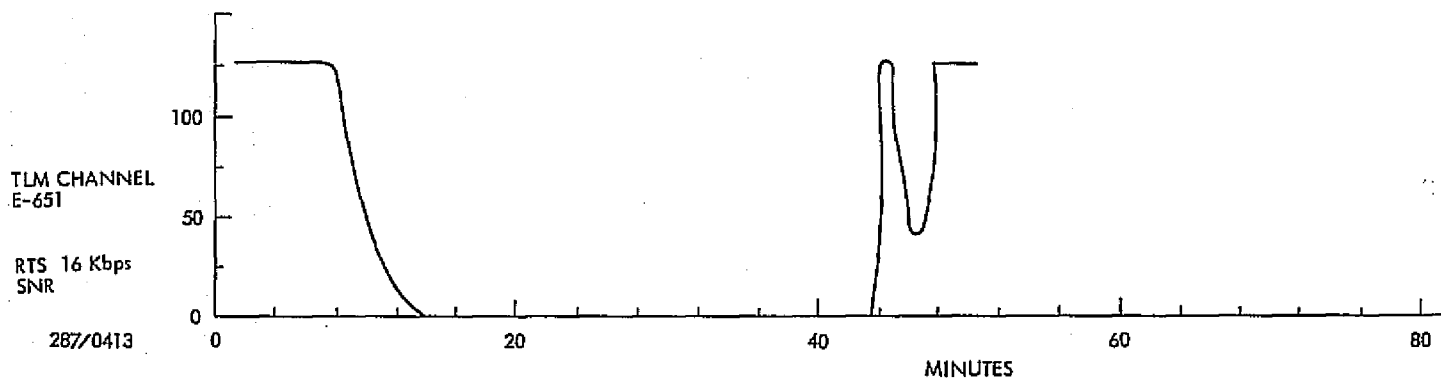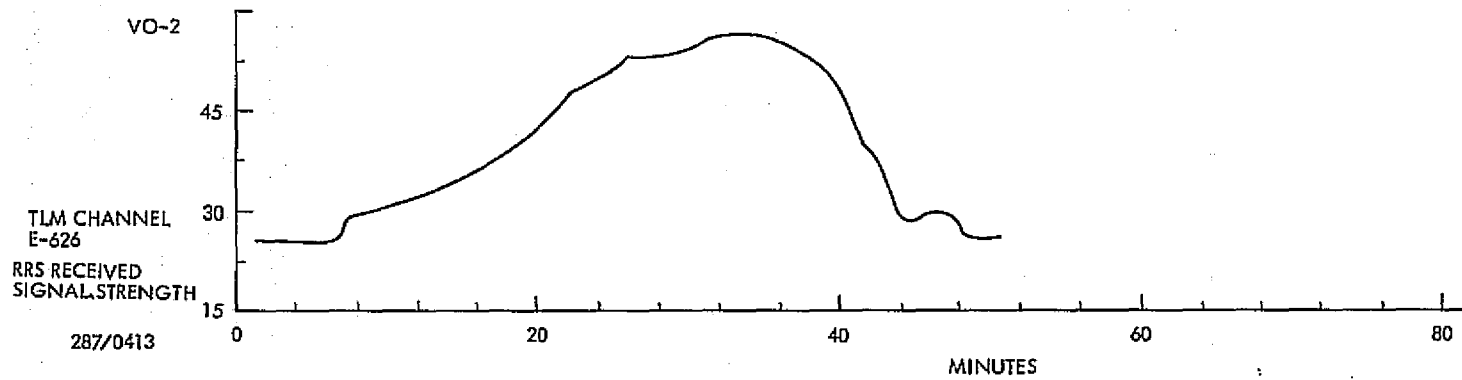
Figure II-11.   Real-Time Digital TV Plot of Relay Telemetry Quantities (Viking 2 SOL 9)

More careful comparison of the RRS AGC with the predicted value is accomplished by use of a plot such as Figure II-12, which is also for Viking 2 SOL 9. The FPAG predicts were available for near real-time comparison with the OPAG actuals. Any deviations could readily be spotted, as well as the effects of such things as the Lander antenna pattern and multipath. It was typical throughout the landed phase that the VO relay subsystems performance fell much closer to the "nominal" predict than to the quasi-sum-of-the-squares (QSS) adverse performance level.

Link bit-error rate as a function of time was computed from plots like II-13, also for Viking 2 SOL 9. The bit-error rate for each VO's RTS at various levels of RTS SNR was predetermined by laboratory measurement before launch. The bit-error rates corresponding to thresholds for each type of relay link data were then drawn on the plot of RTS SNR versus time, giving the times at which the relay link crossed each threshold.

The final comparison of relay subsystem performance versus that predicted was accomplished by a plot similar to Figure II-14 made for each relay pass. The squared dots represent points of SNR vs mean at corresponding times during the pass. The dotted lines indicate the tolerances established and the solid line the expected characteristic, established from laboratory tests. The relay subsystem sensitivity and noise performance was determined for each relay pass from such a comparison. The RRS and RTS performance remained stable and normal from pass to pass, both VO-1 and VO-2.

The relay links were characterized as stable, adequate and, for the most part, predictable. There were three types of relay links: those from VL-1 to VO-1, those from VL-2 to VO-2, and those "crossed relay" links, VL-2 to VO-1. Figure II-15 shows VL-2 SO1 31, in which the data was transmitted to VO-1. Figure II-12 showes the VO-2 data transmitted by VL-2 some 20 days earlier on VL-2 SOL 9. Note the characteristics of the two SOLs are quite different in terms of relay link parameters, but this is attributed nearly entirely to the differing geometry present in the two cases. About the only deviation from prelaunch measurements in the relay subsystem area was that the VO-2 RRS appeared, from data like Figure II-14, to be about 0.5 to 1.0 dB less sensitive than expected. The relay link data base for VO-2 was changed to account for this, and no operational difficulty or data degradation resulted.
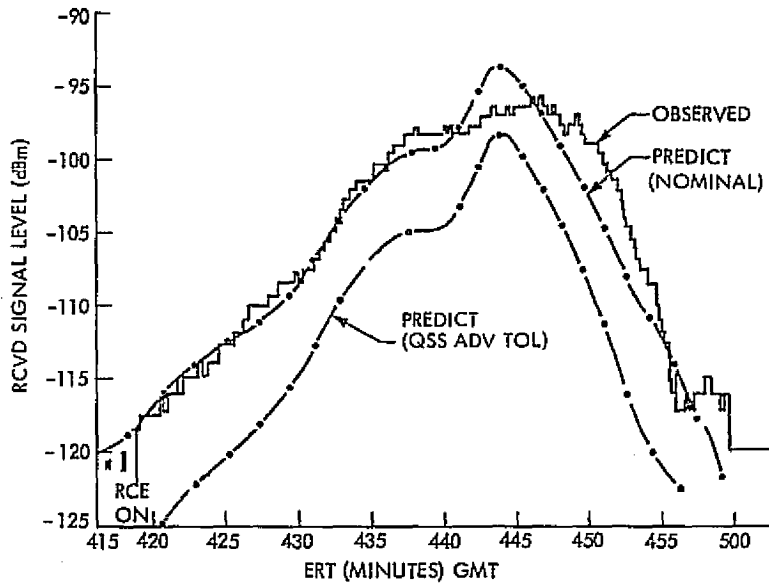
Figure II-12.   Comparison of Predicted and Actual
RSS AGC (Viking 2 SOL 9)
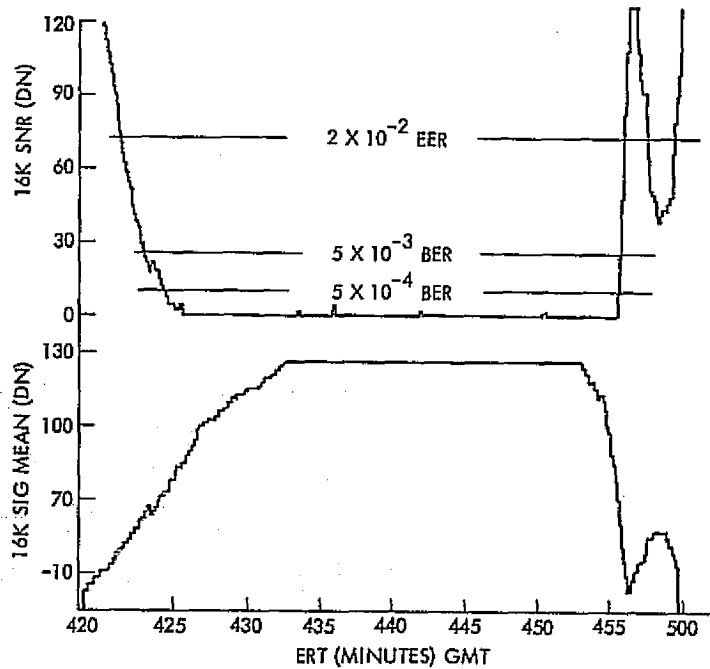
Figure II-13.   Determination of Threshold Bit Error Rate
Times (Viking 2 SOL 9)
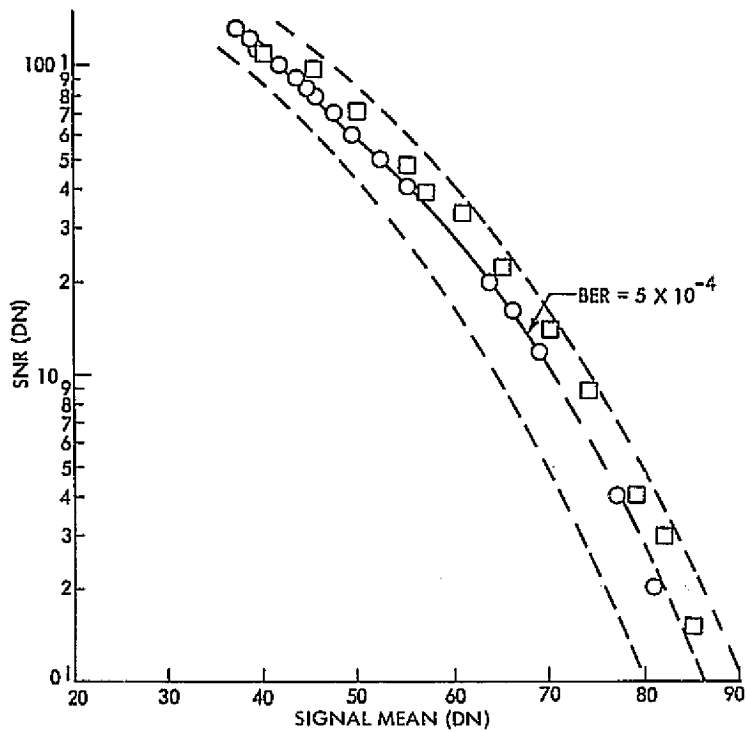
Figure II-14.   Comparison of Predicted and Actual RTS SNR
vs RTS Signal Mean (Viking 2 SOL 9)
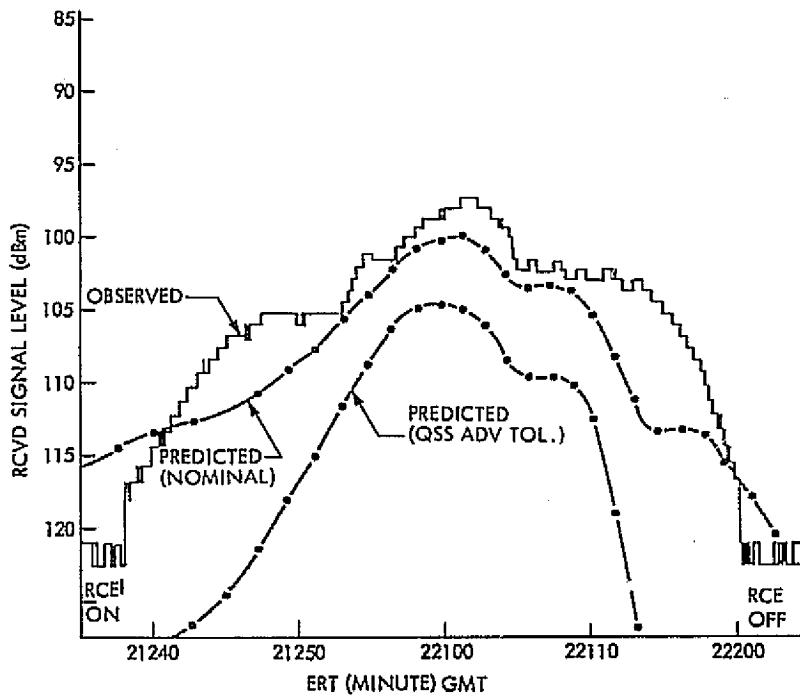
Figure II-15.   Comparison of Predicted and Actual RRS AGC
on Viking Lander 2 to Orbiter 1 SOL 31

Close analysis of the VO relay subsystem telemetry, done in a timely fashion, enabled the vital relay links to be optimized in terms of data quality and data quantity. One example of this occurred about one week after VL-2 touchdown and is displayed in Figure II-12. A three-minute period was observed at the end of the relay link during which the signal level would rise high enough to support the 2×10^{-2} bit-error rate, which was the minimum acceptable for real-time imaging. This signal increase was thought to be the result of a slight gain increase at the edge of the VL antenna pattern. Beginning with SOL 18, this "bonus time" was incorporated into the ongoing Viking 2 sequences.

The "cross relay" links from VL-2 to VO-1 occurred very low on the VL-2 antenna pattern, and there was some concern that the kind and amount of multipath present could not be predicted. Figure II-15 was typical of these passes. Characterization of the multipath was not easy and, indeed, this figure shows a greater deviation between predicted and actual values than other relay passes. "Guaranteeing" link times was made more difficult. The approach taken, which was successful, was to characterize the link residual (from plots like Figure II-15) versus the link elevation angle.

3. Anomalies

There were no significant anomalies in the performance of any of the VO relay subsystems. As previously described in Part I of this report, VO-2 RTS telemetry showed short, abrupt glitches during "link rise" on a few SOLs. These glitches varied up to a maximum of 0.8 dB. They did not cause any degradation in the relay link data, and the source of the variations (even as to whether in the Lander or the Orbiter) could not be determined. No change in link strategy was necessary as a result of these performance variations, best characterized as idiosyncracies.

During several of the early relay passes from VL-2, the Lander transmitter operated at 1-watt rather than the 30-watt level expected. The OPAG Relay Analyst was able to establish quickly, from plots similar to II-12 and II-15, that such was probably the case. Later, upon playback of the relay data

from the VO tape recorder, the Lander telemetered data confirmed this. Relay
link sequences were modified to account for the possible operation at 1-watt,
until corrective action to prevent 1-watt operation could be taken.

E.   RELAY RADIO SUBSYSTEM

1.   Description

The RRS consists of a single UHF receiver, shown in Figure II-2, which is commanded on or off by the CCS. The RRS demodulates the frequency-shift-keyed (FSK) signal, received via the RAS, employing separate demodulators for the 16 kbps and 4 kbps data and routes the signals to the Relay Telemetry Sub-system (RTS). Some of the major receiver parameters are:

(1)   The receiver frequency is held to within ±1 parts in 10^5 of the assigned frequency of 380.963303 MHz.

(2)   The dynamic receiver signal range is approximately 0 dBm to a threshold of -120 dBm (depending on the bit error rate of the overall Orbiter relay communications).

(3)   The receiver noise figure, at the input terminal of the RRS, is maintained below 5.3 dB.

2.   Performance

The performance of the RRS, for both Orbiters during the primary mission, was well within the predicts produced prior to the events of the VO/VL separation/descent and landing. Very little can be written about the RRS by itself since it is only one part in the overall relay communications link, which is discussed in Section I-D. The major task for the OPAG relay analysts was that of providing the predicts of the expected RRS received signal level for the duration of each relay pass, together with the expected RTS outputs of SNR and signal output relative to the predicted RRS signal input. Actual data from each relay pass (one pass per SOL for each Orbiter/Lander) was compared to the predicted data as soon as possible in order that any discrepancies could be ascertained and future mission activities could be planned.

Several in-flight VLC checkout sequences were performed during the cruise period of the mission for Viking 1 and 2. During several of these, VO-1 and VO-2 relay equipment was turned on for assessment of no signal input telemetry conditions and also for ascertaining telemetry data points for operation with

the Lander UHF transmitters in 1 and 10W modes. Due to the VO/VL proximity, the signal level received by the RRS saturated the receiver AGC telemetry channel and only coarse estimates could be made by means of the receiver input current telemetry. Extrapolation of data obtained from the 1 and 10W operation predicted the 30W mode could produce RRS input signals marginally close to the maximum allowable level of +4 dBm. Subsequently, it was decided not to operate either VL in the 30W mode, prior to Mars Landing, in view of the remote possibility of damage to the RRS input circuits.

July 20, 1976 was the historical date of the first Viking Landing. During the preceding VL-1/VO-1 pre-separation checkout the Orbiter relay equipment was turned on and performed as expected. The actual separation-descent-landing phases produced relay link performance data well within that predicted. The second Viking landing took place September 3, 1976, an event marred by an Orbiter anomaly that activated the Loss of Roll Reference routine, occurring directly after the Orbiter/Lander separation. Since this automatic routine switched the S-Band Radio to the LGA, the downlink high-rate data was temporarily lost for the period involving the VL descent/touchdown phase. The RRS signal level, via the Orbiter low-rate telemetry, was the only source of Lander location through touchdown. Once again the Orbiter relay performance was well within the predicted bounds. A more indepth coverage of the Lander/Orbiter relay link performance is to be found in the Viking Lander System Primary Mission Report.

Prior to the landing of VL-1 and VL-2 the Orbiter UHF relay equipment was tested for a total of approximately two hours for VO-1 and VO-2. After VL-1 landing, the Orbiter equipment was turned off and was then turned on for each subsequent relay pass up to July 26, 1976 (SOL 6) for a total of three hours. From this time on the Orbiter relay equipment was left on through Nov 16, 1976. Thus an approximate total operational time of 2,220 hours was accumulated for the VO-1 relay equipment. For VO-2 similar pre-landing test periods totaled approximately 2 hours, then after VL-2 Landing, Sept. 3, 1976, the Orbiter equipment was turned on for each relay pass until Sept. 6, 1976 totaling approximately two hours. After this day the RRS/RTS was permanently on through Nov. 16, 1976 for a grand total of 998 hours.

3.   Anomalies

Only one anomaly relating to Orbiter relay equipment was observed during the primary mission, occurring at the relay link rise of SOL 8, 9 and 10 for VO-2/VL-2. Actual readings of RTS signal and SNR telemetry levels showed a slight perturbation relative to the predicted level. The discrepancy was -0.4 to -0.8 dB for a brief period at the beginning of these passes. The problem appeared to be intermittant, occurring again during VO-2/VL-2 SOLs 13 and 23, with similar effect. No loss of data or deterioration of the relay link performance was caused by this offset. In order to aid in locating the problem source, data was analyzed from (1) VL-1 to VO-1 relay link, which showed no problem, then (2) VL-2 to VO-2 which indicated some samples (as described above), and finally (3) VL-2 to VO-1 having no signs of the anomaly. No data was available from the VL-1 to VO-2 relay link, due to the on-coming superior conjunction and end of the primary mission. However, the situation was constantly monitored in case of subsequent changes, but nothing further was observed by the conclusion of the primary mission. It was, therefore, proposed that this intermittent condition be considered as an Orbiter relay equipment idiosyncracy, until and unless further data became available.

F.   X-BAND TRANSMITTER

1.   Description

The interconnection of the XTX with the other VO telecommunications equip-
ment is shown in Figure II-6. The XTX provides a ranging modulated X-band down-
link signal that is coherent in both carrier phase and ranging modulation phase
to the S-band downlink signal from the RA. The following are some of the major
functional parameters of the XTX:

(1)   The input frequency from the active RA exciter is multiplied by 440
to produce the X-band frequency.

(2)   The detected ranging code input from the RA is modulated by the XTX
onto the X-band carrier signal.

(3)   The XTX output signal is phase modulated and the frequency is coher-
ent with that of the RA oscillator frequency source.

(4)   The RF power output is 200 milliwatts (+23 dBm) into 50Ω.

The VO'75 XTX is a second generation of hardware that was first flown on
the MVM'73 program. Since no redundancy of the hardware was flown, a high
order of reliability and stability was desired in order to carry out the
planned radio science experiments.

2.   Performance

On Nov. 11, 1975 the XTX aboard VO-1 was commanded on for a period of one hour.
All the relevant telemetry data indicated predicted values. With DSS-43
managing to lock on to the X-band downlink with newly installed equipment, just
as a friendly gesture, no signal level could be ascertained since its calibra-
tion had not been done. The VO-1 XTX was turned on permamently as of Nov. 22, 1975,
with all telemetry data repeating the previous turn-on values, although the
XTX temperature stabilized a little higher than had been predicted by the
temperature control analyst. This gave rise to a review of S-band radio
frequency predicts submitted to the DSN. However, there was no need for any
recalibration since the VCO and Auxiliary Oscillator temperature changes were
minimal.

The first in-flight operation of the VO-2 XTX was initialized on Nov. 18, 1975. Again the duration was for one hour, producing the expected values in the XTX telemetry channels. The permanent turn on of this sybsystem was accomplished on Nov. 22, 1975 with a similar 2 to 3°F higher temperature as with VO-1. This was probably due, for both Orbiters, to a lack of previous long term (spacecraft) data in a space environment.

Throughout the mission both VO-1 and VO-2 X-band equipment performed flawlessly. The downlink X-band AGC was used for HGA calibrations, plus providing the basis for a roll reference (star) loss contingency plan. Since the X-band signal is always present at the HGA, the 20 dB loss of S-band transmission due to a switch from HGA to LGA would not make the OPAG completely blind as to Orbiter roll angle. This procedure was particularly prepared for use during MOI; fortunately, it was never required. However, with the VO-2/VL-2 separation, there was a spacecraft anomaly that caused the roll reference loss routine to be initiated. The DSN was requested to carry out the contingency procedure and the X-band AGC data plot provided the pointing angle required for the HGA to be "seen" by the DSN.

On VO-1 the XTX had one brief checkout period of one hour on Nov. 11, 1975 and was permanently turned on from Nov. 22, 1975 through Nov. 16, 1976 for a total of approximately 8,660 hours. Similarly, on VO-2 the XTX was briefly checked out for one hour on Nov. 18, 1975. A few days later it was turned on permanently, from Nov. 22, 1975 through Nov. 16, 1976, for the same total time of 8,660 hours.

3.   Anomalies

There was absolutely no transient or anomalous behavior by the XTX on either Orbiter throughout the primary mission.

G.   S- AND X-BAND ANTENNAS SUBSYSTEM

1.   Description

The S- and X-band antennas provide the means by which the Orbiter radio communications subsystems receive and transmit signals from and to Earth.   The hardware of the SXA includes: the HGA and the LGA plus the required inter- connecting waveguides, cables, and rotary joints.   The interconnection with other telecommunications hardware is shown in Figure II-6.

The HGA is a dual frequency antenna, which transmits at both S- and X-band (simultaneously), but receives only at S-band.   The gain at the S-band transmit frequency (2295 mHz) is approximately 28.5 dB and 27.5 dB at the receive frequency (2115 mHz).   The 3 dB bandwidth is approximately 6 deg. at both receive and transmit frequencies.   The gain at X-band frequency (8415 mHz) is approximately 39.0 dB with a 3 dB bandwidth of 1.6 deg.   The articulated move- ments of the HGA, required for various Orbiter maneuvers, was made possible by use of two dual-frequency rotary waveguide joints.   These joints enabled the azimuth and elevation movements of the antenna by the Orbiter Articulation Control Subsystem (ARTC).

The LGA was used to receive and transmit radio signals by the Orbiter RA during the Near-Earth Phase of the mission and whenever the HGA could not be used, for example, during some orbiter maneuvers.   The LGA gain at the received frequency (2115 mHz) is approximately 7.2 dB with 3 dB beamwidth of 90.0 deg. At the transmit frequency (2295 mHz) the gain is approximately 7.8 dB with a 84.0 deg, 3 dB, beamwidth.

Selection of either of the two antennas is made by means of Earth- originated commands.   The two modes of operation for the SXA are: transmit LGA/ receive LGA and transmit HGA/receive HGA.   The HGA X-band transmission is always available, providing the XTX signal is present, no matter which antenna is selected for S-band transmission.   This latter point was a useful source for a contingency plan derived in case of loss of roll reference during Orbiter maneuvers.   With the HGA in use, the loss of the roll reference star lock will

automatically switch to the LGA via an on-board CCS command sequence. This can (and did) lead to a loss of downlink signal at the tracking station (the sudden loss of 20 dB of signal under some tracking conditions can put the signal below the ground receiver threshold).

2.   Performance

Performance for the SXA subsystem for the duration of the primary mission was completely successful for all up and downlink requirements. During the cruise phase of the mission, the first 90 days were carried out with the use of the LGA. Prior to switching to the HGA for mission use, a special science instrument checkout was performed for VO-1 on Oct. 20, 1975. This entailed switching between HGA and LGA several times within a ten minute period. An interesting plot was produced by the MTC of the playback data of this checkout. The plot consisted of the telemetry outputs of the HGA drive, LGA Drive, and the uplink receiver AGC coarse. Radio analysts were able to verify the 20 dB difference in antenna gains prior to the required switch to the HGA on Nov. 11, 1975 for VO-1. A similar science instrument checkout sequence was carried out on Oct. 16, 1975 for VO- 2, and again on MTC plot was requested of the Orbiter playback data. However, in this case the spacecraft orientation did not make it po-sible to obtain the correct gain difference between HGA and LGA, but at least switching was verified. When the required switch to HGA occurred for VO-2 on Nov. 18, 1975 the uplink receiver AGC-Coarse indicated the expected 19.5 dB increase due to the HGA.

3.   Anomalies

There were no problems or anomalies attributable to any of the SXA equipment on either Orbiter.

H. RELAY ANTENNA SUBSYSTEM

1. Description

The RAS consists of a single feed, symmetrical, low-gain pattern UHF antenna and associated cabling and connectors. The RAS enables the Orbiter to receive Lander UHF signals and feed them to the RAS. The RAS is positioned on one of the Orbiter solar panels such as to provide the required relay link. Both the RAS and RRS were completely new design concepts for the Viking Program, and were necessarily developed to a high degree of reliability by reason of their lack of redundancy. One of the major antenna parameters is: the RAS was designed to receive right-hand circularly polorized waves in a 2 MHz band with the center frequently of 380.963 MHz.

2. Performance

The RAS performance was substantially one part of the VO/VL relay link overall performance, which can be found in the Viking Lander System Primary Mission Report. In view of the data produced via this communications link for the various combinations of Orbiter and Lander, it is safe to consider the RAS to have made the required contribution to the success of the primary mission.

3. Anomalies

Only one anomaly was observed that could have involved the RAS: the VO-2 intermittant perturbation that was discussed in paragraph D.3. Since no conclusive evidence could be recorded as to the actual cause of the signal level shift, and since the RAS is a component of the Orbiter relay equipment, it would therefore become a candidate by association.

SECTION II

GUIDANCE, CONTROL AND POWER

A.   INTRODUCTION

This portion of the report details the operational performance of three subsystems:

(1)   The Attitude Control Subsystem (ACS) provided attitude orientation and control for the Orbiter in the following distinct, but related, modes: cruise, all-axis inertial, inertial roll, maneuver, and thrust-vector control.   The ACS consists of two block-redundant inertial reference units, a Canopus tracker, sun sensors, two block-redundant attitude control electronics assemblies, a dual-reaction control gas system, and rocket engine gimbal actuators.

(2)   The Articulation Control Subsystem (ARTC) provides positioning of the articulated elements of the Orbiter: two axes for the scan platform and HGA and single axis for the SECs.   It is a multiplexed control system consisting of an electronic unit, two scan platform actuators, two HGA actuators, and four SEC actuators.   The ARTC is a dual channel closed loop system using digital control signals, stepper motors, and feedback potentiometers.

(3)   The Power Subsystem (PWR) had two primary functions: to provide a central supply of power for operating electrical equipment on-board the VO, and to provide the required switching and control functions for effective power management and distribution.   Power derived from four photovoltaic solar panels and two rechargeable Ni-Cad batteries was converted and distributed as 2.4kHz single phase, 400 Hz quasi 3-phase, regulated dc (30 and 56V), or unregu-lated dc (25 to 50V).

B. ATTITUDE CONTROL SUBSYSTEM

1. Description

The ACS provided S/C stabilization and orientation throughout the primary mission after S/C separation from the Titan-Centaur launch vehicle. A simplified block diagram of the ACS is shown in Figure II-16. The ACS is shown within the dashed line. Intrasubsystem and intersubsystem interfaces related to the functioning of the ACS are also shown.

a. Functions. The ACS provided the following functions:

(1) Reduced the initial rates after S/C separation and acquired the celestial references (sun and Canopus).

(2) Automatically (in conjunction with the CCS) reacquired celestial references in the event that they were lost.

(3) Maintained the correct S/C attitude during all mission phases following initial acquisition of celestial references.

(4) Performed commanded turns of the S/C to any desired orientation relative to the celestial references.

(5) Controlled S/C attitude and thrust vector orientation during propulsive maneuvers.

(6) Provided control with respect to celestial references for VLC initialization and inertial control during VL separation.

b. Equipment. The ACS consists of the following assemblies: acquisition sun sensors (ACQ S/S), cruise sun sensors (CR S/S), sun gate (SG), Canopus tracker (CT), inertial reference units (IRUs), attitude control electronics (ACEs), reaction control assemblies (RCAs) and gimbal actuators (GAs). These are described briefly in the following paragraphs.

1) Acquisition Sun Sensors. The ACQ S/S assembly consists of four non-redundant identical subassemblies. One subassembly is mounted on each of the four solar panel tips. The ACQ S/S provide pitch and yaw control signals. They have a combined unobstructed 4π steradian field-of-view (FOV).
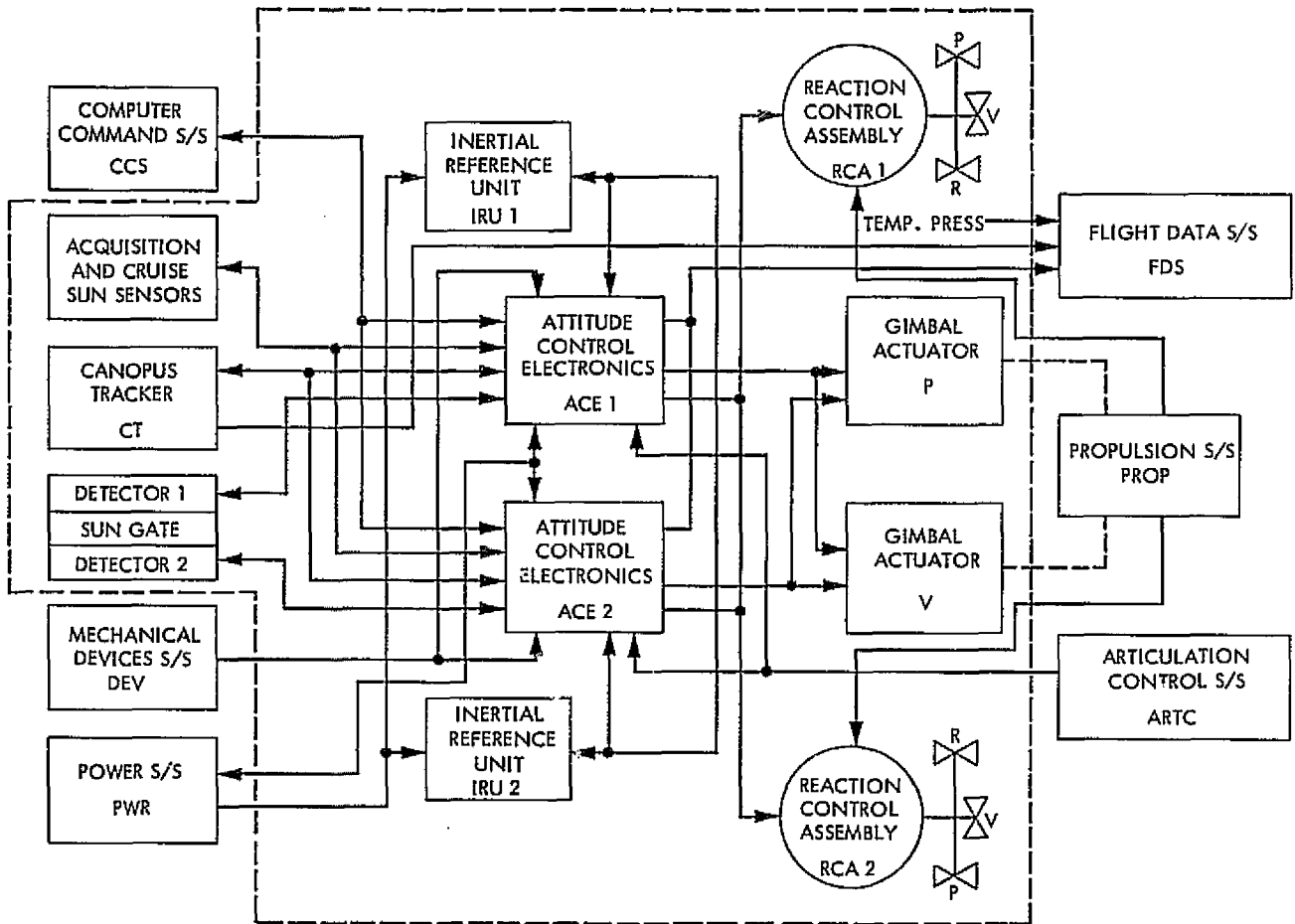
Figure II-16. Simplified ACS Block Diagram

2)   Cruise Sun Sensors. The CR S/S are mounted in a single non-redundant assembly mounted on the solar panel outrigger and provide pitch and yaw control signals. The CR S/S have a FOV which exceeds that of the SG.

3)   Sun Gate. The SG is a single assembly with redundant detectors mounted on the solar panel outrigger. One detector is associated with each ACE. The signal generated by the SG is used to identify a sun acquired logic state.

4)   Canopus Tracker. The CT consists of a single non-redundant assembly mounted on the VO bus. The CT provides a roll axis control signal and a star intensity signal used for star identification.

5)   Inertial Reference Unit. The ACS has two identical IRUs. Only one IRU is required at any given time for control, the other providing standby redundancy. The IRU provides rate and position signals in pitch, yaw and roll, and an acceleration signal in roll.

6)   Attitude Control Electronics. The ACS has two identical ACEs. Only one ACE is used at any given time for control, the other providing standby redundancy. The ACE contains the following:

a)   RCA Electronics. The RCA electronics control the operation of the jet valves and consist of a celestial sensor buffer amplifier, switching amplifier with deadband and minimum on-time, rate estimator, derived rate, position and rate select circuits, and jet valve drivers for each axis.

b)   TVC Electronics. The thrust vector control (TVC) electronics control the operation of the GAs and consist of a pre-aim circuit, gimbal servo electronics, compensator, gain selection, and enable controls for the pitch and yaw axes.

c)   Control Logic. The ACE receives a 14-bit command word input from from the CCS. The ACE logic, in conjunction with these commands, internally generated logic functions, and the ACS Enable and Scan Blow signals, provides direct control over all ACS operating modes.

7)   Reaction Control Assembly. The ACS has two identical RCAs. In normal operation, the RCAs provide torque couples about each axis. In cases of a failure of either assembly, the other assembly provides single jet, bi-directional torque capability about each axis.

8)   Gimbal Actuator Assembly. The ACS has two identical non-redundant GAs used to rotate the PROP rocket engine about the pitch and yaw axes. Each GA contains a dc motor, ball screw driven shaft, and a shaft position transducer.

2.   Performance

a.   Canopus Tracker. The CT is an electro-optical device, illustrated in Figure II-17, that is designed primarily to provide a single-axis error signal that is proportional to the subtended angle between the line-of-sight to a star and a reference axis in the mounting plane of the tracker. The images of any objects within the FOV limits are formed by the objective lens on the image dissector tube photo-cathode.

The cone angle deflection plates in the image dissector tube are utilized to provide five selectable cone angle offsets within the total FOV to allow for seasonal variation in cone angle of Canopus. Three coincident level commands, sent by the ACE, select the position of the cone angle.
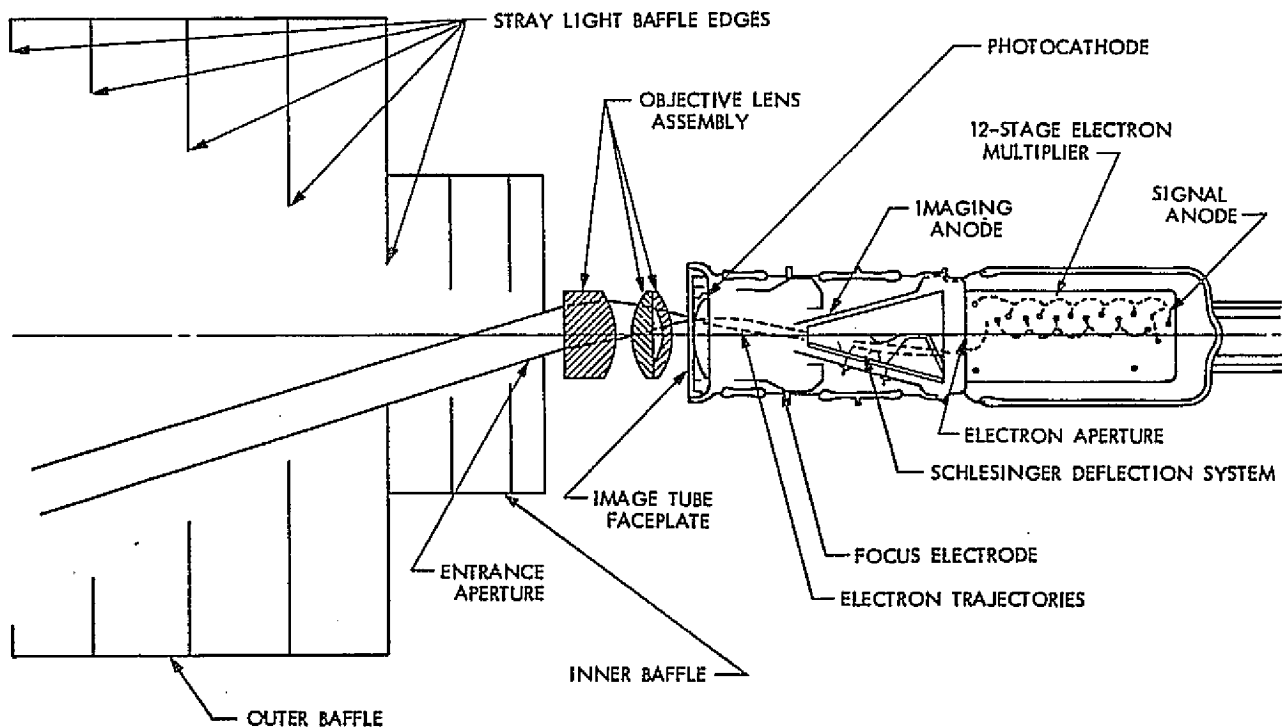
Figure II-17. Canopus Tracker Optical Layout

The FOV is described below, with the aid of Figure II-18.

(1) Total FOV. The CT has an overall unvignetted FOV of ±18.0 degrees minimum in cone and ±5.0 degrees minimum in clock (roll).

(2) Instantaneous FOV. The instantaneous FOV is defined by an aperture within the image dissector tube that has an effective FOV of approximately 1.0 degree (clock by 11.8 degrees (cone).

(3) Scanned FOV. The instantaneous FOV is scanned over a range of ±1.0 degree in clock by means of a sawtoothed waveform. This extends the effective FOV to ±1.5 degree (in clock).

(4) Tracking FOV. The scanned FOV is controlled in clock through a closed internal loop so that it will track a star over the total FOV in clock.

(5) Straylight FOV. Two straylight FOVs are defined, one for planetary interference and the other for Mars satellite interference. The planetary straylight FOV is ±15 degrees in clock by ±33 degrees in cone. The Mars satellite straylight FOV is ±6.5 degrees in clock by ±9 degrees in cone centered about the applicable cone position.

1) Flight Performance. The CT was turned on shortly after launch and the initial canopus acquisition reference verified that the tracker's intensity response, intensity gate, threshold, and tracker scale factor were as predicted.

On Day 260 (17 September 1975), eight days following the launch of VO-2, the Propulsion Subsystem (PROP) was pressured in preparation for the midcourse maneuver. At the end of the sequence, a particle or series of particles caused the CT to lose Canopus and to fail to reacquire it during the subsequent flyback and sweep (FB/S).

The ACS switched to the roll inertial mode and the CCS entered the RRL routine and began issuing FB/S commands on ten minute centers, as expected, for loss of Canopus. FB/S was executed 22 times without successful reacquisition. Since the CT cone angle was due to be stepped from C4 (cone angle 4) to C3 in two days, it was updated to increase sensitivity slightly. Canopus was successfully reacquired on the next FB/S and ACS returned to the celestial cruise mode.
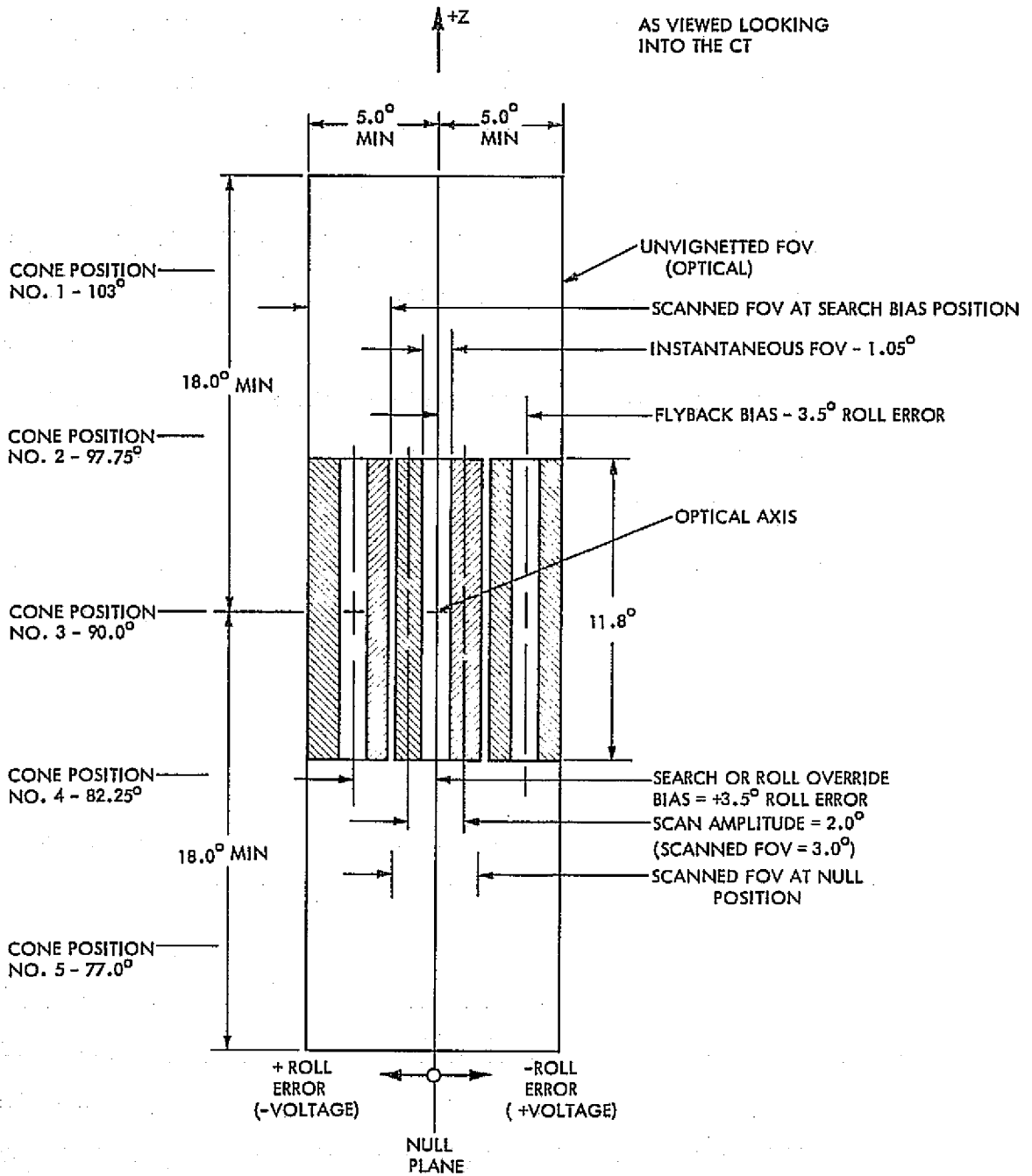
Figure II-18.   Canopus Tracker Controlled Field-of-View Positions

The principal reason the 22 commanded FB/S were unsuccessful is that the CT becomes slightly less sensitive within minutes of looking at dark space. This was estimated to be a 12 mV or 7 percent loss of sensitivity within the first ten minutes (23 mV = 14% = 1 DN of intensity). Thus, by the time the first FB/S was commanded by the RRL at 22:56:35, Canopus was no longer acquirable in Gate (G) G1. This is corroborated by the fact that Canopus intensity was initially 87 DN upon reacquisition but this soon settled down to 86 DN, the expected intensity.

The CT brightness gates are the means by which the CT discriminates on the basis of star intensity. The intent is to reject from acquisition all stars except those within a narrow range of intensity. A given gate is satisfied (allowing acquisition) if the voltage into the gate exceeds a set level. This voltage is proportional to the brightness due to stars or particles within the CT FOV. It is in discussing these gates in terms of Canopus ratio instead of voltage that some confusion arises. This is because the voltage response to a given star is a function of its position in cone and clock, CT aging, and temperature. In establishing the gate settings, the intent was to set G1, for instance, such that a star of 0.70 x Canopus could trigger the gate based on the response in the center of C3 at room temperature at the time the gate was set, about one year prior to launch. It was understood (and part of system design) that it may be necessary to select lower gates during the mission as CT response changes as a function of age.

The primary mission experience greatly enlarged the body of knowledge relative to CT performance in particle and straylight environments. This experience also attested to the wisdom of the design change reducing the tracker internal tracking rate which greatly reduced the number of particle induced star losses. The ACS tracker control logic was a truly outstanding feat of design in anticipation of an almost infinite set of disturbance conditions.

2) <u>Analysis Software</u>. Four Univac 1108 software programs comprising the Celestial Reference Set (CRS) were used to provide apriori knowledge of the tracker environment and the CT responses to the environment during all phases of the primary mission. This knowledge was used to determine the tracker state, i.e., lock star selection, cone angle setting, intensity gate setting as well as to determine whether the S/C was to be in celestial lock or roll inertial during

periods of tracker interferences from Mars' straylight or from the Moons of Mars, Phobos and Deimos. The four software programs were:

(1)   Celestial Reference Program (CELREF) provides predicts of tracker output during spacecraft turns.

(2)   Star Tracker Evaluation Program (STEP) evaluates potential lock stars and the tracker cone angle settings needed for these lock stars.

(3)   Tracker Interference Program (TIP) provides predicts of tracker interferences from Mars straylight and Phobos and Deimos as well as predicts of tracker output as a result of these interferences.

(4)   Limb Interference Program (LIP) provides graphical presentation of events as indicated by the TIP program.

3)   <u>Tracker Straylight Performance.</u>   Both spacecraft were placed in roll inertial numerous times in order to safeguard spacecraft attitude during the primary mission. The majority of these maneuvers due to interference from Mars straylight VO-2 went roll inertial a number of times due to Phobos interferences.

a)   <u>Straylight Relative to VO-1.</u> While the maximum straylight intensity seen by VO-1 was during science and propulsive maneuvers, most occurrences were recorded while on roll inertial (CAMARS). Fifty-one occurrences of straylight while in roll inertial was seen through Nov. 6, 1976. The average maximum footcandle intensity was 0.54×10^{-6} footcandles (~63.2 DN). The corresponding average straylight duration was 15 minutes.

The CT on VO-1 experienced its maximum energy load on June 21, 1976 (MOI), maximum intensity being 0.444×10^{-3} footcandles and the straylight duration being 14.5 minutes.

The total energy seen by VO-1 as a result of straylight was small, being less than 5×10^{-4} footcandle-hours.

b)   <u>Straylight Relative to VO-2.</u> Primary straylight activity was during science and propulsive maneuvers with 19 occurrences recorded through November 5, 1976. The average maximum intensity was 0.91×10^{-4} footcandles (~+40 DN). The average straylight duration during maneuvers was 13.3 minutes. The single

largest straylight occurrence during maneuvers was on August 7, 1976 (MOI), with maximum intensity being 0.444×10^{-3} footcandles (33 DN) and the straylight duration 41 minutes.

Seventeen straylight occurrences were recorded while on roll-inertial (CAMARS). The average maximum intensity was 0.99×10^{-5} footcandles (~57.2 DN) and the average straylight duration was 26.1 minutes.

The total energy seen by VO-2 as a result of straylight was less than 3×10^{-5} footcandle-hours.

c)   <u>Tracker Electronics Performance</u>. During the periods of straylight a phenomenon associated with the tracker electronics surfaced. This phenomenon, termed the darker than dark effect, occurred only during periods of straylight and manifested itself by having telemetry intensity readings which were darker than the tracker output voltage cutoff. This phenomenon was recognized for the first time during the Viking mission. No identifiable occurrence had appeared in previous missions.

d)   <u>Tracker Health.</u> In previous missions major deterioration in the CT was observed, especially where large amounts of straylight were seen by the tracker. The VO trackers have experienced at least as much, if not considerably more, straylight than any previous mission. Daily monitoring of telemetered CT intensity for both VOs as compared to predicted values provided a gauge on the tracker health during the primary mission.

No identifiable decrease in CT performance was seen in the VO-1 CT as a result of either aging or straylight activity.

An apparent 16 percent desensitization of the CT on VO-2 occurred between February 11 and May 7, 1976. Since this time period was prior to orbital straylight, and since the relative shift in the tracker response curve seemed constant through the remainder of the primary mission, the desensitization was attributed to CT tube or electronics aging.

It should be noted that although no apparent permanent desensitization of either tracker was seen due to straylight, it is highly likely that long term effects due to straylight will be seen in the Viking extended mission.

b.   Sun Sensors. There are four sun sensing subassemblies in the VO-75 ACS:

(1)   Cruise Sun Sensor

(2)   Acquisition Sun Sensors

(3)   Sun Gate

(4)   Sun Shutter in the Canopus Tracker

The first three devices will be briefly described and their predicted performance will be compared to observed flight performance. The CT Sun Shutter is used to protect the CT from looking into the sun, but this condition was avoided by operational limitations so that no Sun Shutter flight performance data was observed.

1)   Cruise Sun Sensors. The CR S/S consists of four cadmium sulfide photodetectors installed in a single assembly and mounted on the +y solar panel outrigger, as illustrated in Figure II-19. Each axes sun sensor set consists of two photoresistors mounted beneath a shadow bar and electrically connected in a
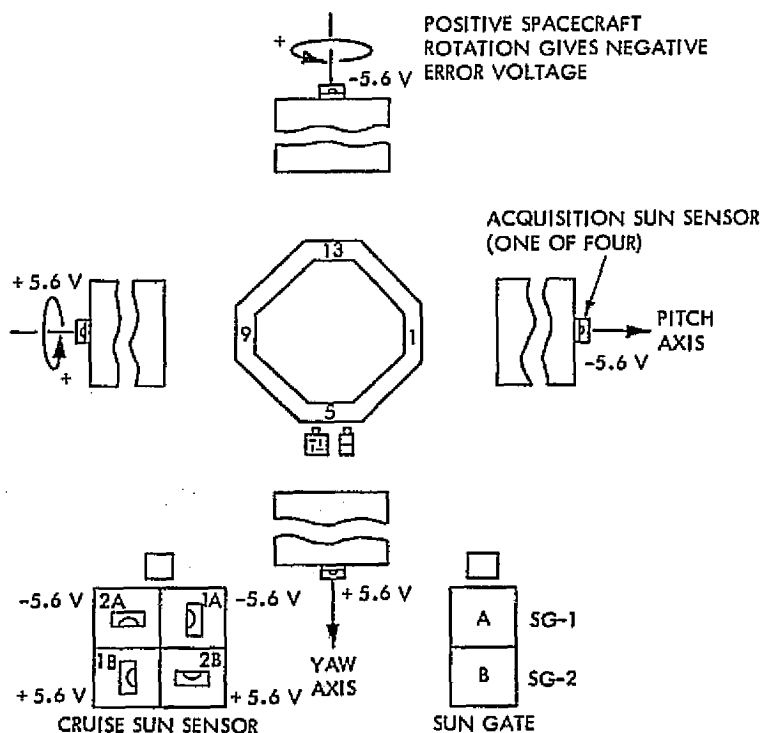
Figure II-19.   Sun Sensor Orientations and Sign Conventions

bridge, as illustrated in Figure II-20. As the Sun moves off the null axis, differential illumination of the detectors produces the electrical error voltage, as illustrated in Figure II-21.

Evaluation of CR S/S flight performance is accomplished by comparing its performance relative to a fixed quantity observable in limit cycle data.

The CR S/S scale factor may be compared to the IRU inertial position scale factor. Table II-5 lists the VO-1 and VO-2 IRU-CR S/S scale factor comparisons that were made.

It therefore must be concluded that the increased rate increments observed in the pitch and yaw axes are the result of an increased cruise sensor scale factor.

2) Acquisition Sun Sensors. The ACQ S/S are a set of four identical three photoresistor detector assemblies mounted on the ends of the solar panels, as illustrated in Figure II-19. The detectors are connected in a bridge arrangement, and their FOVs are such that each axes (six-detector set) has a 4π steradian

$$V_E = \frac{(R_1 - R_2)}{R_1 + R_2}$$
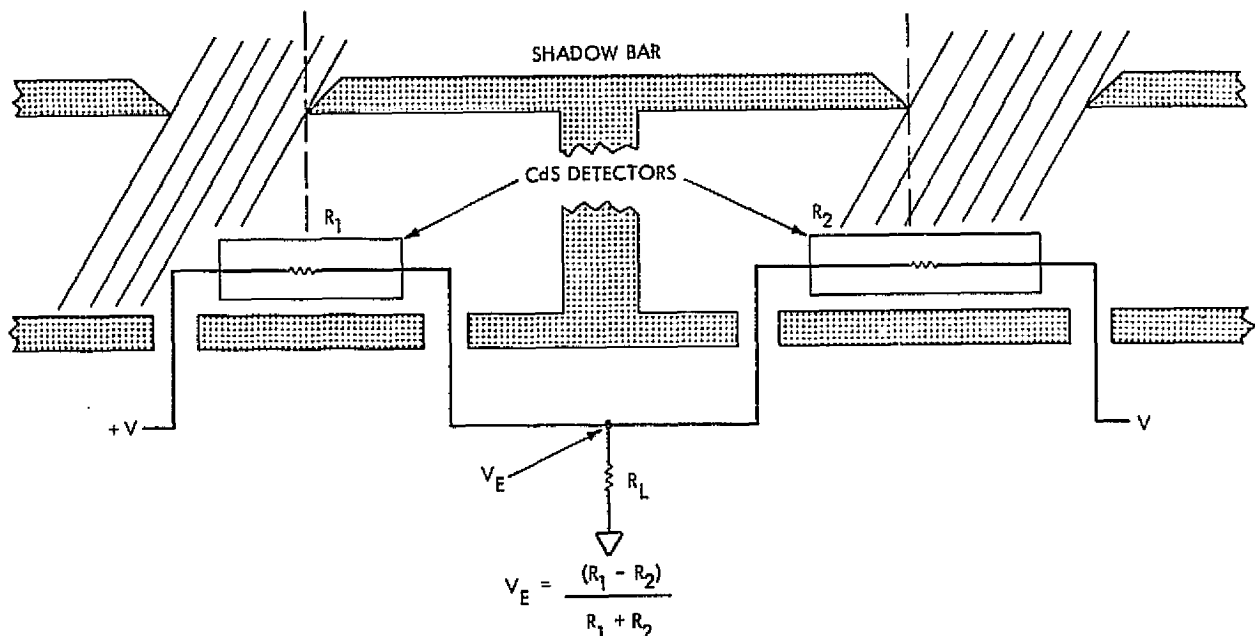
Figure II-20. Cruise Sun Sensor

ACQUISITION SUN SENSOR
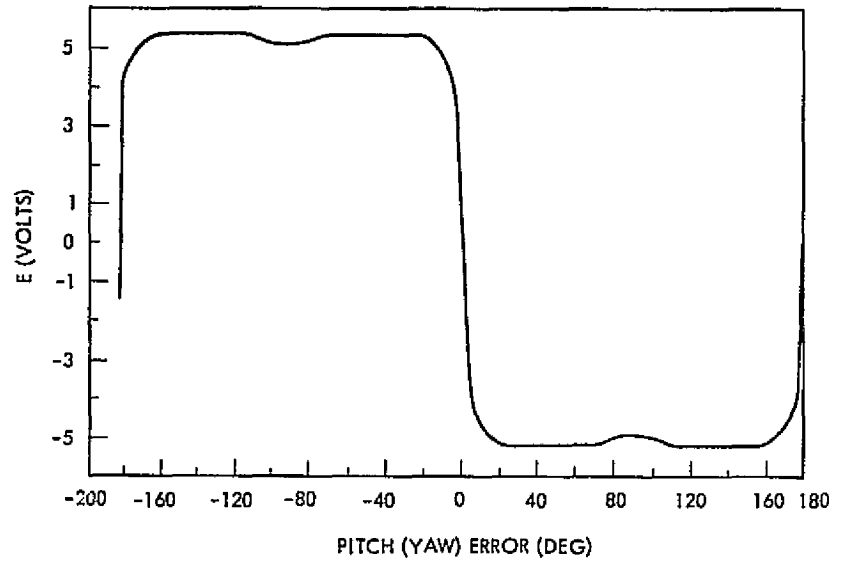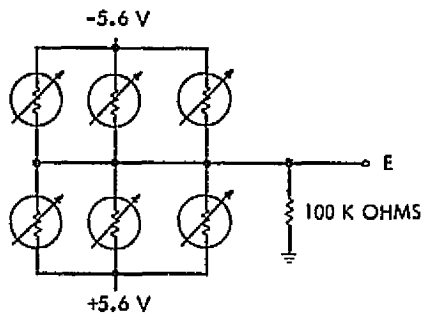
CRUISE SUN SENSOR
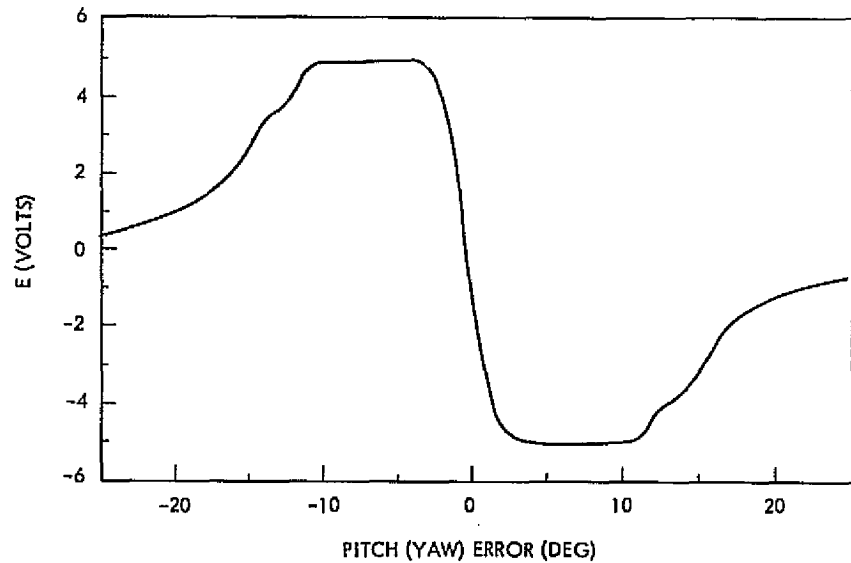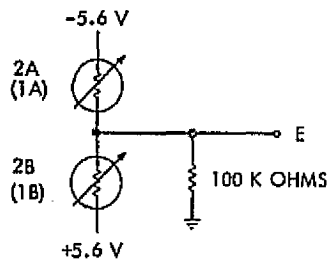
Figure II-21. Sun Sensor Transfer Functions

Table II-5. Ratio of Cruise Sun Sensor to IRU Position Scale Factors

S/C	Date	Axis		Event
		Pitch	Yaw	
VO-2	October 23, 1975	1.94	1.86	IRU 1 CAL
	November 20, 1975	1.91	1.94	ACCEL. CAL
	March 15, 1975	1.99	1.94	IRU 1 CAL
	March 26, 1975	2.0ℓ	2.04	IRU 2 CAL
	May 12, 1976	2.04	2.01	IRU 2 CAL
	July 15, 1976	2.05	2.06	TVC CO.
VO-1	October 30, 1975	2.14	2.21	IRU 1 CAL

FOV. The rear-looking detectors FOV overlap slightly so that an electrical null exists. Any S/C motion will eventually cause the gas jets to be fired and drive the S/C away from this null point toward a stable null point at about zero deg cone. The bridge arrangement and transfer function for a single axis is shown in Figure II-21.

The availability of ACQ S/S flight data was very limited for most of the primary mission.

Launch performance and the conjunction period data demonstrated that the ACQ S/S is a very linear device with a null axis very near the cruise sun sensor null axis. However, it is unreliable during periods when large bright objects are observable by the S/C.

3) Sun Gate. The SG is a single assembly with redundant detectors mounted to the +Y solar panel outrigger. One detector is associated with each of the two ACE units. The SG is positioned so that its optical axis is parallel to and along the -Z axis of the S/C. Each detector consists of a photoresistor masked so that it is sensitive to S/C cone angle but insensitive to clock angle.

The ACQ S/S position is determined for both pitch and yaw at the time sun gate is issued, and the RSS position is the angular offset at the instant of sun gate. These results indicate that sun gate occurred at a cone angle between 4 and 5 degrees at Earth which was the design goal.

Sun Gate angular performance during the solar occultations at Mars could not be evaluated because in the all-axes inertial mode no SG performance data exists.

c.   Inertial Reference Unit. The IRU is comprised of two subassemblies: an inertial sensors subassembly and an inertial electronics subassembly. The sensors in the IRU consist of three, miniature, single-degree-of-freedom, floated, rate-integrating gyroscopes and one miniature, pulse-captured, linear, single-axis pendulous accelerometer. Position information is generated by integrating the rate signals. Precision biases of either polarity can be introduced into the roll and yaw integrator inputs in response to bi-level signals from the ACE, based upon CCS commands into the ACE, to perform commanded turns.

The IRU provides three-axis rate signals for damping and a three-axis inertial reference during those times when the S/C is not locked onto its celestial references. It also provides a signal from which the linear change in velocity of the S/C is derived during PROP engine burns.

Two identical IRUs are provided. Only one IRU is used at any given time, the other providing standby redundancy. Both IRUs were powered during launch and pyrotechnic events to protect the sensors; otherwise, only one IRU was powered. Neither IRU is normally on during cruise. The orientation of the sensing elements is shown on Figure II-22.

The IRU has five operating modes as follows:

(1)   Rate Mode   The IRU provides three-axis rate signals and accelerometer pulses.

(2)   All Axes Inertial Mode   The IRU provides three-axis rate signals, three-axis position signals and accelerometer pulses.
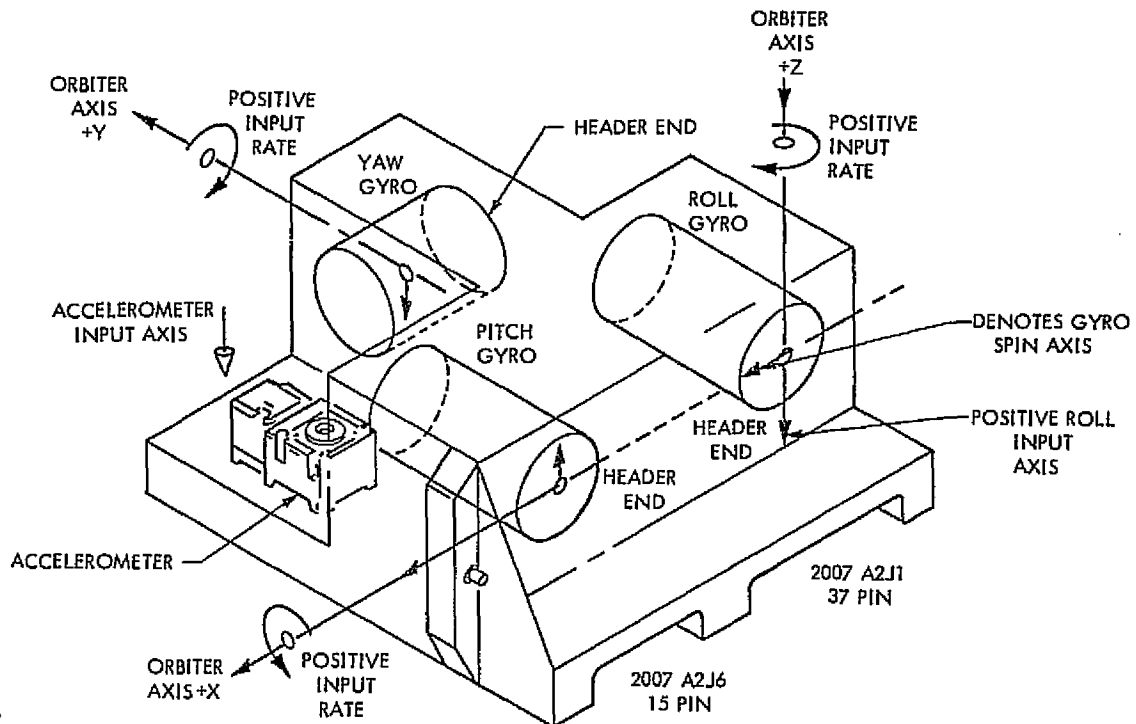
Figure II-22. Inertial Sensor Orientation

(3) Roll Inertial Mode — The IRU provides three-axis rate signals, roll position signal and accelerometer pulses.

(4) Commanded Turn Mode — A turn bias is input to the rate integrator while in an inertial mode. Yaw turns are performed in the all axes inertial mode. Roll turns are performed in the roll inertial or all exes inertial mode.

(5) Inhibit Mode — The IRU is powered, but its rate and position signals and its accelerometer output are inhibited (zero).

The signals derived by the IRU are:

(1)	Rate Signals for RCA Control	The pitch, yaw and roll rate signals are analog voltages proportional to the rates about the respective axes. The scale factor is -28.15 Vdc/deg/sec over the linear range of ±0.5 deg/sec from zero rate input.
(2)	Rate Signals for TVC Control	The pitch and yaw rate signals (roll is also provided for telemetry) are analog voltages proportional to the rates about the respective axes. The scale factor is -7.2 Vdc/deg/sec over the linear range of ±2.0 deg/sec from zero rate input.
(3)	Position Signals	The pitch, yaw and roll signals are analog voltages that are the intergral of the respective rate signal voltages from the time the inertial mode signal is received by the IRU. The scale factor is -2.975 Vdc/deg over the linear range of ±4.5 deg from zero position output.

1)   _Flight Performance._   Each gyro in the IRU package has a set of expected performance parameters established by design and ground testing. Flight verification of these parameters can only be accurately accomplished in a secondary fashion.

One evaluation technique is to compare computer simulations of gyro rate and position signatures during commanded turns to actual performance. A close examination of VO-1 midcourse 1 verifies that the signatures are almost identical, and post-burn analysis indicates turn accuracy was within acceptable tolerances. It was concluded that IRU-1 gyros scale-factors flight performance was well within the design specifications.

IRU drift is evaluated by comparing the S/C celestial position drift while in the inertial mode. The drift calibrations verified that all gyro drift and drift stabilities were within design specifications.

During separation of VL-2, what initially appeared to be a gyro failure resulted in a severe dynamic transient and use of the contingency routine in both the ACS and the CCS. This anomaly will be discussed in detail in another part of this report, but the post anomaly analysis concluded that the probable failure was in the 400 Hz power supply and not within the IRU package.

It is concluded that the VO IRUs performed flawlessly during the primary mission. The true test of these devices will occur during the extended mission when their design life may well be exceeded.

A summary of all the ACS subassembly primary mission operating time is given in Table II-6.

2) <u>Gyro Drift Rate Calibration</u>. Viking Orbiter attitude under gyro control exhibits drift as a function of time. The drift rate of VO gyros is required to not exceed a total variability of 0.54 deg/hr 3 σ and to autocorrelate within 0.15 deg/hr 3 σ over a 10-day period from turn-on to turn-on. Predictability of gyro drift rate is an important factor in maneuver turn design, so several in-flight calibrations were performed to measure this parameter. The

Table II-6. ACS Operating Time

Component	VO-1 (hours)			VO-2 (hours)		
	Through 9/30/76	This Report Period	Total	Through 9/30/76	This Report Period	Total
ACE-1	9666	1006	10672	9123	1081	10204
ACE-2	0	75	75	165	0	165
IRU-1	291	165	456	152	0	152
IRU-2	20	0	20	487	1081	1768
CST	9659	1081	10740	9281	1081	10362
ARTC-E-1	7789	862	8651	7614	892	8506
ARTC-E-2	2927	862	3789	1761	892	2653

method of calibration is to engage gyro control of attitude for an otherwise undisturbed period of 6 to 8 hours, record the apparent positions in VO coordinates of the Sun and the roll reference star as a function of time, and process this data through the MAPS program TRNANG in its gyro drift analysis mode. The accuracy of this process is required to be 0.065 deg/hr in pitch and yaw, and 0.04 deg/hr in roll. Apparent Sun motion and cross coupling of pitch and yaw into roll are taken into account.

Figure II-23 shows the results of the analyses for IRU-1 on VO-1 as a function of time during each of the calibrations. The variability of drift rate is sometimes exhibited over operating time (see pitch calibration No. 3) but mostly from turn-on to turn-on. There appears to be no repeatable correlation with gyro warmups (the test period starts 5 minutes after IRU turn-on, and the operating temperature increases $35^{\circ}F$ in the next 2 to 3 hours). The best predictor of drift rate appears to be the mean value over the entire calibration period and overall calibrations.

Table II-7 summarizes the results of all gyro drift rate calibrations performed during the primary mission. There has been very good agreement (within 0.07 deg/hr) among all measurements of any given gyro, including comparison of in-flight with ground calibrations. The 10-day autocorrelation requirement actually met with good margin over periods of months. The overall variability requirement was also met with good margin (highest measured rate was $1.1\,\sigma$ of this requirement). The accuracy of the calibration process has been within 0.02 deg/hr $3\,\sigma_1$ a factor of 2 or 3 times better than required. The right-hand column of Table II-7 lists the values of gyro drift used for maneuver design.

3) Accelerometer Bias Calibration. The VO-75 accelerometer was set up on the ground to have a positive (therefore measurable) bias in flight, with an overall variability requirement of 300 μg $(3\,\sigma)$. In-flight calibration consisted of turning on the accelerometer in zero-g, recording total number of output pulses as a function of time for 2-1/2 hours, and then processing this record through the MAPS program ACCAL in its accelerometer bias analysis mode. The output is bias as a function of temperature, since the data is taken during the warmup period plus an hour at steady-state temperature. Analysis shows that the bias versus temperature function is quite well represented (within a few μg's) by a best-fit straight line.
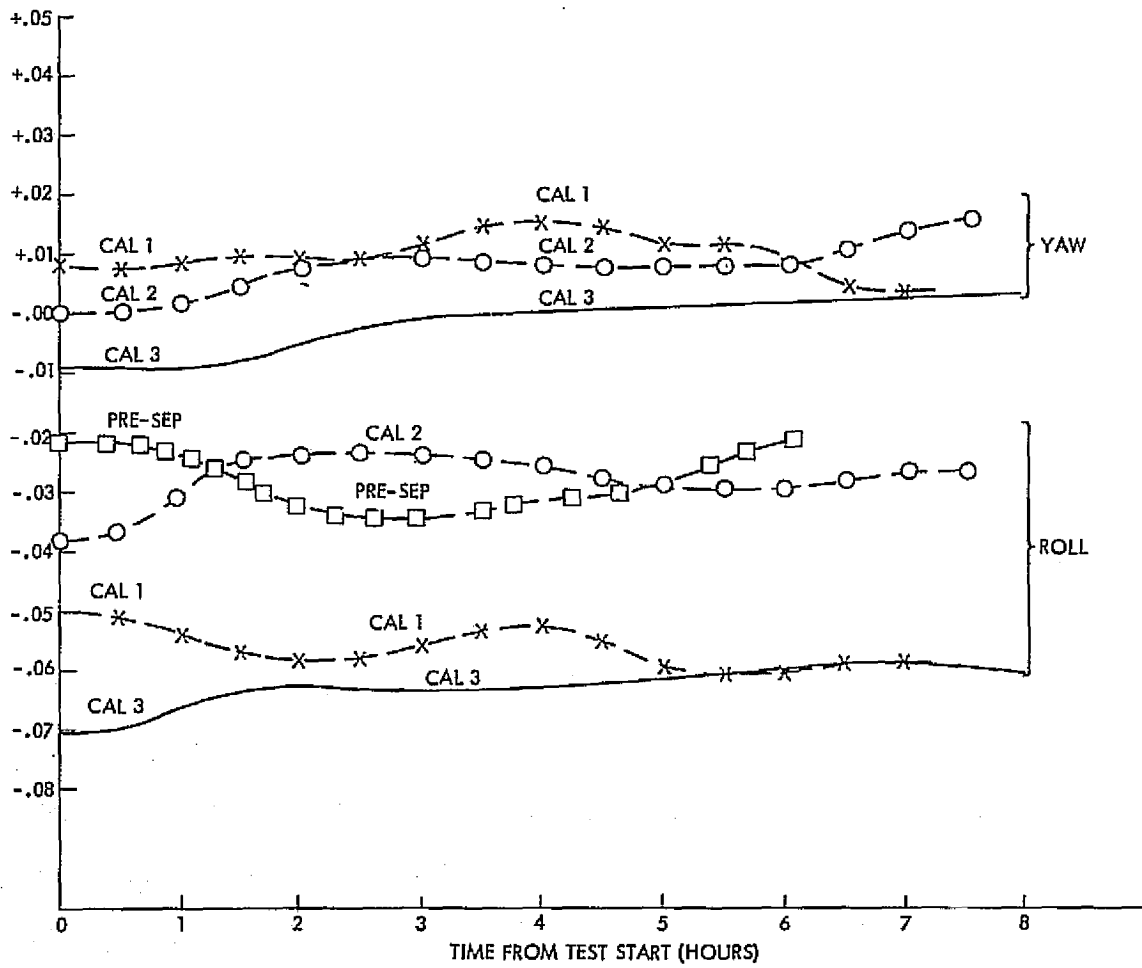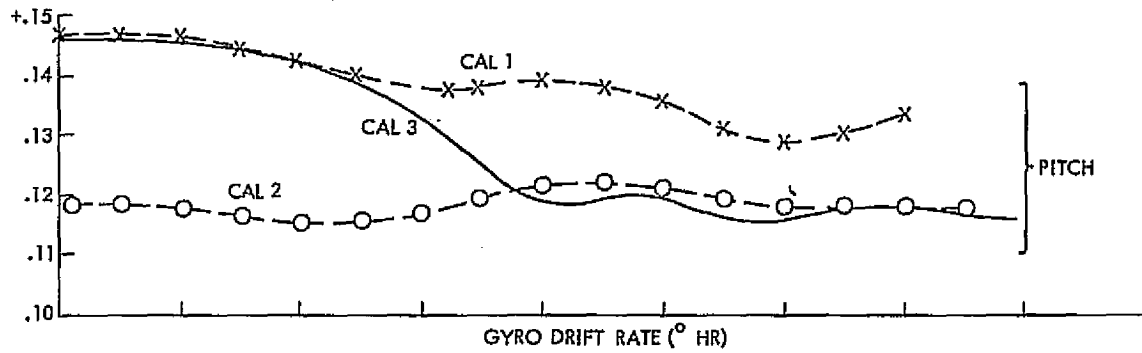
Figure II-23. VO-1 IRU-1 In-Flight Gyro Drift Rate Calibrations

Table II-7. Gyro Drift Rate Calibrations

	Ground Calibration	In-Flight Calibrations				Estimate From All In-Flight Calibrations
		No. 1	No. 2	No. 3	Pre-Sep. Roll Check	
VO-1, IRU-1						
Date		10/30/75	3/18/76	5/25/76	7/1/76	
Pitch Drift Rate (deg/hr)	+0.118	+0.1398	+0.1209	+0.1270	N/A	+0.1292
Yaw Drift Rate (deg/hr)	+0.001	+0.0123	+0.0085	-0.0013	N/A	+0.0065
Roll Drift Rate (deg/hr)	-0.051	-0.0548	-0.0275	-0.0621	-0.0294	-0.0434
VO-1, IRU-2						
Date		82(1976)	N/A	N/A	N/A	
Pitch Drift Rate (deg/hr)		-0.198				-0.198
Yaw Drift Rate (deg/hr)		+0.010				+0.010
Roll Drift Rate (deg/hr)		+0.022				+0.022

	Ground Calibration	In-Flight Calibrations				Estimate From All In-Flight Calibrations
		No. 1	No. 2	No. 3	No. 4	
VO-2, IRU-1						
Date	.	10/23/75	3/15/76	5/12/76	8/26/76	
Pitch Drift Rate (deg/hr)	+0.056	+0.0809	-0.0148	+0.0796	+0.0779	+0.0559
Yaw Drift Rate (deg/hr)	-0.083	-0.0341	-0.0725	-0.0355	-0.0392	-0.0453
Roll Drift Rate (deg/hr)	-0.162	-0.1926	-0.1838	-0.1778	-0.1756	-0.1824
VO-2, IRU-2						
Date		3/26/76	9/3/76	N/A	N/A	
Pitch Drift Rate (deg/hr)		-0.003	N/A			-0.003
Yaw Drift Rate (deg/hr)		+0.1405	N/A			+0.1405
Roll Drift Rate (deg/hr)		+0.0243	-0.033			-0.015

Table II-8 summarizes the results of all accelerometer bias calibrations performed during the primary mission. The change induced by launch is apparent in a comparison of ground-measured bias values with those of the first in-flight calibrations. The most unfavorable comparison is only 0.7 σ of the requirement. Temperature sensitivity showed surprising shifts, but it remained relatively stable in flight. The change of bias with time was in the direction predicted by the manufacturer but at about three times the expected rate. This caused no problem since in-flight measurements are made with frequency sufficient to maintain required knowledge accuracy (150 μg 3 σ, of which 120 μg is for stability).

Table II-8. Accelerometer Bias Calibrations

	Ground Calibration	In-Flight Calibrations			Estimate at EOM
		No. 1	No. 2	No. 3	
VO-1, IRU-1					
Date		11/21/75	3/18/76	5/25/76	
Bias at 75°F (μg)	516.0	454.2	474.0	481.2	481.2
Temp. Sens. (μg/°F)	−1.582	+1.168	+1.444	+1.625	+1.625
VO-1, IRU-2					
Date		3/11/76			
Bias at 75°F (μg)	371.1	400.1			400.1
Temp. Sens. (μg/°F)	−5.354	−2.208			−2.208
VO-2, IRU-1					
Date		11/20/75	3/15/76	5/12/76	
Bias at 75°F (μg)	316.6	387.7	412.0	417.3	417.3
Temp. Sens. (μg/°F)	−0.636	+0.942	+1.220	+1.281	+1.281
VO-2, IRU-2					
Date		3/26/76			
Bias at 75°F (μg)	415.6	461.8			461.8
Temp. Sens. (μg/°F)	−1.804	+1.254			+1.254

d.   Reaction Control Assembly.

1)   Description.   The RCA normally provides the S/C with pure torque couples about the control axes for the purpose of controlling S/C attitude. There are two mutually interchangeable assemblies, as shown in Figure II-24, each of which provides one-half of the torque couple.

The RCA uses compressed nitrogen gas as the propellant.   Each of the gas storage vessels holds 16.0 lb of gas when fully loaded at 4432 psig and 90°F. The specific impulse is 68 sec at 68°F and the jet thrust is 30 mlb.   The effective impulse expended for a 24 msec electrical pulse into a pair of jet valves (minimum impulse bit) is 0.00144 lb-sec.   The distance from the roll axis to the jet valves located on the ends of the solar panels is 16.4 ft.   The pitch jet valves are located at the outer edges of the +Y, -Y solar panels and are oriented so as to nominally produce torque in a plane 0 deg 41 min ccw from the YZ plane, perpendicular to the Z axis.   The yaw jet valves are located at the outer edges of the +X, -X solar panels and are oriented so as to nominally produce torque in a plane 0 deg 41 min ccw from the XZ plane, perpendicular to the Z axis.   The roll jet valves are located at the outer edges of the +X, -X solar panels and

HPM   -   HIGH-PRESSURE MODULE
PSPV -   PROPELLANT STORAGE PRESSURE VESSEL
TT   -   TEMPERATURE TRANSDUCER
TRT$_1$ -   TRANSITION TUBE
PVI$_1$ -   PRESSURE VESSEL ISOLATION VALVE

FV   -   FILL VALVE
FM   -   FILL MANIFOLD
FT   -   PRESSURE REGULATOR
RV   -   RELIEF VALVE
FJ   -   FIELD JOINT
CTH   -   CONVOLUTED TUBE HINGE
CTF   -   CONVOLUTED TUBE FOLD
TRT$_2$ -   TRANSITION TUBE
TM   -   THRUSTER MANIFOLD

JV   -   JET VALVE
N   -   NOZZLE
LPM   -   LOW-PRESSURE MODULE
PYV   -   PYRO VALVE
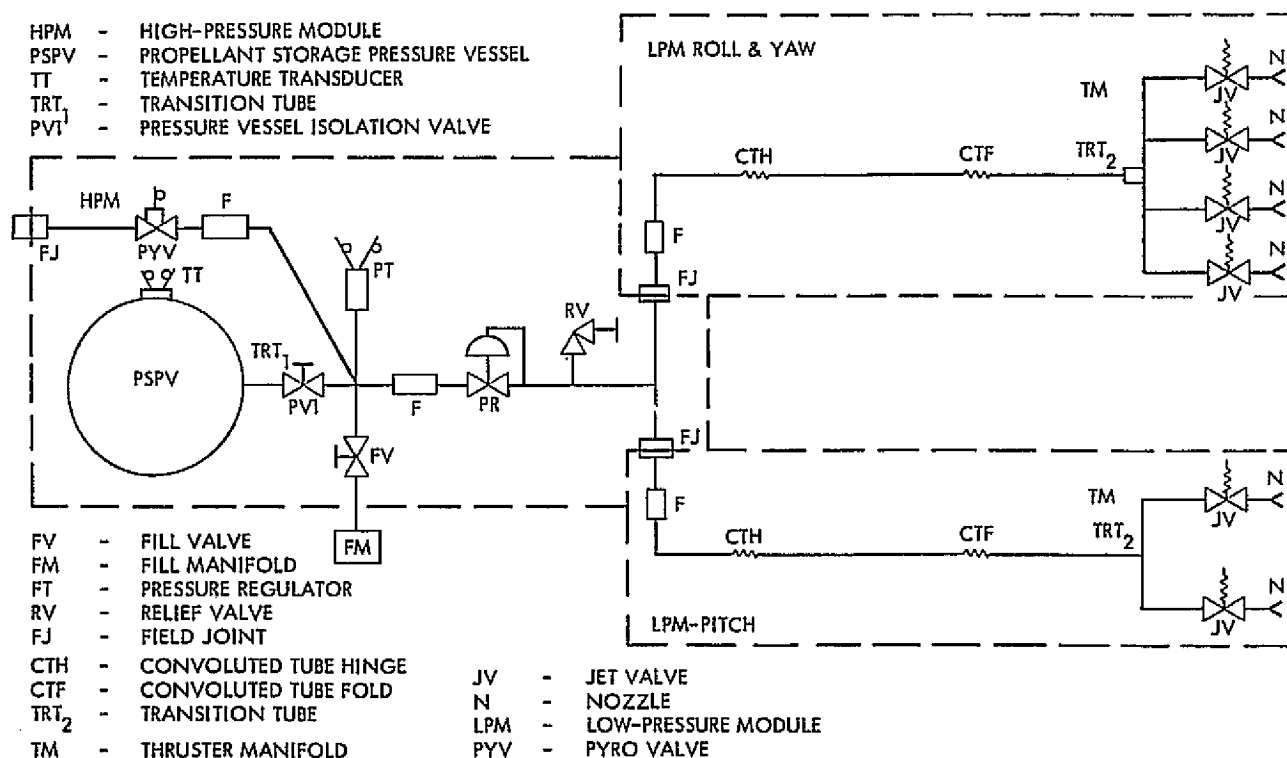
Figure II-24.   Reaction Control Assembly Schematic

are oriented so as to produce torque in the XY plane at an angle of 25 deg from being perpendicular to the X axis. The 25 deg angle provides for reduced gas impingement on the solar panels. The relief valve exhaust plume is directed so as to produce essentially zero net torque.

Each RCA consists of one High-Pressure Module (HPM) and two Low-Pressure Modules (LPMs). The two LPMs are the pitch control module (PCM) and the roll/yaw control module (RYCM). The three modules are interconnected through field joints located in the immediate vicinity of the HPM.

To provide for extended mission life with regard to expendables, the PROP helium gas can be supplied to the RCA. When using helium gas, the jet thrust will be 27.8 mlb.

a)   High-Pressure Module. The primary functions of the HPM are to provide propellant high pressure storage and to provide the propellant at regulated pressure to the RCA low pressure distribution lines. An ancillary function of the HPM is to provide the FDS with signals proportional to the propellant pressure and temperature. The HPM is a self-contained, all welded subassembly.

b)   Low Pressure Module. The LPMs have the function of providing torques about the VO control axes. Each module is a self-contained subassembly.

LPM tubing is routed along the edges of the VO bus to the solar panel outriggers, along the outriggers to the inner solar panel hinge joints at the side opposite the solar panel deployment mechanisms, along the inner solar panel support structure to the outer solar panel hinge joints, and along the outer solar panel support structure to the panel outer edges. The tubing is provided with flexible (convolute) sections in corresponding to the inner and outer solar panel hinge joints to allow for panel folding in the launch configuration and for panel deployment after interplanetary orbit injection.

2)   Flight Performance. Flight performance of the RCA is evaluated based on a set of assumptions. For example, the rate increment in each axis is evaluated as follows:

$$\Delta w = \frac{2.F\ell}{I} \Delta t$$

F is the force produced by expanding nitrogen gas through the gas jet nozzle into a vacuum. The gas jet thrust profile is not constant over the valve poppet opening and closing periods, but for a fixed command open period (Δt) the product $F\Delta t$ is assumed constant. Since the lever arm, ℓ, the inertial I of the S/C axis, and Δw (assuming a known celestial sensor scale-factor) are assumed known and constant, the product $F\Delta t$ can be evaluated. The thrust F is assumed constant at the HPM pressure regulating pressure of 25 psia, and all uncertainties are lumped in Δt. During the first 30 days of flight of both S/C, Δt was calculated to best fit the observed rate increment data, assuming thrust, scale factor, etc., are nominal values, and was calculated to be 0.023 sec.

The most important measure of overall ACS performance is RCA gas usage. In the following paragraphs, the VO methods of gas usage evaluation and prediction will be outlined, and the running sum of the estimates compared to actual gas usage as evaluated from gas bottle temperatures and pressure data.

Total gas usage is the sum of usage in three operational modes:

(1) Celestial Cruise — If a celestial sensor is used for control in an axis, then the gas used in that axis is grouped under cruise usage.

(2) Discrete Events — The gas used when an axis is in the inertial mode determines discrete usage. Table II-9 illustrates when gas usage contributes to discrete usage as a function of inertial mode and axis.

(3) Slewing Usage — The gas usage when the platform and HGA are slewing is determined over and above the celestial cruise usage.

The methods of estimating gas usage and verifying that those estimates are relatively accurate are discussed briefly in what follows.

Celestial cruise gas usage is determined by evaluating the gas jet rate increments for an entire day (once per week) and shortly after each S/C inertia change. This observed usage plus a leakage factor determined celestial cruise usage.

Table II-9. Gas Usage in Non-Celestial Modes

Mode	Discrete Gas Est.		
	Pitch	Yaw	Roll
Roll Inertial	No	No	Yes
All Axes Inertial	Yes	Yes	Yes
Roll Turn	No	No	Yes
Yaw Turn	No	Yes	No
Motor Burn	No	No	Yes

Discrete gas usage was estimated in a number of ways. Limit cycle usage during non-turning, motor burning or science periods was determined in much the same way as celestial cruise usage.

Commanded turn gas usage was evaluated from computer simulation. Comparison of the predicted and observed telemetry signatures (illustrated in the IRU discussion) demonstrated that the simulated dynamic states and corresponding gas usage were very accurate.

Motor burn gas usage was also obtained from actual flight performance data. During MOI it was possible to estimate engine swirl torque from the roll inertial telemetry and this value is directly proportional to gas usage.

Slewing gas usage is evaluated wholly by simulation. A very efficient computer program was developed which determined the amount of angular momentum imported to each axis by a given slew start-and-stop transient. The gas usage in each axis was a function of this momentum, the duration of the slew and operational mode. Validity of the momentum estimates was established by comparing a limited number of slewing flight signatures to comprehensive computer simulations which used the momentum estimation method.

Figures II-25 and II-26 plot the cumulative gas usage for VO-1 and VO-2 respectively vs the gas weights evaluated from gas pressures and temperature measurements. These figures demonstrate that the methods used to evaluate Viking gas usage were very accurate.
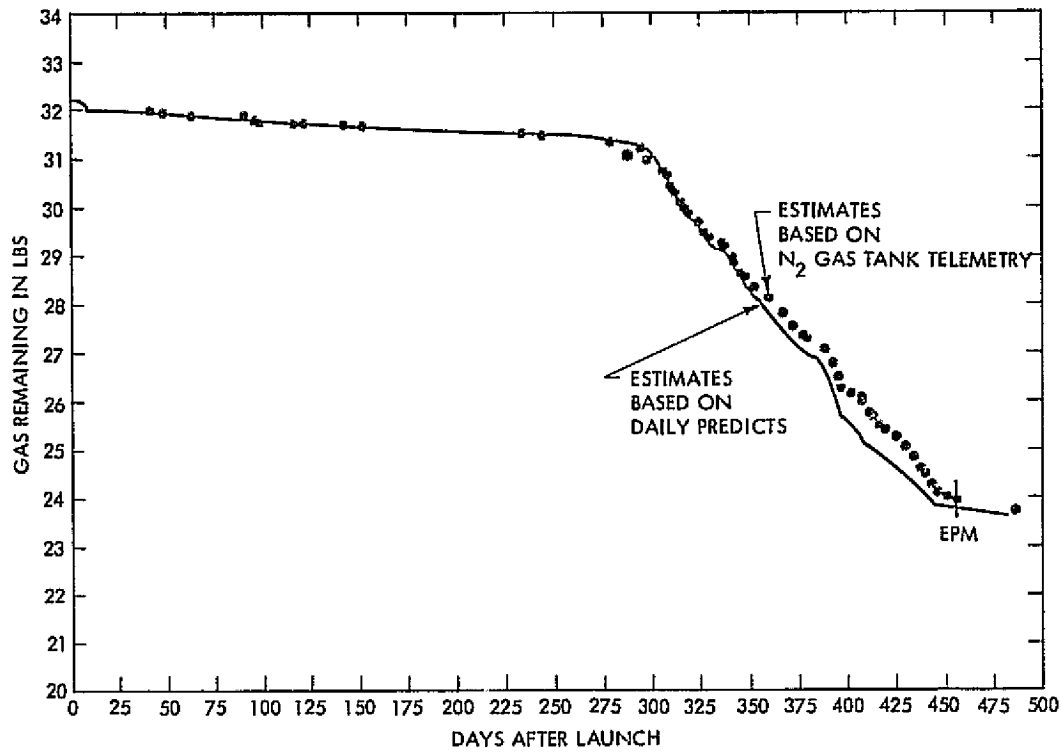
Figure II-25.   VO-1 ACS Gas Usage
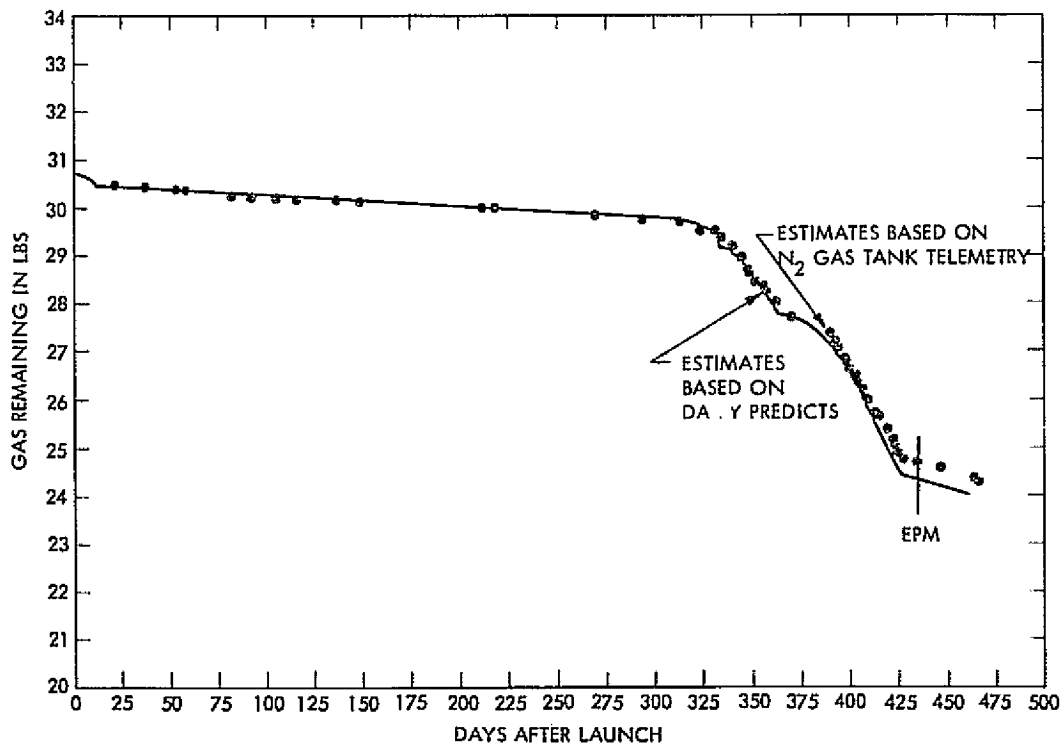
Figure II-26.   VO-2 ACS Gas Usage

II-74

It may be concluded that gas prediction, comparison of the prediction
to the actual gas usage when possible, and model correction for future predic-
tions enabled highly accurate gas usage and attitude control performance evalua-
tions to be made.

e. <u>Maneuver Reconstruction</u>. Standard procedure during Viking mission
operations included reconstruction of S/C attitude for any event that involved
S/C reorientation off celestial reference. Such an event is termed a maneuver,
and maneuver reconstruction is the process of estimating S/C attitude "a posteriori"
using telemetry of the event. If the event involved change of S/C velocity (Δv)
it was a propulsive maneuver and required also an "a posteriori" estimate of the
Δv imparted to the S/C.

1) <u>Propulsive Maneuvers</u>. Two methods of propulsive maneuver reconstruc-
tion were used on Viking. Ultimately, the most accurate method of determining
the total effect of a velocity change maneuver is by feeding radio tracking data
through the orbit determination process. This is done by the FPAG and is docu-
mented elsewhere. The OPAG reconstructed propulsive and non-propulsive maneuvers
as a regular practice. The OPAG process estimated S/C orientation (and ΔV as
applicable) by updating the parameters of a computerized S/C model using
information from telemetry of the event. Though somewhat less accurate in
estimating the total effect than the FPAG method, the OPAG process provides
needed insight into S/C parameters and has been used in near real-time to sup-
port the detailed design of S/C sequences.

Table II-10 is a compilation of the best reconstruction estimates available
at the end of the primary mission for all propulsive maneuvers. Total pointing
error estimates are given for all reconstructed maneuvers; those flagged with
asterisks were based solely on the OPAG process, and the others are the result
of FPAG's reconstruction.

The insight afforded by the OPAG reconstruction process led to some inter-
esting discoveries. The net estimation error in the center-of-mass (CM) and
thrust misalignment for both S/C was detected and measured by the exercise of
this process, and it afforded an estimate of factors to correct subsequent
maneuvers. Comparison of FPAG reconstructions with OPAG results led to separa-
tion of the two error sources, the effects of which are seen only as a sum by

Table II-10. Propulsive Maneuver Performance

S/C	Event	Date	ΔV Magnitude (m^2/sec)	Total Pointing Error (deg.)	Total Pointing Error (per unit σ)**	ΔV Mag. Error (m/sec)	ΔV Mag. Error (per unit σ)
VO-1	M/C	8/27/75	4.6844	0.296	0.77 σ	−0.0004	0.03 σ
VO-1	AMC1	6/10/76	50.5396	0.186*	0.46 σ	n.e.	n.e.
VO-1	AMC2	6/15/76	60.1424	0.161*	0.39 σ	n.e.	n.e.
VO-1	MOI	6/19/76	1097.272	0.291*	0.64 σ	n.e.	n.e.
VO-1	MOT1	6/21/76	80.0530	0.345*	0.84 σ	n.e.	n.e.
VO-1	MOT5	7/8/76	25.713	0.344*	0.90 σ	n.e.	n.e.
VO-1	MOT6	7/14/76	2.736	0.312*	0.72 σ	n.e.	n.e.
VO-1	SK-2	8/3/76	2.2279	0.203*	0.47 σ	n.e.	n.e.
VO-1	MOT7	9/11/76	21.327	0.163*	0.43 σ	0.023	0.89 σ
VO-1	MOT8	9/20/76	3.7077	n.e.	n.e.	n.e.	n.e.
VO-1	MOT9	9/24/76	22.9257	n.e.	n.e.	n.e.	n.e.
VO-2	M/C	9/15/75	8.1085	0.186	0.47 σ	−0.0357	1.55 σ
VO-2	AMC	7/28/76	9.2227	0.380*	0.97 σ	n.e.	n.e.
VO-2	MOI	8/7/76	1102.087	n.e.	n.e.	n.e.	n.e.
VO-2	MOT1	8/9/76	4.0770	0.167*	0.38 σ	n.e.	n.e.
VO-2	MOT2	8/14/76	1.7760	0.082*	0.17 σ	n.e.	n.e.
VO-2	MOT3	8/25/76	42.7215	0.284	0.71 σ	+0.0124	0.28 σ
VO-2	MOT4	8/27/76	11.2920	0.243	0.64 σ	−0.0176	0.92 σ
VO-2	MOT5A	9/29/76	5.0060	0.120	0.27 σ	−0.0013	0.08 σ
VO-2	MOT5B	9/30/76	342.551	0.737	1.63 σ	−0.3842	1.16 σ

*Estimated from S/C telemetry only, no radio tracking estimate available.

**Standard deviation of design performance level guaranteed in Functional Requirement V075-4-2007

Note: "n.e." means no estimate was made of error magnitude, although S/C performance was verified to be within required bounds.

the thrust vector control system. This comparison was performed for the MOT-3 through MOT-5 maneuvers of VO-2 and was prompted by the production of an unusually large period error by the MOT-5 plane-change burn. The reconstruction analysis confirmed that the maneuvers before the VL-2 separation event showed significantly different error characteristics than those after the event. The analysis also demonstrated that a combination of changes had occurred. There was insufficient data to reestimate the error sources but the groundwork was laid for completion of this task in the extended mission.

2) Non-Propulsive Maneuver Reconstruction. Non-propulsive maneuvers (NPMs) were reconstructed for the purpose of refining S/C attitude information. This improved attitude data was then fed into the Scan Platform Operations Program Set (SCANOPS) when it was used in the generation of refined scan platform pointing information for scientific data records. The method of reconstruction is similar to that used to reconstruct propulsive maneuvers with the initial scan platform pointing vector at the maneuvered attitude being the vector about which the pointing data applies.

As of November 6, 1976, a total of 51 NPMs had taken place on both spacecraft, 36 of which were reconstructed. (There were four types of non-propulsive maneuvers which were processed.) The breakdown summary is given in Table II-11.

Table II-11. Non-Propulsive Maneuver Reconstruction Summary

Type	VO-1		VO-2		Grand Total
	Total Maneuvers	Total Reconstructed	Total Maneuvers	Total Reconstructed	
Roll Turn	15	10	27	17	
Yaw Turn	1	1	0	0	
Roll-Yaw	1	1	0	0	
Roll-Yaw-Roll	6	6	1	1	
Total NPMs	23		28		51
Total Reconst		18		18	36

For the RYR maneuvers on VO-1 through Rev 10 (no further data was input after this) an examination of the pictures taken from the maneuvered attitude seemed to indicate a systematic maneuver execution error on the order of 0.5 deg. An extensive analysis was undertaken and an examination of the reconstruction process and the error sources involved revealed no extraordinary oversights or errors.

3. Anomalies

Only two events occurred relative to ACS hardware that can be truly classified as anomalies. A few minor procedural errors occurred during the primary mission that gave rise to unexpected performance characteristics. However, these isolated cases were quickly analyzed and the hardware found to be operating as expected for the particular situation. The two hardware anomalies that presented themselves during the mission were:

(1) Failure of IRU-1/400 Hz Inverter at VL-2 separation.

(2) Suspected partial failure of the RCA half-gas pressure regulator during solar occultations.

a. <u>IRU/400 Hz Inverter</u>. On September 3, 1976, VL-2 separated from VO-2 in preparation for its de-orbit burn and subsequent landing on Mars. While the Lander adhered to its timeline, the Orbiter suffered a failure at separation which caused it to depart significantly from its nominal sequence. The failure resulted in a total loss of gyro functions from the primary IRU, causing loss of roll attitude control and extreme instability in pitch and yaw control. Thanks to standby redundancy in the Orbiter implementation, onboard fault detection and correction software, and timely analysis and response from flight operations personnel, all VL-2 data was acquired by VO-2 and returned to Earth, in spite of the failure.

1) <u>Anomaly as Seen From Earth</u>. At or within seconds after the separation event there was a failure on board the Orbiter which either <u>was</u> a short in the 400 Hz gyro power supply or <u>caused</u> such a short. High solar panel currents indicated the short's presence, and subsequent power telemetry indicated that the input current to the 400 Hz inverter went to zero. Loss of the 400 Hz inverter caused the gyros to run down. Without gyro error signals, the roll attitude began to drift, and underdamped oscillations in the pitch and yaw limit cycles began to build up.

Before ground analysts could comprehend what was happening, low-rate data sync was lost, followed ten seconds later by loss of lock on the S-band carrier. Although the S-band carrier was reacquired shortly thereafter, the carrier level was down 20 dB, and no lock on the data could be obtained.

2)   Deduction and Confirmation of Anomaly Mechanism. Initial analysis following loss of data indicated that excessive gas jet firings would have resulted from the underdamped oscillations. This excessive activity would have caused an internal spin-up detector in ACE-1 to exceed its threshold, thus generating an ACE changeover interrupt to the onboard computer (CCS). The CCS response to the interrupt would include a switch of the S-band radio function from the HGA to the LGA, a switch from ACE-1 to its back-up ACE-2, and a termination of the CCS pre-programmed sequence. Indeed, following commands to reduce the Orbiter data rate, engineering telemetry confirmed that the CCS had properly responded to the ACE changeover interrupt, and the Orbiter was operating on ACE-2. ACE-2 logic circuits had selected IRU-2, and the attitude control function was once again normal. This anomaly is covered further from a power subsystem viewpoint in paragraph II-D.

b.   RCA Half-Gas Pressure Regulator. Shortly after the Solar occultation period on October 15, 1976, a positive pitch torque of between 200 to 300 dyne-cm was noted and a small negative yaw torque increase over previous observed yaw torque was noted. Figure II-27 shows the torque signature on October 16, 1976 (day 290) starting at 24 hr 34 min.

1)   Disturbance Torque Characteristics.

(1)   The disturbance torque appears in both the pitch and yaw axes simultaneously and their magnitudes are related in the ratio of about 6:1 for pitch to yaw torque. No disturbance was noted in roll. Figure II-28 illustrates the disturbance torque history with the following qualifications:

(a)   The disturbance torque appears after the solar-Earth occultation on October 14, 1976 (UTC day 288) at 09:00 but appears to go away by 15:00.
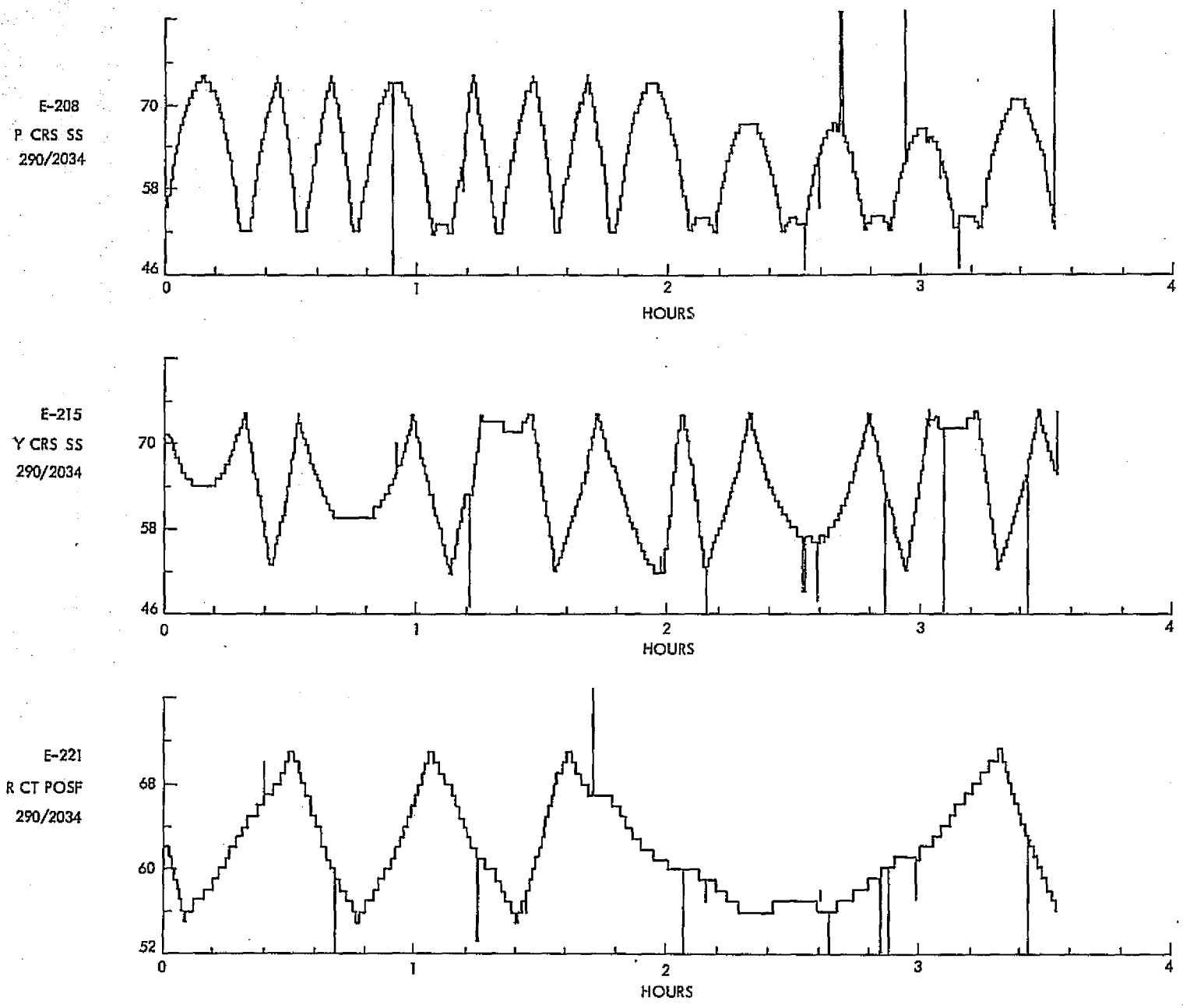
Figure II-27. Disturbance Torque Signature of VO-1
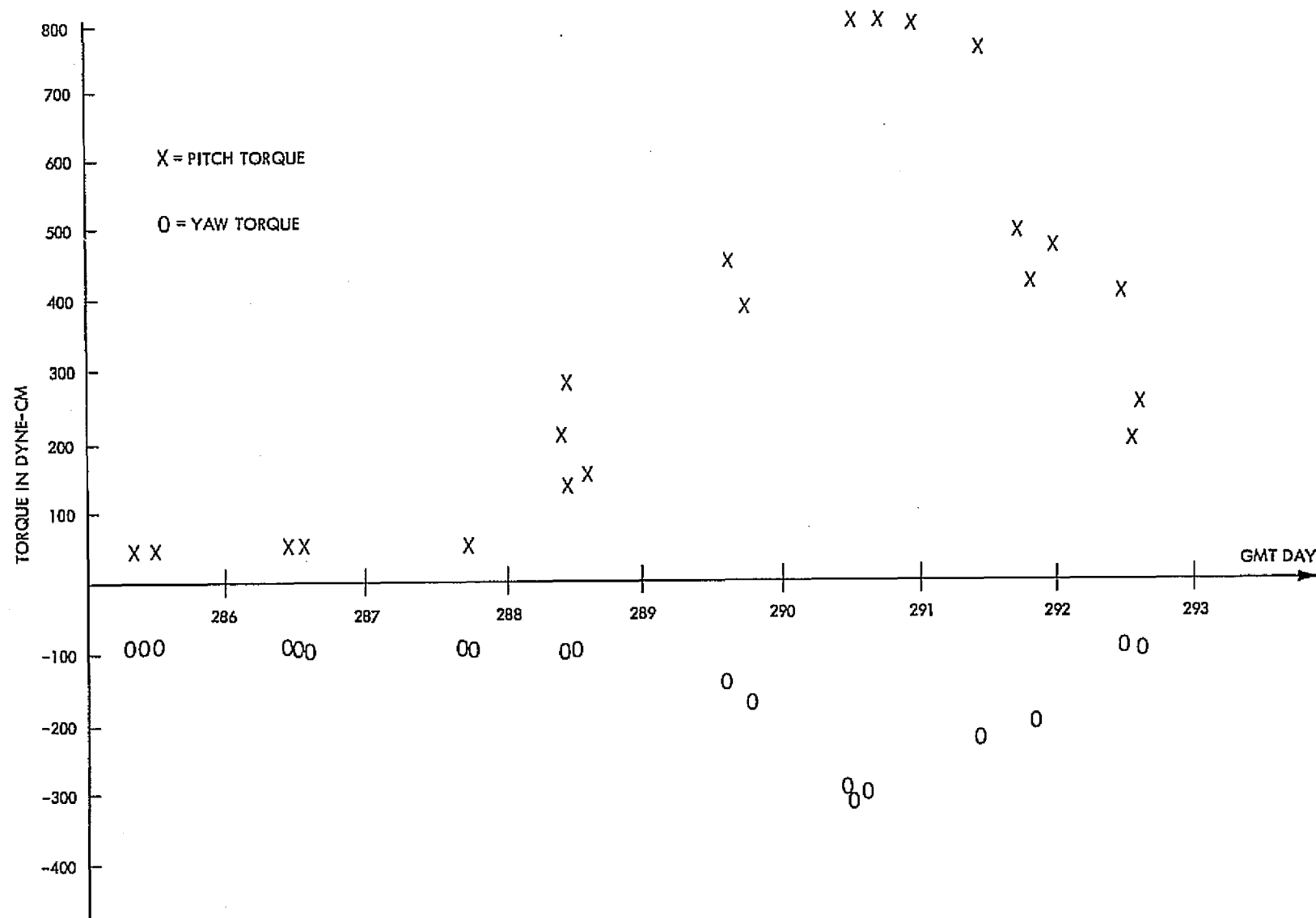
Figure II-28.   Samples of Disturbance Torque in VO-1 Pitch/Yaw Axes

(b)   The disturbance torque reappears after solar occultation on October 15, 1976 at 09:00 and traces the trajectory in Figure II-28 until about October 18, 1976 at 16:00 (day 292).

(c)   There are a number of short recurrences subsequent to October 18, 1976, at 16:00 but all are short in duration and relatively low in magnitude.

(2)   The observed gas jet rate increments in all axes, plotted in Figure II-29, show a marked increase just after solar occultation on October 12 at 08:00, remain high until about 11:00, and return to normal at about 13:00. A similar sequence is repeated on October 13 from about 08:00 to 10:00. At about 09:00 on October 14, the rate increments again increase sharply after solar occultation, but on this day there appears the first indications of pitch and yaw disturbance torques. These high rate-increments remain for approximately 6 hrs. Following solar occultation on October 15, 1976, at 10:00, the rate increments jump sharply (and the pitch and yaw disturbance torques also were much higher than the day before). The rate increments remain at a fairly high level until about October 21 at 16:00 when they drop suddenly and remain low until solar occultation on October 22, at 14:00, when they increase for a short period before gradually decaying to normal at about 00:00 on October 24. There have been no periods of large rate increments or torques in excess of 100 dyne-cm since October 24, 1976 (Day 298).

(3)   The temperature of the RCA bottles from October 11 to 15 ranged from $61^{\circ}F$ to $57^{\circ}F$ with the minimum reached about 30 min after exit of occultation. Flight acceptance test limits for the HPM are $32^{\circ}F$ to $132^{\circ}F$.

    2)   <u>Potential Disturbance Sources</u>. The initial reaction to the disturbance torque observed in the limit cycles was to assume a RCA gas jet valve leak. However, since there is no disturbance torque noted in the roll axis, it may be concluded that the fixed ratio of the observed disturbance torques in pitch and yaw, and the probable direction of the thrust, limits the source of the thrust and excludes any leaking RCA valve.
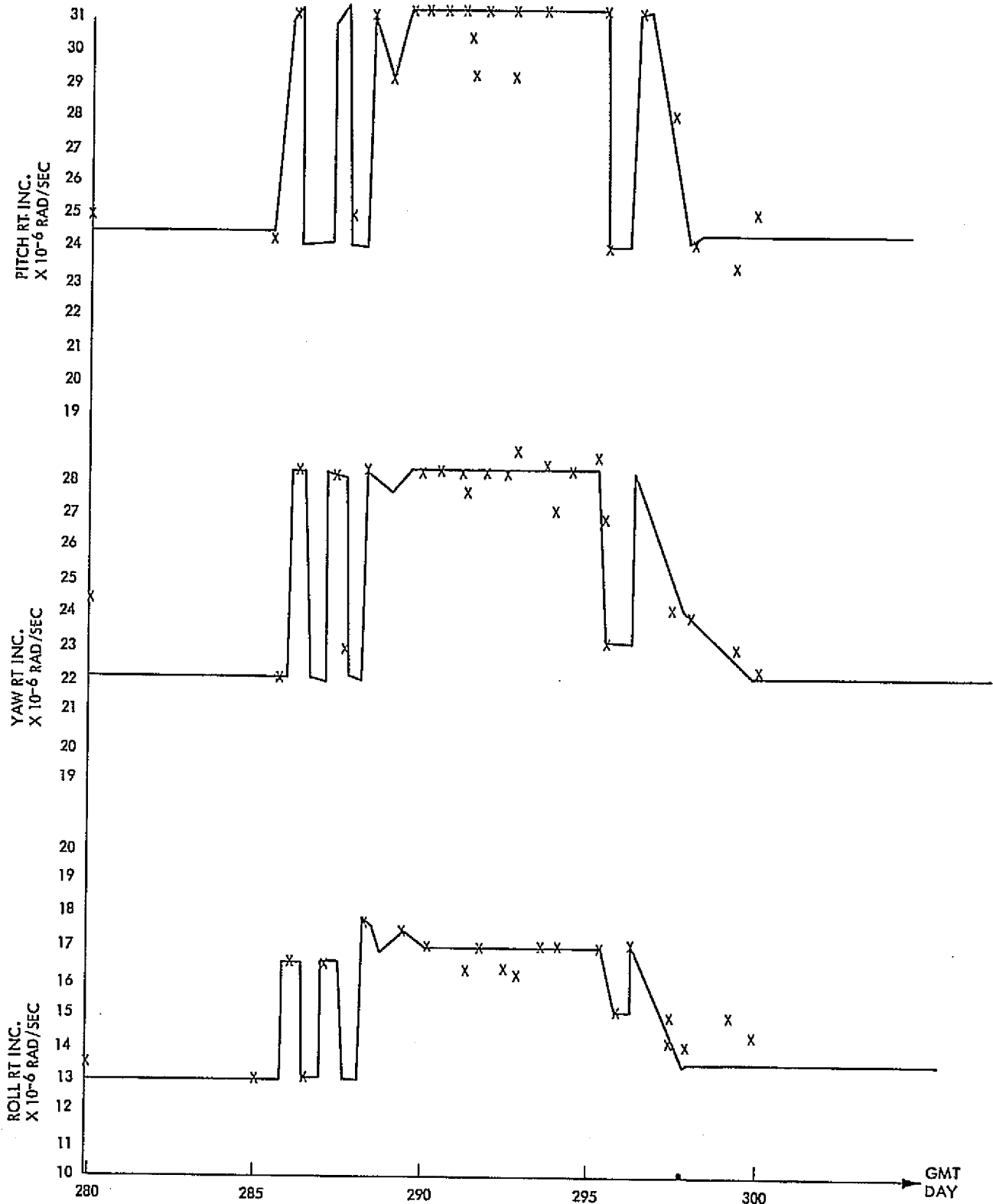
Figure II-29.   Observed Minimum Gas Jet Rate Increment Trends

Located in the middle of the disturbance torque envelope is the RCA vent tee. The vent tee is designed to minimize the effect of vented nitrogen gas, and, for low flow rates, should produce a negligible net thrust and disturbance torques.

However, the observed increased gas jet rate increments are a manifestation of an elevated low pressure module pressure in one RCA half gas systems. If this vent tee were plugged, the ratio of the pitch and yaw torques and their polarities would be compatible with the observed values.

3) Conclusions. There is some justification for assuming that the lighted Mars limb may result in Sun Sensor scale factor changes just prior to and immediately after solar occultation. These scale factor changes would be observed as rate increment changes in the pitch and yaw axes only and should be observable during each occultation. The fact that roll rate increments increased along with the pitch and yaw increments, and that these changes were not detected after each occultations, seems to eliminate the lighted Mars limb effects as one of the causes of the observed disturbances.

Gas jet rate increments point to a pressure regulator failure to regulate at 25 psi during a portion of the solar occultation period, and for a portion of this period the excessive pressure may have caused the relief valve to vent. This venting would have caused the observed disturbance torque signature if one of the vent tee outlets were obstructed.

Current gas bottle usage figures indicate that during the disturbance period, the +X/+Y bottle used more gas than the -X/-Y bottle. This amount of gas is consistent with the estimated amount used for limit cycle usage as a result of the increased regulator pressure and venting.

C.   ARTICULATION CONTROL SUBSYSTEM

1.   Description

a.   Functions.   The ARTC provides closed-loop positioning of the artic-
ulated elements on the VO; namely, the scan platform, HGA, and solar energy
controller (SEC) blades in response to command angles in the form of coded
commands from the CCS.   A simplified block diagram of the ARTC is shown in
Figure II-30.   The ARTC is shown within the dashed lines.   Intrasubsystem and
intersubsystem interfaces related to the functioning of the ARTC are shown.

The ARTC provides the following functions:

(1)   Position control of the scan platform (two axes)

(2)   Position control of the HGA (two axes)

(3)   Position control of the four sets of SEC blades (one axis)

The scan platform (Figure II-31) is a two-degree-of-freedom (clock and
cone) gimballed support structure upon which the science instruments VIS, IRTM
and MAWD are mounted.

The HGA, Figure II-31, is mounted on a two-degree-of-freedom azimuth (AZ)
and elevation (EL) gimballed support structure for the purpose of keeping the
antenna pointed toward the Earth.

The SEC assemblies, of which there are four, consist of louvered blades
used for maintaining temperature control of the PROP tanks by regulating the
Sun radiation on the interior of the VO.

b.   Equipment.   The ARTC, Figure II-30, consists of the following
assemblies: articulation control electronics (ARTC-E), scan actuators, antenna
actuator, and SEC actuators.   These are described briefly below.

1)   Articulation Control Electronics.   The ARTC-E accepts CCS position
commands and provides drive signals to the commanded actuator stepper motor to
slew the actuator until its position, as indicated by a feedback (FB) potentiom-
eter (POT), agrees with the position command.   Except for the actuator drivers,
the ARTC-E consists of two identical control channels to provide redundancy and
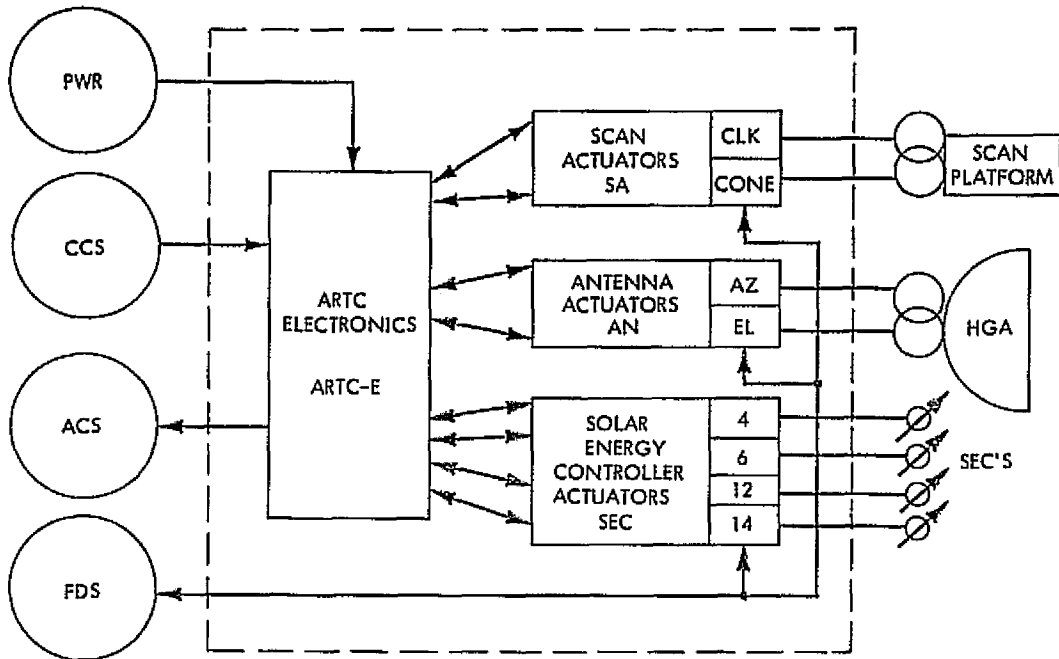
Figure II-30. Simplified ARTC Block Diagram
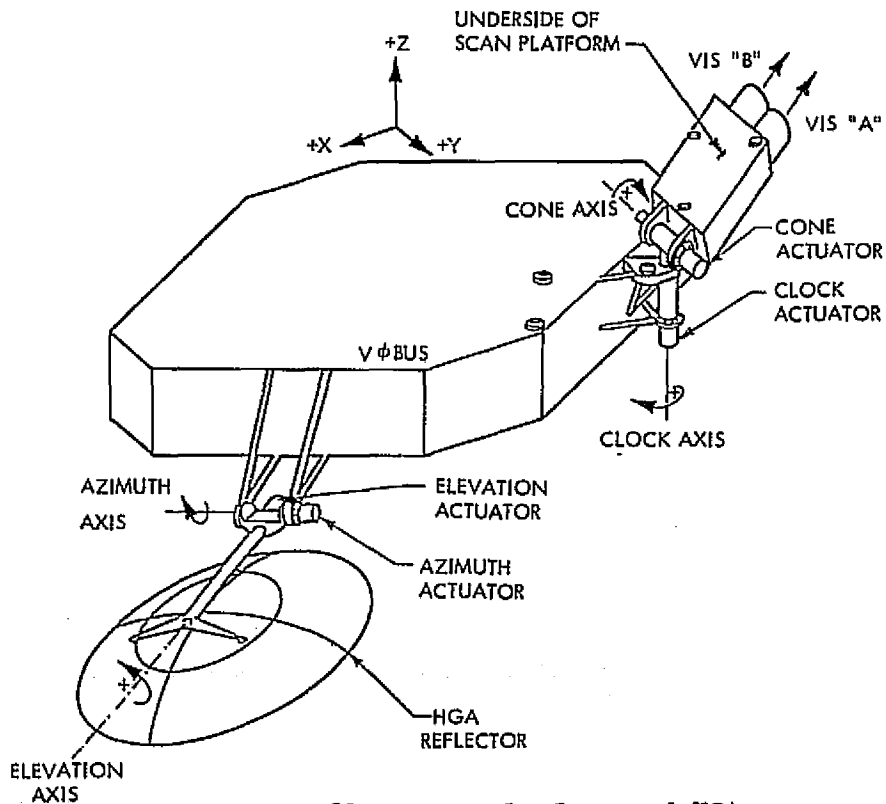
Figure II-31. Scan Platform and HGA

the ability to slew any two actuators simultaneously. The electronics in each of the two channels are multiplexed to allow the position of any one of eight actuators to be controlled with a single set of electronics.

2) Actuators. All three types of actuators are identical to concept but differ in size, weight, torque, angular range and slewing speed. All are stepper motor driven. Stepper motor rotation is fed through a gear train to the actuator shaft. Each actuator has two redundant FB POTs, one dedicated to each of the two ARTC-E channels. Each actuator also has a coarse telemetry POT, and the scan and antenna actuators have a fine telemetry POT. The three scan actuators are identical and interchangeable, as are the four SEC actuators. One scan actuator and one antenna actuator is used for the HGA.

c. Operating Modes. The operating modes relate to the actuator that is being slewed and the rate at which it is be slewed. In addition, there is an idle mode in which the ARTC is inactive except for passively restraining the articulated elements from moving with friction and motor detent torque. The ARTC is placed into the idle mode at power turn-on, after completion of each actuator slew and if a power drop-out occurs. A simplified ARTC functional block diagram is shown in Figure II-32.

1) Slew Rate Modes. The ARTC-E is capable of selecting the high-rate slew mode or the low-rate slew mode, as commanded by the CCS. In the high-rate slew mode, ARTC-E gates 100 Hz stepper motor drive pulses to the ARTC-E actuator outputs. In the low-rate slew mode, ARTC-E gates 24.5 Hz stepper motor drive pulses to the ARTC-E actuator outputs. The position control loop is not enabled when a slew rate command is issued.

2) Position Control Mode. The design uses a corrective mechanization in which the control error is corrected at discrete intervals and at a constant rate independent of the error magnitude. The error detector determines the polarity of the error and provides a signal to the reversible counter indicating the proper sequence for the actuator drive pulses. When the clock pulses are transmitted to the actuator through the motor driver, the feedback signal is corrected at the rate of one step per clock pulse until the error crosses null.

CONTROL CHANNEL NO. 1

50 VRMS
2.4 kHz → POWER SUPPLY

CCS INPUTS → INPUT UNIT

POSN CMD

ADDR
RATE
PARITY
ACTUATOR

SLEW CONTROL

SYSTEM ENABLE

ANALOG MULTIPLEXER

POSN

ERROR DETECTOR

RESET
SYSTEM SET
RATE SELECT
ACTUATOR SELECT

REVERSIBLE COUNTER

PULSE SEQUENCER

DUAL RATE CLOCK

DIGITAL MULTIPLEXER

DRIVERS (8)

ACTUATORS (8)

SCAN STATUS

SCAN SLEW STATUR TO ACS

INPUTS → CONTROL CHANNEL NO. 2

POSN

Figure II-32. Simplified ARTC Functional Block Diagram

2.   Performance

With over 8,500 hours operating time on each Orbiter during the primary mission, ARTC performance has been excellent. Both the electronics as well as the eight actuators have performed in an entirely nominal manner.

Tables II-12 and II-13 summarize the VO-1 and VO-2 ARTC primary mission activity. It can be observed from these tables that most ARTC activity was due to scan platform slewing. The combined total of VO-1 and VO-2 slews was 38,000; approximately 97 percent (36,900) were scan platform slews, 2.4 percent (900) were HGA slews, and 0.6 percent (200) were SEC slews.

a.   <u>High-Gain Antenna Calibration.</u> The VO HGA is a dish antenna with two degrees of freedom. During the course of the primary mission, the HGA was used primarily to receive commands from the Earth, send science and engineering data back from the Orbiter, and relay data from the VL.

Table II-12. VO-1 ARTC Primary Mission Summary

Actuator	Number of Slews			Total Travel Degrees
	Chan 1	Chan 2	Total	
Clock	10,189	842	11,031	57,322
Cone	7,621	4,028	11,649	96,437
Azimuth	172	0	172	180
Elevation	308	0	308	605
SEC 4	36	0	36	630
SEC 6	27	0	27	629
SEC 12	27	0	27	629
SEC 14	27	0	27	629

Total operating time: Chan-1 8,651, Chan-2 3,789

Total On/Off cycles: Chan-1 5, Chan-2 12

Table II-13.   VO-2 ARTC Primary Mission Summary

Actuator	Number of Slews			Total Travel Degrees
	Chan 1	Chan 2	Total	
Clock	6,710	399	7,109	19,484
Cone	4,093	3,025	7,118	65,177
Azimuth	148	6	154	567
Elevation	284	8	292	581
SEC 4	30	0	30	456
SEC 6	21	0	21	425
SEC 12	21	0	21	433
SEC 14	21	0	21	433

Total operating time: Chan-1 6,506, Chan-2 2,653.

Total On/Off cycles: Chan-1 5, Chan-2 12.

Because of the large distance of the VO from the Earth, and the relatively small amount of power available for transmitting data by the VO HGA, a tight pointing requirement had to be imposed.   The requirement was that at no time should the angle offset between the Earth and the HGA pointing direction exceed 0.75 degrees and that this angle should be kept as small as possible.   Since the VO oscillates slightly about its ideal orientation (this oscillation is called limit cycle motion), and since the HGA moves in discrete, as opposed to continuous, steps, a certain amount of "pad" is necessary in judging what pointing accuracy and control meets the overall pointing requirement.   Specific numbers for the pad are included in Table II-14.

There are many components of the Orbiter that affect the pointing of the HGA, and since none of these can be built perfectly, a measurement process, called a "calibration," is performed to detect and compensate for any error sources built into the system.   Part of the calibration procedure is made by making careful on-the-ground measurements.   This is, however, not enough, since launch forces and other disturbances may cause antenna misalignments.

Table II-14. HGA Pointing Calibration Results (Data Evaluated
at 0° Azimuth, 0° Elevation)

X-Band Pointing	Post-Calibration		Pre-Calibration	
	VO-1	VO-2	VO-1	VO-2
Residue Calibration Error (deg)	0.02	0.06	0.300	0.130
Altitude Limit Cycle Motion (deg)	0.412	0.412	0.412	0.412
Command Resolution Error (deg)	0.160	0.160	0.160	0.160
Total	0.592°	0.632°	0.872°	0.702°

Note: A 3σ uncertainty of about 0.03 degrees should be associated with the total in each case.

The in-flight calibration is designed to detect misalignments after launch. The basic idea is to move the HGA around in a pattern, measure changes in signal strength received on Earth and, from this, calculate the position of the HGA boresight relative to where it was thought to be nominally pointed.

During the course of the Viking Primary Mission, there were four in-flight calibrations on VO-1, and three on VO-2.

Table II-14 shows the final result of the HGA caliabration. The final results are given in the first two columns. By comparing the final calibration results to the initial ground calibration an estimate of the pointing accuracy improvement due to inflight calibration can be made. Columns 3 and 4 of Table II-14 present the estimated uncalibrated pointing accuracy for VO-1 and VO-2, respectively.

It should be noted that VO-2 had more ground testing, hence accounting for the smaller difference between calibrated and uncalibrated pointing accuracy.

b. Scan Platform Calibration.

1) In-Flight Sequence Objectives. The in-flight calibration of the attitude control (sun and star) sensors, scan platform alignment, and VIS alignment is necessary to be able to point the scan platform mounted science

instruments, including the VIS, and to determine their pointing directions from downlink telemetry to the accuracy required for science experiments and optical navigation. The requirements on the accuracy with which the scan platform must be positioned (Pointing Control) is 5 deg (99 percent) and the accuracy with which the scan platform position must be determined (Pointing Knowledge) is 0.25 deg (99 percent). These requirements apply when the spacecraft is on celestial references.

For each VO five distinct picture sequences were planned to calibrate the scan platform: instrument check-out, and Scan Cal I to IV. The primary objectives for each of these sequences were:

(1)   Instrument Check-Out: This sequence was primarily designed to provide early information on the totally new technique of a two-camera operation for optical navigation using the Earth in one camera and stars in the adjacent camera. In addition, this sequence provided early indications of camera response characteristics and a limited scan platform calibration.

(2)   Scan Cal I: Initially this sequence was intended to remove any large scan platform offsets before going into a complete calibration sequence. However, based on the good results of the instrument check-out sequence, this sequence was changed into a complete scan platform calibration sequence.

(3)   Scan Cal II: Primary objective was to verify the results of Scan Cal I, and to photograph Mars and determine critical approach optical navigation processing procedures.

(4)   Scan Cal III: Intended to verify scan platform pointing control and knowledge after MOI and before VL separation.

(5)   Scan Cal IV: Complete calibration sequence to develop model parameters that apply to the entire region available to the scan platform after VL separation.

2)   Instrument Checkout Sequence. The instrument checkout sequence con-
sisted of an initial picture pair of stars, followed seven days later by two
picture pairs with the Earth in one camera and stars in the other camera which,
at the time selected for the pictures, was possible only with a S/C roll maneu-
ver. The purpose of the star pair scheduled seven days prior to the Earth
pictures was to obtain added confidence that the VO hardware was working properly
and that the VIS cameras and the science instrument platform pointing was under-
stood. This precaution was taken since any one of a number of malfunctions or
misunderstandings could cause gross overexposure of the vidicons when taking the
Earth-star pair.

3)   Scan Platform Calibration Sequence I.

a)   Picture Sequence Design. During the cruise phase, the first VO scan
platform calibration sequences were scheduled on February 9, 1976 for VO-1 and
February 13, 1976 for VO-2 to remove any large offsets in platform pointing.
These sequences originally consisted of six five-picture strips and one three-
picture swath of stars. However, based upon the results of processing the Earth
and star pictures taken during the initial instrument checkout sequences con-
ducted in October 1975, it was determined that offsets were characterized well
enough so that Scan Cal I could be used to provide a more comprehensive scan
platform calibration and meet many of the objectives originally intended for
Scan Cal II. Scan Cal II could now be used for verification of the Scan Cal I
results and used for optical measurement processing studies in preparation for
the important optical navigation sequences.

Scan Cal I consisted of 19 one-picture swaths, six two-picture swaths and
two three-picture swaths for a total of 37 pictures. Figure II-33 depicts the
scan pointing for Scan Cal I in the clock cone space.

b)   Results. The pointing results in Tables II-15 and II-16 are
specified in terms of a camera M-N-L coordinate system where a positive rotation
around M decreases the camera clock angle and a positive rotation around.
N increases the camera cone angle. The errors are characterized by their stan-
dard deviations and extreme values.
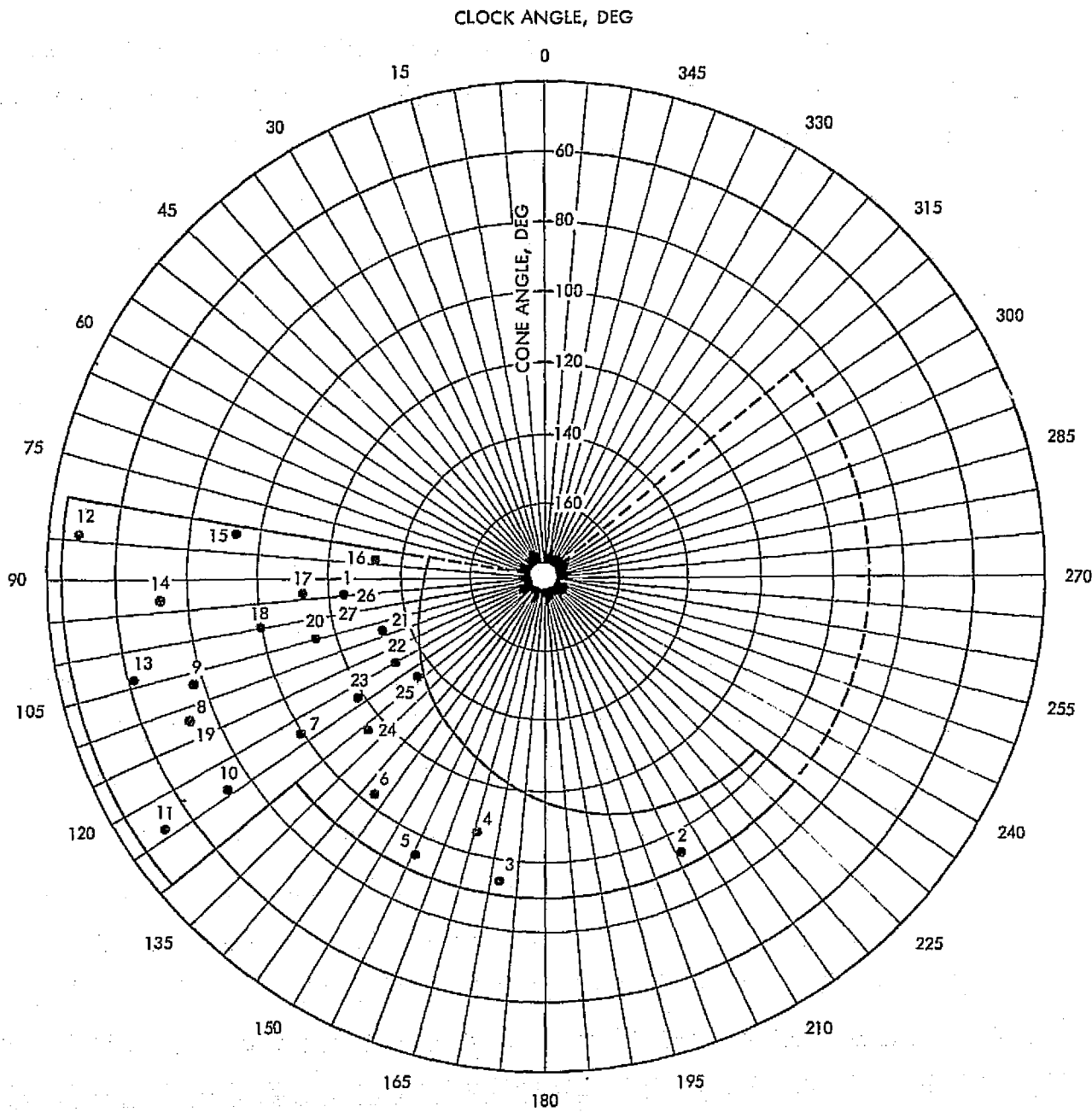
Figure II-33. VO-2 Scan Cal I Instrument Pointing History

Table II-15. Pointing Knowledge Error (Degrees) for Scan Cal I

	VO-1	VO-2
σ_M	0.019	0.014
σ_N	0.018	0.014
Maximum Total Error	0.044	0.034

The results indicate the 99 percent requirement for pointing knowledge (0.25 deg) and control (0.50 deg) were met. Table II-15 indicates Scan Cal I a-posteriori statistics were near the limit of removing all non-random error sources.

4)   Scan Platform Calibration Sequence II.

a)   Picture Sequence Design. The second scan platform calibration sequences were scheduled on April 12, 1976 for VO-1 and on April 15, 1976 for

Table II-16. Pointing Control Error (Degrees) for Scan Cal I

	VO-1	VO-2
σ_M	0.166	0.149
σ_N	0.156	0.178
Max M	0.20	0.35
Min M	-0.40	-0.29
Max N	0.30	0.38
Min N	-0.32	-0.40
Maximum Total Error	0.50	0.49

VO-2. These sequences consisted of a total of 24 pictures each (three four-picture swaths, two three picture swaths, and six one-picture swath).

b)   Results. The error parameter sets estimated in Scan Cal I were used. The results shown in Tables II-17 and II-18 indicate that the 99 percent requirements for pointing knowledge (0.25 deg) and control (0.50 deg) were still being met.

Table II-17. Scan Cal II Results (VO-1)

Pointing Knowledge Error (Degrees)		
	M	N
Mean	−0.014	+0.003
σ	0.029	0.010
Maximum	0.030	0.013
Minimum	−0.062	−0.022
Maximum Total Error	0.063	
Pointing Control Error (Degrees)		
	M	N
Mean	−0.03	0.012
σ	0.15	0.12
Maximum	0.23	0.14
Minimum	−0.35	−0.24
Maximum Total Error	0.36	

Table II-18. Scan Cal II Results (VO-2)

Pointing Knowledge Error (Degrees)		
	M	N
Mean	00.022	0.022
σ	0.038	0.025
Maximum	0.044	0.044
Minimum	−0.114	−0.039
Maximum Total Error	0.120	
Pointing Control Error (Degrees)		
	M	N
Mean	0.07	0.04
σ	0.17	0.12
Maximum	0.32	0.33
Minimum	−0.23	−0.20
Maximum Total Error	0.40	

5)   Scan Platform Calibration Sequence III.

a)   Picture Sequence Design. During the optical navigation pictures, the scan platform offset in the cone direction changed approximately −0.15 deg on VO-1 after the first approach mid-course correction maneuver. This offset was conjectured to have been introduced as a result of not moving the platform against the stops prior to the maneuver. All subsequent maneuvers were done with the platform near the stops for both Orbiters and no new negative offsets were observed. Scan Cal III was primarily designed to verify scan platform alignment after the large MOI engine burn and not for calibration purposes.

These sequences consisted of just a few pictures spaced throughout the available scan platform region.

(b) <u>Results</u>. Scan Cal III for VO-1 occurred on July 7, 1976 and the results of processing these three pictures are shown in Table II-19. Table II-19 demonstrates that the pointing knowledge was less than 0.1 deg and the negative cone bias observed in approach appears to be reduced to -0.10 deg.

On Rev. 4 August 11, 1976 for VO-2, six star frames were taken in order to verify the existing scan platform alignment model parameters used in pointing control and knowledge computations for the scan platform. The results of processing these six pictures are given in Table II-19, which indicates that the pointing for VO-2 had not been affected by MOI and that the camera pointing knowledge is well within the requirement of 0.25 deg.

Table II-19. Scan Cal III Results

VO-1 Pointing Knowledge Error (Degrees)		
	M	N
Mean	0.028	-0.052
σ	0.039	0.006
Maximum Total = 0.093		
VO-2 Pointing Knowledge Error (Degrees)		
	M	N
Mean	0.01	0.00
σ	0.01	0.04
Maximum Total = 0.064		

6) <u>Scan Platform Calibration Sequence IV.</u>

a) <u>Picture Sequence Design</u>. Scan Cal IV was designed to help character-ize any offsets introduced in orbit by engine burns and, primarily, to provide calibration parameters that apply over the entire scan platform region which was significantly increased after the Lander was separated. Also, a scan plat-form pointing was investigated where high-rate slews (1 deg/sec) were used

to point the scan platform. The results of the VO-1 sequence are shown in Table II-20. Scan Cal IV was cancelled on VO-2 since the bioshield base cover was left attached and prevented the scan platform from using the extended region.

Table II-20. VO-1 Scan Cal IV Results

Pointing Knowledge Error (Degree)		
	M	N
Mean	−0.021	+0.097
σ	0.070	0.033
Maximum Total = 0.18		

3.   Stowing Procedures for Propulsive Maneuvers

a)   Scan Platform. Up to and including the first Mars Orbit Trim (MOT-1) on VO-1 and the VO-2 first Approach Midcourse Correction (AMC-1) it was standard procedure to stow the scan platform prior to each burn in what was then called platform stow position. This position (which was approximately 222.5 deg clock and 90.6 deg cone for both Orbiters) located the scan platform just above Bay 6, with the underside of the scan platform clearing the bus by about 0.5 inch. This stow position will be herein called "soft-stow"—as opposed to "hard stow" where the scan platform is lowered further in cone until there is actual physical contact between the scan platform and the bus.

It was observed during VO-1 AMC-2, MOI, and MOT-1 propulsive manuevers that the scan platform cone position changed during the burn. A careful analysis of this phenomenon showed that transient loads on a soft-stowed scan platform during engine turn-on transients were large enough to move the scan platform in case by slipping the clutch of the cone actuators. It was further shown that during VO-1 MOT-1 the slippage was sufficient for the scan platform to have impacted the base at about 5 degree-per-second and that the problem would

become worse as the spacecraft became lighter. In fact, it was shown that a light spacecraft propulsive maneuver would throw a soft stowed scan platform against the bus with velocities of about 35 degrees-per-second at impact.

Since high-speed scan platform impact on the bus could adversely affect the integrity and calibration of both the scan platform itself, as well as of the instruments mounted thereon, it was decided to eliminate such risks by "hard stowing" the platform--down into physical contact with the stops. All VO-1 and VO-2 propulsive maneuvers after June 30, 1976 have been done with hard-stowed scan platform. No further movement of the scan platform during burns has been observed.

b) <u>High-Gain Antenna.</u> Just as it happened with the scan platform, the HGA was also observed to move during some of the propulsive maneuvers, such as the VO-1 midcourse No. 1, AMC-1 and -2, and MOT-1.

Analysis of this anomaly showed that loading of the HGA during engine firings was sufficient to overcome the friction holding the antenna positions, causing it to move within the backlash of the azimuth and elevation actuators (in the case of the HGA the loading is not large enough to cause clutch slippage). This movement was considered undesirable and potentially hazardous.

Although the HGA could conceivable be put into a "safe position" prior to each burn, it is very desirable (from operational and reliability consider-ations) that there be no such constraint on the system. An alternate solution which alleviates the problem considerably, by reducing significantly the loads on the actuators, is to command the HGA to its normally desired position in such a manner that windup of the actuator will occur during engine start up. Over 90 percent of the allowable azimuth and elevation ranges this positioning can be accomplished with an increasing AZ or EL position command as the last HGA command before the burn. This alternate procedure has been used on all VO-1 and

VO-2 propulsive maneuvers since June 30, 1976 and although movement of the HGA has continued to occur during burns, the procedure minimizes the stress loads on the HGA actuators.

D.   POWER SUBSYSTEM

1.   Description

The PWR was designed and built to provide all the electrical power needs of the VO during the launch, cruise, (MOI) and Mars orbital missions phases. In addition, the subsystem provided electrical power on demand to the VL power subsystem until VL separation at Mars.

The function of the VO PWR is to provide usable electrical power necessary for operation of the VO and the VL. This power is supplied by redundant switching and control networks, energy conversion and power conditioning equipment. Figure II-34 is a simplified functional block diagram of the VO PWR. The PWR electronics and controls are located in two equipment bays (10 and 12) while separate bays are provided for each of the two batteries.

Most of the power conditioning modules in the PWR are block redundant. Reliability of regulated power is achieved by the use of a main and standby power chain. Each power chain consists of one booster regulator (B/R) and one 2.4 kHz inverter. The design features irreversible, automatic transfer from the main to the standby chain should a fault occur in the main chain. Two 30 Vdc converters operate in an active parallel redundant configuration, and the 30 Vdc bias supplies are quadruply redundant with a redundant pair located in each of the two PWR equipment bays. The battery chargers are also redundant since switching permits a given charger to recharge either of the batteries. The B/R, 2.4 kHz inverter, and 30 Vdc bias supplies operated continuously during the mission from the time the S/C is powered at launch. The 400 Hz inverters and 30 Vdc converters operate when needed. Redandant share mode detectors and the boost converters operate to assist in placing the power operating point on the solar array when a share mode is detected under normal S/C operating conditions.

The solar array (S/A) is the principal electrical power source for the VO. The array consists of four solar panels spaced 90 deg about the bus, with two subpanels per solar panel. Each subpanel is identical and all are
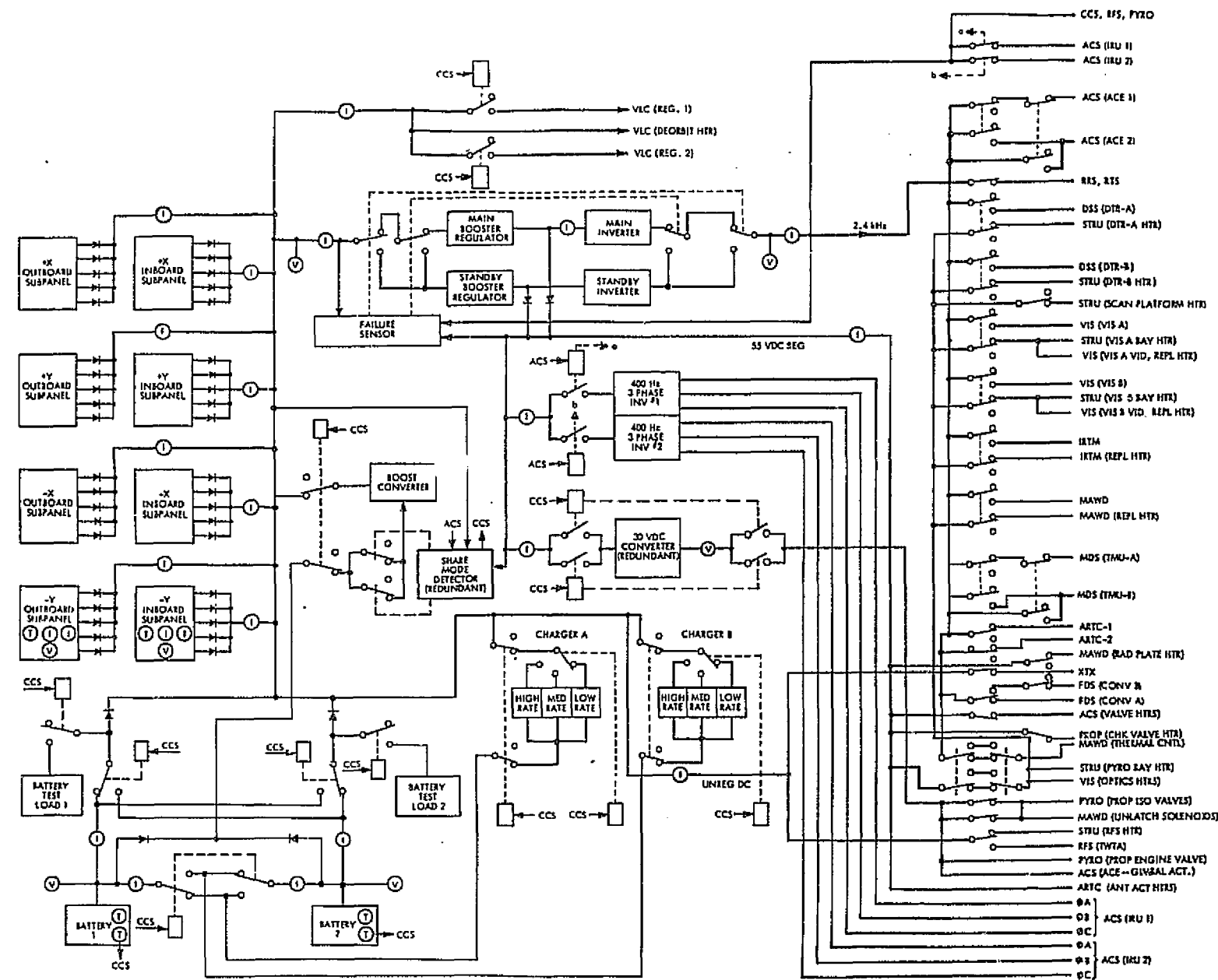
Figure II-34. Power Subsystem Functional Block Diagram

electrically and mechanically interchangeable. Five solar cell module circuits or sections are mounted on each subpanel, and each section is connected in parallel with, and is diode isolated from, the rest. Each solar cell section is shunted and voltage limited by six series-connected zener diodes that are physically mounted on spars on the rear of the subpanels. The eight subpanels are also electrically connected in parallel to form the solar array, incorporating a total of 34,760 solar cells mounted on a substrate with a total area of 15.2 m^2 (164 ft^2). The solar panels are folded and stowed parallel to the S/C Z-axis at launch. When the S/C is Sun-acquired, as it is during most of the mission, its attitude will be controlled to maintain the array within 0.25 deg normal to the Sun in order to convert solar energy to the electrical energy.

Two identical, 26-cell rechargeable nickel-cadmium batteries are estimated to have a total capacity of 2100 watt-hours at launch. The batteries are a secondary electrical energy source. They automatically provide (necessary) S/C electrical power when the array can not supply the entire S/C electrical load, or for the occasions when the S/A is not illuminated. Both or either battery can be used. The batteries are estimated to have a total capacity of 1900 watt-hours at Mars encounter.

Two identical battery chargers serve to charge the batteries, each at one of three different rates: trickle-rate at 0.77 amp, medium-rate at 2 amp, or at high-rate at 3 amps. The 3 amp rate provides the highest charge efficiency. The 2 amp charge rate is used when the S/C load, during a recharge period, reaches levels that exceed S/A capability prohibiting the use of the 3 amp rate. The trickle charge rate is used to bring a battery to its fully charged state after initial charging at the medium or high rate. It is also used to maintain a battery at full charge.

Unregulated power at a voltage range of 25 to 50 Vdc is available on the VO to power the VL, TWTA, and the XTX. The battery chargers are also powered from the unregulated bus and so is the B/R. All other electrical power used on the S/C is first conditioned for the users through the B/R module.

The B/R boosts the 25 to 50 volt unregulated power to 56 Vdc. The 2.4 kHz inverter module uses the B/R output to produce the S/C 50 V rms power supply. The balance of the B/R output is routed through fault-isolating redundant diodes, to the PWR redundant bus, which becomes the source of regulated dc power for the S/C at approximately 55.2 Vdc. The redundant bus powers the 30 Vdc converters, the 400 Hz inverters, the 30 Vdc bias supplies, share mode detectors, and most of the heaters used on the VO.

All of the science instruments and most of the engineering subsystems are powered by the 2.4 kHz inverter. Each of the 400 Hz, 3-phase inverters is hard-wired to ACS IRU. The 30 Vdc converters are actively redundant and are designed to supply the power requirements of the attitude control gimbal actuator drivers, MAWD spectrometer unlatch solenoids, propellant isolation valves and the propulsion bi-propellant engine valve.

The PWR interfaces with all other S/C subsystems because it supplies power to all subsystems. In the majority of cases, the action at the interface is a switching function which turns power on or off to a particular subsystem. However, some interfaces are more than simple switching functions. These are discussed below.

a. Computer Command Subsystem.

(1) Switch closure commands issued as discrete commands (DCs) to PWR are routed through the CCS, whether they originate as ground commands or as stored commands in the CCS.

(2) In the event of a rise in battery temperature above $100^\circ F$ an interrupt is triggered in the CCS resulting in an automatic "charger off" command being issued to the appropriate charger.

(3) The CCS will automatically reduce S/C loads if an undesirable power share mode state continues beyond a prescribed time period.

(4) The PWR supplies continuous (unswitched) 2.4 kHz power to CCS.

(5) The PWR supplies uninterrupted 30Vdc bias power to the CCS for use by CCS as switch-closure driver power for all S/C subsystems.

b.   Flight Data Subsystem.

(1)   The PWR provides analog voltage inputs to FDS from transducers within the PWR. These voltages represent, and are proportional to, the various voltage, current, and temperature measurements taken for engineering data. The PWR telemetry structure is shown in Figure II-35.

(2)   FDS is supplied an informational digital serial bit stream from power status channels 1 and 2.

(3)   The FDS is the source for a 4.8 kHz signal primarily used as a frequency reference in the main and standby 2.4 kHz inverters.

c.   Attitude Control Subsystem.

(1)   The PWR provides 400 Hz, 3 phase, 27.2 Vac rms to the ACS IRU-1 and -2 gyro spin motors through two (redundant) 400 Hz inventers, one inverter for each IRU.

(2)   Setting and resetting of the inverter relays is controlled by ACS only.

(3)   The ACS sun sensor circuit issues a continuous sun gate signal to the share mode detector when the solar array is sun acquired within its dead band of 5.0 $\pm$1.5 degrees.

2.   Performance

The VO-1 and VO-2 PWR operational performance through the 15.5-month primary mission has been almost completely normal. The only outstanding anomally occurred on VO-2 when 400 Hz inverter-A ceased operating within seconds following the separation of VL-2. Both PWRs provided all the electrical power needs of both VLs prior to separation and the VOs throughout the primary mission. All mission planned engineering and science sequences were performed without PWR imposed restrictions.

Spacecraft restrictions were imposed during the VO-1 occultations when both DTRs had to be turned off for fifteen occultation passes near the peak of the occultation season. Battery energy conversation was required during

Power Subsystem Telemetry Structure diagram.

SOLAR SUBPANELS:

E - 105 → VLC
E - 103 → TWTA, XTX
E - 101
E - 077
E - 085
E - 078
E - 086
E - 079
E - 087
E - 080
E - 088
E - 092
E - 104
E - 084

+X I/B, +X O/B
+Y I/B, +Y O/B
-X I/B, -X O/B
-Y I/B, -Y O/B

M B/R   S B/R
E - 111   E - 109   E - 102
400, 3φ   400, 3φ
IRU No. 1   IRU No. 2
DC HEATERS
E - 110   30 VDC
PROP VALVES
MAWD
PYRO
ACE
E - 106

M 2.4 KHz INV   S 2.4 KHz INV

E - 108
E - 107
E - 094
V E - 095
T E - 096
CHARGER A   CHARGER B
E - 098
V E - 099
BATTERY No. 1   BATTERY No. 2
E - 093   E - 097
T E - 100

CCS
PYRO
RFS
IRU
ACE
RRS, RTS
DTR-A, B
VIS A, B
IRTM
MAWD
TMU-A, B
ARTC-1, 2
FDS
MAWD HTRS

ALSO:

E-075 PWR STATUS No. 1	E-082 -Y I/B Voc
E-076 PWR STATUS No. 2	E-083 -Y I/B Iscr
E-006 BAY 10 TEMPERATURE	E-089 -Y O/B Isc
E-007 BAY 12 TEMPERATURE	E-090 -Y O/B Voc
E-081 -Y I/B Isc	E-091 -Y O/B Iscr

Figure II-35.   Power Subsystem Telemetry Structure

that time period due to simultaneous occurrence of Earth and Solar occultations which prevented observation of S/C performance. This precaution was taken to ensure S/C survival should a battery fail and because a single battery could not support an unrestricted load during the peak occultation period.

The performance indicators of both VO PWRs have been nearly identical throughout the primary mission. This trend, developed early in the mission, is seen by a comparison of power signatures recorded one day after the launch of each S/C. The comparison is tabulated in Table II-21. The higher VL input current accounts for the 0.3 A higher S/A current and the 10W higher orbiter power. VL power demands were random due to several thermostatically controlled heater circuits.

A principal indicator of PWR performance is the unregulated bus voltage. This parameter is shown in Figure II-36 for the primary mission period. Approximately 15 days following the launch of VO-2 the unregulated bus voltages were the same. The condition prevailed for the remainder of the primary mission even though the cruise trajectories differed slightly. Unregulated bus voltage limiting provided by the solar array zener diodes started in the time period between October 15 and November 15, 1975. Peak zener diode array power dissipation of approximately 600W occurred near February 1, 1976. The bus voltage after February was influenced primarily by decreasing solar intensity and S/A temperatures. Changing load demands did not affect the bus voltage telemetry indication due to the 0.244V telemetry resolution and the low zener diode impedance. VO-1 batteries supported 14 off-Sun maneuvers (including launch) as compared to four for VO-2 batteries. VO-1 also entered a 37 orbit occultation season during which the batteries reached a 45 percent depth-of-discharge (DOD). The maximum occultation period was 140 minutes.

Battery charge voltages increased 0.2 to 0.5V during the long cruise period at the 0.7 trickle charge rate. Battery discharge voltage degradation of approximately 0.3V near 40 percent DOD was seen at each VO MOI and during the occultation season of VO-1. Pre-launch simulated battery life tests indicated this amount of degradation could be expected. The maximum mission battery DOD was 45.0 percent on VO-1 during the VO-1 occultation season.

Table II-21. Spacecraft Power Signatures

Parameter	Viking 1	Viking 2	Δ
Unreg. bus voltage	43.135	43.132	----
S/A current	9.8	10.1	-0.3A
S/A temperature -Y inbd.	129.1	129.9	-0.8°F
-Y outbd.	128.9	125.1	3.8°F
Orbiter power (less chargers)	384.6	394.9	-10.3W
RFS/XTX current in	2.042	2.070	-0.028A
VLC current in	1.789	2.041	-0.252A
B/R current in	5.085	5.044	0.041A
B/R output power	205.4	205.0	0.40W
2.4 kHz inverter power in	116.6	115.6	1.0W
Reg. heater bus power in	86.0	86.8	-.8W
30 V converter	0.0	0.0	0.0
400 Hz inverter (A & B)	0.0	0.0	0.0
Other loads 30V bias	1.1	1.1	0.0
Red. dc bus diode	1.5	1.5	0.0
Batteries			
Voltage 1	37.323	37.263	0.060V
Voltage 2	37.081	37.087	0.006V
Temp. 1	60.1	59.9	0.2°F
Temp. 2	63.1	62.2	0.9°F
Battery adjacent bay temp.			
Bay 10	62.709	63.002	-0.293°F
Bay 12	67.788	67.410	0.378°F

Maximum S/A loading occurred during the VL separation sequence. The bus load reached a peak of 724W of which the VL was using 270W. The S/A load margin was estimated to be 95 W. This was the closest the VO PWR came to a share mode while the S/C remained at the Sun-acquired attitude. No measurable S/A degradation occurred during the primary mission.
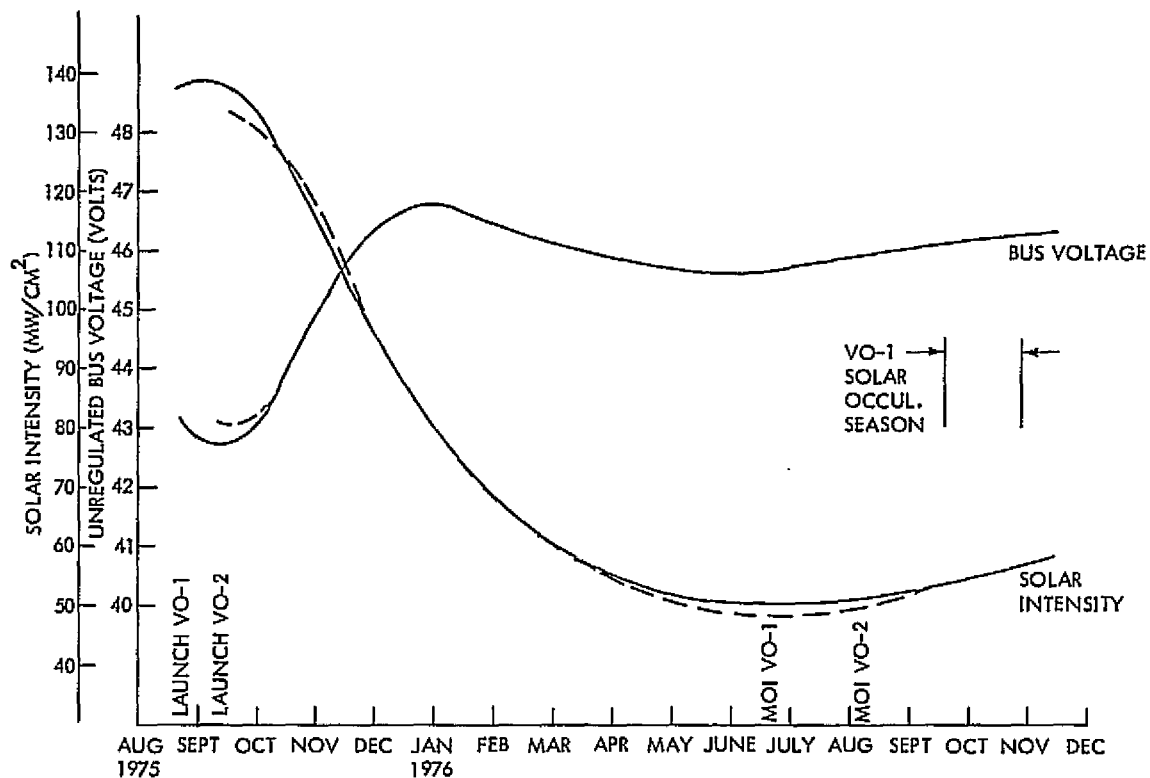
Figure II-36. Unregulated Bus Operating Voltage and Solar Intensity Summary

All power conditioning modules with the exception of VO-2 400 Hz inverter A have performed without any measurable degradation. Each main B/R and 2.4 kHz inverter have operated continuously at approximately 54 percent and 47 percent of their rated capacity for most of the mission. The average power transfer efficiency was between 94 percent and 95 percent for each of these two modules. Peak loading of these modules was 74 percent and 81 percent during several off-Sun science sequences at Mars. The remaining power modules (30V converter and both 400 Hz inverters) were operated as needed at 30 percent and 75 percent of their rated capacities.

a.   Launch. The performance of the PWR for each S/C was normal and as expected during this phase of the mission. All power related activities prior to T-7 minutes were normal for each S/C.

The battery/system voltage profiles are shown in Figures II-37 and II-38 during the period from T-7 to approximately 80 min after launch. Solar acquisition of each S/C was approximately 42 min for VO-1 and 50 min for VO-2. All four batteries on the two S/C discharged less than 6.0 AH each during the T-7 minutes to Sun acquisiton period. Performance of the batteries during the pre-launch and ascent was normal.

The mission profile for VO-1 and -2 required that the S/C enter the Earth's shadow after the ascent and prior to S/C separation from the Centaur second-stage vehicle. Exit from the Earth's shadow occurred 42 minutes after launch for VO-1 and 50 minutes after launch for VO-2. The S/A assumed total S/C power support upon exiting from the Earth's shadow just seconds prior to the sun-gate indication. No share-mode was indicated by the boost converter during the Sun acquisition mode of either S/C. Performance of the PWR parameters through this phase of the launch sequence were normal and as predicted.

The S/A performance for both total power and unregulated dc voltages were as predicted. An unbalance of solar panel currents between inboard and outboard subpanels indicated a non-optimum load sharing of the solar panels on each S/C. This phenomenon was directly attributed to temperature gradients along each solar panel wing and its location relative to the S/C axis. Total solar panel power capabilities were not impacted by the unbalance of solar panel currents.

After Sun acquisition the S/C was conditioned (bio-cap separation, etc.) for Canopus acquisition and near-Earth cruise. Upon completion of Canopus acquisition battery charging was initiated.

b. <u>Cruise.</u> The long cruise phase of each VO mission began approximately five minutes after lift-off when the trans-Mars injection maneuver was completed. VO-1 remained in the cruise phase for 305 days while VO-2's cruise phase lasted 331 days. There were no PWR problems encountered during either S/C cruise period.

S/C activity which influenced VO PWR operation was generally the same throughout the cruise phase. It wasn't until the VO-1 pre-MOI propulsion pressurization sequence that any real differences in the two cruise phases occurred. The unregulated bus load was relatively constant at 430 ±25W. The
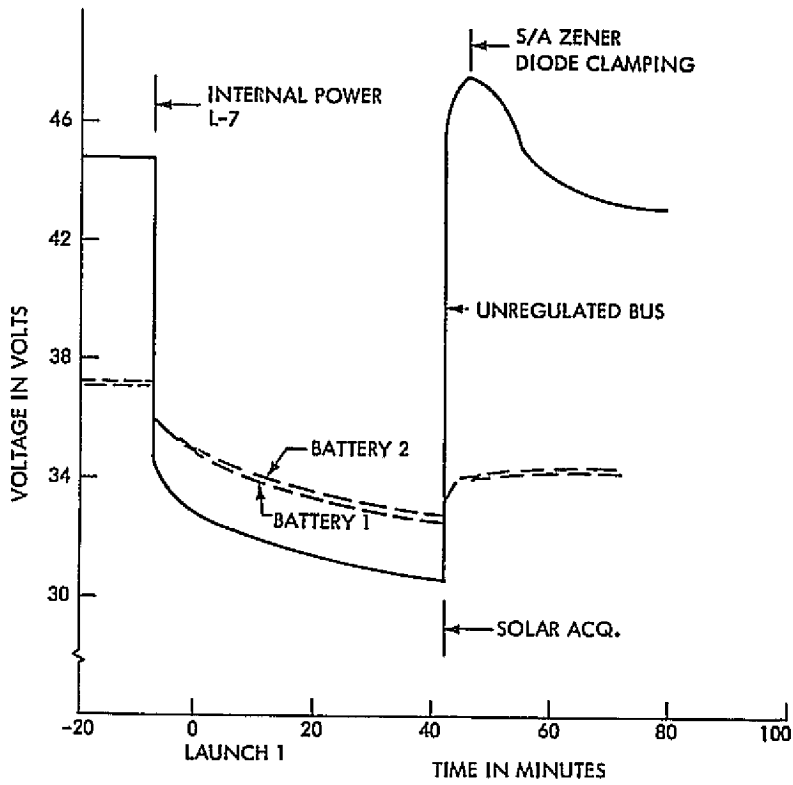
Figure II-37.   VO-1 Power Subsystem Voltages
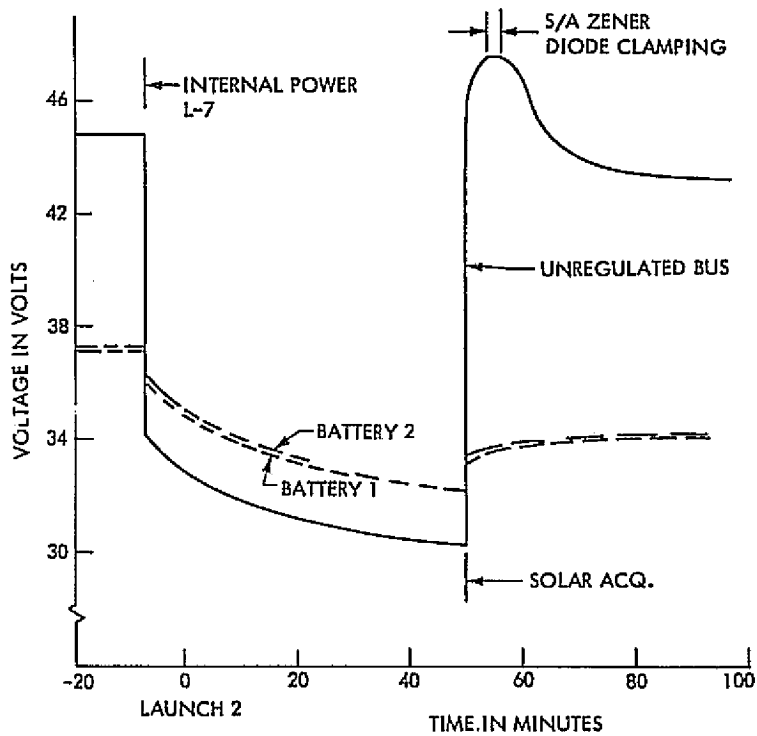
Figure II-38.   VO-2 Power Subsystem Voltages

50W tolerance is due to VLC and MAWD thermal control heater on/off cycles. Both S/C trajectories required minor corrections following the trans-Mars trajectory insertion. The propulsive maneuver attitude of VO-1 at 79.5 deg yaw resulted in a share mode where the batteries supported 40.4 percent of the load and reached a DOD of about 2 percent. VO-2 did not enter a share mode, as expected, at its yaw attitude of 53.2 percent. The estimated S/A maximum power margin at the unregulated bus was 483W while the total bus load 503W, including a 50W charger load (25W/charger) at the trickle charge rate. Other sequences during the cruise phase which required battery support were the approach midcourse maneuvers.

The S/A load sharing improved significantly when the HGA was unlatched on each VO. The effect of the HGA in the (Launch) stowed position on the +X and +Y inboard subpanels was to increase these panel temperatures. The unstowed position placed the HGA in more of a plane with the subpanels and thereby reduced its thermal influence. Both batteries on each S/C were charged at a trickle charge rate (0.7A) for the entire cruise phase. Once in the entire mission the chargers were turned off for a special VL checkout near mid-cruise. It was not necessary to turn the chargers off for this particular sequences. However, the sequence paralleled (simulated) the VL separation sequences and, since it would be repeated for separation the chargers were turned off.

During the long trickle charge period each of the four batteries showed a voltage increase of up to 0.5V. This was expected based on past Mariner flight experience. The increase is attributed to a slow change in the electro-chemical process which involves a slight increase in cadmium crystal size and a balancing of the oxygen gas evolution/recombination process caused by the constant overcharge. The pre-launch trickle charge voltage characteristics are repeated following a discharge exceeding 10 percent DOD.

c.   Mars Orbit Insertion. The MOI sequence for each VO placed the greatest demand on the PWRs since launch. Spacecraft attitude during MOI was 101 deg and 111 deg in the yaw axis for VO-1 and VO-2, respectively. At an

attitude greater than 90 deg yaw the PWR depends totally on battery power and, since the batteries had been in trickle charge since launch, there was some apprehension about the required 40 percent DOD. However, the AMC maneuvers performed just days prior to MOI provided battery discharge data which showed battery performance was normal and as expected following the cruise period. Figures II-39 and II-40 show typical unregulated bus voltage and battery voltage/discharge current profiles seen during the MOI sequences. The end-of-discharge battery voltages were lower by approximately 0.2V from pre-launch data. It was estimated from earlier battery life tests that the long cruise period could cause as much as 0.5V degradation.

Power margins of 121 and 147W existed on the B/R and 2.4 kHz inverter during MOI peak loading. The VL was loading the unregulated bus at approximately 60W, while the TWT and XTX loads were 99W total.

d. Orbital Performance. The demand on the PWR increased considerably during orbital operations. The MAWD and IRTM instruments and both DTRs were turned on following MOI and remained on with few exceptions for the rest of the mission. MAWD and IRTM were turned off only for propulsive maneuvers.
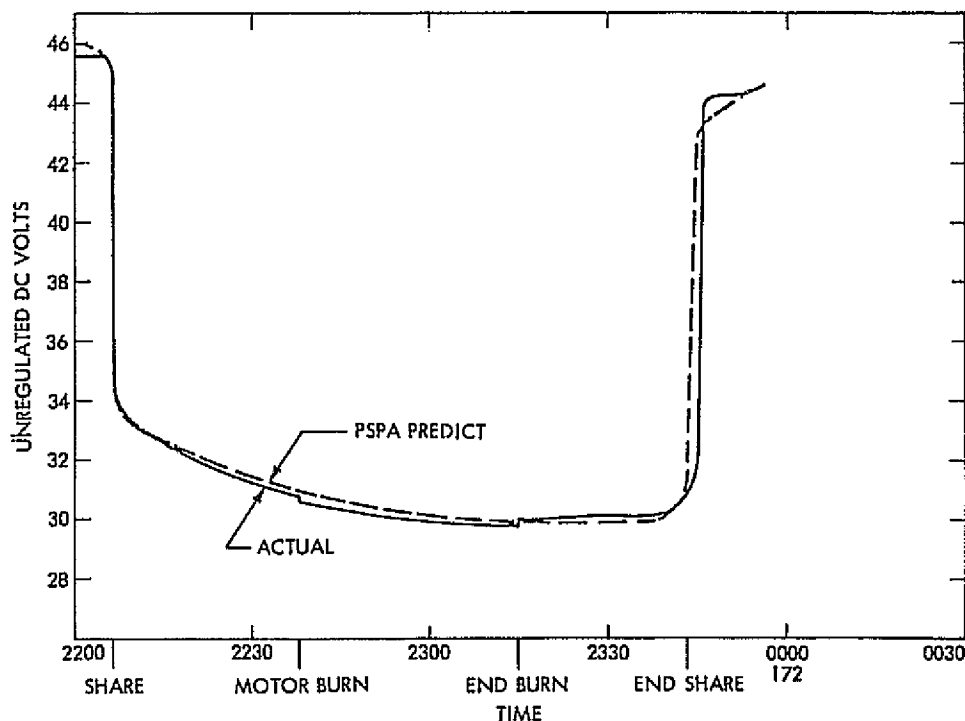
Figure II-39. VO-1 Unregulated Bus Voltage (MOI)
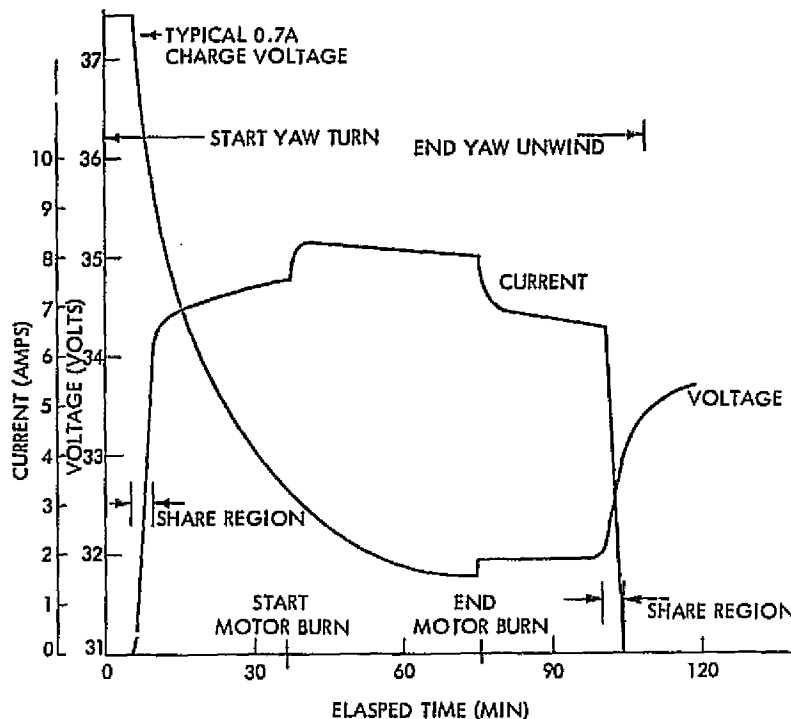
Figure II-40. MOI Typical Battery Discharge Characteristics

Following separation of the Landers, the relay radio and scan platform heaters were also turned on. The VO-2 scan platform heater was not turned on because the thermal influence of the aft-bioshield remained along with the aft-bioshield. The PROP check valve heaters were turned on prior to MOI.

The orbital power demand on the unregulated bus increased only 20W over the cruise loading of 450W. This power increase is small since the IRTM, MAWD, and DTR instruments have replacement heaters which were on during the cruise phase. The average bus load dropped to 425 ±15W upon separation of the VLs.

PWR performance margins during orbital operations were adequate to support all Sun-line science and relay radio sequences without entering a share mode condition. Power margins remained adequate even during periapsis passes where the S/A maximum power capability was reduced by as much as 90W due to increased solar panel temperatures.

The S/A maximum power capability at the unregulated bus is shown in Figure II-41. During orbital operations the maximum unregulated bus load, including high-rate battery charging, approached 650W during non-propulsive science sequences. Maximum power loadings on the regulated buses were between 85 and 90 percent of the bus power ratings.

1)   Viking Lander Separation. The VL separation sequence placed the greatest load on the unregulated bus at separation minus 2.75 hours. At that time in the sequence the VL load peaked at 270W and remained there for almost 1.5 hours. The S/A load margin dropped approximately 95W and the unregulated bus voltage dropped almost 0.6V to 45.2V. Pre-separation PWR performance predictions indicated the above power margins existed with both chargers on, and as a result the pre-separation sequence block was changed to allow the chargers to remain on.

At the time of VL-2 separation, 400 Hz inverter-A ceased operating. This was evidenced by reduced power on the redundant 55.2 Vdc bus and decaying gyro motor speed. The failure of the 400 Hz inverter is discussed further in paragraph 3. Automatic safing routines turned 400 Hz inverter-B on within
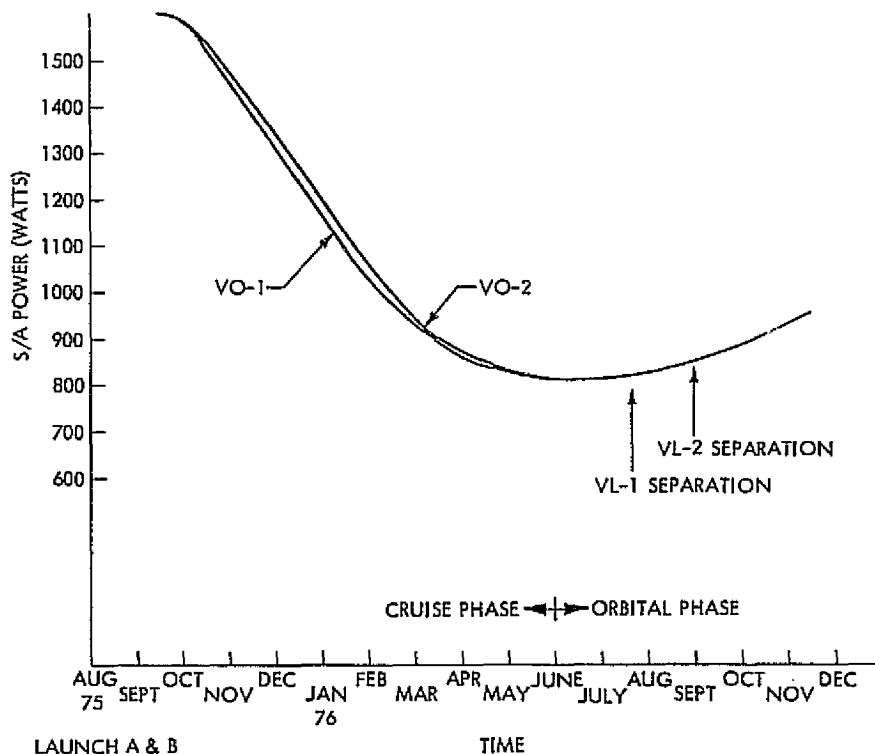
Figure II-41. Solar Array Maximum Power at Unregulated Bus

minutes of the failure. Inverter B has remained on since separation, and no attempts have been made to test inverter A.

2) <u>Occultation Season.</u> VO-1 entered a 37-orbit occultation season, 396 days after launch, on September 18, 1976. The occultation period reached a maximum of 2.3 hours, causing battery DOD to peak at 45 percent. Battery performance was normal throughout the occultation season. The minimum battery voltage was 31.25 V @ 0.7A and 45 percent DOD. The unregulated bus voltage never dropped below 29.25V. A summary of the battery DOD during the occultation season is shown in Figure II-42. The change in battery DOD, as seen at occultation 17, was a result of reducing S/C loads for safety reasons. Earth occultations prevented determination of S/C operations during peak solar occultations, so a survival power mode was adopted for 15 of the occultations.

e. <u>Predictions</u>. PWR performance for proposed sequences was predicted using the Power Subsystem Performance Analysis (PSPA) computer program developed for the Viking program. PSPA was used to predict profiles of the S/A and zener diode characteristics, battery discharge rates, temperature, and DOD
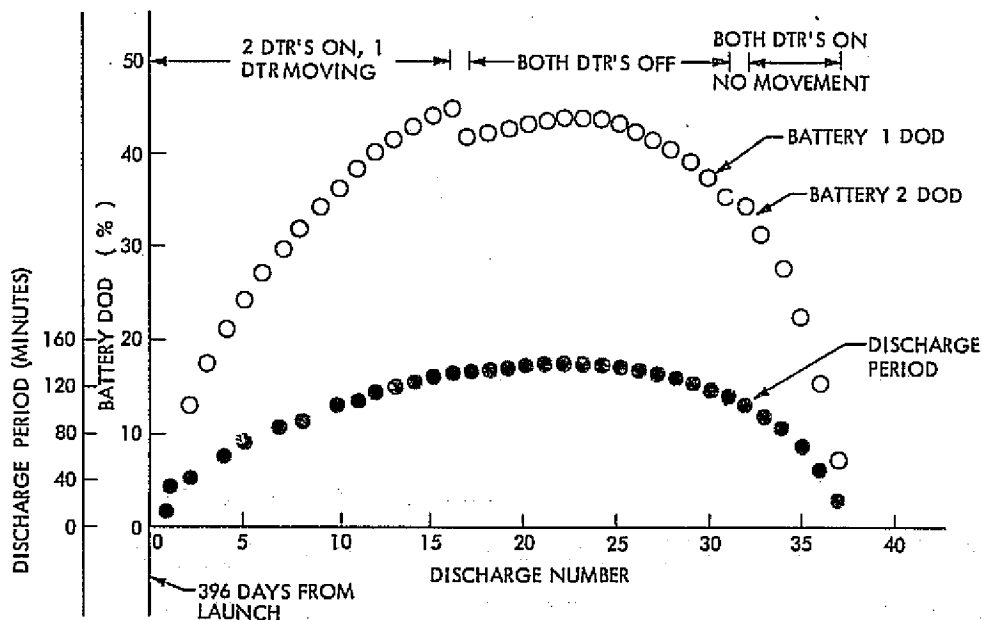
Figure II-42. VO-1 Occultation Season No. 1

and load margins on the unregulated and regulated power buses. It was also used to predict PWR share modes and power margins on the regulated and unregulated load buses. The predictions were within 2 percent of actuals.

Two principle performance parameters predicted by PSPA are the unregulated bus voltage and battery DOD. With the knowledge of these two parameters a S/C sequence could be easily evaluated for overall acceptability. When a particular sequence, such as MOI, was reviewed in terms of S/C survival should an anomaly occur, special PSPA supported analyses were easily made. The only sequences that were altered due to special anomaly reviews which were supported by PSPA were those which involved simultaneous solar and Earth occultations during peak solar occultation periods. PSPA predicted that a single battery could not support a standard power loading. By varying the load and running PSPA, a set of load profiles was developed from which acceptable S/C sequences could be generated to limit battery DOD and assure S/C survival in the event of a battery failure.

PSPA predicts have been used to evaluate PWR performance for both S/C launches, each propulsive or non-propulsive maneuver when applicable, VL pre-separation sequences, and occultation sequences. The VL Bioshield Assembly (BPA) power regulators did not have to be turned off for any VO sequence (as planned prior to launch) based on PSPA predicts. All battery charge times were computed based on DODs predicted by PSPA.

3. Anomalies

The failure of 400 Hz inverter-A on VO-2 was the only failure experienced by either VO during the primary mission, relative to the PWR.

Anomalies were investigated and were fully explained to be normal performance or characteristic of the PWR operation. The following paragraphs briefly discuss some of the anomalies.

a. <u>Battery Charging.</u> The original design feature of the chargers was to automatically transfer from high or medium charge to low charge rate when battery voltage reached 38.25 ±0.25V or battery temperature reached 85 ±3°F. This was never implemented during flight. It was found early in the S/C flight

test program that premature charge rate switchover via an automatic PWR rate low-rate charge command would occur if the battery terminal voltage was near its trip point and a relay closure command was issued by CCS. Also, if the command issued by CCS was in the same command matrix as the low rate charge commands, additional undesirable commands would be issued. The problem manifests itself in the design of the command matrix where all the command sinks are in parallel, causing a common intercept at four points instead of two when two simultaneous source signals are present (one issued by PWR and one by CCS). All battery recharging was timed to low rate with CCS issuing the low-rate charge commands.

b.   Solar Array Load Sharing.   Following launch, after VO-1 left the Earth's shadow, a large variation of the eight solar subpanel currents was noted. The highest-to-lowest subpanel current differential was 1.26A, and the difference between subpanels on a common axis ranged from 0.91 to 1.1A. This was initially attributed to the large thermal gradients (16°C) along the four ten-foot solar panel axes, later confirmed by a detailed analysis of the S/A operating in the near-Earth environment. The PSPA computer program was used to support the investigation.

The subpanel load sharing improved as the solar intensity diminished and S/A temperatures dropped. Marked improvements in load sharing occurred following unstowing of the HGA near Earth and separation of the aft-bioshield at Mars.

c.   30V Converter Gimbal Load Activity.   A fluctuating input current was seen at the B/R and 30V converters following several 30V converter turn-ons during the primary mission. Since this phenomenon was not observed following every 30V converter turn-on, it was investigated.

When the 30V converters are turned on, power is automatically provided to the gimbal drive motors for engine positioning. Normally, pre-aim commands are sent to the gimbals shortly after power is applied. If the commanded positions are within ±0.05 deg of the present position, no power is consumed. However, if the above condition is not satisfied or the engine nozzle position changes within the 0.05 deg deadband due to torques during a maneuver, the position control servo system will reposition the engine. The position controller is a bang-bang servo system with derived rate type feedback for stability and, therefore, the engine repositioning takes place with short drive pulses.

The pulsing phenomena was observed on both VO-1 and VO-2 during system tests due to gravity induced loads on the gimballed engines. While in flight, the pulsing was random due to varying conditions of induced torque during maneuvers or repositioning.

d.   400 Hz Inverter. At or within seconds after the VO-2/VL-2 separation event there was a failure onboard the Orbiter which either was a short in the 400 Hz inverter-A gyro power supply or a filure at the output that caused such a short. High solar panel currents indicated the short's presence, and subsequent power telemetry indicated that the input current to the 400 Hz inverter then went to zero as a result of blowing the 2.0A fuses. Loss of the 400 Hz inverter caused the gyros to run down. Without gyro error signals, the roll attitude began to drift, and underdamped oscillations in the pitch and yaw limit cycles began to build up.

Following the loss of 400 Hz inverter-A, excessive gas jet firings resulted from the underdamped S/C oscillations. This excessive activity caused an internal spin-up detector in ACE-1 to exceed its threshold, thus generating an ACE changeover interrupt to the onboard computer (CCS). The CCS response to the interrupt switched attitude control to ACE-2, and ACE-2 eventually selected 400 Hz inverter B. Attitude control was eventually returned to ACE-1 via ground command but inverter B was never turned off.   .

Post-failure lab tests on a 400 Hz inverter and associated analysis indicated that the internal short was in one of three possible diodes or one of six possible switching transistors. Because of the coincidence with Lander separation, the actual failure cannot be termed strictly "random." However, the assumed separation shock environment at the inverter, being comparatively mild, cannot account for the failure either. Other causes that were postulated appeared even less likely. In particular, structural margins and path geometry argue against fragmentation/penetration by separation hardware. Of even lower likelihood is the possibility of static discharge between the separated Lander and Orbiter. This possibility was dropped after it was determined that no significant voltage differences could be generated by any mechanisms known to exist in the spacecraft's environment.

Load induced failure was also considered, but difficulties existed with this failure mechanism due to the very fast burn-out characteristics of the gyro flex-leads and the absence of back-EMF modes. Of course, since mechanisms of secondary breakdown are not well understood, and every transistor can be postulated to have unique breakdown sensitivities, a theory could be postulated that two gyro flex-leads shorted together--for even the infinitesimal period before they burned out--and caused a switching transistor to short, due to secondary breakdown. But the low shock environment seen by the IRU argues against the two flex-leads shorting together.

While is virtually certain that an internal short developed in the 400 Hz inverter, it cannot be stated with any significant degree of confidence what the prime cause was for that short. The failure mechanism--weak part, loose particle in the part, a flex-lead short (leading to secondary breakdown)-- is unknown.

SECTION III

TEMPERATURE CONTROL AND MECHANICAL SUBSYSTEMS

A.   INTRODUCTION

1.   Temperature Control

The VO temperature control was designed to accommodate greatly varying thermal environments including system test, on-pad checkout, near-Earth to at-Mars solar intensities as well as inflight configuration variations. During flight, the spacecraft is nominally Sun oriented. Transient conditions result from off-sunline maneuvers and propulsion burns.

Variations of the temperature control techniques proven on past Mariner-type spacecraft were utilized in the VO temperature control design. In addition, solar energy controllers (SECs) — a new temperature control device — were used for the first time. Individually commanded, four of these devices regulate solar energy into the propulsion module for temperature control purposes.

The VO temperature control was designed to perform with the aft-bioshield present through VL separation and without it for the balance of the mission. This was accomplished by thermally isolating the Orbiter from the Lander. The aft-bioshield is covered with a multi-layer insulation blanket to eliminate radiative coupling and the VL adapter truss tubes have low conductive titanium end fittings at the VO attach points to minimize conductive losses.

2.   Mechanical Devices Subsystem

Mechanical devices are used on the VO to perform the required functions of separation, release, deployment and latch, and energy dissipation. More than 70 devices must function properly to permit nominal mission operations to occur.

3.   Structure Subsystem

The Structure Subsystem's primary function was to integrate the spacecraft systems structurally by providing efficient load paths and alignment for all flight equipment.

4.   Cabling Subsystem

The Cabling Subsystem provided the necessary electrical interconnections between all VO equipment, and interfaced with the VLC and launch vehicle.

B. TEMPERATURE CONTROL

1. Description

The Orbiter temperature control design utilizes both active and passive techniques to create a thermally favorable environment. Louvers with bimetallic actuators, solar energy controllers, and controllable electrical heaters are examples of active control. Paints, coatings, material finishes, thermal capacitance and conductance, multilayer insulation blankets, and sun shades represent the passive techniques employed. Except for the heaters, the active components are characterized by having moving parts, whereas the passive technique relies on a thermal property of the material, such as its specific heat, thermal conductivity, infrared emittance, and solar absorptance.

During flight, conduction and radiation are the primary heat transfer modes. Generally, conduction is utilized to distribute and transfer energy to a radiating surface. However, convective cooling by propellants is utilized to thermally stabilize the engine during firings of long duration. Also, during the long burns, the flow of propellants effectively cool the propellant tank domes near the engine, and the expansion of the propellant pressurant (helium) cools the components through which it passes and locally helps to lessen the impact of thermal soakback following the firings.

Off-Sunline maneuvers and solar occultations typify transient conditions experienced by the spacecraft. The thermal capacitance of the VO primarily keeps temperatures acceptable during these short time periods (of less than four hours). Except for these periods, the spacecraft is always Sun oriented.

Thermally, the VO is visualized as comprising four assemblies: the appendages, bus, propulsion module, and scan platform. The appendages and scan platform are thermally decoupled from the bus and the propulsion module. There is a strong thermal coupling between the propulsion module and bus. The scan platform temperatures are influenced by the solar panels and relay atenna when articulated to those vicinities. The VL aft-bioshield affects only the temperatures of the scan platform and certain appendage items. Because of the VL, the scan platform was mounted on the side of the bus, and some Sun-illuminated scan platform positions result.

a.   Appendages.   Thermally, appendage items are those elements not included as part of the bus, propulsion module, or scan platform.   Generally, those items are passively controlled and thermally decoupled from the bus.   As a result, their temperature sometimes varied over a large range during the primary mission.

Generally, an appendage is not a single item but is an assembly of many different elements having different functions and different temperature requirements.   In addition, these different elements view different environments, i.e., Sun, shade, radiating surfaces, both Sun and shade as might occur during a maneuver, etc.   As a result, it is sometimes necessary to apply several different temperature control techniques to an appendage assembly.   Table II-22 is a brief summary of the appendage temperature control design and illustrates the variation in predominately passive temperature control techniques employed.   The attitude control jet assembly is the only appendage element with an active commandable heater.

Table II-22.   Appendage Temperature Control Technique Summary

Appendage Item	Temperature Control Technique		
	Multilayer Blanket	Surface Finish	Heaters
HGA Assy*	X	Polished and White Paint	4 W per actuator
Solar Panel Assy*	X	Polished and White Paint	
LGA Assy	X	Polished and White Paint	
Relay Antenna Assy		Polished, Gold, Black and White Paint	
Attitude Control Assy		Polished and White Paint	2 W per jet assy (commandable off/on)
Sun Gate/Cruise Sun Sensor*	X		
Canopus Tracker*	X		
Separation Devices	X		
*Temperature is monitored during flight.			

b.   Bus.   The bus is that part of the Orbiter where most of the
electronics are housed and, as a result, where the majority of the energy is
dissipated.   As indicated in Table II-23, the bus is divided into 16 bays.   A
bay is that volume (typically containing electronic equipment) bounded by the
upper and lower rings, the outboard shearplate, and an open inboard face which
views the propulsion module.   Depending upon the desired temperature range and
heat generating characteristics of each bay over the mission profile, the white
painted shearplate is exposed (large constant energy dissipation), louvered
(variable energy dissipation), or blanketed (none or very small energy
dissipation).

Table II-23.   Bus Temperature Control Features

Bay (Subsystem) See Fig. II-43	Shearplate Side	Propulsion Module Side	Louver Opening Range °F	Replacement Heater Power W
1 (RFS, MDS, XTX)	Louvered	Open	55 to 80	0
2 (CCS)	Louvered	Open	55 to 80	0
3 (ACS)	MLI Blanket	Open	N/A	0
4 (DSS)	Louvered	Open	55 to 80	10
5 (ACE, ARTC)	Louvered	Open	65 to 90	0
6 (FDS)	Louvered	Open	55 to 80	0
7 (Scan Plat. Struc.)	MLI Blanket	Open	N/A	0
8 (SCI)	Louvered	Open	55 to 80	10
9 (BAT)	Louvered	Shielded	45 to 70	0
10 (PWR)	Louvered	Open	55 to 80	0
11 (ACS)	MLI Blanket	Open	N/A	0
12 (PWR)	Louvered	Open	55 to 80	0
13 (BAT)	Louvered	Shielded	45 to 70	0
14 (DSS)	Louvered	Open	55 to 80	10
15 (PYRO, RRS, RSS)	Louvered/ MLI Blanket	Open	55 to 80	4 (Continuous)
16 (RFS)	Open	Open	N/A	16 or 64

The bus rings are more than 90 percent blanketed. The inboard face of the bus is open to the propulsion module except for the battery bays, which are blanketed to suppress thermal coupling with the propulsion module. Polished aluminum shields are used to cover the outboard bus corners and the open areas between adjacent bays. As required, heaters automatically replace normal electrical heat dissipation when a subsystem is turned off. Significant temperature control features about each bay are shown in Table II-23. Except for Bay 7, the temperature of every bay is monitored.

Typical of Mariner- and Viking-type spacecraft is the large variation in bus power dissipation. 38 different power profiles were identified for the Orbiter, and the power in a particular bay can vary by more than 100 percent. Louvers dampen the temperature excursions caused by these power variations. The louvers are attached to the outboard white-painted side of the shearplate, and electronics are thermally coupled to the inboard side. As the shearplate temperature increases above the initial opening temperature, the louvers are driven open by bimetallic temperature-sensitive blade actuators. At the louver full-open position, the shearplate becomes a very effective radiator. The low emittance aluminum louvers when closed are an effective radiation shield. The louver actuation temperature range is tailored to maintain each bay within required temperature limits. There are eleven full and one half-louver assemblies on the bus. Full-closed to full-open requires approximately a 25°F rise in shear plate temperature. Table II-23 gives the approximate louver full-close to full-open temperature range.

c.   Propulsion Module. Both active and passive temperature control techniques were employed in the propulsion module. As illustrated in Figure II-44, the main body of the propulsion module is surrounded by an insulated enclosure created by the multilayer propulsion module blanket, bus blanket, and bus. Gradients and temperatures within this enclosure are controlled by introducing solar energy through the four commandable SECs.

Energy from the SEC is initially reflected off the white painted portion of the tankage assembly and pressurant control assembly, and re-reflected throughout the enclosure. The thrust plate and propellant isolation assemblies had been painted white to help diffuse the solar energy. The outboard portion
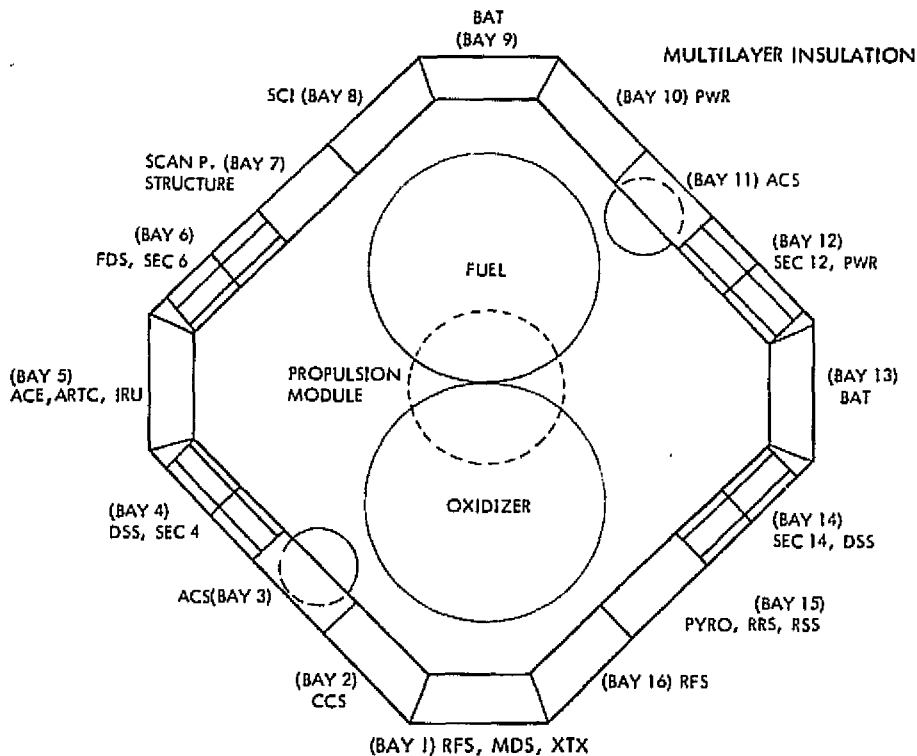
Figure II-43.   Orbiter Bus
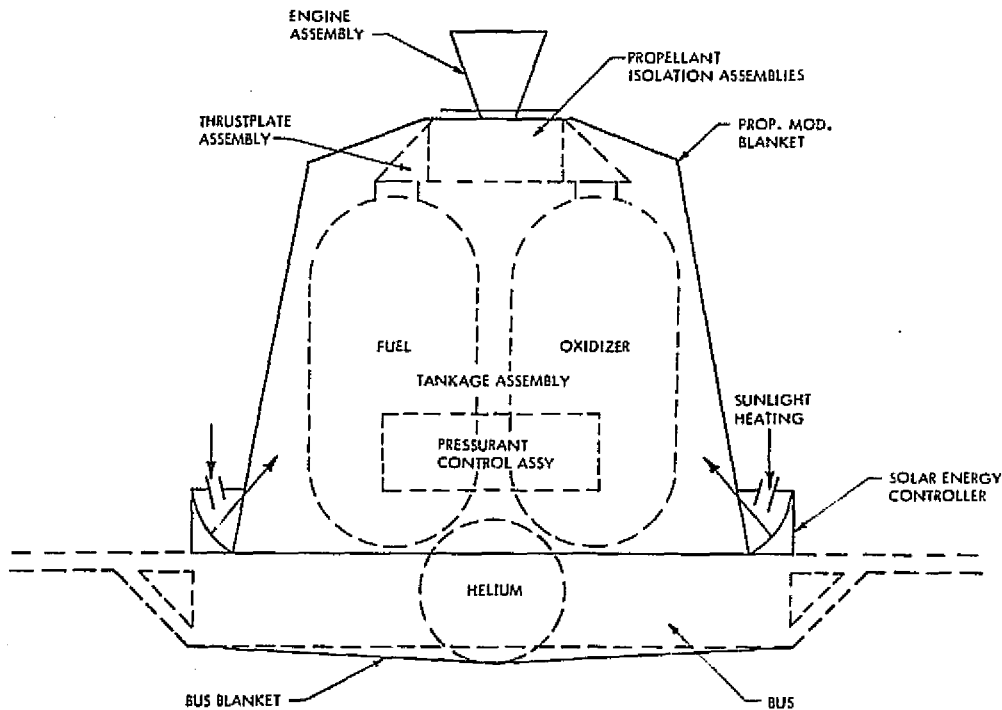
Figure II-44.   Propulsion Module Temperature Control

of the pressurant control assembly has a multilayer blanket to prevent overheating near Earth.

Except for the convective cooling during engine burns, the engine assembly is passively temperature controlled. Various optical finishes were utilized to couple the engine assembly to the rest of the propulsion module and to divert to space the large continuous solar input to the nozzle. (Except for maneuvers, the nozzle exit plane is always normal to the Sun.)

Temperatures are monitored throughout the propulsion module. A 0.25 W heater applied heat at each pressurant check valve to keep liquid propellant away from this interface, thus reducing the possibility of diffusion of the pro-pellants into the common pressurant system.

The SEC is a new temperature control device and is schematically repre-sented in Figure II-45. On command, louver blades are positioned to permit the desired amount of solar energy to be reflected into the propulsion module where additional dispersion of the energy takes place by multiple reflections off of surfaces, given high solar reflective finishes. (Thermally, the propulsion
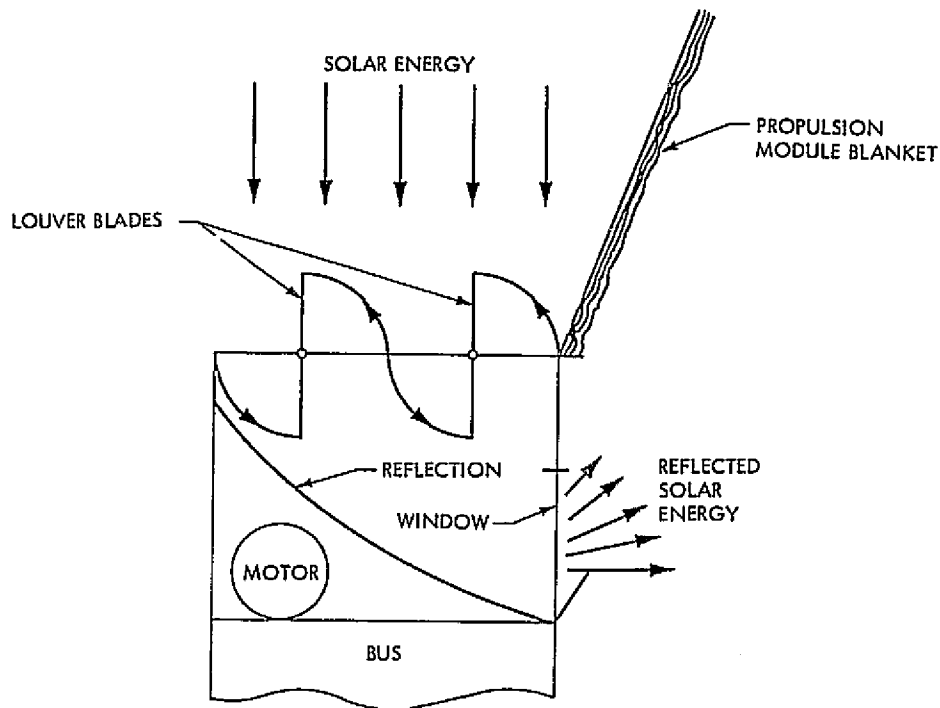
Figure II-45. Solar Energy Controller

module is like a white room with white furniture.) Command actuation gives the SECs the versatility required for meeting the temperature requirements of the propulsion module. For example, during launch the SECs were open 20 deg to increase the VO air venting area. After launch, prior to pressurizing the tanks for the near-Earth midcourse maneuver, the SECs introduced 80 to 100 W continuously for several days to warm the propellants to the pressurizing temperature. Following the midcourse correction burns, the SECs were reopened to heat the propellant lines between the bipropellant valve and solenoid latch valves prior to closing the latch valves to assure the lines would not overpressurize during cruise. The SECs were gradually opened as the spacecraft approached Mars but closed at Mars to lessen the thermal soakback following the long orbit-insertion burn. In orbit the blade positions are adjusted periodically to maintain the propulsion module temperatures. As required, additional energy is temporarily introduced to lock up the propellant lines.

d.   Scan Platform. The Mars Atmospheric Water Detector (MAWD), the Infrared Thermal Mapper (IRTM), and the Visual Imaging Subsystem (VIS) are thermally coupled together by the scan platform structure, as illustrated in Figure II-46. Louvers, like those used on the bus bays, are mounted opposite the camera electronics. Heaters automatically come on to replace the electronics' dissipated power when the instruments are turned off. Additional heaters on the structure are commanded on as required. For the most part, all non-functional surfaces (view ports, etc.) were covered with multilayer insulation blankets.

The MAWD has two servo-controlled heaters. One maintains the optics at a near constant temperature. The other, in combination with a radiator, maintains the detector at a low, near constant temperature (-76°F). The white painted radiator has a commandable heater which prevents condensing of outgassing contaminants.

A shadow shield to partially shade the scan platform extended outboard of Bays 6, 7 and 8. The platform support structure attached to the bus at Bay 7. Temperatures were monitored in several locations on each of the science instruments.
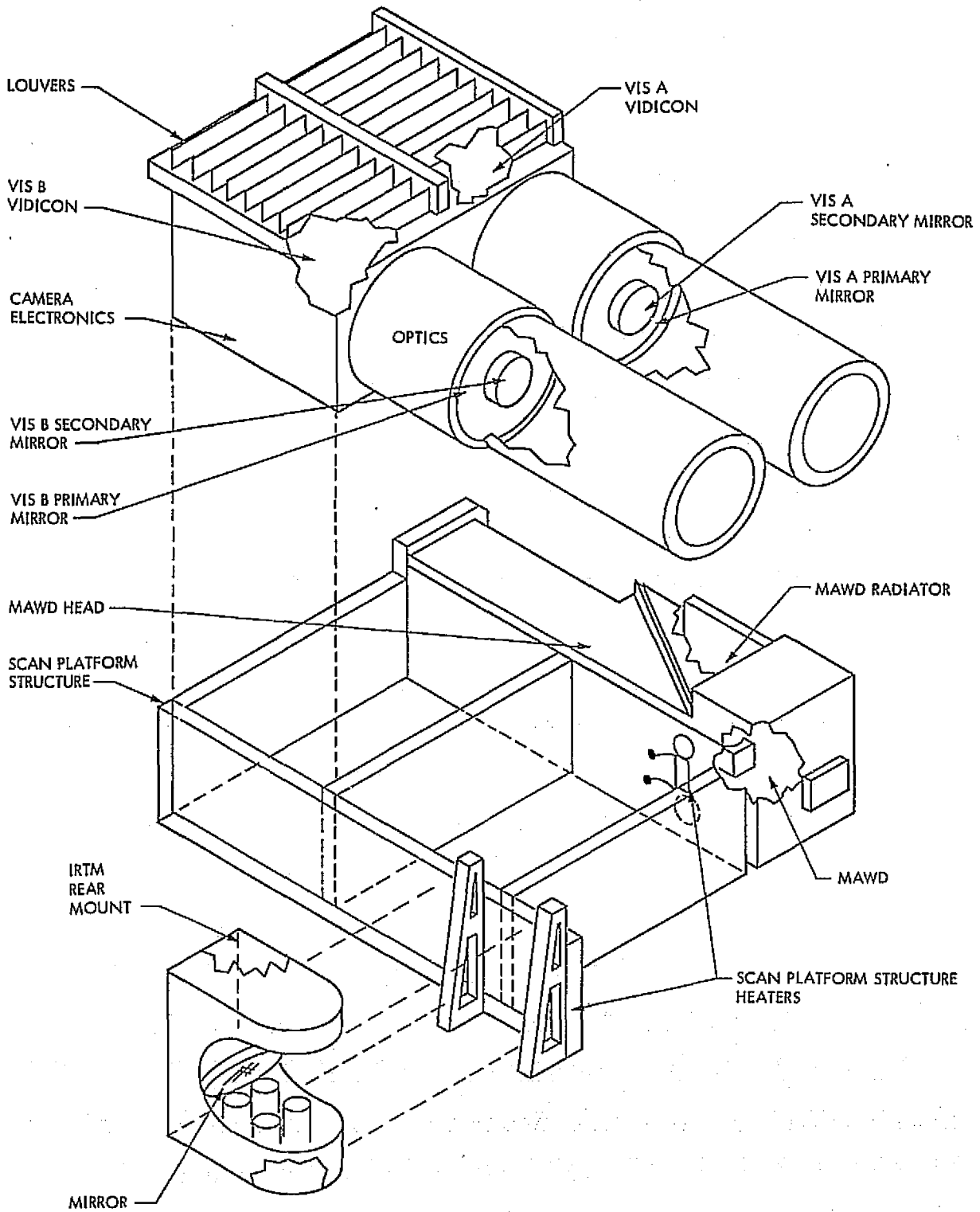
Figure II-46. Scan Platform

2.   Performance

The temperature control design performed its function extremely well. There were no abnormalities, and temperatures have been well within the required limits. To understand the temperature control performance implies an appreciation of the environmental extremes to which a Mars-bound spacecraft is exposed.

Checking out a fully assembled Orbiter at Cape Kennedy required power-on for periods of up to 16 hours. In the free convective environment on an assembly building, the VO temperatures approached the upper limits, and only by selectively managing the power to various subsystems was it possible to keep temperatures below the upper allowable limits. The same checkout on the launch vehicle was performed with no problem because of the shroud cooling system. However, the shroud cooling resulted in propellant temperatures so low that after-launch pressurizing of the Orbiter propellant tanks could not be accomplished until significant warming of the propellants had occurred. The SECs reduced the warming time to days rather than weeks, which enabled a more efficient mid-course maneuver.

Normally, a spacecraft is Sun oriented. However, off-Sunline maneuvers must be performed routinely enroute to Mars. Because of radio contact requirements, the off-Sun position is rarely the same, and any portion of the spacecraft can be temporarily subjected to the Sun. The Sun's intensity decreases 64 percent from Earth to Mars. At Mars, the spacecraft can be in the shadow of the planet (no solar) for up to four hours, and planetary heating of the spacecraft as it daily approaches the planet is not insignificant.

Most of the engine burns were of short duration. However, the burn for Mars orbit insertion was approximately 40 minutes, and the resulting thermal soakback was large. The effect was significantly reduced by temporarily decreasing, from 60 to 0 W, the energy input from the solar energy controllers.

The Orbiter temperature control design has performed successfully under all of these environmental conditions. A summary of this performance is given in Table II-24, which presents the requirements and the actual flight temperatures for several points in the primary mission.

Table II-24. Temperature Control Summary

Flight Temperature Sensor	Earth Cruise		Cruise Operating Requirements		Mars Orbit Aphelion		Mars Orbit Perihelion**		Solar Occul (Min)	Short Term Transient Requirements <4 hrs		Mars Orbit Insertion (Max)	
	VO-1 °F	VO-2 °F	Min °F	Max °F	VO-1 °F	VO-2 °F	VO-1 °F	VO-2 °F	VO-1 °F	Min °F	Max °F	VO-1 °F	VO-2 °F
BUS													
Bay 1 (RFS/MDS)	***	***	45	90	***	***	***	***	***	41	122	65	65
Receiver VCO (Bay 1)	69	71	50	110	68	69	69	70	66	-	-	69	70
X Band Transmitter (Bay 1)	64	63	50	95	88	85	88	86	84	32	122	88	86
Bay 2 (CCS)	73	74	55	110	67	67	67	67	64	50	110	68	68
A/C N2 Bottle (Bay 3)	71	74	41	122	62	60	61	60	59	41	122	63	63
Bay 4 (DTR-A)	67	68	50	90	64	61	63	61	60	50	104	64	66
Bay 5 (ACS/ARTC)	72	75	55	92	68	75*	65	66	70	55	92	73	74
Accelerometer (Bay 5)	69	70	55	110	63	76*	62	61	73	55	110	76	78
Roll Gyro (Bay 5)	69	71	55	167	64	100*	62	63	98	30	167	101	103
Bay 6 (FDS)	77	79	41	104	71	70	70	70	69	41	122	73	74
Bay 8 (VIS/MAWD)	72	73	41	113	62	60	62	62	60	41	122	63	65
Battery 1 (Bay 9)	62	61	41	70	59	56	59	57	61	35	91	60	59
Bay 10	65	65	50	104	61	60	60	60	67	41	122	64	67
A/C N2 Bottle (Bay 11)	68	71	41	122	59	58	58	57	59	41	122	61	62
Bay 12 (Power)	67	69	50	104	64	63	62	63	65	41	122	67	67
Battery 2 (Bay 13)	64	63	41	70	61	58	60	58	60	25	91	62	61
Bay 14 (DTR-B)	66	66	50	90	63	61	62	60	66	50	104	64	67
Bay 15 (PYRO/RRS/RTS)	65	66	50	95	59	58	58	58	***	50	95	60	59
Relay Radio Subs. (Bay 15)	***	***	45	90	***	***	***	***	59	50	95	57	60
Bay 16 (RFS)	***	***	45	90	***	***	***	***	***	41	122	***	***
Traveling Wave Tube (Bay 16)	111	109	45	149	100	99	102	100	97	45	149	100	99
Auxiliary Oscillator (Bay 16)	75	74	50	110	67	67	68	68	65	45	149	67	67
PROPULSION MODULE													
Oxidize Check Valve	82	75	55	90	-	64	70	70	***	30	90	***	***
Engine Injector	***	***	30	200	77	***	***	***	***	30	400	296	293
Engine Valve	128	128	30	150	74	73	84	84	***	30	320	235	227
Fuel Line	***	***	30	105	67	***	***	***	***	-	-	74	67
Fuel Tank T1	84	78	55	100	67	65	65	65	62	30	120	68	67
Fuel Tank T2	74	72	55	100	63	63	61	62	60	30	120	58	66
Oxidizer Line	84	89	30	105	68	67	64	64	***	-	-	74	69
Oxidizer Tank T1	86	85	55	100	68	67	66	66	63	30	120	63	68
Oxidizer Tank T2	74	74	55	100	65	64	63	63	63	30	120	57	66
Helium Tank	72	74	35	100	63	62	60	60	61	30	100	65	63
SCAN PLATFORM													
VIS													
VIS 1 Vidicon	66	65	50	80	65	64	65	64	66	20	90	65	65
VIS 1 Primary Mirror	***	***	40	80	***	***	***	***	***	20	90	***	***
VIS 1 Secondary Mirror	60	59	40	80	57	56	58	57	59	20	90	61	57
VIS 2 Vidicon	65	65	50	80	64	63	63	63	64	20	90	63	64
VIS 2 Primary Mirror	***	***	40	80	***	***	***	***	***	20	90	***	***
VIS 2 Secondary Mirror	58	58	40	80	55	55	55	56	56	20	90	57	56
IRTM													
Base Plate	41	42	0	60	33	33	35	37	33	-14	60	34	35
Replacement Heater	***	***	0	60	***	***	***	***	37	-14	60	***	***
Mount	***	***	0	60	***	***	***	***	38	-14	60	***	***
MAWD													
MAWD Head	70	67	50	90	69	67	69	67	69	50	90	69	67
MAWD Radiator Plate	52	54	-150	-76	-128	-119	-111	-112	-132	-150	-96	-106	-103
MAWD Detector	***	***	-112	-76	***	***	***	***	***	-112	-76	***	***
APPENDAGES													
-Y Outboard Subpanel (Backside)	139	130	-30	190	0	-7	43	36	-251	-310	200	-142	-112
-Y Inboard Subpanel (Backside)	129	125	-30	190	-10	-15	40	35	-251	-310	200	-153	-115
Canopus Tracker (Bay 12)	65	67	20	100	57	56	56	56	56	20	115	60	62
Cruise Sun Sensor	91	91	10	120	27	28	45	46	-13	-40	120	27	33
Scan Platform Clock Actuator	55	59	14	122	40	41	41	43	37	14	122	41	47
High Gain Antenna Actuator	79	85	14	122	61	62	75	77	34	-10	122	61	61

*IRU on continuously since Lander separation - a nonstandard condition.
**Predicted from cruise temperatures for the same heliocentric distance as Mars Perihelion.
***These measurements are not available in the major format or are back-up sensors.

VO-1 and VO-2 temperatures, while not identical, were very nearly so, indicating consistency of the design. An exception is Bay 5, where the VO-2 IRU-2 has been on continuously since VL separation. This condition drives the temperature up from the standard operating mode (IRUs off) which had temperatures very close to those for VO-1.

C.   MECHANICAL DEVICES SUBSYSTEM

1.   Description

The Viking Orbiter Mechanical Devices Subsystem had the responsibility of performing the following mission functions:

(1)   Structurally attach the spacecraft to the spacecraft adapter and, upon command, release and separate the spacecraft from the Centaur and spacecraft adapter assembly.

(2)   Upon Centaur separation, issue electrical signals to four different subsystems or functions to effect separation indications and enable functions.

(3)   Constrain and damp the panels during the launch phase and, upon Centaur separation, unfold the solar panels and latch them in their cruise configuration. During cruise and orbit, damp the solar panels.

(4)   Constrain the relay antenna during the launch phase and, upon Centaur separation, deploy it to the required position.

(5)   Constrain the HGA during the launch phase and release it after spacecraft separation from the Centaur.

(6)   Support and damp the LGA during the launch phase.

(7)   Constrain and support the scan platform during the launch phase and, upon command, release the latching constraint and allow the scan platform freedom of movement.

(8)   Create a variable emittance condition at the VO equipment bay shearplates.

(9)   Allow a commandable amount of solar energy to enter the propulsion module cavity.

(10)   Structurally, attach the VLC and VLC Adapter to the VO and, upon command, release and separate the VLC Adapter and aft-bioshield from the Orbiter.

Each requirement will be discussed in more detail and in the order previously listed because it follows a convenient time line not unlike the mission profile following launch.

a.   Release and Separation Devices. The Viking Spacecraft (Orbiter and Lander) was bolted at four places to the spacecraft adapter using a multiphase high-tensile bolt equipped with a built-in strain gauge to control preload at the joint. The bolt was located on the spacecraft side of the separation interface and a pyrotechnically actuated segmented nut was located on the adapter side of the interface. Each nut and bolt pair was torqued to a preload (as read by a strain gauge) of 11,600 lbs tension. Upon a command issued by Centaur, the release nuts pyrotechnic devices were fired, the nut released and the bolt ejected into a bolt catcher. Separation was effected by four separation springs located adjacent to the release nuts giving a relative velocity between the spacecraft and the Centaur and adapter assembly. Identical release and similar separation springs were used to separate the VLC Adapter from the Orbiter.

b.   Pyrotechnic Arming Switches (PAS). During the separation event, the two PAS switches were actuated by relative motion of about 0.3 in. between the VO and the spacecraft adapter, and signals issued to the following areas:

(1)   PYRO Arming Power

(2)   MAWD Unlatch Enable

(3)   Separation Indication to FDS

(4)   Separation Indication to CCS

c.   Low-Gain Antenna Dampers. During the launch phase, the LGA was supported and damped by two LGA dampers of a modified M'71 design located such that their axes are about 90 deg to each other and attached to the antenna at about a third of the distance up from its base. The center-line of each damper intercepts the center-line of the antenna at about a 45 deg angle and extends over the LGA base at the spacecraft separation plane.

d.   Solar Panel Devices. Each solar panel assembly was double folded during launch and held in the launch position by the solar panel flyaway release rod at the outboard hinge and by the tip release latch at the inboard hinge. During launch, the flyaway rod and the panel are allowed to move through lateral

motion in two directions and be damped by three boost dampers attached between the flyaway rod and the spacecraft adapter. During separation, after about 1-1/4 inches of relative motion, the solar panel slides off the end of the fly-away release rod and the panels are then free to deploy. Initial deployment rotation is only about the inboard hinge axis. This rotation continues for 55 deg until the solar panel tip latch at the inboard hinge disengages a cam, allowing the tip latch pin to disengage the solar panel tip. When the tip latch pin is disengaged, the solar panel outboard hinge rotation starts. The outboard hinge rotation takes about 7 sec to complete the 180 deg of rotation and to latch. The outboard panel is completely unfolded and latched before the inboard hinge motion completes its 90 deg of motion and latch. When the solar panels are in the deployed position and latched, the device is then in a configuration to damp the solar panel motions induced by engine firing or scan platform slewing.

e.   Relay Antenna Deployment Device. The relay antenna was folded up next to the back of the outboard +X subpanel during the launch phase. Simultaneous with the panel tip release, the relay antenna is unlatched by relieving the force on a spring-loaded control cable. This control cable pulls a clevis pin and allows the antenna spring strut to deploy the antenna to its required position.

f.   High-Gain Antenna Latch. The HGA was constrained in the stow position during launch by a pin puller which preloads the antenna reflector against two snubbers on the bus. Actuation of the pin puller releases the HGA so that it can be pointed by the two-axis drive actuators.

g.   Scan Platform Latch. During launch the scan platform structure was preloaded against three structural hard points on the bus by a manifolded set of three pneumatic launches. About five days after launch, by command, a pyro-technically actuated valve vents the nitrogen gas in the manifolded latches which releases the preload and allows unlatching to take place. Prior to the unlatch command, the pressure in the system is monitored for leaks by data read out in the engineering telemetry stream.

h.   Louvers. During the cruise and orbit portions of the primary mission, the bus and scan platform temperature control was partly accomplished by the use of louver assemblies. These assemblies are made of highly polished aluminum frame and blades which are actuated by bi-metal actuators. In the open position, a highly emittive surface is exposed to space. In the closed position, the polished blades cover the emittive surface. The start of opening set point temperature is manually adjustable and is selected and set prior to launch. The VO louvers are similar to those flown on Mariner spacecraft.

i.   Solar Energy Controller. The SEC is a temperature control device that allows sunlight to enter an opening and reflect the solar energy into the propulsion tank cavity. The SEC opening is variable by virtue of two louver blades that are mechanically linked together and motor actuated by command.

2.   Performance

The functions of several devices were instrumented for direct indication of proper performance. These include solar panel deployment, relay antenna deployment, SEC blade position, spacecraft separation and the scan latch pressure. Proper function of other devices, such as the release devices, dampers, and louvers, can be inferred by the fact that other monitored functions were not impaired.

All mechanical devices hardware performed as designed.

a.   Spacecraft Separation. The spacecraft separations for both launches were analyzed by using information from both the Centaur gyro rates and the VO inertial reference package.

Predictions were generated based on known physical properties such as CG location and moments-of-inertia. Also, connector drag forces and connector locations were used in generating the predicted separation tip-off rates.

The results of the in-flight data analysis of both launches indicated minor reductions in separation clearance; the separations were near perfect.

b.   Aft-Bioshield Separation. The aft bioshield and Lander adapter separation normally occur a few days after Lander separation. The VO-1 aft-bioshield separation occurred successfully. During VL-2 separation from VO-2

an anomaly occurred that caused the Orbiter to switch from one IRU to the second unit. It was speculated that the pyrotechnic shock from the release nut may have caused the anomaly. Therefore, the aft-bioshield separation was never commanded for Viking 2.

D.   STRUCTURE SUBSYSTEM

1.   Description

The Structure Subsystem is divided into four groups of hardware assemblies:

(1)   The major structural elements which include the bus structure and the two degree of freedom scan platform, the spacecraft and VLC adapters and the structural parts of the propulsion module.

(2)   Multilayer insulation blankets and shields.

(3)   Electronic assembly chassis and shearplates.

(4)   Miscellaneous small items including the flight loads accelerometers.

2.   Performance

Structural member loads were monitored by the launch loads instrumentation for both VO-1 and -2. There were no indications of failure or anomalies in the Structure Subsystem during the primary mission.

E.   CABLING SUBSYSTEM

1.   Description

The Cabling Subsystem provided the necessary electrical interconnections between all Orbiter equipment. This is accomplished through the system cabling harnesses, the subsystem electronic assembly's harnesses, and the interface cabling from the VO to the launch vehicle and the VLC. There are 41 electrical harnesses in the Orbiter.

2.   Performance

The Cabling Subsystem performed throughout the mission with no anomalies.

SECTION IV

DATA HANDLING

A.   INTRODUCTION

The Orbiter on-board data system consists of the CCS and its associated flight software, the FDS, and the DSS. The Earth-based sequence implementation and subsystem modelling software, which interfaces with the flight software and provides the inputs to that software, are not described herein. In general, the basic functions of the three hardware subsystems are described below. Paragraphs B through D provide details of the functional design, performance, and anomalies for each of the subsystems of the Orbiter Data System; CCS, FDS, and DSS, respectively. Anomalous operation caused by ground software or operational problems are not discussed in this report.

1.   Computer Command Subsystem

The CCS decodes uplink data bits, and sends verified commands to VO subsystems and the VLC by issuing short duration relay closures or sending digital data through isolated switches. The commands are issued in real-time based on direct ground commands or in a sequence according to the programs stored in the CCS memories. The stored sequence can be altered by interrupts initiated by board the VO or by commands initiated on the ground in accordance with the particular reaction programmed into the CCS.

2.   Flight Data Subsystem

The FDS provides for the processing of VO or VLC engineering and VO science data for real-time transmission by the MDS or recording by the DSS. Also, the FDS provides control and timing signals for the VIS, MAWD, and IRTM, as well as timing for the MDS, PWR, CCS and DSS. The desired data mode, data rate, and engineering telemetry format are selected by sending coded commands to the FDS.

The FDS includes functional elements for processing engineering infrared science and visual imaging data, timing and control units, two memories, and two power converters.

3.   Data Storage Subsystem

DSS records VO data from the FDS and VL data from the Relay Telemetry Subsystem. These data are played back through the MDS and RFS to Earth.

The DSS consists of two basically identical and completely independent record-ers, each with a total storage capacity of 5.6×10^8 bits ov VO visual imaging data plus a minimum of 4.0×10^7 bits of data composed of any combination of FDS high-rate data (VO engineering and infrared science data) and relayed VL data. Each recorder has the capability to record VO visual imaging data on seven tracks simul-taneously at 2.112 Mbps, record VL data at either 4 or 16 kbps on track 8, record FDS high-rate data (VO engineering and infrared science data) at 2 kbps on track 8, and playback recorded data at 1, 2, 4, 8 or 16 kbps. FDS high-rate data may be played back at 1, 2, 4, or 8 kbps.

B.   COMPUTER COMMAND SUBSYSTEM

1.   Description

a.   <u>Functional Description</u>. The CCS is configured as a block-redundant computer. Each half of the subsystem is an independent special purpose computer containing a power supply, processor, memory, and an output unit. All inputs are applied to both halves of the CCS, and either half is capable of providing all mission requirements. The utilization of a dual computer provides both redundancy and extended command capability. The two processors operate asynchronously and may be programmed to perform different functions simultaneously. When critical command outputs are required, the processors may be operated in a tandem or parallel mode. A block diagram of the CCS is shown in Figure II-47.

The Orbiter system provides 2.4 kHz power, 2.4 kHz timing, and data in the form of interrupts (pulses) or levels (binary data) as inputs to the CCS. The CCS outputs coded commands (CC) in the form of 14-bit digital data words; it outputs discrete commands (DC) in the form of mechanical relay closures to command the other subsystems of the spacecraft. In addition, each output unit provides the FDS telemetry channel with CCS data and status.

The processors operate independently; however, their outputs are cross-connected to allow both processors to access either output unit. The processors can also exchange data words by using an output unit as the exchange media. A control signal is exchanged by the processors, allowing one processor to disable the other processor's output unit access, in order to prevent a defective processor from issuing extraneous commands to the spacecraft.

b.   <u>Detailed Description</u>.

1)   <u>Power Supply</u>. The CCS power supply subassembly provides the operating voltage for its associated processor, memory, and output unit. In addition, it provides a buffered 2.4 kHz square wave to the processor and output unit for timing.

2)   <u>Processor</u>. The CCS processor resembles a general purpose computer; however, several special purpose features have been implemented to facilitate its functions within the CCS. It is basically a serial machine, but memory access and some data transfers are performed in parallel. The processor is composed of
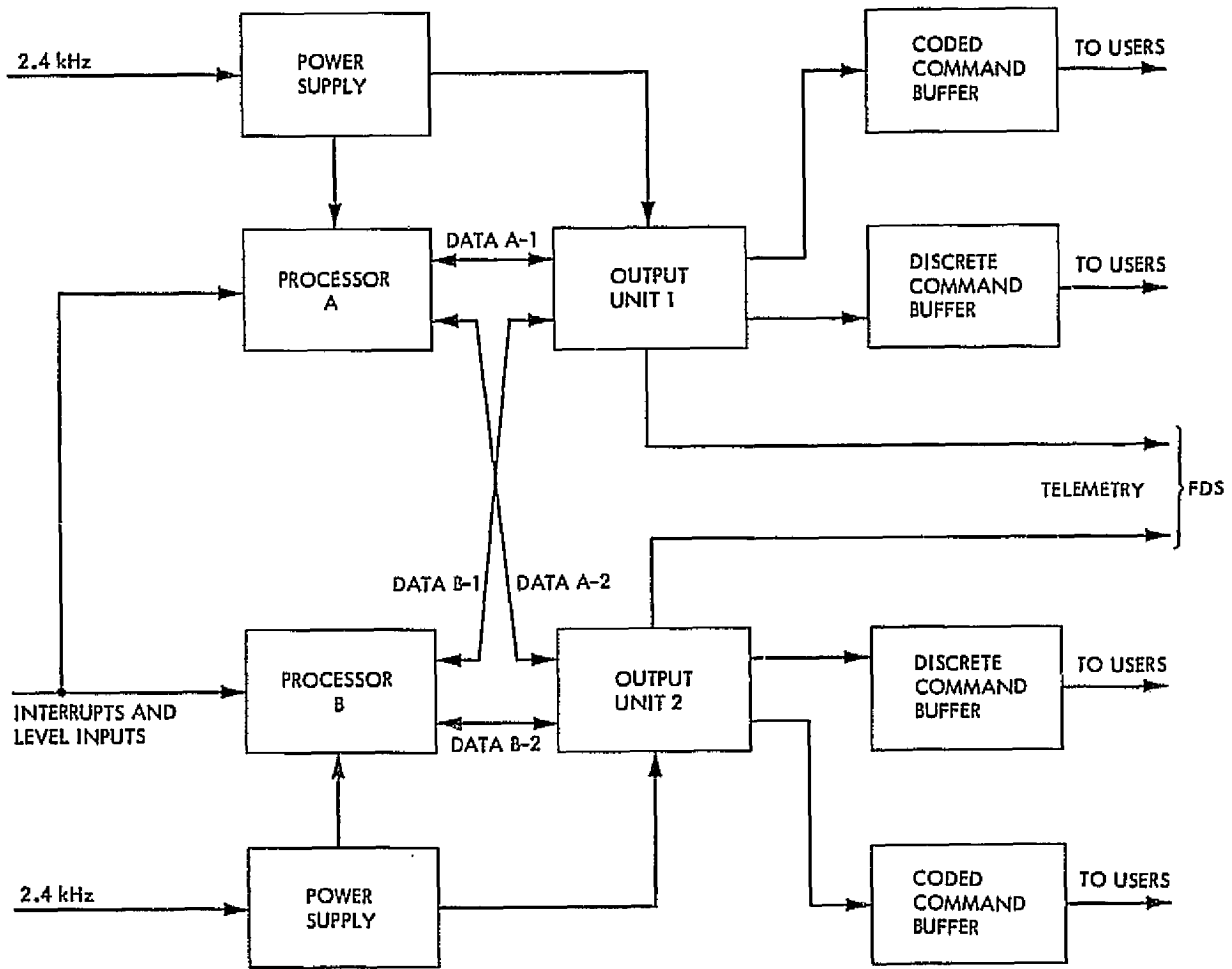
Figure II-47. CCS Hardware Functional Block Diagram

a central processor, interrupt processor, clock, and a timing generator. The central processor executes the software program using a repertoire of 64 instructions, controls the output units, and monitors itself for internal errors. The interrupt processor receives the interrupts and level inputs from the VO subsystems and from within the CCS, establishes their priorities, and makes them available to the central processor for execution of the associated software program. Spacecraft timing is coordinated via the 2.4 kHz power source which is phase locked to the FDS master oscillator frequency. Internal CCS timing is derived from an asynchronous 4 MHz oscillator.

3)   CCS Memory. The CCS Memory consists of a 5-mil plated wire memory stack with associated read/write electronics to provide storage for 4096 18-bit words. Each quarter of the memory may be separately controlled (by external wiring) to be read-only, write-protected, or read-write. In the CCS configuration, the lower half of memory is write-protected, requiring that a special instruction be executed by the processor prior to any write initiating instructions addressed to this area. The upper half of memory is configured read-write.

4)   Output Unit. The CCS output unit is a special purpose input-output device for the processors. It serves the dual purpose of interprocessor communications and CCS-to-spacecraft system output interface. The interprocessor communication function is used to pass 18-bit data words between processors. The CCS-spacecraft system output interface is used by the processors to issue DC and CC commands to the spacecraft. In addition, the output unit provides the telemetry output for the CCS.

5)   Command Execution Operating Modes. The CCS operates in three command execution modes: individual, parallel, and tandem. The execution modes are controlled by the processor software program and implemented by the output unit.

a)   Individual Mode. In the individual mode, the processors operate independently, using available output units for command executions. The processors may execute different software programs in this mode.

b)   Parallel Mode. The parallel mode is used when redundancy is required to insure that a command output occurs. The processors operate in essentially

the same sequence as for the individual mode; however, both processors perform the same software routine, each accessing a different output unit.

c)   Tandem Mode. The tandem mode is used when redundancy is required to insure that a correct command output occurs only at the required time. Both processors and one output unit are required to execute a tandem event. The initiating processor executes input/output (I/O) instructions which send data to the output unit and then verify it. This data represents the next event in the processor's sequence. A demand interrupt to the other processor is generated. In response to the demand interrupt, the opposite processor directs an I/O instruction to the output unit. This instruction contains the next data word in the processor's sequence; and it contains an order word that directs the execution of the data word if the word from this instruction is identical to the word already in the output unit data register. A miscompare results in no execute and a reject interrupt to the processors.

6)   Processor to Processor Communication. Processors can exchange 18-bit data words by a sequence similar to the tandem execution mode. The originating processor sends a data word to an output unit and a read interrupt to the other processor is generated. In response to the read interrupt, the processor executes an I/O instruction to read the waiting output unit data register and shift the word from the originating processor into the accumulator of the receiving processor accumulator.

7)   Telemetry Modes. The CCS provides the FDS with 28-bit telemetry words. The readout rates are controlled by the FDS. Status integration is selectable within each output unit (OU).

c.   Flight Software Description. The CCS flight software is the means by which the CCS executes its functions. It can be divided into five main functional units as shown in Figure II-48. Each is described below.

1)   Input Conditioning. The input conditioning unit contains those routines necessary to monitor and direct the interrupt and level inputs to the CCS. The monitoring consists of noting the occurrence of an interrupt, counting the number of occurrences of a specific interrupt, or determining which level

CCS INTERRUPTS
CCS LEVEL INPUTS

INPUT CONDITIONING
TRAP
INTERRUPT MANAGEMENT

COMMAND DECODING

EVENT GENERATION
DATA ACQUISITION
AND PLAYBACK
MASTER TABLE DRIVER
ACCELEROMETER
CONTROL
LAUNCH HOLD RESET
ERROR RECOVERY

OU DRIVER

TELEMETRY PROCESSING
TELEMETRY
CHECKSUM

CC/DC
COMMANDS

TELEMETRY
PROCESSOR
WORDS

TO CCS OUTPUT UNITS
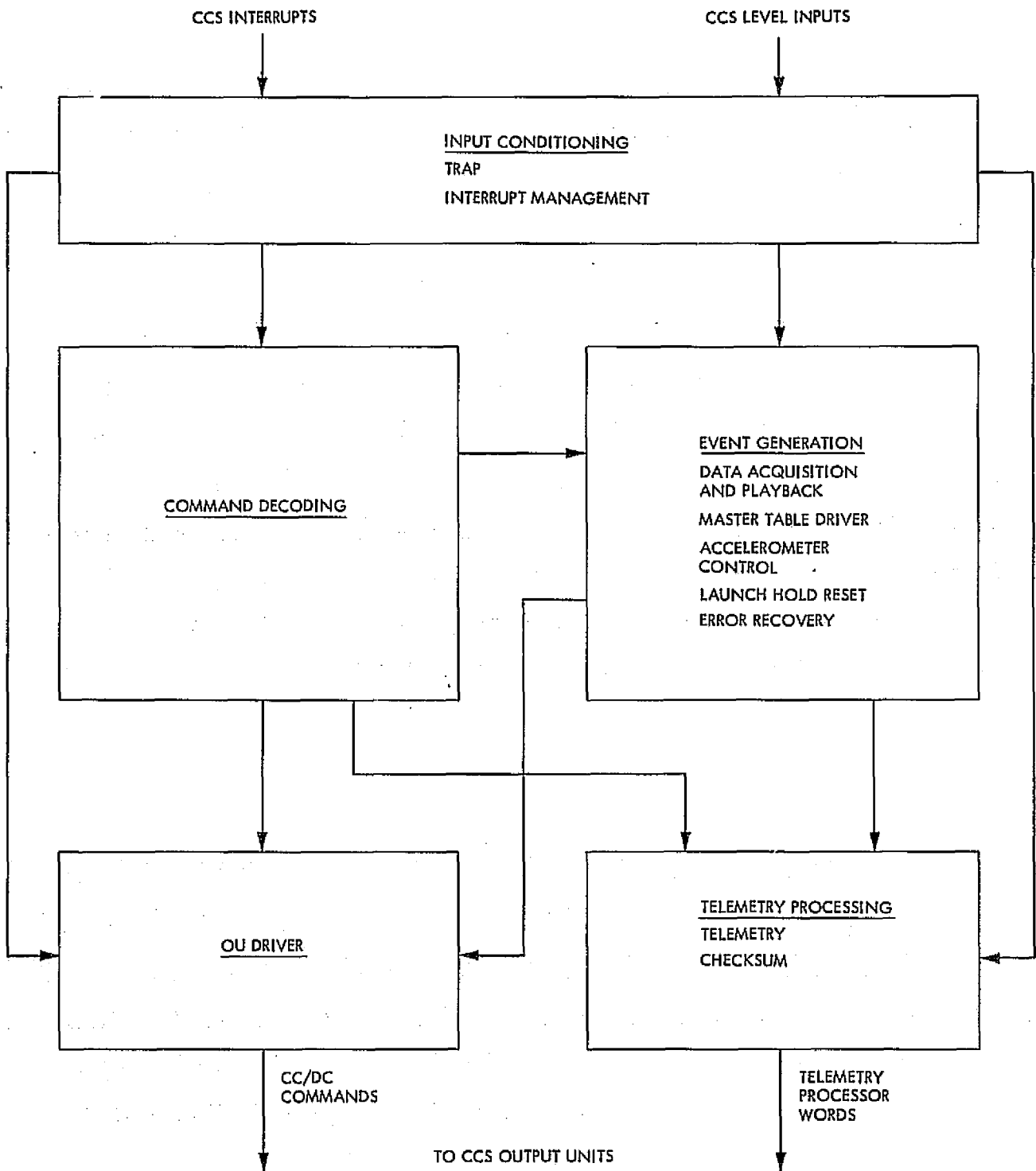
Figure II-48. CCS Software Functional Block Diagram

inputs have changes. The directing of the input consists of transferring program control to the appropriate routines.

2)   Command Decoding. The command decoding unit contains the routine of the same name which is required to decode the base and block command formats. The routine contains a 50-word buffer for the temporary storage of block commands. DC and CC commands which are decoded for execution are passed on to the OU driver. The routine is also responsible for the execution of processor commands. Single-bit error correction and multiple, bit error detection capability is provided through a row-and-column parity bit scheme.

3)   Event Generation.

a)   Data Acquisition and Playback. The data acquisition and playback sub-unit contains those routines tailored for the gathering, storing, and playing back of VO data. The routines are designed to do all the sequencing necessary for their particular function while being controlled by a minimum number of parameters. This concept minimizes the data transmission and storage required for these commonly used sequences.

b)   Master Table Driver. The master table driver unit is primarily responsible for keeping track of timing interrupts and initiating event sequences at the appropriate times. These events and their associated times are stored in tables which are primarily loaded from the ground. It can also activate routines and, when requested to do so, will inform a routine that a specified time interval has passed.

c)   Accelerometer Control. The accelerometer control routine keeps track of accelerometer pulses, puts out accelerometer related telemetry, and initiates engine shutdown when a specified number of accelerometer pulses have been received.

d)   Launch Hold Reset. The launch hold reset routine is responsible for the CCS launch associated operations. This includes the conditioning of the CCS immediately prior to launch and the initialization of the CCS after spacecraft separation.

e)   Error Recovery. Error recovery routines are responsible for the detection, analysis, and correction of specific anomalous spacecraft conditions. These conditions can be internal or external to the CCS and can be hardware or software in nature.

4)   Output Unit Driver. The OU driver routine is responsible for buffering and issuing CCs and DCs to the spacecraft. These commands can be issued in the tandem or individual (includes parallel) mode as required.

5)   Telemetry Driver. The telemetry driver routine is responsible for buffering processor telemetry information and passing it to the FDS through the output units. An additional function is gathering memory readout information.

2.   Performance

Except for the two anomalies described in paragraph 3, each Orbiter CCS performed as expected, well within the subsystem design, and all functional requirements were met. Because of the discrete digital nature of the subsystem, there are no appropriate consumables or trend type parameters to observe or analyze. As a matter of interest, however, the following command-related numbers are provided (all values are from launch through November 15, 1976):

VO-1:

Commands Received*:   2251

Commands Issued:	Output Unit	DC	CC
	1	3659	74 968
	2	520	499

VO-2:

Commands Received*:   1656

Commands Issued:	Output Unit	DC	CC
	1	2532	46 774
	2	460	514

---

*Commands Received tally counts each command block as one command.

3.   Anomalies

  a.   Post-Launch Checksum Discrepancy.

  1)   Summary. The VO-2 CCS Processor-B Checksum, which was automatically computed and read out via telemetry at the first post-launch CCS hours pulse, was 144724(8) rather than the predicted value of 144753(8). Subsequent investigation (i.e., CCS memory readout) showed that location 4416(8) contained 705200(8) rather than the predicted value of 705227(8). This was the only discrepancy revealed in all of the analysis performed, and the processor functioned normally both prior to and after the anomaly.

  2)   Analysis.

  a)   Software. Four software areas were investigated in detail:

  (1)   Line-by-line check of the code involving this address.

  (2)   Review of the acceptance tests of routines using this address.

  (3)   Retests of routines with meaningful variations.

  (4)   Independent review of the code, possible interactions, and possible environmental uniqueness.

  b)   Hardware. Three hardware oriented investigations were conducted:

  (1)   Multiple runs of launch/hold reset configuration on the prototype CCS.

  (2)   Possible failure modes tested on the breadboard.

  (3)   Detailed review of the design specifically oriented toward single/ double failures, noise possibilities, and interference possibilities.

  c)   Hardware/Software System. A review was made of the Orbiter system for possible single failure implications plus a detailed review of all pre- and post-separation telemetry data for indications of problems. The detailed investigations revealed only one functional single-point failure which could have caused the checksum anomaly. The failure would cause the WAIT instruction residing in the instruction register to appear as a SENT instruction (one-bit change). The instruction register flip-flop could have changed state or one of 31 gates could have temporarily failed for as short as 64 μsec. Any of these 32

failures would cause the serial clearing of the wait condition code. If this occurred between launch minus 10 minus and separation, the resultant link stored in location 4416 would be 705200(8) instead of 705227(8). That would cause the checksum error and, since the WAIT condition code is re-established at separation, no other evidence would exist, as is the case.

Subsequent successful operations and the maintenance of the non-zero wait condition code shows that the failure must have been transient in nature. Every complete readout of this processor's memory provided a check for the recurrence of the anomaly; none have been observed. The failure could have been introduced directly electrically or indirectly mechanically. Several of the electrical failures were demonstrated on the breadboard with identical results.

The CCS subsystem hardware, software, and spacecraft interfaces were reviewed for normal and abnormal interactions which could account for the anomaly. None were found.

From the available data a detailed account of CCS activities during the anomalous period was reproduced. There was only one timing uncertainty. Both possibilities were again checked for possible normal and abnormal interactions which could have caused the anomalous condition. None were found.

The spacecraft states and modes were reviewed and found to be normal throughout the anomalous period. In fact, the only anomalous condition was the Processor-B location 4416 and the resultant checksum error.

Since the hardware failure noted in item (2) was being checked continuously, other tests of areas unique to the anomalous condition were conducted even though none could be accounted for by a single-point failure. Briefly those tests were:

(1) Processor-B/OU-2 in both Orbiters were switched to the non-integrate mode so processor activity could be monitored. No abnormal activity was found.

(2) Processor-B self-test entry and exit counters were checked since the three complete memory readouts showed them to be different by one. They were found to be equal and the difference accountable to a documented CCS idiosyncrasy.

(3) Location 4416 was read and checked 10,000 times. All values were 705200(8).

(4) Location 4416 had 705227(8) written into it, read out of it, and checked 10,000 times. All values were 705227(8).

(5) The NOP, TRA, STL 4416 instruction sequence was checked 10,000 times to be sure the NOP was not clearing the condition code. It was not.

(6) The initial establishment of the wait condition code was checked 10,000 times. Each time the value was 27.

(7) The RET* instruction was checked 10,000 times to see if it would maintain the 27 WAIT condition code. It did.

(8) When the wait condition code was cleared by the normal response of processor B to loss of Canopus on September 17, 1975, it was re-established to 27 on February 15, 1976. This provided the capability to observe any recurrence each time a readout was taken. Readouts taken since then for various reasons throughout the mission have shown that the anomaly has not recurred.

One test which was not performed was to exercise the SENT instruction. This instruction is not used in the flight software which uses a functionally equivalent STL and TRA. Since the suspected anomaly was a false decode of a SENT instruction, its use might point out a softness in the hardware. It was decided to not exercise the SENT instruction because:

(1) The actual failure mode is being continuously checked.

(2) Since the CCS does not use the SENT instruction, its function is not necessary for the health of the CCS.

(3) If the SENT instruction was exercised, a softness in the hardware could cause an unpredictable response and jeopardize an otherwise healthy processor.

The launch sequence was not duplicated on VO-3 since the problem was internal to the CCS.

3) Closeout. Based upon the above analysis and test results, the fact that the processor correctly executed all activity both before and after the anomaly, and finally the fact that the only functional single-point failure

which could account for the anomaly produces a functionally "don't care" condition (clearing of the wait condition code), the failure reports were closed out by attributing it to a transient associated with the launch environment.

b.   CCS Memory Bit Failures

1)   Summary.   After VO-1 exited from Earth occultation (still in solar occultations) on October 11, 1976, it appeared that CCS processor-B had erroneously responded to loss of the Sun as if its Sun-acquisition routine had not been disabled as required by the sequence of events. Subsequent CCS memory readouts indicated that the memory was correctly loaded and that the memory was configured correctly. Later, another check of the memory indicated that a word was in error and that bit-17 of memory location 6727 contained a "1" rather than an "0". Had this bit been a "1" at the time of the anomaly, the subsequent events could be explained except that it must have had to return to the "0" state for the readouts. Several tests were conducted and a considerable amount of analysis, both at JPL and the memory manufacturer (SCI), has been performed. During tests conducted on the processor just prior to the superior conjunction load (and end of the primary mission), three additional memory locations were observed to exhibit similar symptoms, two more in bit-17 and one in bit-18. As of the end of the primary mission, the problem remains unsolved and additional testing and analysis is planned to begin early in December, 1976.

2)   Analysis.

a)   Tests Conducted. Five VO'75 CCS memories on the ground have been subjected to the CCS Memory Subassembly Test since the failure. The memories tested were:

> Evaluation Unit (1)
>
> VO-3 A & B   (2)
>
> Prototype A & B (2)

The subassembly memory test is automatic, consisting of several test modes including the adjacent bit disturb (ABD) test as conducted on VO-1 Memory B. The two tests are in every way identical. There were no failures encountered in the testing of the five memories.

No further testing is planned at this time; however, the memories are available should some special tests later be defined and adequately justified as being meaningful to the problem.

b) <u>In-Depth Analysis to Date</u>. In parallel with the testing, an effort was started to ascertain from the records at JPL and at the manufacturer whether there are any identifiable causes for the VO-1 Memory B problem and any reason to believe that through any other deficiency we may expect more widespread problems with other VO memories. Significant data determined to date:

(1) The wire in VO-1 Memory B was plated in the period from March 6, 1974 to April 11, 1974.

(2) The stack tester was performing normally when this particular stack was converged.

(3) Wire sample data was checked and found to adhere to specifications.

(4) All planes in the memory had wire changes during convergence. Bit-18 was changed on wire change No. 1.

(5) Bit-17 wires (on a plane not presently in question) were changed as a result of a subassembly test failure (after convergence testing of the stack).

(6) Adjacent tunnels are involved.

(7) The second ABD test conducted on VO-1 Memory B suggested a pattern of data toggling from bad to good. This is inconsistent with the typical failure mode of bad plated wire but is consistent with degrading electronics. Typically, bad wire will degrade to a point and then fail completely with insufficient output.

To this point we are unable to conclude if the Memory B problem is caused by bad wire or by component parametric drift. Post conjunction (Extended Mission) tests on VO-1 and VO-2 may contribute to some conclusion. There are still issues to be checked in the data at JPL and the manufacturer.

C.   FLIGHT DATA SUBSYSTEM

1.   Description

   a.   General Description. The FDS performs two basic functions:

   (1)   Provides reference frequencies for timing and control directly to
          the MDS, DSS, PWR and the instrument payload and, indirectly, via
          the 2.4 kHz power system, to the CCS.

   (2)   Collects both science and engineering measurement data, provides
          signal conditioning, provides analog-to-digital conversion, (where
          required), and then formats the data into serial bit streams which
          are passed to the MDS for transmission to Earth or to the DSS to be
          recorded.

   The FDS consists of six major functional blocks:

   (1)   Timing and Control

   (2)   Engineering

   (3)   Infrared Science Data

   (4)   Visual Imaging Data

   (5)   Memory

   (6)   Power Conversion

These are described in the following paragraphs. A functional block diagram is
provided in Figure II-49.

   b.   Detailed Description.

   1)   Timing and Control Block. The timing and control block includes the
redundant oscillators, timing chains, and CC decoding logic; the engineering
sequencing and control logic; the science sequencing and control logic; and the
power-on-reset circuitry.

   2)   Engineering Data Block. This block performs digital and analog
measurements that can be made at relatively low rates with no more than 7-bit
precision. Analog signal measurements are: 0 to 100 mV, ± 1.5V, and 0 to 3V.
Digital measurements consist of the following four types:
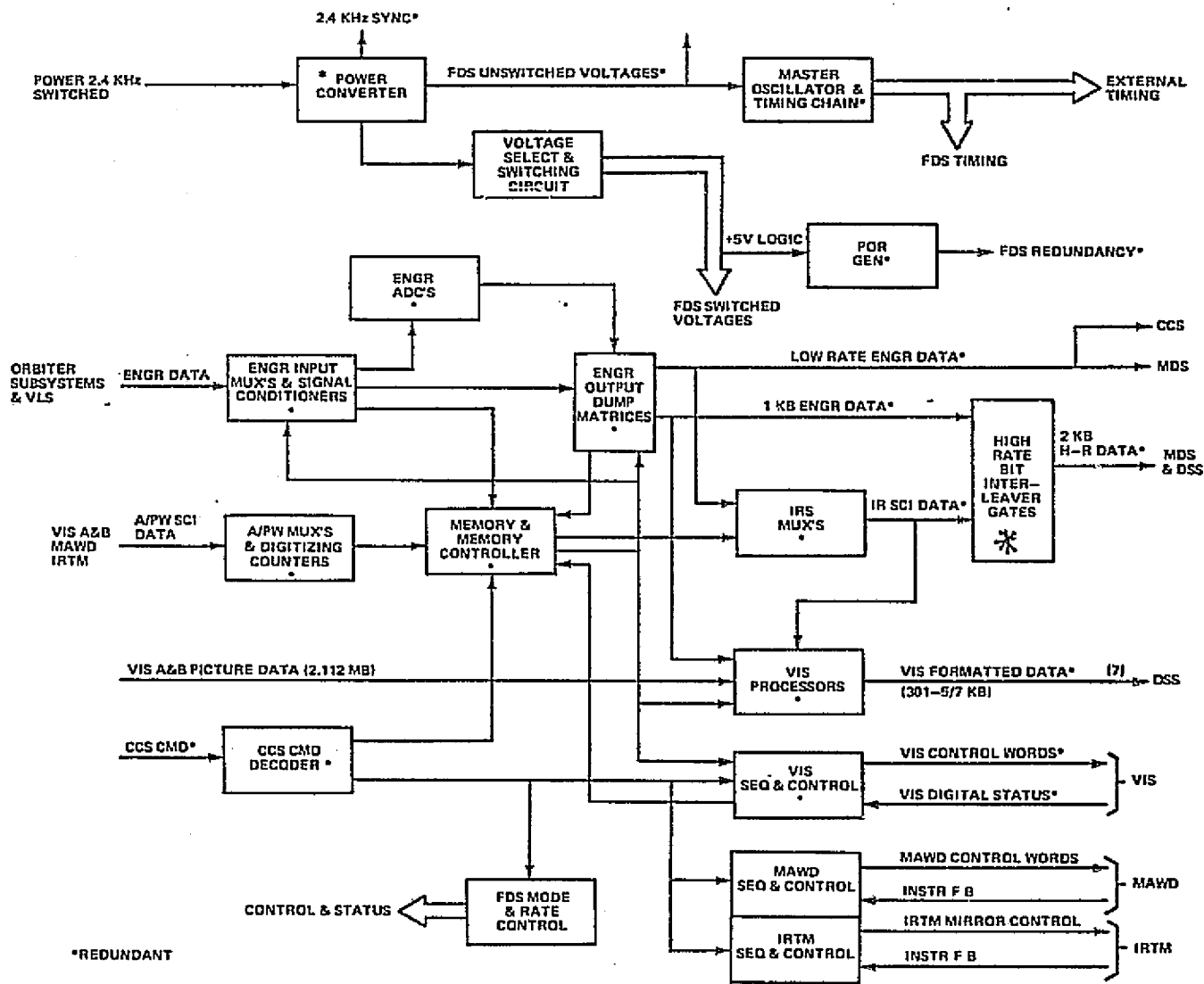
Figure II-49. FDS Simplified Functional Block Diagram

(1)	External Shift Register	The subsystem being measured contains a register that is shifted out by the FDS.
(2)	Bi-level	The subsystem being measured sends a logic voltage level (either a "1" or a "0") that is sampled by the FDS.
(3)	Timer	The subsystems being measured send a pulse that is used by the FDS to gate a signal of a known frequency into a counter.
(4)	Counter	The subsystem being measured sends pulses that increment a counter in the FDS.

3) Infrared Science (IRS) Data Block. The IRS Multiplexers assemble the IR Science Format. Two identical, redundant outputs are generated by separate FDS hardware to be bit-interleaved with 1 kbps engineering data (or "all ones") and transmitted to DSS and MDS, and also to be imbeded into the VISID (TV flyback) data.

Most of the IRS format is buffered in FDS Memory and is generated already multiplexed by reading the memory at appropriate times.

4) Visual Imaging Data Block. The Visual Imaging Data Block receives 2.112-MHz data from the VIS Analog-to-Digital Converter (ADC). It processes this data from serial format to seven tracks of parallel data suitable for recording on a DTR. The logic circuits that perform this function, referred to as the VIS Processor, consist mainly of steering logic and rate buffering.

Processed data on the seven tracks to the DSS occurs at a rate of 301-5/7 kbps (per track). A single VIS line format requires 4-8/33 msec to send and contains 1280 bits. Except for track ID, the first 76 bits of the format for a given VIS line are the same for all seven tracks. The track IDs are abitrary three-bit sequences uniquely identifying each of the seven tracks.

5) Memory Block. The memory block encompasses two identical plated-wire memories, designated Memory-A and Memory-B, and two associated memory controllers. Each memory provides random access storage and retrieval of 1024

words of digital data, for a total of 2048 words of 8 bits each. The memories
are mounted on a common subchassis but are otherwise completely separate and
independent. The memories operate in complete synchronism. Each memory includes
the plated-wire mats and all associated electronics but excludes power conver-
sion and power conditioning. Address bits and data to and from either memory
are transferred in parallel. The memories are interrogated without destroying
the stored data. Stored data does not change as a result of power interruptions.
Normal operation of the memory is inhibited by internal circuitry when any of the
supply voltages are outside of predetermined tolerance limits, approximately ±6
to ±8 percent. If this condition occurs during a READ or WRITE cycle, the memory
completes the cycle. The functional modes of operation are controlled by
appropriate commands on the memory cycle initiate line and on the memory mode
line. These are: write, read and standby.

6)   Power Conversion Block. The Power Conversion Block includes two
identical power converters, each of which converts the 2.4-kHz input power to the
specific voltages required to operate the FDS circuits, logic, relays, and
memories. The power converter function also includes relay switching for the
outputs of the power converters. The two power converters are used as a redun-
dant set where one is active and the other is standby redundant.

7)   Data Modes, Rates, and Formats. The FDS supplies data to the TMU of
the MDS over two pairs of transmission lines. One pair furnishes low-rate data,
while the other pair supplies high-rate data. The low-rate is also supplied to
the CCS via a single line to both CCS processors. High-rate data and VIS data is
also supplied to the DSS for recording. The various data modes produced by the
FDS are listed in Table II-25.

2.   Performance

Other than to state that each FDS executed all commands and output all
control signals as designed throughout the mission, very little performance-type
information is appropriate to present. However, daily records of FDS Master
Oscillator frequency were maintained for both VO-1 and VO-2 because of its
importance in spacecraft sequence timing.

Table II-25.   FDS Data Modes

Mode	Rate	Channel	Can Be Recorded	Remarks
IR Science Data plus Engineering A (Eng-A)	2 kbps*	High	Yes	IR science data includes imbedded Engineering B or C.
VIS DATA	301-5/7 kbps	Recorded	Yes	Includes imbedded Engr. and IRS data in flyback.
Engineering B (Eng-B)	33-1/3 kbps	Low	Yes**	Can be either the fixed, or any of four programmable formats.
Engineering C (Eng-C)	8-1/3 bps	Low	Yes**	Can be either the fixed, or any of four programmable formats.
Engineering D (Eng-D)	8-1/3 bps	Low	No	Derived from Eng-A.

*1 kbps IR science data bit-interleaved with 1 kbps Eng-A data (IRS first) to provide a 2 kbps data stream.   Eng-A is "all ones" when Eng-B or Eng-C selected.

**Only as imbedded in IRS data.

Graphical plots of VO-1 and VO-2 FDS Master Oscillator frequency offsets during the mission have been made (see Figures II-50 and II-51). Also included on these plots are Bay 6 (FDS) temperature profiles during these periods. As seen in the figures, the FDS Master Oscillator frequence offset is directly related to FDS temperature:

$$VO-1 \text{ frequency offset} \approx 0.9 \text{ Hz/}^{o}F$$

$$VO-2 \text{ frequency offset} \approx 0.6 \text{ Hz/}^{o}F$$

3.   Anomalies

There were no FDS anomalies on either Orbiter throughout the primary mission.
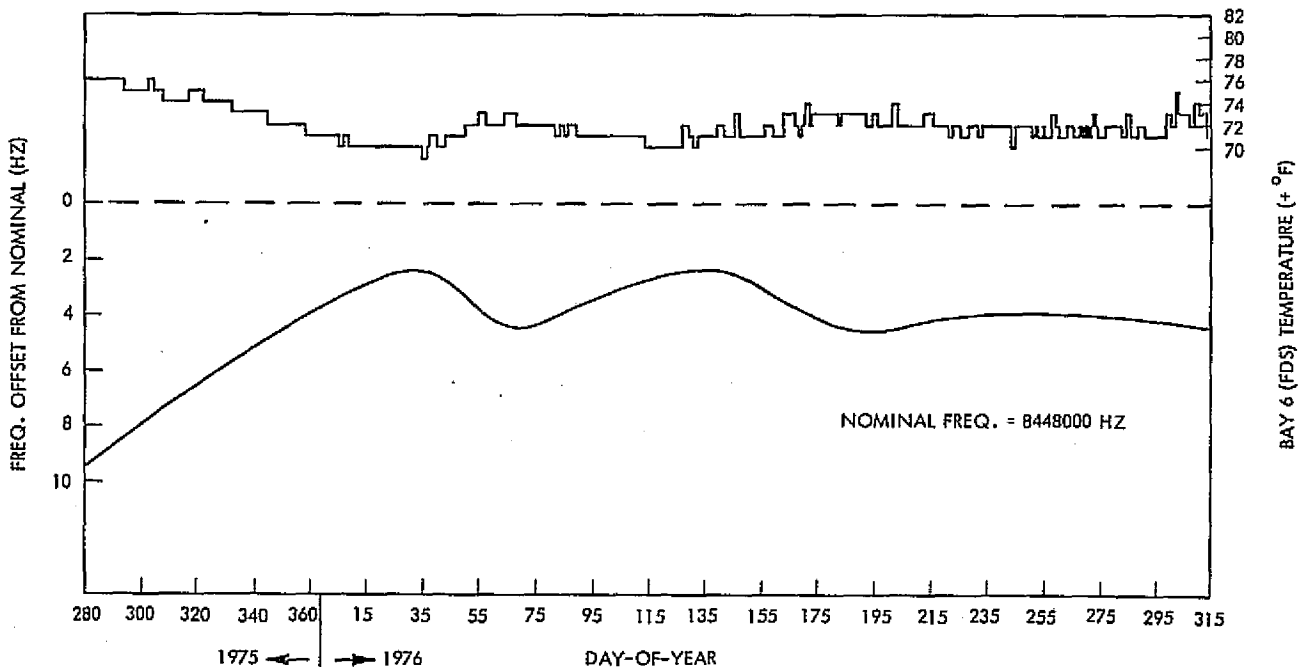
Figure II-50.   VO-1 FDS Master Oscillator Frequency
Offset and Bay 6 Temperature Profile
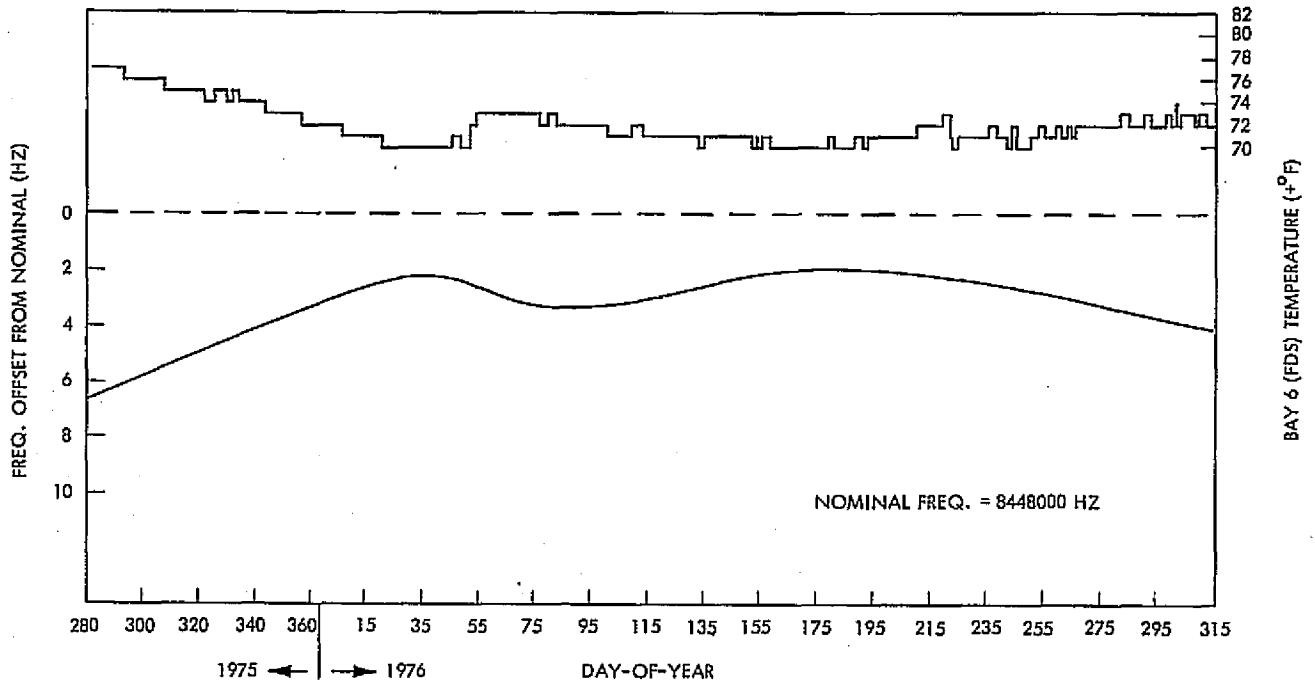
Figure II-51. VO-2 FDS Master Oscillator Frequency
Offset and Bay 6 Temperature Profile

D.   DATA STORAGE SYBSYSTEM

1.   Description

a.   <u>General Description.</u> The DSS consists of two Digital Tape Recorders (DTR's) and performs the following major functions: (1) store science data received from FDS; (2) store high-rate engineering data received from FDS; (3) store VL Data received from the Relay Telemetry Subsystem (RTS); and (4) play back the stored data through the MDS at 1, 2, 4, 8, or 16 kbps. The DTRs are independent and identical (except for slight dynamic differences due to their electromechanical configuration). A functional block diagram is provided in Figure II-52. Each DTR consists of a 9-track tape transport (DST) and the electronics (DSE) required to store and play back data. Control inputs to the DTRs to select mode, bit rate, track, and tape direction are via commands from the CCS.

VIS data from FDS is multiplexed on 7 parallel lines to either DTR. The data rate for each line is 301-5/7 kbps. Full resolution pictures will be recorded by either DTR in the VIS record mode. Science or engineering data from the FDS at 2 kbps or VL relay data from the RTS at 4 or 16 kbps is recorded on track 8. Simultaneous recording of more than one data source or bit-rate will not be possible on any DTR.

b.   <u>Detailed Descriptions.</u>

1)   <u>DST.</u> The DST is a coplanar reel-to-reel tape recorder, using seamless belts to transmit motion from motor to tape and provide speed reduction. This kinematically complex, peripheral belt, capstan differential drive design, provides uniform tape tension, bidirectional operation, and smooth tape motion at low speed. The transport is comprised of 13 separate rotating components. Rotating subassemblies utilize precision preloaded instrument ball bearings. High precision bearings are essential to minimize torque disturbance which causes non-uniform tape speed at the magnetic heads (flutter). Many of these components rotate at just 3 rpm during the 1 kbps playback rate.
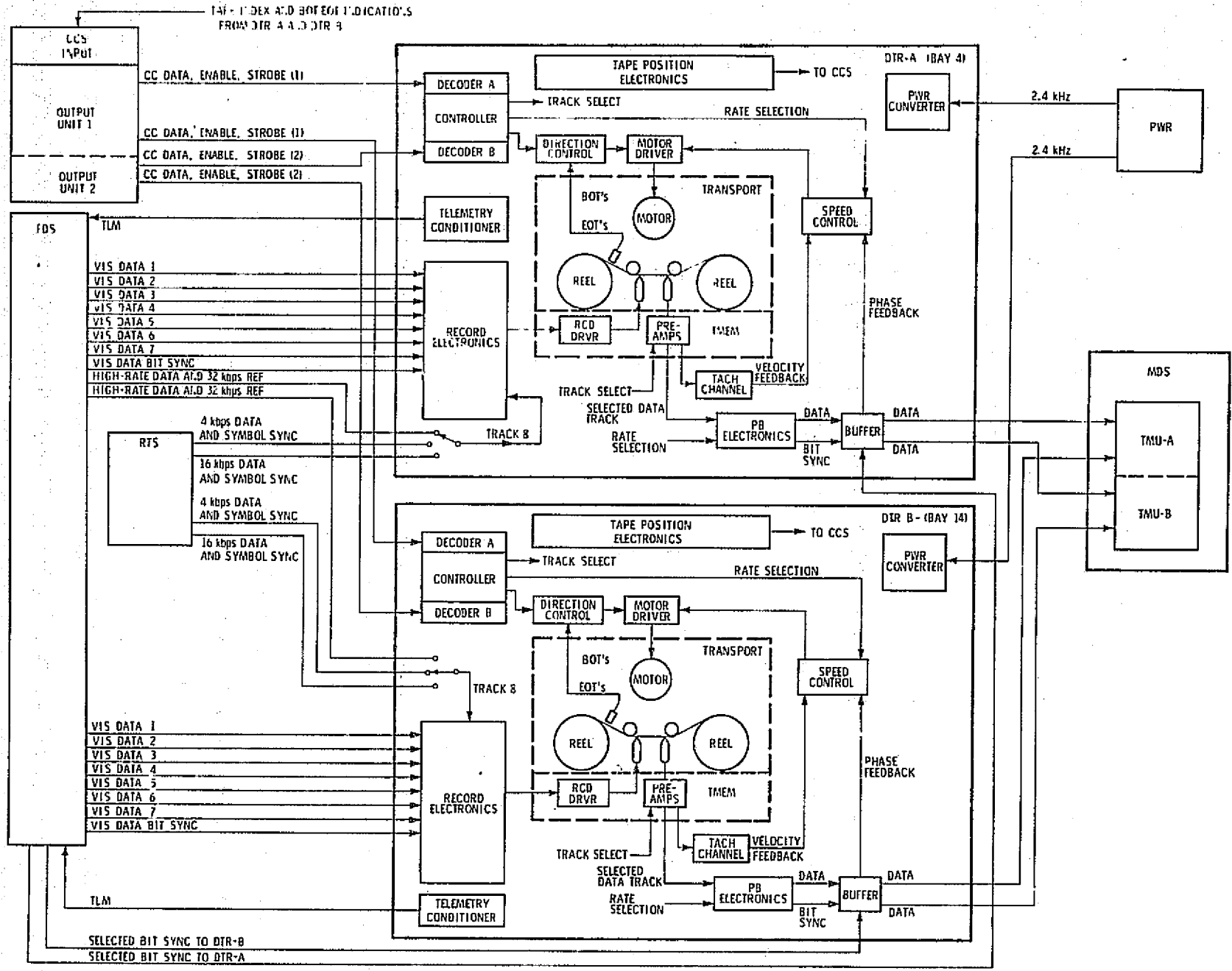
Figure II-52. DSS Block Diagram

A damper mechanism is built as part of the left reel assembly of the DST. This damper reduces the transport resonance frequency by the usage of rubber damper material installed in the mechanism.

The magnetic tape used in the DST is one-half inch wide, type 900, manu- factured by 3M. A tape map is shown in Figure II-53. During operation, the tape shuttles from reel-to-reel, motor power being supplied from the DSE. The end-of-tape (EOT) or beginning-of-tape (BOT) condition does not correspond to physical tape end; rather, a signal is generated when the tape reaches a pre- pared window at 90, 60 and 30 feet from each physical end-of-tape. Normal logic interlocks prevent movement, other than run down, beyond the first EOT signal.

2) DSE.

a) Record Electronics. The record electronics selects the proper data source and conditions the data for transfer to the DST. VIS data is recorded on tracks 1 through 7, while the data for track 8 may be selected from any of three sources (RTS 4 kbps, RTS 16 kbps, or FDS 2 kbps). Data is played back one track at a time by turning on one of the eight preamplifiers in the Trans- port Mounted Electronics Module (TMEM). The playback data signal from the TMEM is further amplified, filtered, gain compensated, and peak detected. The filter constants and gain compensation adjustments are switched by rate enable lines to ensure that the signal amplitude to the peak detector remains approximately the same for all five playback rates. These adjustments are necessary since the magnetic head output amplitude doubles for each doubling of tape speed. The peak detector senses both positive and negative peaks such that its output represents the Miller code form of the data previously recorded.

The output of the peak detector is sampled by a one-half bit period inte- grating amplifier. The timing pulses to initialize the integrating amplifier and to store the output level are derived from the bit synchronizer Phase Lock Loop (PLL). The detected data is converted to NRZ format and sent to the data buffer. A bit synchronizer PLL locks to the playback data and generates the bit-sync timing signals. The PLL allows the bit-sync information to be recorded from the playback data in the presence of moderate dropouts and flutter. The bit synchronizer PLL determines the location of the Miller code data transition
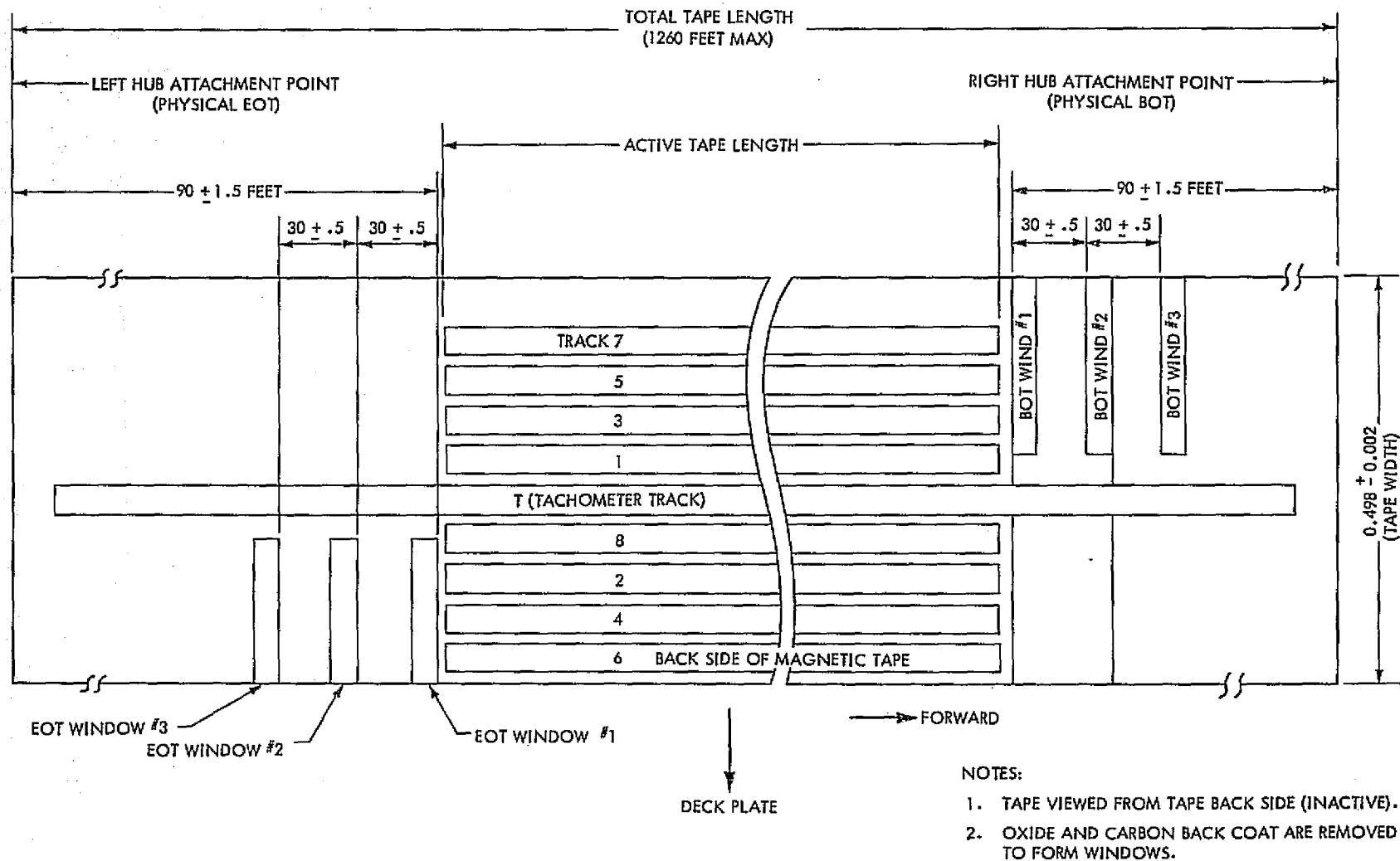
Figure II-53. Magnetic Tape Map (Transport Frontal Profile)

and resets the integrating amplifier so that each data transition will be coincident with the reset pulse. After the detected Miller code data has been converted to NRZ format, it is routed through a buffer. The buffer transfers the data from the bit sync clock to a stable external clock from the FDS. This removes the flutter from the data that is inherent in the system when operating the motor under servo control.

VIS data from the FDS comes to the DTR on seven separate lines and is simultaneously recorded on tracks 1 through 7. The data rate of each line is 301-5/7 kbps. The VIS bit sync is divided by two and used to convert the data input from NRZ format to Manchester code. Manchester code is formed by the EXCLUSIVE-OR combination of the NRZ data and the square-wave clock (at data-rate frequency). The seven lines of Manchester data are routed to the TMEM where they are divided by two to form Miller code such that data and bit sync information are recorded on each track. VL data is recorded on track 8 while the tape is running at speeds corresponding to either 4 of 1y kbps. FDS data is received at a 2 kbps data rate but is symbol encoded to a 4 kbps rate and recorded at the 4 kbps tape speed.

b) Playback Electronics. The purpose of the playback electronics is to recover the playback data signal and derive a bit sync clock. The DTR may be operated at any one of five selectable tape speeds during the playback mode. Ideally, the input and output buffer clocks would be exactly the same frequency, the counter would remain in the middle of its counting range, and the output data would be taken from the middle of the 48-bit register. In reality, the servo control with the frequency loop alone is not accurate enough to maintain an average zero frequency difference between the input and output clocks. When differences in frequency do occur, the 6-bit counter gradually begins to drift toward one end of its counting range, the counter's position is detected by a phase detector circuit which consists of two digital-to-analog (D/A) converters which are the complement of each other. The outputs from the phase detector are routed to a difference amplifier and filter which converts the difference to a phase-error signal. The phase-error signal is added into the servo control loop through the summing amplifier and corrects the motor speed in the direction which brings the buffer counter back to its center position.

In playback, the counter is clocked up by data bit-sync and clocked down by a fixed frequency from FDS. In a synchronous record, the counter is clocked up by the selected record bit-sync and clocked down by the tach clock signal. This action allows the buffer to partially compensate for tape speed perturbations.

c) Tape Position Counter. The tape position logic is a counter which divides the tach clock by a count of 10,000. This results in either an increment or a decrement pulse to CCS for every three inches of tape, depending on whether the tape is moving in the forward or reverse direction. This unit of measure is referred to as a Tape Increment Count (TIC) and is measured from BOT, where BOT is TIC 200(10). The increment and decrement pulses are used by the CCS to maintain current tape position.

3) Operating Modes. Each DTR has seven basic operating modes. Mode selection is controlled by commands from CCS. The receipt of a BOT or EOT event will automatically switch the DTR to the ready mode from any of the other operating modes. The modes are described below.

a) Ready Mode. As the name implies, the ready mode is in essence a standby mode with the DTR waiting to perform its normal record or reproduce function. During ready mode, the 2.4 kHz primary power input is applied but the tape is not in motion and the magnetic heads in the DST are not enabled. The power-on-reset circuit forces the DTR to the ready mode.

b) Playback Mode. The playback mode reproduces previously recorded data and routes the detected data to the MDS for subsequent transmission to Earth. Any single track may be selected for playback at one of the five playback rates (1, 2, 4, 8, or 16 kbps) with the exception of FDS 2-kbps recorded data which may only be reproduced at the four lower rates. The playback direction, rate, and track are selected by CCS command. Tracks 1 through 7 contain VIS data and may be reproduced in either direction. Track 8 is used for asynchronous recording (RTS 4 kbps, RTS 16 kbps, or FDS 2 kbps) and should only be reproduced in the direction it was recorded for best bit-error performance.

c) <u>Slew Mode.</u> The slew mode is used to position the tape at the desired location prior to starting a record or playback sequence. The tape speed may be selected from any of the five playback rates or the VIS record rate. The record heads are disabled during slew mode so that there is no erasure of stored data. At any of the playback speeds, data is reproduced in the same manner as the playback mode except the data is available only via the direct access cable. Slew rate and direction are selected by CCS command.

d) <u>Record VIS Mode.</u> During the VIS record mode, data is simultaneously recorded on tracks 1 through 7. The DST motor is operated at synchronous speed and moves the tape at 45.26 in. per sec. The VIS data is received from the FDS on seven parallel lines at 301-5/7 kbps and may be recorded in either direction, though throughout the primary mission it was operationally constrained to the forward direction.

e) <u>Record FDS 2-kbps Mode.</u> FDS 2-kbps data is symbol encoded to 4 kbps and recorded on track 8. The DST motor is operated asynchronously under servo control as a tape speed of 0.6 in per sec to maintain the same packing density· as VIS data. The data may be recorded in either direction.

f) <u>Record VL 4-kbps Mode.</u> The RTS 4-kbps data is selected as the data source and recorded on track 8 during the VL 4-kbps mode. The tape direction may be selected by CCS command and the tape speed is servo controlled at 0.6 in. per sec to maintain the same packing density as VIS data.

g) <u>Record VL 16 kbps Mode.</u> VL data from the RTS 16-kbps source is recorded on track 8 in the selected direction during the VL 16-kbps mode. Packing density is maintained by operating at a tape speed of 2.4 in. per sec under servo control.

2. Performance

a. <u>General.</u> All four flight recorders remain completely operational with no measurable degradation. Table II-26 summarizes the amount of data that has been recorded and played back in flight.

Table II-26. In-Flight Record-Playback Statistics
at End of Primary Mission

Recorder		No. of VIS Pictures Recorded	Minutes of VL Relay Data Recorded	Minutes of FDS Data Recorded	Hours of Playback at				
					1 kb	2 kb	4 kb	8 kb	16 kb
VO-1	DTR-1	2613	1710 (16 kb)	5469 (2 kb)	0	53	148	577	31
	DTR-2	2535	1570	5945	0	66	190	515	32
VO-2	DTR-1	3062	1135	6064	0	25	36	400	34
	DTR-2	2708	735	6367	0	28	66	309	24
TOTALS		10918	5150	23845	0	172	440	1801	121

b.   Evaluation. Throughout the primary mission, an evaluation was main-
tained in an effort to detect degradation or trends in the DSS performance. As
it was not possible to conduct a bit error test in flight, it was always a matter
of subjective judgement to use the DSS telemetry measurements, RF link infor-
mation, and thr ground data processing system status to access the performance.
It was concluded that the in-flight performance was as good as or perhaps some-
what better than the pre-launch status. This conclusion is based on the follow-
ing analysis.

1)   Dropouts. A list of dropouts, their location and affected tracks
was maintained for each DTR before launch. Early in the primary mission, play-
backs with a good link performance, and problem-free ground processing revealed
no tape-related performance problems. Unfortunately, late in the mission the
link or processing problems prevented a thorough reassessment of the tape con-
dition. It can be stated, however, that no dropout areas could be detected
throughout the primary mission.

2)   Buffer Level. The buffer level telemetry measurement indicates from
what area in the 48-bit buffer playback data is being taken. The servo was
originally set up such that with no noise or flutter the buffer would be exactly

centered. This allows a +24 bit excursion before an error occurs. This measurement has built-in memory such that the telemetry sample is given the largest excursion since the last sample. Thus, from observing the signal over many samples, the average value and the variation (which depends on the amount of flutter) can be determined. The buffer of all four DTRs was monitored continuously. The average level has remained centered. No unusual excursions which might represent increased flutter levels or which might be linked to bit errors was observed.

3)   Lock Detector. During playback the lock detector indicates the lock status of the bit sync phase-lock loop. If the loop drops lock during playback, bit errors are almost sure to occur. The telemetry measurement indicates whether the loop was out of lock since the last sample. Only twice during the primary mission was an out-of-lock occurrence observed.

4)   Motor Voltage. The motor voltage indicates the voltage required to drive the motor. Any change in transport friction or electronic gains would cause the servo to shift the average value of this measurement. The average level and excursions on all four flight units have remained the same as their pre-launch values.

c.   Consumables. Recorder lifetime was specified in the following terms:

(1)   Total feet of tape across the heads, 1.5×10^6 feet

(2)   Passages of any given section of tape across the heads, 6500

(3)   Total number of Start/Stop cycles: 1×10^4

A summary of actual performance values for each DTR is presented in Table II-27 and Figure II-54. Table II-27 presents a summary of Start/Stop cycle activity and number of feet of tape across the heads for each DTR. Figure II-28 presents a histogram for each DTR showing the number of passages (ordinate) of various sections of each tape across the heads with samples taken at specific locations (abscissa) along the tape. These locations are measured in TICs (3-in. intervals) from BOT to EOT.

Table II-27. Consumable Status at End of Primary Mission

Recorder		Parameter	Subsystem Tests	System Tests	In-Flight	Total At End Of Primary Mission	System Tests Plus In-Flight* Total
VO-1	DTR-A	Total Hours on	303	540	4,528	5,371	5,068
		Start/Stop Cycles	3,783	3,672	5,293	12,748	8,965
		Tape Footage Across Heads	467,307	476,204	870,435	1,813,946	1,346,639
	DTR-B	Total Hours on	336	742	4,219	5,297	4,981
		Start/Stop Cycles	5,615	2,648	5,005	13,368	7,753
		Tape Footage Across Heads	403,408	403,494	756,387	1,563,289	1,159,881
VO-2	DTR-A	Total Hours on	459	348	3,313	4,120	3,661
		Start/Stop Cycles	5,080	1,284	3,403	9,767	4,687
		Tape Footage Across Heads	519,186	190,371	475,028	1,184,585	665,399
	DTR-B	Total Hours on	419	644	3,088	5,151	3,732
		Start/Stop Cycles	4,513	1,687	2,381	8,581	4,068
		Tape Footage Across Heads	437,815	307,590	431,450	1,176,855	739,040

*Functional Requirement Spec: 1,500,000 Feet of Tape Across Head
                                             10,000 Start/Stop Cycles

VO-1
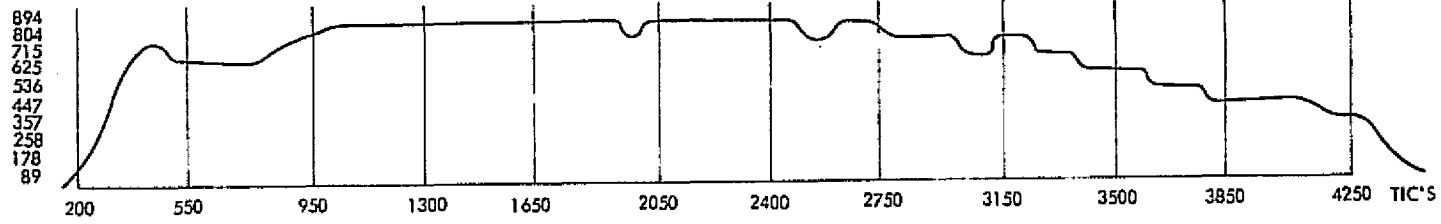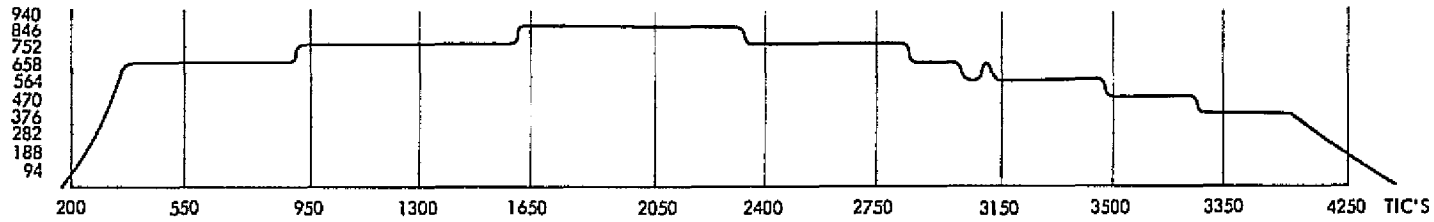
DTR A

DTR B

VO-2

DTR A
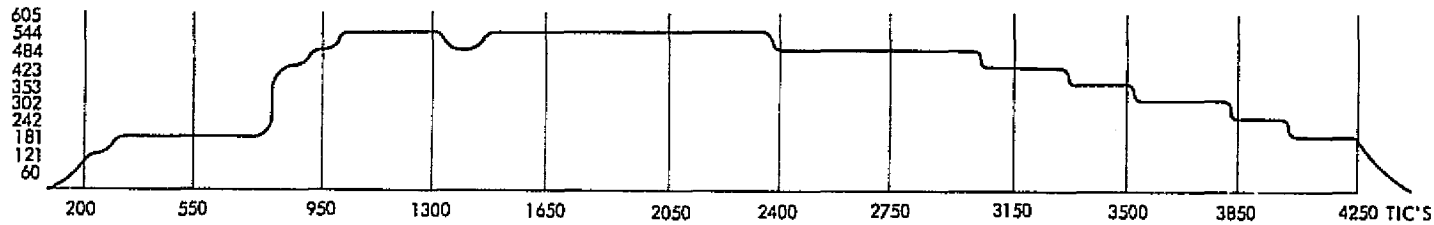
DTR B
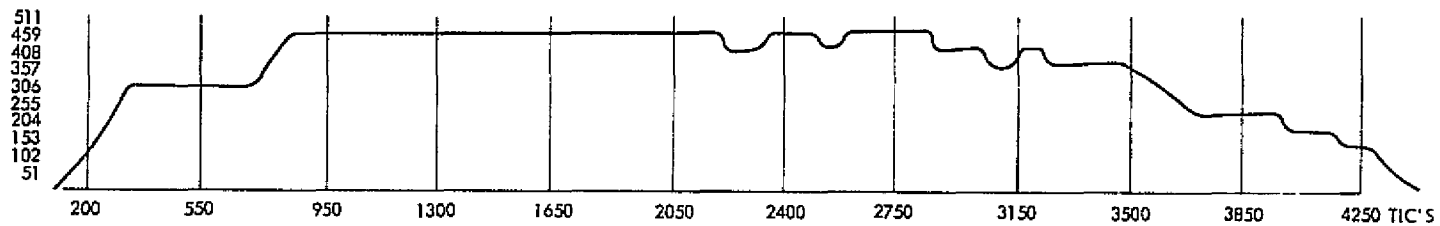
Figure II-54.   DTR Tape-Across-Head Histograms

3. Anomalies

a. Summary. During an 8-kbps VIS playback on VO-2 DTR-B, track 4, reverse direction, the tape motion suddenly changed to synchronous speed in the same (reverse) direction. Upon reaching the correct TIC value, the CCS commanded the DTR to 8-kbps playback, track 5, forward direction as required, and the DTR responded correctly. It functioned in a perfectly normal manner both prior to and following the anomaly.

b. Analysis. All appropriate DTR logic was independently analyzed by both the Contractor (Texas Instruments) and JPL DSS personnel in an attempt to locate failure mechanisms which would explain the anomaly. All Orbiter telemetry data was intensively reviewed both prior to and during the anomaly in an effort to characterize both the DSS and Orbiter System performance and environment in a search for clues to a possible explanation. Significant facts observed from telemetry were:

(1) No evidence of a CCS command or other unusual spacecraft activity could be found at the time of the anomaly.

(2) The DTR mode status word was sampled and indicated synchronous speed just after the anomaly occurred. This status is decoded from the DTR control logic which isolates the problem to the control logic and removes the possibility of a servo or transport problem.

(3) Analysis of the events, timing, and playback data after the anomaly confirm that the DTR did actually go to the sync speed.

(4) Rate control logic was correctly reset with the track-5 command.

The only failure mode which fits all of these facts is the change of one of the rate control flip-flops from a "0" to a "1". Since the above-mentioned logic design analysis also pointed to that flip-flop as being the only clear candidate, it is assumed that it was indeed the culprit. Since other parts could have indirectly been involved, the history of all parts which could have been remotely involved was reviewed by the parts specialists. No significant conclusions were drawn from this investigation. A series of special tests was conducted on the DTR but its response was normal and its performance since the anomaly to date has been normal.

c.   <u>Close Out.</u> Since the DTR functioned normally both before and after the anomaly and no operational constraints were deemed necessary as a result of the analysis, the DTR was returned to full service. The specific cause of the failure is unknown though it must have been transient in nature, possibly due to a system noise transient, a particle in the IC, an intermittent IC, or a degraded noise susceptibility. The operation of the DTR continues to be carefully analyzed.

SECTION V

PROPULSION AND PYROTECHNICS

A.   INTRODUCTION

1.   Propulsion Subsystem

The Orbiter Propulsion Subsystem (PROP) is a modular element of the Viking spacecraft designed to produce, upon command, a directed impulse to accomplish up to four Interplanetary Trajectory Corrections (ITC), a Mars Orbit Insertion (MOI) maneuver, and up to twenty Mars Orbit Trim (MOT) maneuvers. The PROP subsystem is a fixed thrust, multi-start, pressure fed, earth-storable bipropellant system utilizing the propellants Nitrogen Tetroxide (N_2O_4) and Monomethylhydrazine (MMH) with helium for pressurization. Multiple restart capability of the rocket engine is provided by an electromechanical bipropellant valve. Ten pyrotechnic valves and two latching solenoid valves provide positive isolation of the propellant and pressurant during various mission phases. All electrical signals to actuate the valves and fire the squibs come through the Pyrotechnic Subsystem.

2.   Pyrotechnic Subsystem

The VO Pyrotechnic Subsystem (PYRO) provides the following functions: squib actuation of all required VO electro-explosive devices, electrical energy storage and power switching for initiation of the VO electro-explosive devices (except the spacecraft release devices), and switching of electrical power for actuation of the solenoid valves used in the VO PROP. The spacecraft release devices, although included in the PYRO, were initiated (fired) by the Centaur pyrotechnic control unit in the Launch Vehicle. The PYRO includes a total of 22 pyrotechnic devices (with 31 total squibs), consisting of eight release nuts, one pinpuller, two normally-open pyrotechnic valves and 11 normally-closed pyro-technic valves.

B.   PROPULSION SUBSYSTEM

1.   Description

The Orbiter PROP is a modular element designed to deliver in excess of 870,000 lbf-sec of propulsive impulse to the Viking Spacecraft. In summary, it was designed to be capable of:

(1)   Providing a total velocity change of 1480 mps to a 7556-lbm spacecraft with a usable propellant mass of 3055 lbm.

(2)   Providing, in a single burn, an MOI velocity increment of up to 1325 mps.

(3)   Performing up to four ITCs, one MOI, and 20 MOTs.

(4)   Performing a firing within 32 hours after the preceding firing.

(5)   Providing a minimum impulse capability of 120 lbf-sec.

(6)   Performing an engine firing within 240 sec following termination of the last attitude orientation maneuver.

(7)   Producing thrust with very small swirl disturbance, i.e., less than 4.0 in-lbf of real torque about the roll axis.

(8)   Functioning without degradation in performance for 510 days after launch in a vacuum and gravity-free environment within a temperature range of 30° to 90°F.

The VO PROP is a fixed thrust, multi-start, pressure fed, earth-storable bipropellant system utilizing the propellants Nitrogen Tetroxide (N204) and Monomethylhydrazine (MMH) with helium for pressurization. A two-axis gimballed engine and electromechanical actuators provided thrust vector control in the pitch and yaw directions during engine operation. PROP, with its structure, is a mechanically defined module with eight subassemblies and is depicted in Figure II-55.

The eight subassemblies are functionally and physically independent and extended the modular design concept into the subsystem. The subassemblies are as follows:

PRESSURANT TANK
ASSEMBLY

GAS SHARE ASSEMBLY

PROPELLANT TANK
ASSEMBLY - OXIDIZER

PRESSURANT
CONTROL ASSEMBLY

PROPELLANT
TANK ASSEMBLY-FUEL

PROPELLANT
ISOLATION ASSEMBLY - FUEL

PROPELLANT ISOLATION
ASSEMBLY - OXIDIZER

ROCKET ENGINE ASSEMBLY
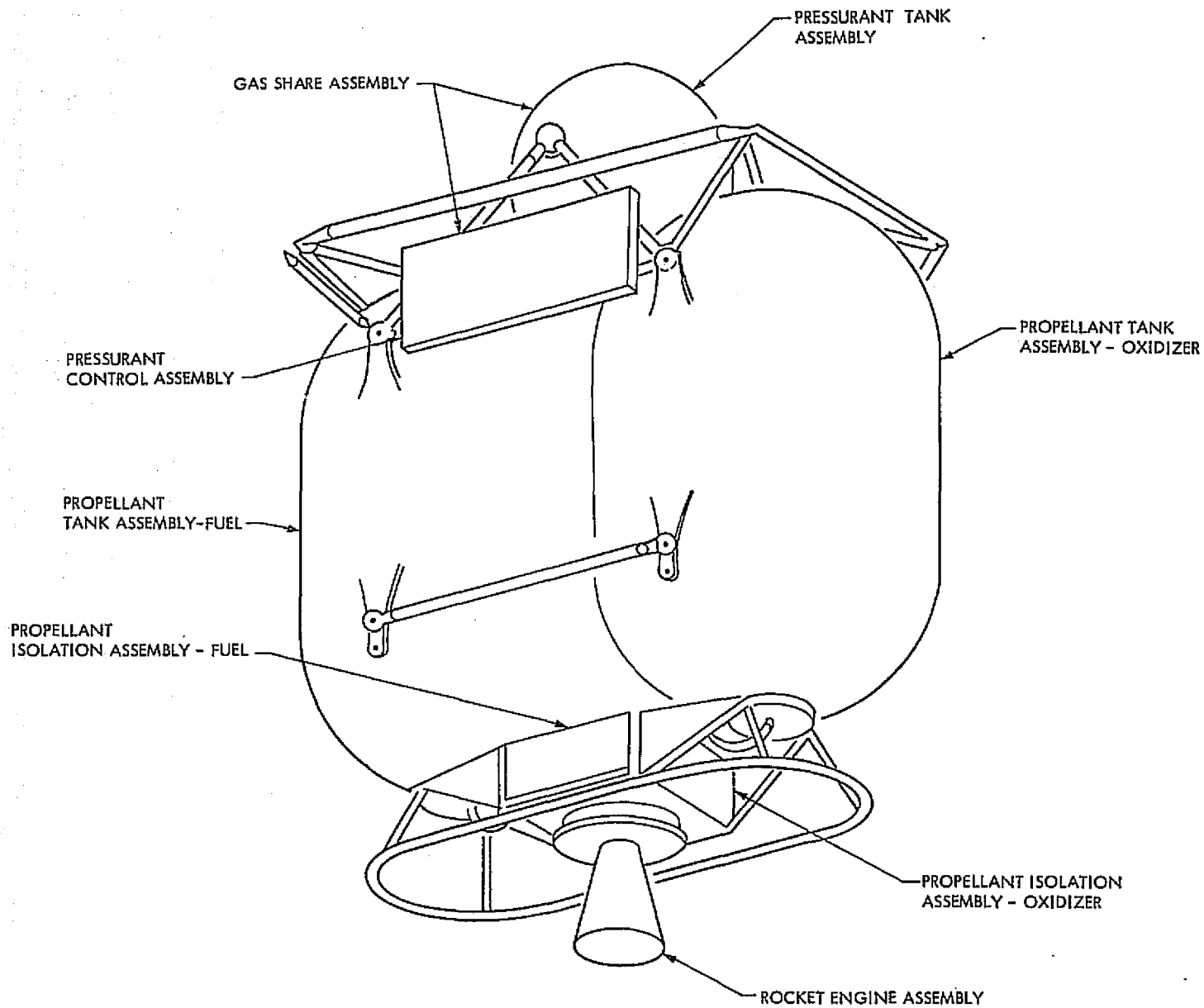
Figure II-55. Propulsion System

(1)   Pressurant Tank Assembly (PTA)

(2)   Pressurant Control Assembly (PCA)

(3)   Propellant Tank Assembly--Fuel and Oxidizer

(4)   Propellant Isolation Assembly (PIA)--Fuel and Oxidizer

(5)   Rocket Engine Assembly (REA)

(6)   Gas Share Assembly (GSA)

Two identical propellant tank assemblies and two identical propellant isolation assemblies are integrated into the subsystem to store and control the flow of propellants--oxidizer and fuel.

The basic operation of the subsystem can best be described from a propulsion schematic, Figure II-56. Propellants flow from the propellant tanks, through the propellant isolation assemblies, and into the rocket engine combustion chamber. There they mix and chemically react, creating gaseous reaction products which are accelerated through the engine and ejected at high velocity. The combustion chamber nominally operates at a pressure level of 116 psia while the propellant tanks operate in the 240 to 250 psia range. The pressure level in the propellant tanks is maintained by a regulated pressurant gas (helium) in-flow through the pressurant control assembly. The pressurant gas is withdrawn from the pressurant tank which will vary in pressure from approximately 3700 psia early in the mission to 243 psia (depending on utilization strategy) at the end of the mission. The pressurant and propellant isolation assemblies provide fluid filtering and positive isolation of the pressurant gas supply and the propellant liquids during long periods of cruise.

The gas-share assembly is not an integral part of the PROP. Gas share is an add-on feature which provides a capability to transfer propulsion pressurant gas to either of the reaction control assemblies in the ACS. Gas transfer to ACS is not a normal function of PROP and was not required to be utilized during the primary mission (its use is anticipated at some point in time during the extended mission).
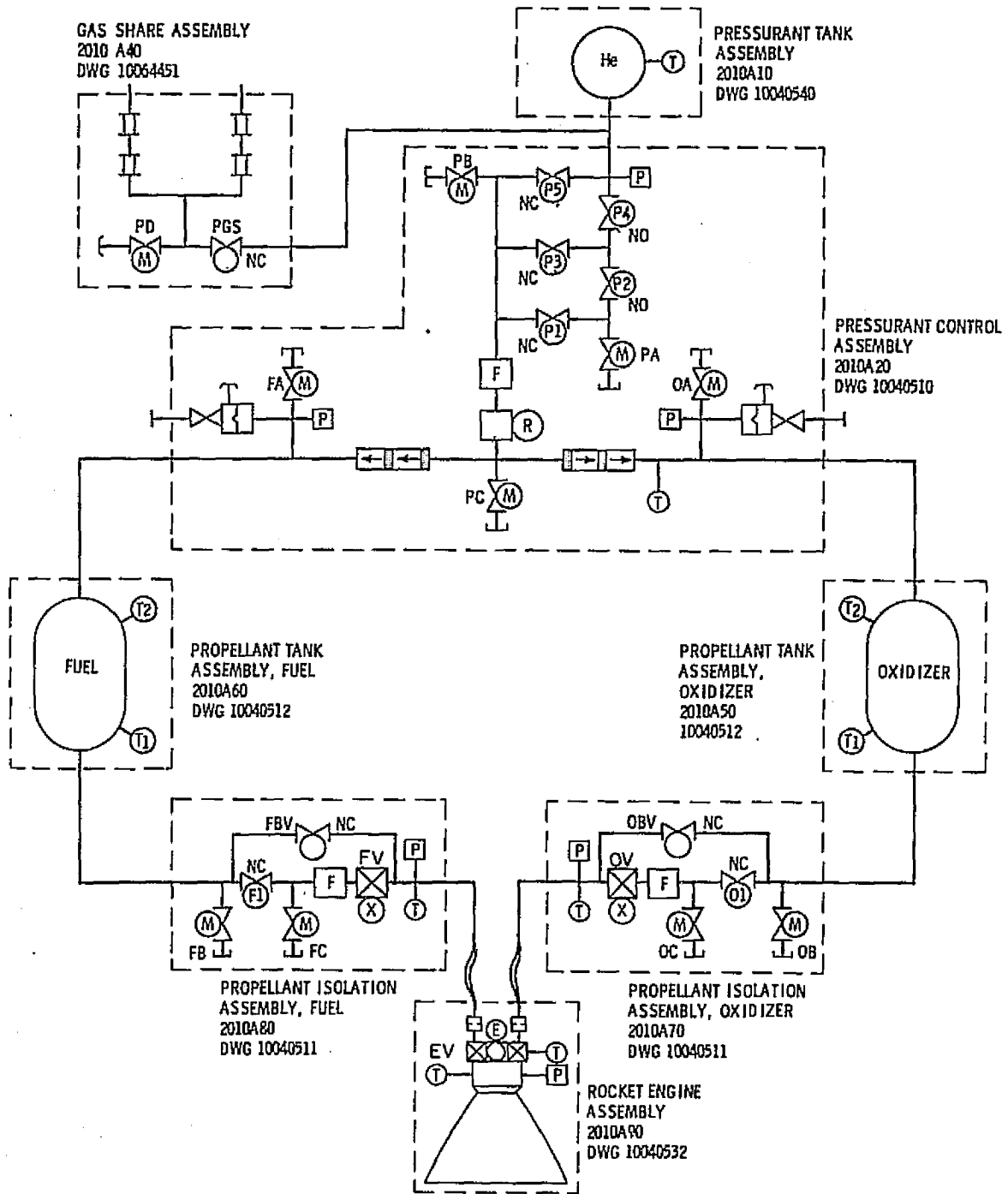
Figure II-56. Propulsion Subsystem Schematics

A typical PROP mission sequence is shown in Table II-28. At launch, the high-pressure helium supply and the propellants are isolated by the pyrotechnic valves P1, P3, P5, O1 and F1, as shown in Figure II-56. Prior to the first propulsive maneuver, the engine valve (EV) and the solenoid isolation valves (FV and OV) must be opened to vent trapped air downstream of the propellant isolation valves. After closing the engine valve, propellants are allowed to flow to the engine valve by opening the two normally-closed pyrotechnic valves, O1 and F1. Propellant tank pressurization is accomplished by opening the pyro valve, P1. The PROP is now prepared for operation and the propulsive maneuver is performed by opening the engine valve (which allows pressurized propellant to flow into the thrust chamber) to undergo hypergolic ignition until the desired velocity increment is achieved. The maneuver is terminated by closing the engine valve (removing electrical power).

2.   Performance

a.   Flight Events. The actual flight sequence of events involving PROP and PYRO for VO-1 and VO-2 are shown in Tables II-29 and II-30, respectively. The events for both subsystems followed closely the pre-launch nominal sequence of events with the exception of the redesign of the approach maneuvers required on VO-1 and VO-2 to compensate for the helium regulator leakage problem. A detailed discussion of the VO-1 regulator leakage problem and the redesign of the approach maneuvers is presented in paragraphs b and c.

During the primary mission, eleven propulsive maneuvers were conducted on VO-1, nine on VO-2. Maneuver durations ranged from the 39.4-min. VO-2 orbit insertion maneuver, the longest engine burn in space to date, to a 2.8-sec Mars orbit trim, MOT-8 on VO-1. The MOI burn duration for VO-1 (37.6 min) was only slightly shorter than the VO-2 MOI.

Separation of VL-1 from VO-1 was achieved on July 20, 1976, followed the next day by separation of the aft-bioshield and VL adapter structure. Both events were successful and without incident. VL-2 separation from VO-2 was achieved on September 3, 1976. Coincident with Lander separation, the primary inertial reference unit (IRU-1) failed, resulting in a momentary break in communications and a switch to IRU-2. IRU-1 could not be recovered and because

Table II-28. Typical Propulsion Operational Sequence

Maneuver (Mission Time)	Event	Typical Velocity Change (mps)	Typical Burn Duration (sec)
First Cruise Phase (Separation + 2 days)	Vent Prop Lines	DNA	DNA
Midcourse No. 1 (Launch + 5 days to Launch + 20 days)	Open Prop Iso Valves and Vent Open Prop Lines (O1, F1) Pressurize Prop Tanks (P1) Execute Rocket Engine Firing Close Prop Iso Valves Isolate Pressurant Source (P2)	10	25.6
Midcourse No. 2 (MOI - 30 days to MOI - 5 days)	Open Prop Iso Valves Pressurize Prop Tanks (P3) Execute Rocket Engine Firing	6	15.3
Midcourse No. 3 (MOI - 30 days to MOI - 5 days)	Execute Rocket Engine Firing	0.2	0.5
Mars Orbit Insertion (MOI)	Execute Rocket Engine Firing	1175	2445.1
Preseparation Orbit Trims Phasing (Up to 10 Burns) (MOI + 1 day to MOI + 30 days)	Execute Rocket Engine Firing Isolate Pressurant Source, P4, as required Close and Op-n Prop Iso Valves Between Burns (as required)	225.6 Total DNA DNA	363.3 Total DNA DNA
Separation Orbit (Up to 10 Burns)	Execute Rocket Engine Firing	134.0 Total	91.6 Total
	Mission Total	1550.8*	2941.4

*Corresponds to a ΔV of 1484 mps for the VO, with VLC attached for all firings.

Table II-29. VO-1 Flight Sequence of Events

Date	Event	Time ERT, UTC	Engine-On Time In Seconds		Velocity Change (ΔV), MPS	Maneuver Weight Lbs	ACS GN_2 Remaining Lbs
			Predict	Actual	Predict		
8/20/75	Launch	21:22	–	–	–	7769.5	32.3
8/21/75	Line Vent	00:38	–	–	–	7650.5	32.3
8/26/75	Pressurize (P1,O1,F1)	22:07	–	–	–	7650.5	32.3
8/28/75	M/C-1	18:30	12.03	12.07	4.684	7650.2	32.0
9/16/75	Isolate Press. (P2)	17:17	–	–	–	7637.5	31.9
9/17/75	Close Prop. Iso. Valves	17:30	–	–	–	7637.5	31.9
6/04/76	Open Prop. Iso. Valves	16:05	–	–	–	7636.7	31.1
6/07/76	Press. (P3)	17:23	–	–	–	7636.7	31.1
6/10/76	AMC-1	11:17	123.97	122.39	50.540	7636.7	31.1
6/15/76	AMC-2	14:17	143.67	143.09	60.000	7503.8	31.0
6/19/76	MOI	22:38	2271.02	2256.3	1097.270	7348.7	30.9
6/21/76	MOT-1	17:43	131.25	130.63	80.050	5018.3	30.7
7/07/76	Isolate Press. (P4)	23:20	–	–	–	4879.5	29.6
7/08/76	MOT-5	00:58	41.04	41.11	25.713	4879.5	29.6
7/14/76	MOT-6	07:30	4.38	–	2.736	4835.7	29.3
7/20/76	Lander Sep.	08:51	–	–	–	4831.0	29.2
7/21/76	Sep. Aft Bioshield	02:00	–	–	–	2503.5	28.9
8/02/76	SK-2	03:19	1.73	–	2.228	2311.0	28.4
9/11/76	MOT-7	19:24	16.19	16.26	21.327	2307.7	26.9
9/20/76	MOT-8	22:36	2.84	–	3.708	2290.2	26.4
9/24/76	MOT-9	15:31	17.38	17.40	22.926	2285.4	26.4

Table II-30. VO-2 Flight Sequence of Events

Date	Event	Time ERT, UTC	Engine-On Time In Seconds		Velocity Change (ΔV), MPS	Maneuver Weight Lbs	ACS GN$_2$ Remaining Lbs
			Predict	Actual	Predict		
9/09/75	Launch	18:39	–	–	–	7766.0	30.8
9/10/75	Line Vent	00:28	–	–	–	7647.0	30.8
9/17/75	Pressurize (P1,01,F1)	12:37	–	–	–	7647.0	30.8
9/19/75	M/C-1	16:30	21.1	21.30	8.11	7646.7	30.5
10/06/75	Isolate Press. (P2)	19:22	–	–	–	7625.1	30.3
10/07/75	Close Prop. Iso. Valves	17:20	–	–	–	7625.1	30.3
7/26/76	Open Prop. Iso. Valves	17:19	–	–	–	7624.4	29.6
7/27/76	AMC	01:19	25.08	25.01	9.223	7624.3	29.5
8/06/76	Press. (P3)	22:11	–	–	–	7624.2	29.4
8/07/76	MOI	11:49	2374.8	23.62.7	1100.8	7599.8	29.4
8/09/76	MOT-1	17:35	7.11	7.08	4.077	5185.9	29.2
8/14/76	MOT-2	08:51	3.06	–	1.776	5178.3	29.0
8/25/76	MOT-3	18:09	72.64	72.74	42.728	5175.0	29.0
8/27/76	MOT-4	20:46	19.07	19.19	11.292	5098.8	29.0
9/03/76	Lander Sep.	19:40	–	–	–	5078.7	28.9
9/28/76	MOT-5A	04:54	4.58	–	5.0	2749.6	27.5
9/30/76	MOT-5B	21:29	299.4	298.32	342.551	2744.8	27.5
10/05/76	Isolate Press. (P4)	19:58	–	–	–	2436.9	27.4

it was suspected that the pyro event (shock) during Lander separation could have caused the IRU failure, the decision was made not to separate the aft- bioshield and VL adapter on VO-2. This separation would have involved a second pyro shock and might have endangered the remaining IRU. The aft-bioshield and adapter, weighing 191 lbs. remain attached to VO-2.

b. <u>Pressurant System.</u> The helium tank pressures at launch were 3705 psi and 3703 psi for VO-1 and VO-2, respectively, representing 10.7 lbs of helium in each tank. The first indication of pressurant system performance was the initial pressurization, August 26, 1975 on VO-1 and September 17, 1975 on VO-2. Average VO-1 flight tank pressure following pressurization was 254 psi, within one psi of the average value for the regulator family assuming a check valve lockup ΔP of 4 psi. Average VO-2 flight tank pressure following pressurization was 250 psi and was assumed to have been an anomalous lockup. A check of the component data, however, revealed that the regulator for VO-2 (S/N 007) represented the lower limit of the regulator family while VO-1's regulator was near the upper limit. The <u>final</u> difference in the system lockup pressures (6 psi) was representative of ground test data and both regulators were considered to be operating normally. Both VO-1 and VO-2 systems operated normally during their respective midcourse maneuvers and were subsequently locked up, P_2 closed, for the long cruise period.

On June 7, 1976 pyro valve P3 was actuated to repressurize the propellant tanks on VO-1 in preparation for the approach mid-course correction. Initial tank pressures were normal. However, the propellant tank pressures continued to increase at a rate of 0.68 psi/hr, indicating that the regulator had not achieved a leak-tight reseat. At the observed pressure rise rate the tank pressures would have reached the pressure relief system burst diaphram rupture pressure of 320 psi in 95.6 hrs ($\approx$4 days) or 8 days prior to MOI (reference paragraph 3.b.).

Several options were explored, with the object of preventing rupture of the burst diaphrams without actuating the last remaining normally-open pyro valve (P4) to isolate the helium system. Actuation of P4 would have introduced a single point MOI failure mode, since there would have been only one valve left (P5) to reopen the helium system for MOI. While pyro valves are considered

extremely reliable, it was felt that this action assumed an unnecessary risk as long as other options were available. In the option selected, the approach mid-course correction maneuver was redesigned to accommodate a longer engine-on time and thus increase the possibility of flushing out any small particle(s) that might be lodged under the regulator valve seat. The delayed maneuver consisted of a 50 mps change in velocity, lasting 125 sec on June 10, 1976. Following the maneuver the leak continued, however, and a second maneuver of 60 mps was required on June 15 to maintain the tank pressures at an acceptable level for MOI.

The MOI maneuver for VO-1 was conducted on June 19, 1976 from initial pro-pellant tank pressures of 283 psi. Regulator performance during MOI was normal in all respects. Regulator leakage continued following MOI; however, the pro-pellant tank pressure rise rates were acceptably small due to the large post-MOI ullage volumes. The first MOT maneuver, 80 mps, was conducted on June 21, 1976. On July 7, the helium system was isolated by closing pyro valve P4 in accordance with the nominal sequence of events. Six subsequent maneuvers in the primary mission were conducted in the blowdown mode.

Since the cause for the regulator leakage could not be uniquely determined, it was assumed that a reasonable probability existed for a similar occurrence when pyro valve P3 was opened on VO-2. To accommodate this possibility, the sequence of events was rearranged so that the approach mid-course correction was done in the blowdown pressure mode. P3 opening was delayed until just 13-1/3 hours before the MOI to minimize tank over-pressurization in the event of a leak. Regulator lockup following the P3 event was normal. During the 13-hour pre MOI period 3 of the 4 pressures increased one DN indicating possible low rate leakage. The starting propellant tank pressures were 255 psi for the MOI on August 7, 1976. The helium system was not isolated (P4 closed) until October 5, 1976, following the sixth MOT maneuver. Regulator performance during this period was normal, with no leakage visible on telemetry measurements.

    c.   <u>REA and Feed System.</u> Performance of the rocket engine is measurable only indirectly through the observed chamber pressure and the engine burn time to achieve a given spacecraft velocity increment. Comparison of the predicted maneuver duration, computed by the propulsion system mathematical model (PSOP) using the observed pressures and temperatures and the nominal system performance

characteristics, with the actual duration as determined by the on-board accelerometers, provides a good overall assessment of system performance. Table II-31 presents a comparison of the predicted and actual maneuver durations for maneuvers over 5 sec in duration. The actual duration is derived from the accelerometer status channel which is sampled in 5 sec intervals. Accuracy of the derived maneuver times, when more than one sample is available, is ±0.024 sec. This is significantly more accurate than that which could be determined from chamber pressure which is sampled only every 0.224 sec (high-rate data). The table shows that the difference, predict minus actual, is within 0.2 percent of actual with a one-sigma spread of approximately one-half percent for both subsystems. Assuming a normal distribution, the three-sigma tolerance for maneuver duration predictability is approximately 1.5 percent. This is well within the system specification for maneuver predictability of ± 2 percent.

A comparison of the actual (flight data) and predicted rocket engine chamber pressure during the MOI maneuver for VO-1 is presented in Figure II-57. The dual DN values from 100 sec to the end of the maneuver indicate a 73/74 ON toggle. The true chamber pressure during this period is right at the threshold of 74 DN (115.9 psi). Agreement between predicts and flight data is very good, as evidenced by the ability to predict maneuver duration. Figure II-57 is typical of the propulsive maneuvers for both VO-1 and VO-2.

d.   Propellant and Pressure Management. Both propulsion subsystems performed without incident, excluding the regulator leakage problem, performing a total of 20 propulsive maneuvers with a total cumulative duration of 5562.7 sec (over 1.5 hours). A summary of the propulsive maneuver parameters is presented in Table II-32 for VO-1 and VO-2. The velocity increment imparted, propellant expended and the initial propellant and helium tank pressures for each maneuver are given. The status of the pressurant system (helium regulator) is also shown along with the maximum engine valve soak-back temperature following each maneuver.

Total propellant expended during the primary mission for VO-1 was 2856 lbs, leaving 283 lbs for the extended mission. Assuming that the subsystem continues to operate as indicated to date, the maneuver capability remaining is 242 mps.

Table II-31. Maneuver Duration Predictability

VO-1				
	Duration in Seconds			**Delta (% Actual)**
Maneuver	Predict	Flight Actual	Delta (Pred.–Actual)	
MC	12.03	12.07	-.04	-0.35%
AMC-1	123.97	122.39	1.58	1.29%
AMC-2	143.67	143.09	0.58	0.41%
MOI	2271.02	2256.30	14.72	0.65%
MOT-1	131.25	130.63	0.62	0.47%
MOT-5	41.04	41.11	-0.07	-0.17%
MOT-7	16.19	16.26	-0.07	-0.43%
MOT-9	17.38	17.40	-0.02	-0.12%
			AVG =	0.22%
			1σ =	0.55%
VO-2				
MC	21.10	21.30	-0.20	-0.94
AMC	25.08	25.01	0.07	0.28
MOI	2374.80	2362.70	12.10	0.51
MOT-1	7.11	7.08	0.03	0.42
MOT-3	72.64	72.74	-0.10	-0.14
MOT-4	19.07	19.19	-0.12	-0.62
MOT-5	299.40	298.82	0.58	0.19
			AVG =	-0.08%
			1σ =	0.51%
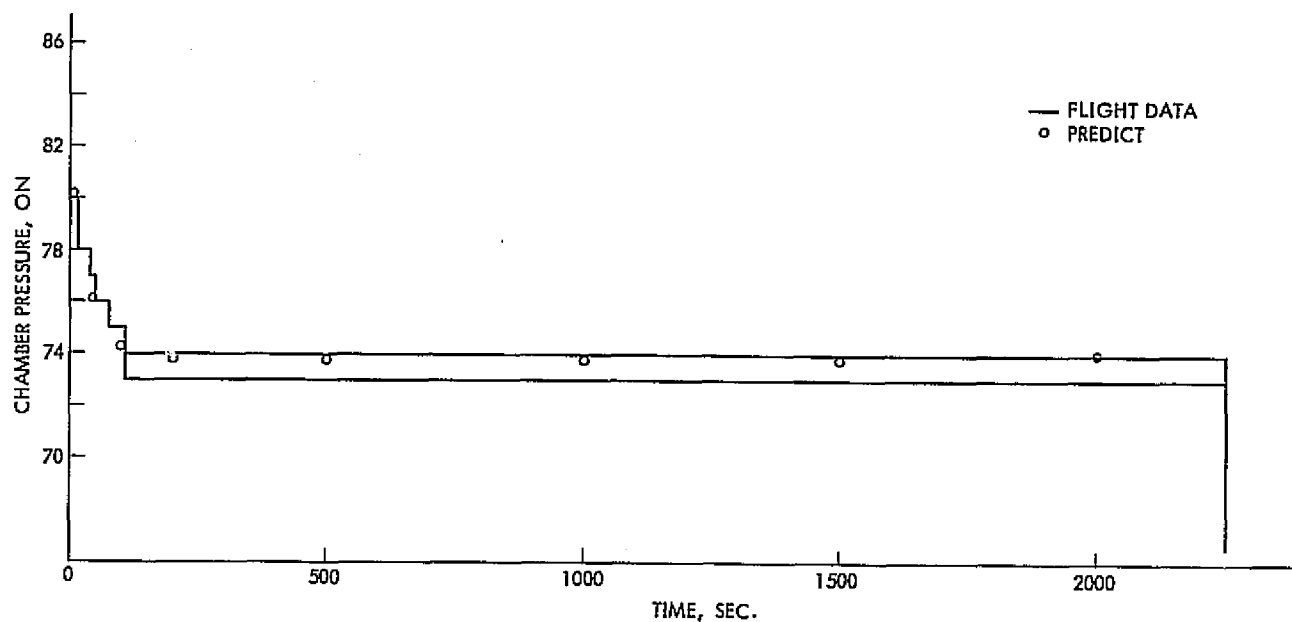
Figure II-57. Rocket Engine Chamber Pressure vs Time

Total propellant expended for VO-2 was 2880 lbs, leaving 261 lbs for the extended mission. Remaining maneuver capability for VO-2 is 193 mps. Remaining maneuver capability for VO-1 and VO-2 was calculated on the basis of usable propellant less the residuals. The residuals are that portion of the propellants, 44 lbs total, set aside to compensate for the uncertanties in the system performance characteristics.

3.   Anomalies

a.   Propellant Tank Temperatures During VO-1 Propellant Warmup. During the first seven hours of Aug. 23, 1975, 48 hours after the start of propellant warmup, fuel tank temperature, TF1, toggled between the initial value of 58 DN and a lower value of 54 DN, finally reaching a low value of 53 DN at 08:00 hours. Toggling continued but in an upward direction for the next 24 hr with the fuel tank temperature returning to the initial value of 58 DN. For an additional 30 hr the toggling continued in a generally increasing trend consistent with overall spacecraft heating.

Table II-32. Propulsive Maneuver Summary

Event	Velocity Change (ΔV), MPS	Expended Propellant, Lbs.		Starting Tank Press. PSI			Helium Reg. Active	Max. Eng VLV Temp, F°
		Oxid	Fuel	Oxid	Fuel	Helium		
VO-1								
Launch	–	–	–	99	114	3607	No	–
M/C-1	4.684	7.5	5.0	257	257	3446	Yes	166
AMC-1	50.540	81.1	51.8	304	304	3224	Yes	216
AMC-2	60.000	94.4	50.5	305	305	3099	Yes	216
MOI	1097.270	1396.4	934.0	283	283	2968	Yes	235
MOT-1	80.050	83.2	54.5	267	261	1044	Yes	211
MOT-5	25.713	26.1	17.4	263	264	933	No	183
MOT-6	2.736	2.8	1.9	260	261	933	No	106
SK-2	2.228	1.1	0.7	260	261	933	No	101
MOT-7	21.327	10.2	6.8	260	261	933	No	146
MOT-8	3.708	1.8	1.2	258	260	933	No	97
MOT-9	22.926	10.9	6.3	257	260	933	No	151
VO-2								
Launch	–	–	–	102	100	3936	No	–
M/C-1	8.11	13.0	8.6	252	251	3442	Yes	183
AMC	9.223	14.9	9.5	240	236	3346	No	157
MOI	1100.8	1448.2	965.5	255	255	3299	Yes	227
MOT-1	4.077	4.5	2.9	265	255	1195	Yes	116
MOT-2	1.776	2.0	1.3	264	255	1195	Yes	97
MOT-3	42.728	46.3	30.0	266	255	1195	Yes	198
MOT-4	11.292	12.1	7.9	260	255	1164	Yes	151
MOT-5A	5.0	2.9	1.9	258	258	1110	Yes	107
MOT-5B	342.551	185.0	123.3	257	257	1110	Yes	213

Initially the toggling of the fuel tank temperature was assumed to be an indication of either a failing temperature transducer or a data processing error. Subsequent fuel tank temperature data over the next 12 days responded in a normal manner to the changing spacecraft thermal state, indicating normal transducer operation. A check of other engineering measurements in the FDS data-deck containing fuel tank TF1 produced no abnormal data variations during this time period. The absence of any similar data disturbances in adjacent measurements, coupled with the subsequent normal operation of the fuel tank temperature, indicated that the temperature variations observed on Aug. 23 were real.

Propellant tank bottom skin temperatures TF1 and TO1 are presented as a function of time in Figure II-58 and II-59 for fuel and oxidizer, respectively. The subject fuel tank temperature variation is the 5° (5 DN) temperature drop at the start of Aug. 23 (see Figure II-58). A second rapid drop in the fuel tank wall temperature occurs at the start of the yaw turn just prior to the midcourse propulsive maneuver on Aug. 27, 1975. The oxidizer tank temperature (see Figure II-59) illustrates two rapid temperature drops similar to those noted in
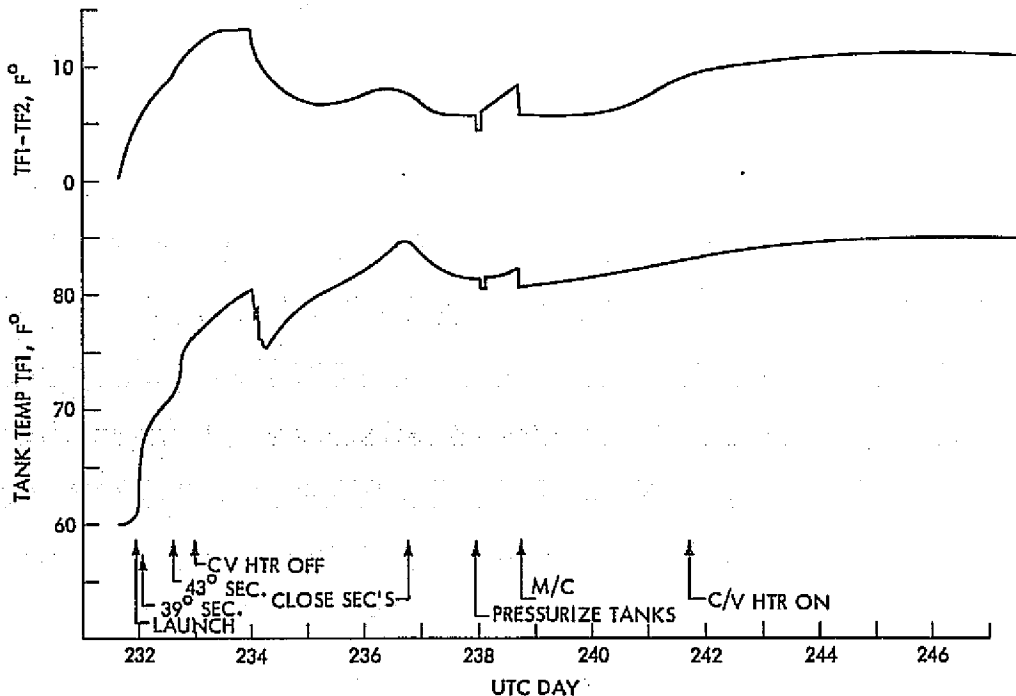
Figure II-58. Fuel Tank Temperature Profile (VO-1)
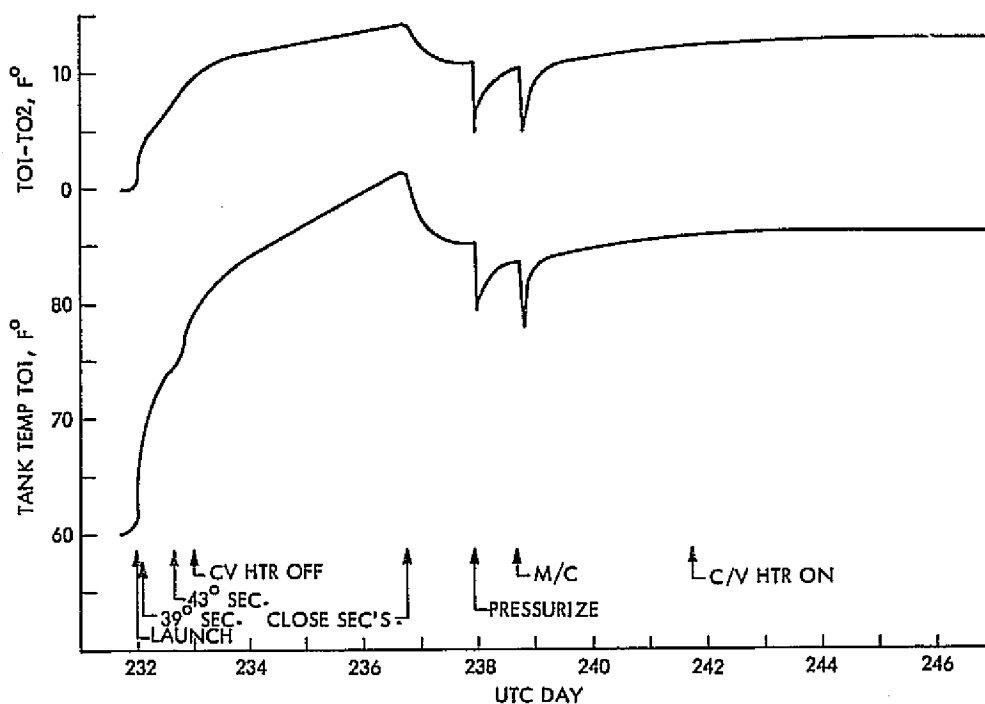
Figure II-59. Oxidizer Tank Temperature Profile (VO-1)

in the fuel tank: at propellant tank pressurization (Aug. 26) and again at the start of the yaw turn just prior to the mid-course propulsive maneuver.

The only mechanism in the propellant tanks capable of producing the rapid tank wall temperature changes in a zero-g environment is propellant circulation. Large temperature gradients are produced in the propellants during the warmup period due to the concentrated solar heating of the tank walls. The thermal gradient in the radial direction is computed to be 20 to 25°F after 3-4 days of SEC heating. The temperature gradient in the longitudinal direction, based on telemetry data, ranged from 10° to 15°F. Temperature gradients in the fuel tank tend to be smaller than those in the oxidizer tank due to the higher heat conductivity of the fuel.

Initiation of propellant circulation requires application of a force large enough to cause some physical movement of the propellant within the tank. Once started, however, propellant movement will continue for some time (possibly days) since the only damping forces are viscous in nature. Only two events during the early portion of the cruise period were expected to produce sufficient forces to initiate propellant circulation: propellant tank pressurization and the mid-course propulsive maneuver.

During propellant tank pressurization, the incoming gaseous helium is directed toward the tank top and sweeps down the tank wall, setting up a toroidal vortex circulation pattern in the tanks. The repositioning of the ullage bubble due to the incoming gas imparts a force to the liquid to initiate circulation. The rapid $6^\circ F$ drop and $4^\circ F$ recovering of the oxidizer tank wall temperature following pressurization (see Figure II-59) is indicative of the existence of the relatively large temperature gradients in the oxidizer. The oxidizer temperature disturbance at the mid-course maneuver is nearly identical to that at pressurization. The temperature drop was $5^\circ F$ with complete recovery within 10 hr.

Fuel tank wall temperature during propellant pressurization toggled only ±1 DN from its initial value for a two-hour period. During the 22 hours between pressurization and the M/C maneuver, the fuel tank wall temperature increased 1 DN. The oxidizer tank during the same period increased 4 DN. Fuel tank temperature drop prior to the M/C maneuver was 2 DN. These small fuel tank wall temperature variations, as compared to those in the oxidizer tank, indicate that the temperature gradient in the fuel was significantly smaller than that calculated at the end of warmup ($\approx 20^\circ F$). Since this calculated thermal gradient (based on no propellant mixing) was apparently nearly non-existent, it is evident that significant mixing occurred in the fuel tank prior to propellant pressurization. The 5 DN drop in fuel tank wall temperature on Aug. 23 (≈ 4 days prior) is apparently indicative of this circulation. The only disturbance in the spacecraft during this time period was high-rate slewing (fast rewind) of the DTR. This event occurred less than 30 min prior to start of the observed fuel tank temperature variation. The start of the DTR slewing was evidenced by

increased movement about the S/C yaw axis. The DTR movement, possibly combined with attitude control reaction, is thought to have provided the necessary initial propellant (fuel) movement.

b. VO-1 Regulator Leakage. The helium pressurant system was reactivated, after the 265 day cruise period, on June 7, 1976 by opening valve P_3 in the PCA. Following initial tank pressure lockup at 258 psi, which was near normal, the tank pressures continued to increase, thus indicating that the regulator had failed to effect a leak-tight reseat. Pressure rise rate in the propellant tanks was 0.68 psi/hr corresponding to a helium leak rate of 3.4 x 10^{-3} lbs/hr. The approach maneuver (AMC-1) was delayed one day and redesigned for a 50 mps velocity change to achieve an engine duration of 125 sec, significantly longer than originally planned. This charge was made on the assumption that the leak could be caused by a particle caught in the regulator seat area which might be flushed out by helium flow. The longer duration reduced the tank pressures sufficiently to actuate the regulator.

The helium leakage did not stop following AMC-1 but did decrease significnatly. Pressure rise rate after AMC-1 was 0.33 psi/hr, corresponding to a leak rate of 2.0 x 10^{-3} lbs/hr. Tank pressure increased to 305 psi by June 15, 1976 and a second maneuver of 144 sec duration was performed to reduce the tank pressurp to lockup, 258 psi. The leak rate was further reduced after AMC-2 to 1.7 x 10^{-3} lbs/hr. By the start of the MOI maneuver on June 19, 1976 (Day 171) the tank pressures had increased to 283 psi. Regulator performance during MOI was nominal in all respect. Post-MOI helium leakage was 4.0 x 10^{-4} lbs/hr, which when combined with the increased ullage volume, resulted in a propellant tank pressure rise rate of 0.02 psi/hr. By the start of the first MOT maneuver on June 21, 1976 (Day 173) the tank pressures had increased to 264 psi. Pyro valve P4 was closed on July 7, 1976 (Day 189) to isolate the helium system. Propellant tank pressures during the regulator leak period are shown in Figure II-60. The helium leak rates are summarized in Table II-33.
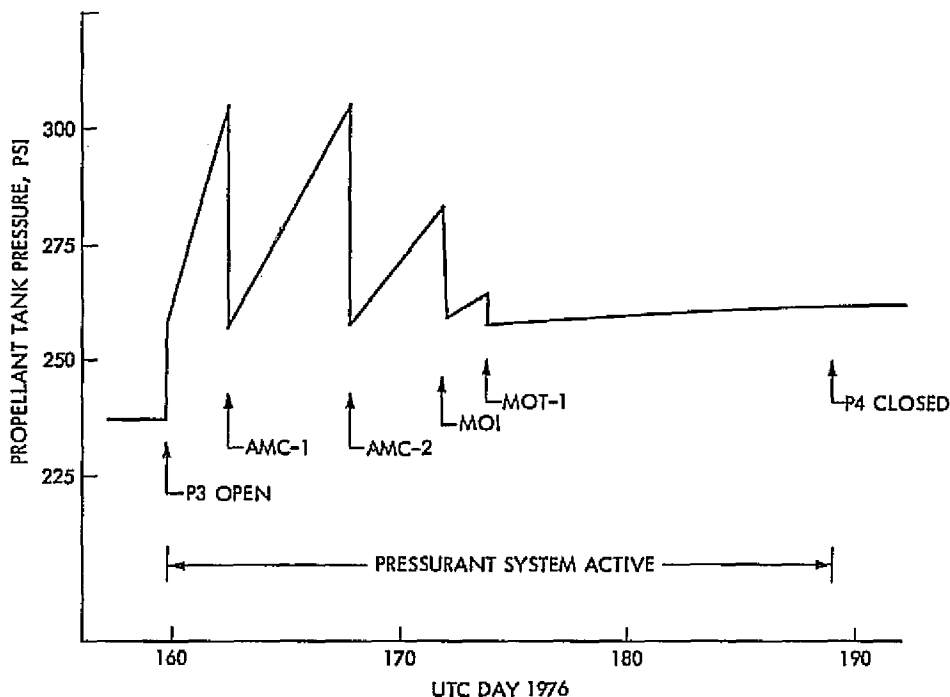
Figure II-60. Average Tank Pressure Second Pressurant
System Activation (VO-1)

Table II-33. VO-1 Regulator Leakage Summary

Event	Ullage (Oxid/Fuel, in^3)	Press Rise Rate, psi/hr	He Leakage (GHe flowrate, lbm/hr)
Post P-3	8099/4037	0.68	3.4×10^{-3}
Post AMC-1	9647/5668	0.33	2.0×10^{-3}
Post AMC-2	11445/7571	0.22	1.7×10^{-3}
Post MOI	38086/36978	0.02	4.0×20^{-4}

C.   PYROTECHNIC SUBSYSTEM

1.   Description

    a.   General. PYRO provides the following functions: squib actuation
of all VO electro-explosive devices, electrical energy storage and power
switching for the initiation of the VO electro-explosive devices (except space-
craft release devices), and switching of electrical power for the actuation of
solenoid valves used in the VO PROP.

    Table II-34 lists all hardware associated with PYRO. There are a total
of 31 electrically initiated hot-wire squibs per VO, in addition to a Pyrotechnic
Switching Unit (PSU), used for actuation of squibs, and a Propulsion Actuation
Unit (PAU), used for actuation of the PROP solenoid valves. The approximate
location of the squibs and electro-explosive devices is shown in Figure II-61.
The PSU and PAU are electronic subassemblies located in Bay 15 of the VO.

    A block diagram of PYRO is presented in Figure II-62. As shown in the
figure, the spacecraft separation release device squibs are initiated (fired) by
the Centaur pyro control unit. The other VO PYRO squibs are fired by the VO
PYRO PSU, as commanded by the CCS. The PROP solenoid valves are actuated with
power from the 30 Vdc converter, when switched by the PAU, as commanded by the
CCS.

    The 31 squibs used in the VO PYRO consist of four different sizes. The
four squib configurations have the same basic design, but each type has a differ-
ent quantity of explosive charge, as dictated by the requirements of the device
which is to be actuated.

    The squib explosive matchhead is initiated (fired) when current is switched
to and flows through the electrical bridgewire. Two of the four squib types have
a single bridgewire and are used in redundant pairs, in the HGA pinpuller and
release devices. The other two squib types have dual bridgewires and are used
in explosive valves (one squib per valve).

TABLE II-34.   PYRO Hardware

Device	Devices Per S/C	Squibs Per Device	Squibs Per S/C
Spacecraft Separation Bolts	4	2	8
High-Gain Antenna Unlatch Pinpuller	1	2	2
Scan Platform Unlatch (NC Valve)	1	1	1
Propellant Isolation Valves (NC)	2	1	2
Pressurant Isolation Valves (NC and NO)	5	1	5
Aft-bioshield/Adapter Separation Bolts	4	2	8
PIA Bypass Valves (NC)	2	1	2
PROP and ACS Gas Share Valves	3	1	3
Pyrotechnic Switching Unit (PSU)	1	–	–
Propulsion Actiation Unit (PAU)	1	–	–
TOTAL SQUIBS PER ORBITER	–	–	31

The squib is threaded into a port in the device which is to be actuated, with an O-ring making a pressure seal. When the explosive matchhead is initiated, or when the explosive output charge ignites, the resultant pressure generated within the device is so directed as to produce a force (e.g., on a piston) which results in the desired mechanical action.
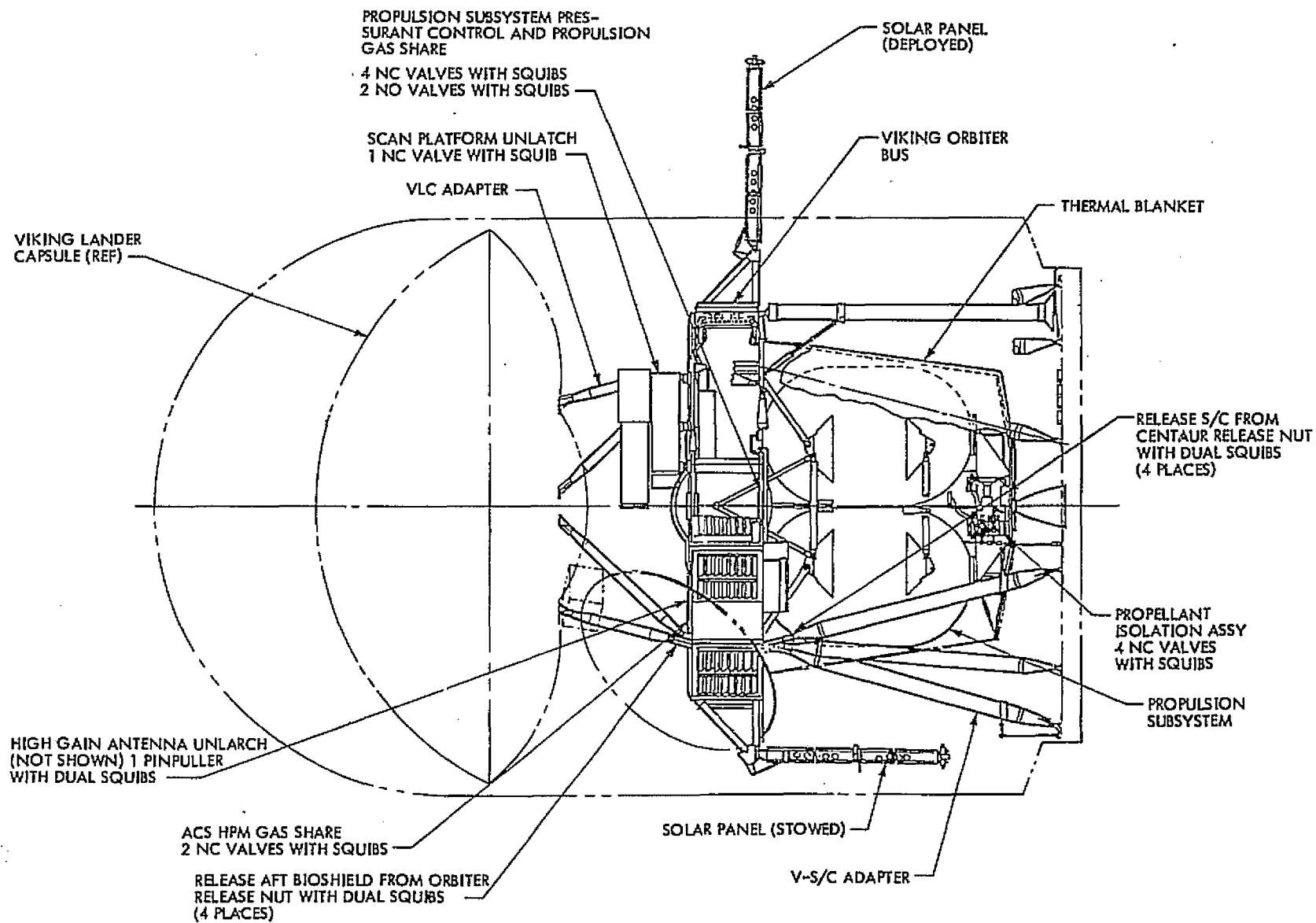
Figure II-61. Pyro, Squib Locations on Orbiter
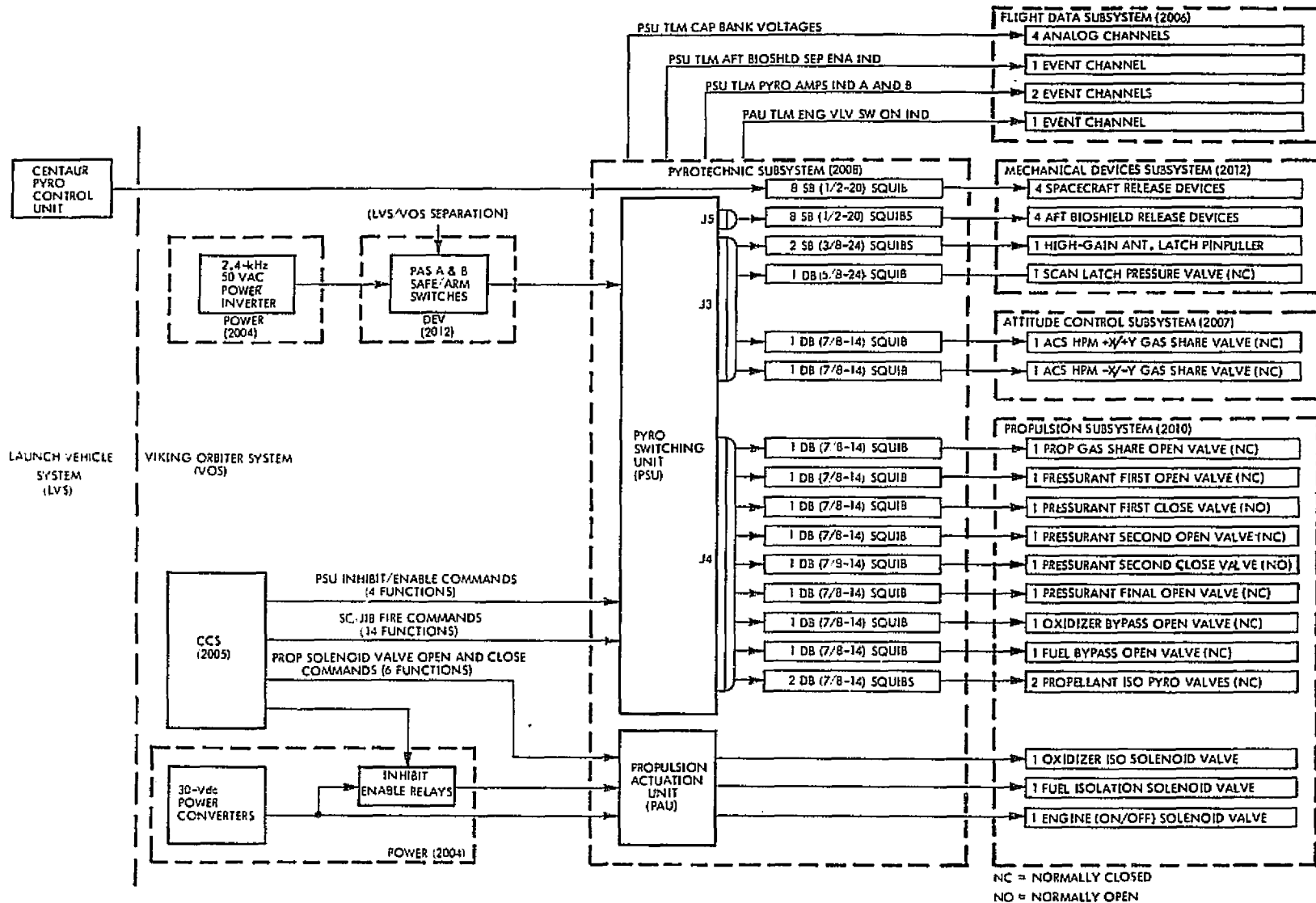
Figure II-62. Pyro and Interfaces Functional Block Diagram

b.   Pyrotechnic Switching Unit. The PSU is configured in an active, parallel redundant, manner for discharge firing of hot bridgewire squibs. The PSU also provides for enable/inhibit (charge/discharge) control of the energy-storage capacitor banks.

Upon receipt of the appropriate command from the CCS, the energy stored on capacitor banks is switched to specific squib bridgewires. The requirement on the PSU is that the energy delivered to each squib bridgewire shall be not less than 75 mj within one ms, and the initial peak current shall not exceed 25A. For nominal conditions, the minimum delivered energy will be approximately 150 mj in one ms, and the initial peak current will be in the range of 15 to 20A.

At each squib firing event, a pulse transformer in the return side of each redundant half of the PSU senses the current flow. The pulse from the transformer activates a pulse-stretching circuit which provides a momentary closure of a transistor switch that outputs to the FDS. The FDS provides a telemetered indication that the specific event was sensed.

c.   Propulsion Actuation Unit. The PAU receives power from the 30 Vdc converter within the PWR. Upon receipt of the appropriate command from the CCS, the PAU switches 30 Vdc power to open or close solenoid valves within the VO PROP. The 30 Vdc used by the PAU for command excitation and for actuation of the PROP engine valve is provided to the PAU whenever the 30 Vdc converters are turned on. The 30 Vdc used by the PAU for actuation of the PROP propellant isolation solenoid valves is supplied to the PAU via an inhibit/enable relay circuit located within the PWR; thus, this power may be turned off during certain critical periods.

2.   Performance

The PYRO subsystems on both VO-1 and VO-2 performed flawlessly throughout the primary mission. Table II-35 lists all of the PYRO events performed by both Orbiters.

Of the 22 pyrotechnic devices per Orbiter, 16 were actuated on VO-1 and twelve on VO-2. The difference between Orbiter pyrotechnical event totals was

the four separation bolts on the VO-2 aft-bioshield and VL Adapter that were never actuated. The decision to indefinitely delay the aft-bioshield separation on VO-2 resulted when IRU-1 was lost after VL-2 separation. It was suspected that a pyro event (such as an explosive bolt) during this separation may have produced sufficient shock to cause the IRU failure.

Six remaining pyrotechnic devices that were not actuated on either orbiter are the following: the final pressurant isolation valve (P5), the two propellant isolation assembly bypass valves (FBV and OBV), and the three valves associated with the gas share option. Each of these valves was intended only as a failure or contingency option.

As seen in Table II-35, there were 12 duty cycles on the engine valve (counting the line venting and maneuvers) and four cycles on the latch valves for VO-1. On VO-2 there were ten duty cycles on the engine valve and three cycles on the latch valves. All valve commanding on both orbiters was normal in all respects.

3. Anomalies

There were no anomalies on either orbiter in PYRO.

TABLE II-35. Primary Mission PYRO Events

| Event | 1975 | |
	VO-1	VO-2
1975		
Spacecraft Separation, HGA	Aug. 20	Sept. 9
Scan Platform	22	11
Open Latch Valves	22	11
Open/Close Engine Valve	22	11
01, F1, P1	26	17
Maneuver	27	19
P2	Sept. 16	Oct. 6
Close Latch Valves	17	7
1976		
Open Latch Valves	June 4	July 26
P3 (VO1)	7	–
Maneuver	10	28
P3 (VO2)	–	Aug. 6
Maneuver	15	7
Maneuver	19	9
Maneuver	21	14
P4 (VO1)	July 7	–
Maneuver	9	25
Maneuver	14	27
Close Latch Valves	–	Sept. 2
Lander Separation	20	3
Close Latch Valves	21	–
Aft Bioshield Separation	22	–
Open Latch Valves	Aug. 2	28
Maneuver	3	29
Close Latch Valves	15	–
Open Latch Valves	Sept. 11	–
Maneuver	11	30
Maneuver	20	–
Maneuver	24	–
P4 (VO2)	–	Oct. 5
Close Latch Valves	Oct. 28	28

SECTION VI

SCIENCE INSTRUMENTS

A. INTRODUCTION

1. Infrared Thermal Mapper

The purposes of the Infrared Thermal Mapper (IRTM) scientific experiment were to determine the surface temperature of Mars, determine the temperature of the Martian upper atmosphere, map observable variations in thermal inertia and spectral emissivity, search for regions of thermal imbalance, determine the temperature of any frost or clouds, and investigate the nature of any condensation phenomena.

The IRTM supported the Viking Landers by determining the Martian surface characteristics at the VL-2 proposed landing sites. In addition, IRTM observations were made over the VLs, complementing the VL meteorological experiments.

2. Mars Atmospheric Water Detector

The Mars Atmospheric Water Detector (MAWD) instrument measures the radiation at five wavelengths in the 1.38 μm water vapor absorption band. Figure II-63 shows computed spectra for water vapor in this band and the spectral location of the five lead sulfide (PbS) detectors which are used in the water vapor measurement. The energy incident upon the detectors is predominately reflected solar radiation received after two passes through the Mars atmosphere; the contribution to the received radiation from the thermal energy emitted by the Mars surface is negligible at this wavelength.

In essence, the radiance measured at the three positions corresponding to water vapor absorption lines are taken as ratios to the radiances of the remaining two (continuum) wavelengths to enable the absorption of the water vapor and hence its abundance to be determined.

3. Visual Imaging Subsystem

The purposes of the Visual Imaging Subsystem (VIS) experiment were to aid in the selection of landing sites for the Viking Landers, monitor the regions

surrounding the Landers, and provide additional spatial and temporal coverage of Mars in order to increase our knowledge of the planet and to aid in the selection of future landing sites. Prior to MOI, pictures of the whole planet were to be obtained to provide coverage of areas not readily accessible from orbit and to detect changes from the 1971 seasons. Additionally, star field pictures would be taken to improve the precision of approach navigation. After VL landing, observations were to be made of specific regions of Mars geological interest and of atmospheric phenomena such as cloud and haze layers.
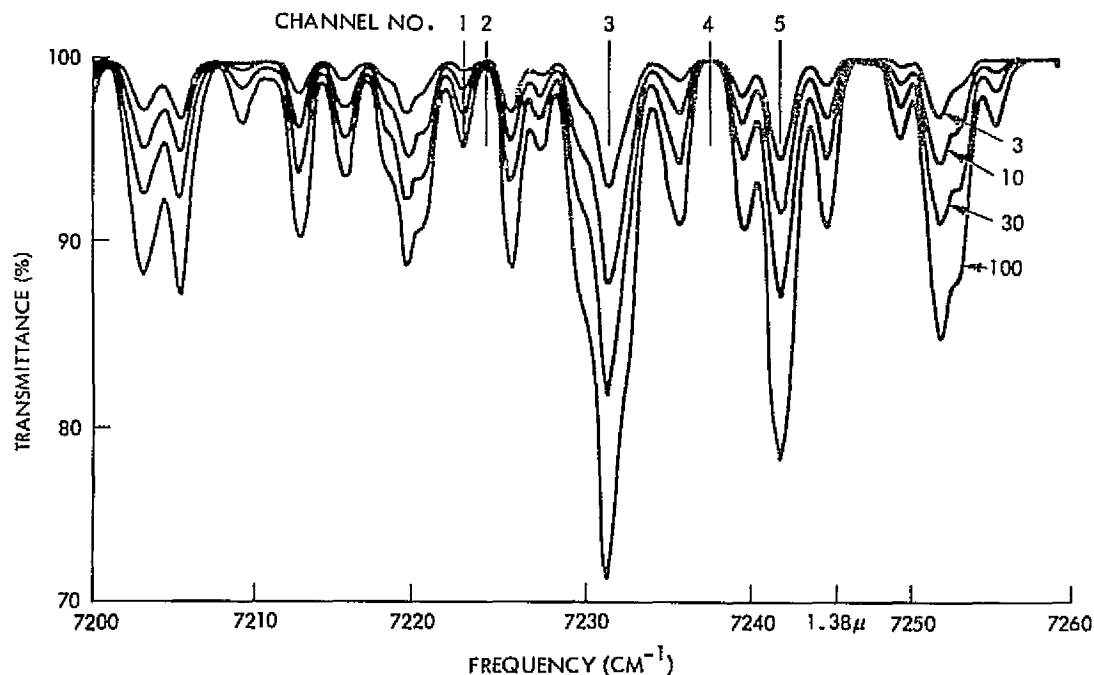
Figure II-63. MAWD Absorption Spectra

B.   INFRARED THERMAL MAPPER

1.   Description

The IRTM (see Figure II-64), is a 28-channel infrared radiometer. Thermal emission from an internal calibration source, space, or the planet is selected by positioning a scan mirror to one of three discrete positions. The radiation is reflected from the scan mirror into four telescopes. Each of the four telescopes has interference filters or special optical materials which pass radiation in selected wavelength bands. In the focal plane of each telescope are seven antimony-bismuth thermopile detectors to measure the radiation in each of the spectral bands, transmitted across a telescope's filter. The fields-of-view of each group of seven detectors are arranged in a chevron pattern; each detector's field-of-view is typically 5.2 mr. The EMF produced in each thermopile is amplified and converted to a level and format compatible with the FDS. Peridocally, diagnostic IRTM instrument engineering functions are substituted in place of the IR data. An essential feature of the thermopile amplification electronics is the DC restore capability. The IRTM is DC restored by viewing space and then null biasing each IR amplifier channel. The IRTM may operate in any of four selectable modes: Fixed Planet, Fixed Space, Fixed Reference, or Normal. During Normal Mode operation the scan mirror is stepped to all three positions by a timed sequence.

Thermal emission from the Martian surface is measured in four bands: 6.1 to 8.3 μm, 8.3 to 9.8 μm, 9.8 to 12.5 μm, and 17.7 to 24 μm. Seven detectors respond to reflected sunlight in the band from 0.3 to 3.0 μm. One detector measures radiation between 14.56 and 15.41 μm, in the CO_2 vibration band, to measure the stratospheric temperature. The response of all channels is nearly linear with flux, and is digitized into 1023 DNs. The maximum response of the solar band corresponds to 75 percent of a perfect white diffuser at normal incidence at the mean Mars distance from the Sun. The thermal bands have maximum temperatures between 300° and 330°K. The fields are splayed out in the cross-track direction. A detector's typical 5.2 ma field-of-view covers an 8-km circle on the surface at periapsis altitude. The angular resolution,

PREAMPLIFIER COVER

SPACE VIEW

TELESCOPE "D"

TELESCOPE "B"

TELESCOPE "A"

DIGITAL ELECTRONICS

PREAMPLIFIER (1 OF 4)

DETECTOR PLATE

PRIMARY MIRROR

PRIMARY BAFFLE

CONE BAFFLE

SECONDARY MIRROR

TELESCOPE "C"

SPIDER BAFFLE

SCAN MIRROR/ROTOR ASSEMBLY

PLANET VIEW
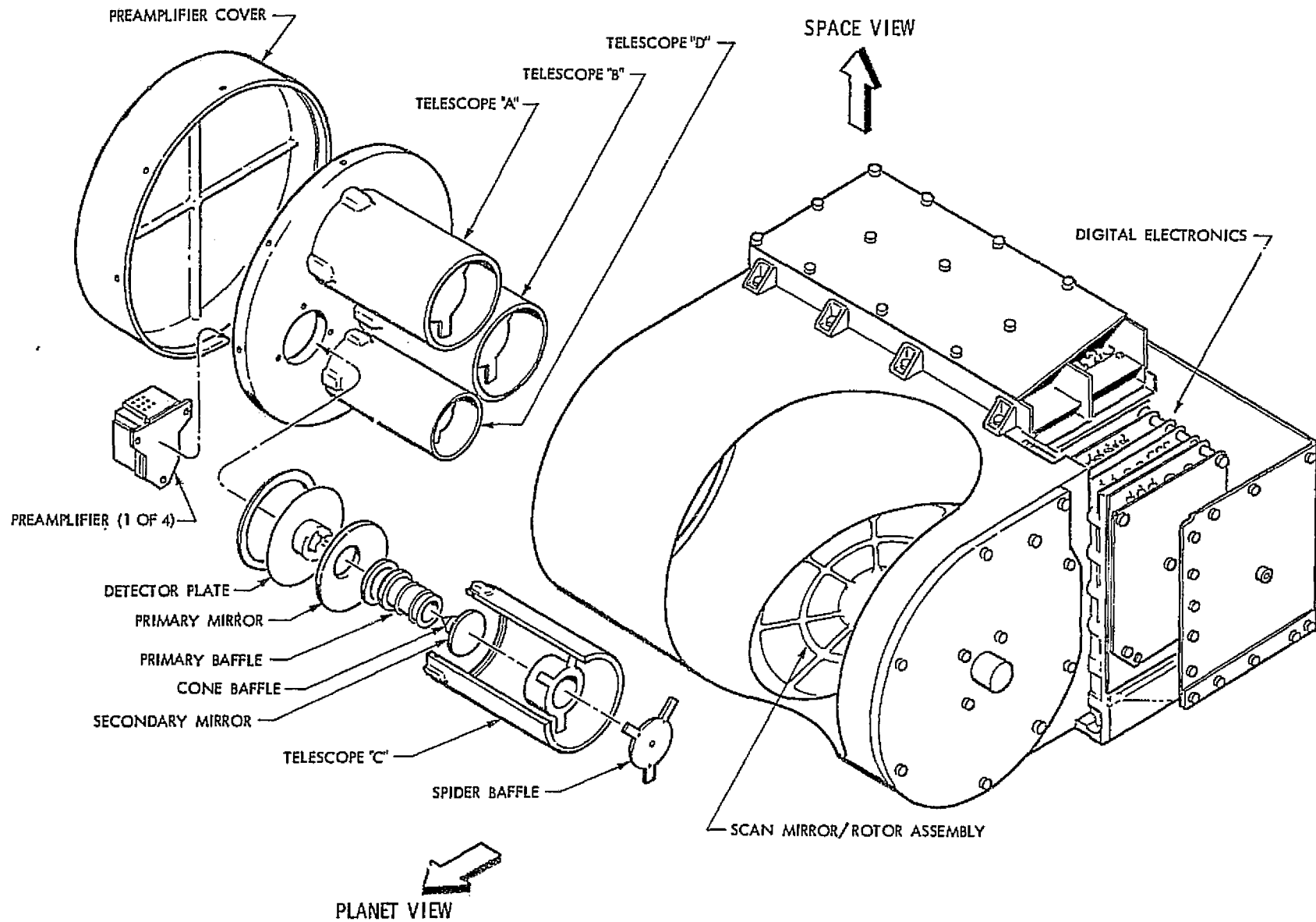
Figure II-64.   Infrared Thermal Mapper

detector configuration, sample rate, and scan platform slew rate were designed to allow uniformly spaced, non-redundant, continuous coverage so that the IRTM experiments can produce two-dimensional images in the solar and thermal bands.

2. Performance

VO-1 was launched on August 20, 1975 with IRTM S/N 005. During the Earth-Mars transit period both instruments were periodically exercised to determine their operational characteristics in a space environment; in addition, approach science data was obtained during the week preceding MOI. Following MOI both IRTM instruments have been utilized exclusively for scientific observations.

a. Cruise. The instruments installed on VO-1 and VO-2 were checked to verify the instruments response to all commands. This proved the Orbiter/Instrument interfaces were intact and that the instruments were fully operational. Additional sequences were implemented to determine the following:

(1) Thermal inputs from the Lander Capsule, and the +Y solar panel.

(2) S-band RFI from the HGA.

(3) IRTM off-axis response (a measurement of input signal amplitude from beyond the 5.2 mr field-of-view of each detector).

1) Orbiter Heat Inputs. The effect of heat from the Orbiter upon operation of the IRTM instrument was determined by slewing the scan platform through the limits of its operational area. The signal level from all 28 IRTM science data channels was plotted with respect to scan platform position; thus, changes in IRTM data levels vs scan platform position were mapped. Changes in instrument response were noted when the IRTM moved between shaded and sunlight areas and when the IRTM approached the warm +Y solar panel or the warm Lander Capsule.

IRTM data was not affected by any of the scan platform positions in the steady state case. However, when scan platform changes of position produced a difference in the heat input to the instrument, changes in magnitude of the IR data occurred. The 18 to 24 micron "A" Telescope channels were the most

sensitive to transients. The observed rates of change were of small enough magnitude that valid data could still be obtained while the IRTM was operating in the Normal mode. When operating in the Normal mode, a DC Restore is performed every 72 seconds. Utilization of this DC Restore feature reduced changes in the data to an acceptable level.

2)   S-Band RFI. During developmental testing the IRTM was checked to determine if any RF signals present on the Viking Orbiter/Lander or present in the spacecraft testing environment would affect instrument operation. It was determined that IRTM data was degraded by the 2295 MHz S-band and 380 MHz UHF transmissions. The 380 MHz signal is generated by the Lander relay radio, which would not be utilized during IRTM data acquisition sequences. Therefore, the requirement to be immune to RFI from the Lander relay radio was waived. The susceptibility to S-band RFI was a concern since the Orbiter would continually be transmitting at 2295 MHz during IRTM data acquisition. Analysis indicated that the main source of S-band energy would be from the Orbiter HGA, and that negligible effects resulted from the Orbiter LGA operation. A parallel effort was initiated in order to further define and solve this concern. Tests were performed on the antenna range which mapped the HGA S-band near-field at various points where the IRTM could be positioned by the scan platform. Simultaneously, the flight model IRTM instruments were modified to reduce their susciptibility to RFI. The antenna range tests indicated that the maximum RF field on the Orbiter would be less that 100 mW/m^2. By grounding each IRTM detector center tap at the detector, and sealing all accessible openings between the aperture cavity and the area which houses the preamplifiers and detectors, the IRTM rejection on S-band RFI was raised above 100 mW/m^2.

During cruise checkout no RFI problems were observed on the VO-1 IRTM; however, RFI was observed on the VO-2 IRTM, where the S-band field strength at the IRTM was approximately 800 mW/m^2. Review of instrument prelaunch test data indicated that the IRTM on VO-1 was less susceptible to RFI and would not be affected by a S-band field of 800 mW/m^2. Two RFI tests were performed. The first test was performed on Oct. 17, 1975. The HGA was at a cone angle of 0 deg

and a clock angle of 331 deg; the scan platform was at a cone angle of 45 deg and
a clock angle of 126 deg where the highest field from the HGA was expected.
Table II-36 is a listing of the VO-2 IRTM response to RFI for the Oct. 17, 1975 test.
The values shown represent the average difference in DN for periods when power
was applied to the HGA and when power was applied to the LGA. Differences less
than 2 DN were not considered significant. The second RFI test, performed on
Dec. 16, 1975, was expanded to include additional scan platform positions, and the
HGA was at a cone angle of 22 deg and a clock angle of 249 deg. Very small
RFI effects were observed.

The probable mechanism for the relatively high RFI levels observed on the
first test was that the IRTM had an unobstructed view of the HGA feed. On the
second test the higher HGA cone angle obscured the HGA feed from the IRTM.

Based on the two RFI tests it was concluded that the RFI will occur only
on VO-2, IRTM S/N 005. RFI will occur when the HGA is at low cone angles and when
the scan platform is in the region of 45 deg to 70 deg cone and 117 deg to
126 deg clock. In addition, the IRTM will be most sensitive to RFI when the
instrument scan mirror is in the space position.

3)   Off-Axis Response. The IRTM field-of-view was slewed across the
planet disk numerous times during the week preceeding Mars encounter. An
accurate measurement of off-axis response was obtained by slewing the instrument
from looking at space to looking at the planet's disc. The results of these
measurements indicated that the "off axis" response is near the theoretical
minimum, that is, diffraction limited. The IRTM has an extremely sharp field-
of-view, providing precise measurement of well-defined areas of the planet
surface.

b.   Orbital. The instruments on both Orbiters have properly responded
to all commands issued to them.

1)   Heat Inputs/Thermal Transients. During the early orbital operations,
the Orbiters' scan platform slew range was limited by the presence of the
Landers. Before Lander separation, thermal transients produced negligible

TABLE II-36. VO-2 RFI Test Results Oct. 17, 1975

IR CH. NO.	MIRROR IN PLANET	MIRROR IN SPACE	MIRROR IN REFERENCE
1	--	-1.3	-1.2
2	--	-1.5	-2.4*
3	--	-1.3	-3.2*
4	--	+1.0	-1.8
5	--	-1.2	-1.0
6	--	-2.5*	-2.6
7	--	+0.7	-2.5*
8	-0.2	-0.6	-0.2
9	+0.2	+0.2	+0.3
10	+0.2	+0.4	-0.2
11	+0.4	+1.7	-0.7
12	+0.2	+1.3	-0.5
13	-0.1	+0.6	-0.7
14	+0.9	-0.1	-0.3
15	+0.8	+10.2*	+2.1*
16	-0.4	+3.7*	+1.4
17	+1.7	+8.9*	+1.8
18	+1.2	+9.3*	+0.7
19	+1.0	+15.0*	+1.5
20	0.0	+3.0*	+0.1
21	+1.6	+2.3*	-0.1
22	+0.5	+0.5	+0.3
23	-0.6	+0.4	-0.2
24	-0.4	+0.3	0.0
25	-0.6	+0.5	+0.3
26	+0.4	+0.2	+0.4
27	+0.4	0.0	-0.5
28	-0.6	-0.2	-0.2

*DN As Indicating RFI

-- Data Not Available

effects upon the IRTM science data. Following the Lander and bioshield separation from VO-1, a significant increase in the magnitude of thermal transients was observed. The increase of thermal transients induced drifts in the IR data. The increase in thermal transient magnitudes is caused by:

(1) After VO-1 Lander/bioshield separation, the planetary heat load at periapsis doubled. Prior to separation an increase of IRTM temperature of approximately 5°F occurred at each periapsis. After separation, the temperature change increased to approximately 10°F. This effect is attributed to blocking of some percentage of the planetary input by the capsule.

(2) After VL-1 separation, the scan platform was able to slew over a much greater range. Thus, the solar and planetary heat inputs varied considerably due to large changes in the IRTM aspect angles relative to Mars and the Sun. In addition, many sequences are now able to occur where the instrument would be positioned in Sun light and then be slewed to an area where the Sun was blocked by the Orbiter bus.

The aforementioned thermal transients occur during the interval of periapsis ± 45 min. The effect of the transients is being adequately controlled by spacing IR data acquisition sequences as far apart as practicable; this permits the IRTM to become nearly thermally stable from changes induced by scan platform pre-positioning. Also the IRTM DC restore feature is in effect immediately prior to and during each IRTM data acquisition sequence; so that thermal changes are cancelled (zeroed out) at an interval of once every 72 sec.

c. Motor Operation. The IRTM scan mirror may be positioned to any one of three discrete positions for data acquisition: planet, space, or reference. The scan mirror is driven by a stepping motor. 50 motor steps are required to move the mirror between planet and space or between space and reference. 100 motor steps are required to move the mirror from planet to reference. During flight operations all VO-1 and VO-2 motor stepping was as expected, 50 or 100 steps occurred in all cases when transiting between positions.

d.   Trends of Engineering Functions.   All stable IRTM functions have been
analyzed to determine if trends or excessive dispersions are occurring.
Functions analyzed were: the 28 average space IR values during periods when the
IRTM is fully DC restored, the 21 DC monitor channels, and the three power supply
monitors.   No drifts or excessive noise has been observed on any channel for
either the VO-1 or VO-2 IRTM instruments.

e.   Gain Stability of IR Channels.   Based on data received when the IRTM
mirror is in the reference position, a periodic check is made of the gains for
each of the 28 IRTM science data channels.   The response for each of the 21 IR
data channels is normalized to the current reference plate temperature which is
measured by thermistors.   The response of the seven albedo data channels is
derived from a lamp stimulus; no normalization is required.   The gains of all
IR channels, telescopes A, B, and C, have been consistent.   Gradual gain
increases were observed in the albedo channels, Telescope D, which appear to
have leveled off after increasing approximately three percent.   At this time
we are unable to determine if the apparent increase in response is an increase
in the gain of the albedo channels or an increase of the albedo stimulus lamps
intensity.

3.   Anomalies

The encoder anomaly occurred 14 times during Revs 53 and 54.   The IRTM
was operating in normal mode throughout the period when the anomaly occurred.
Therefore, the mirror was stepping from the planet position to the space posi-
tion every 71.68 seconds.   Normally, the mirror steps from planet to space
and then stays in the space position for three complete IR frames (3.36 seconds).
The mirror then steps either to the reference position or it returns to the
planet position.   In the anomalous cases the mirror stepped normally to space
and paused only for approximately 60 or 100 ms.   Figure II-65 depicts the
normal and anomalous mirror motions.   IRTM scientific data was adversely
affected each time the anomaly occurred.   In the nominal case, the mirror
arrives at the space position and 1.12 sec later a 985 ms DC restore is
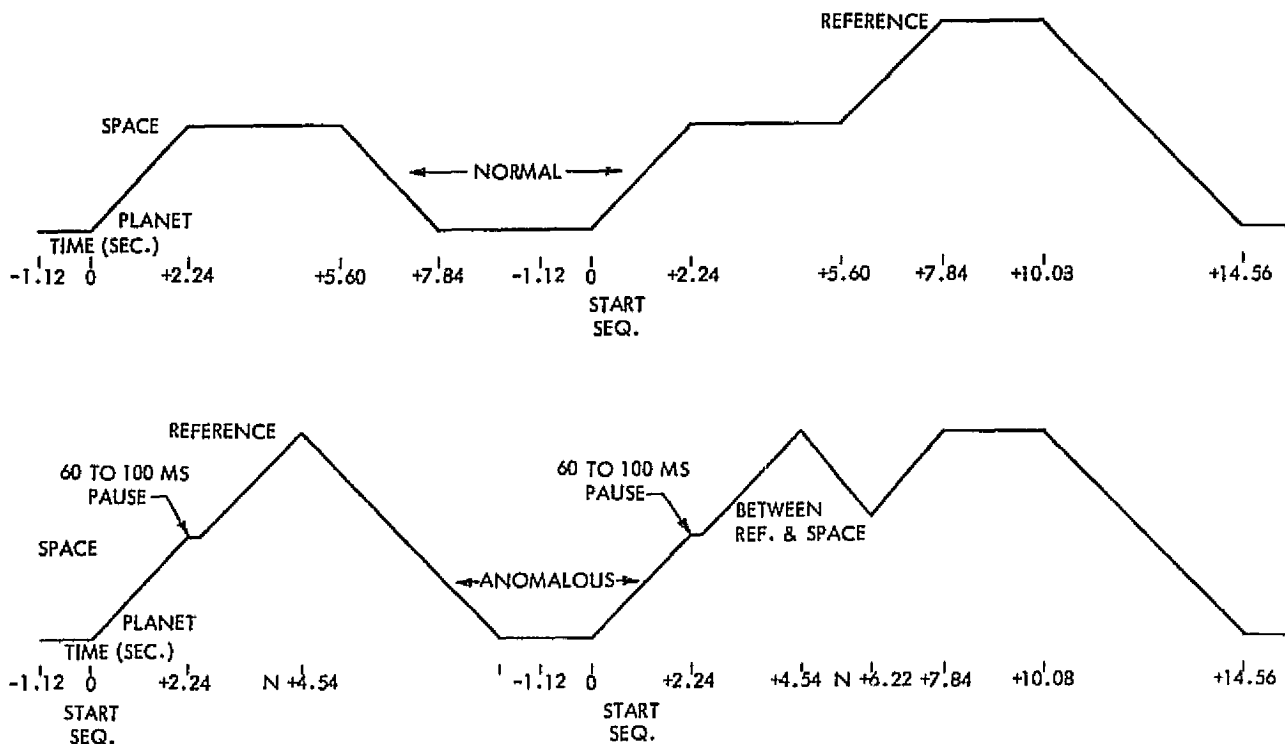
Figure II-65.   IRTM Mirror Motions

implemented, whereby all 28 IR amplifier channels are null biased with the
IRTM viewing space. In the anomalous case the DC restore sequence is initiated
when the mirror pauses at the space position but, since the mirror continues
towards the reference position, the null biasing occurs when the IRTM thermal
reference plate is in view, approximately 1.12 sec later. By null biasing the
the amplifiers on the warm reference surface (approximately 275°K, the
planet data values were negatively saturated until the instrument was DC restored
four times. Thus, approximately five min of data were lost each time the anomaly
occurred. During Revs 53 and 54, 13 percent of the planet to space transitions
were anomalous. Considering possible failure modes, the most probable cause of
the anomaly is an intermittent condition within the IRTM mirror position encoder.
Furthermore, the intermittence is unique to the encoder space contacts. The

encoder has redundant 0.016 in. tabs at the space location. A "true" space indication is indicated when either of two redundant pins make contact with the space tab, the pins are unique to the space tabs. Figure II-66 depicts the encoder disk with its associated brush block pins. Closure of either of the redundant space contacts activates a 2 ms debounce circuit on the base of a transistor switch which generates the space "true" signal level. Thus the voltage level indicating that the encoder is at the space position is true from first closure until open + 2 ms. Considering the anomaly signature, a momentary pause at the space position rather than stopping for 3.36 sec, the following anomaly model is proposed:

(1) The 50-step motor sequence occurs.

(2) After the issuance of the 50th step the encoder generates a space position "true" signal based upon first contact between a brush block and a space tab.

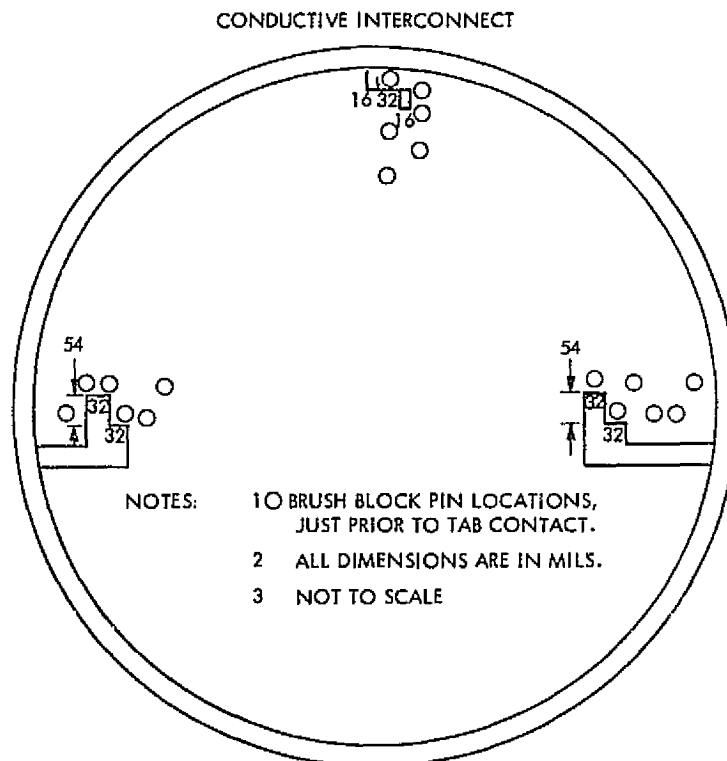(3) 67 ms following Step 50 power is removed from the stepper motor coils.

CONDUCTIVE INTERCONNECT

Figure II-66. IRTM Mirror Position Encoder

(4) Upon removal of power from the stepper motor, Step 50 plus 67 ms, the motor drive shaft may move changing the encoder space tab/brush block pin relative position by as much as a 0.7 mil.

(5) This is the point where the anomalies occurred.

(6) Due to the 0.7 mil change in angular position the continuity between the brush block pins and the space tabs was opened.

There are two possibilities which account for the loss of the space indication from the encoder when power is removed from the stepper motor coils. In both cases it is assumed that the brush block pin/encoder disk space tab relationship change up to ± 0.7 mil beginning at the time when power is removed from the motor coils.

(1) If the brush block pins moved off the encoder disk tabs edge, loss of the space position signal would occur and the anomaly observed would result. However, this model is not considered likely since both brush block pins and encoder disk tabs tend to increase in size with wear, so with increased usage the brush block pins would be less susceptible to loss of contact with the tabs.

(2) If one or both brush block pins move to an area on the tabs that is contaminated with a resistive coating, the loss of the space position signal would occur, causing the observed anomaly. This is the most probable cause of the intermittent IRTM operation since:

(a) With increased usage encoder output signals tend to become noisy.

(b) The low current through the pin/tab contact points could easily become intermittent due to contaminates.

(c) The IRTM brush block pins have relatively flat ends, decreasing self cleaning.

(d) The problem appears to be transitory and non-temperature dependent. Thus, there is a possibility that the space tabs became contanimated but were subsequently self-cleaned.

Following the observation of the IRTM mirror stepping anomaly, the
instrument was turned off with the mirror in the planet position. The instru-
ment was then turned back on and operated in the fixed planet mode; all
instrument functions were normal. During Revs 70 through 85 the instrument was
commanded from fixed planet to fixed space 51 times; no recurrence of the
anomaly was observed. During Rev 84 the instrument was commanded to normal
mode for 25 minutes, the same mode in which the anomaly initially occurred.
21 transitions from the planet position to space were observed with no
recurrence of the anomaly.

4.   Conformance to Scientific Objectives

The in-flight performance of the IRTM has been entirely as expected. The
spatial resolution, gains, and spectral bands are as designed for both instru-
ments; thus, conformance to IRTM scientific objectives has been attained.

C.   MARS ATMOSPHERIC WATER DETECTOR

1.   Description

The instrument is a fixed grating monochromator of Pfund-Littrow design, using a five-element radiation cooled PbS detector. Radiation from the planet is focused through a tuning fork chopper onto the input slit of the monochromator by a (25 mm, f/5) telescope which views the surface via an external scanning mirror. The instantaneous field of view (IFOV) of the instrument is 0.92° by 0.12° which, at a periapsis altitude of 1500 km, gives a projected area of 24 x 3 km on the surface (see Figure II-67).

Figure II-68 is the MAWD optical layout schematic. Radiation enters the fore-optics section and is reflected from the scanning raster mirror, through the order isolation filter, and onto the first telescope mirror. It is focused onto the entrance slit and enters the monochromator section. The radiation is collimated by a 550 mm focal length paraboloid and then falls on a 1200 line per mm grating. The dispersed energy is reimaged by the collimating mirror onto the detectors, which are in the same plane as the entrance slit. The signals from the detectors are individually and simultaneously amplified, synchronously demodulated, and integrated for approximately 260 msec. After integration is complete, the channels are sampled by the spacecraft data system and converted to serial digital words for transmission to Earth. The raster mirror is stepped every 280 msec
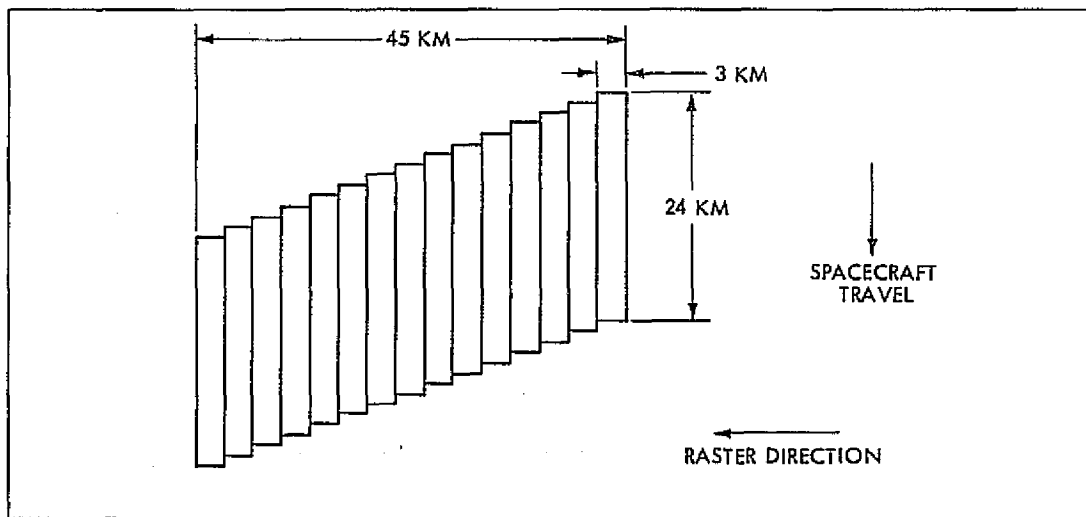
Figure II-67. MAWD Surface Track
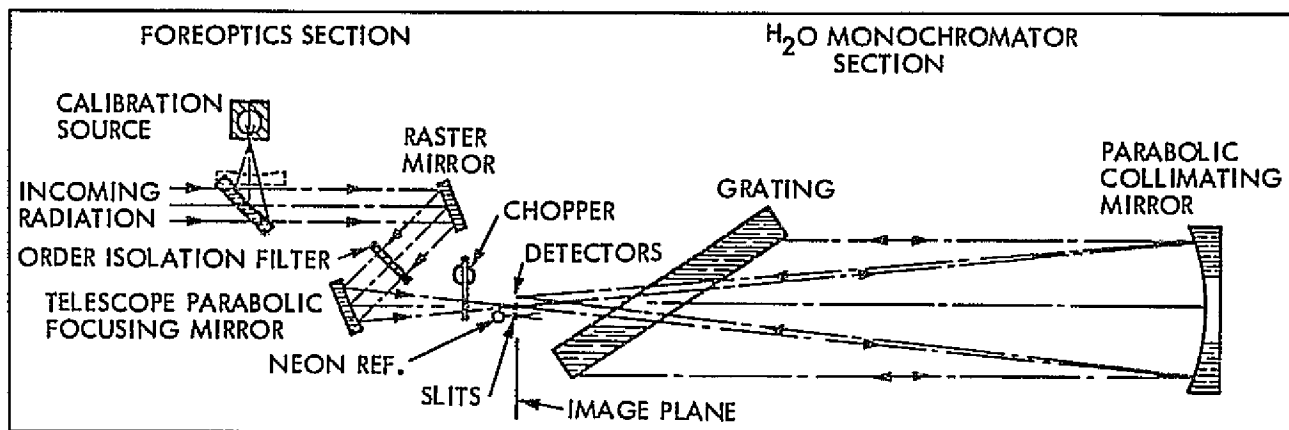
Figure II-68. MAWD Optical Layout

through 15 positions to provide a scan of the planet surface. The scan direction can be reversed to provide the mirror image of the track illustrated. Return to the initial position also taken 280 msec so that each raster is 4.48 seconds. During each flyback of the raster mirror (or every 16th frame) the wavelength servo system is actuated. This includes turning on neon lamps which are located beyond the order filter and chopper. Silicon detectors are radiated by the neon line at 0:6931 um, two detectors are used to fix the spectrum by means of a servo loop controlling the grating position, and two detectors monitor the beam position normal to the dispersion plane for the purpose of field of view correction.

The responsivity of each PbS detector is measured every 64 rasters (4.78 min) by inserting into the telescope field-of-view radiation from an intensity source and blocking radiation normally viewed by the telescope.

In order to monitor the purity of the spectra the wavelength scan mode provides a look at the total spectra. This mode provides calibration of channel gains, continuum levels, spectral resolution, and total absoprtion characteristics. To scan the wavelength lock is bypassed and the grating is stepped through 20% of a resolution element (0.2 cm^{-1}) each time the raster is reset. After 160 such

steps, which take the grating from its mean position to one end of its travel, back through its full travel and to its original position, the wavelength servo spectral coverage over the total wavelength range of the instrument (sixteen wavenumbers per detector). Both the water vapor (PbS) and the neon (Si) detectors are monitored during the wavelength scan.

a. Operating Mode. The instrument has four operating modes, as follows:

(1) Planet scan, raster forward, reverse or stationary, wavelength lock.

(2) Wavelength scan during planet scan, raster forward, reverse or stationary.

(3) Intensity calibrate, raster IFOV 8, with or without wavelength scan.

(4) Sounding mode, with instrument viewing sunlight from a diffuse reflector on the Orbiter, after it has passed through the Mars atmosphere.

b. Design Parameters.

Spatial Resolution: 0.12 x 0.92 deg (3 km x 24 km at 1500 km altitude)

Wavelength Servo Accuracy: ±0.25 wavenumber (cm^{-1})

Resolution: 1.25 cm^{-1} (0.0002μm)

Radiometric Accuracy: ±10% absolute ±1.0% relative, ch to ch.

SNR: 50 for spectral irradiance of 3.5 x 10^{-7} W.$(cm^{-1})^{-1}$.cm^{-2}.$ster^{-1}$

Data Rate: 280 bps

2. Performance

Prior to launch the MAWD radiator plate heater was turned on, maintaining the plate and associated detectors above 10°C for 50 days on VO-1, and 30 days on VO-2 after launch. The radiator looks into deep space which cools the detectors to -70°C; this temperature would allow the spacecraft outgassing

materials to collect on the detectors and radiator plate without the heater. Telemetry measurements indicated neither VO-1 nor VO-2 instruments had been contaminated at the time the heaters were turned off.

Approximately 28 hr after each launch, the MAWD shutter and grating were unlatched by three solenoid actuations. Concerns that they would not properly respond were alleviated when the correct response to the unlatch command was receive

First visibility into the post-launch condition of the instruments was on October 16, 1975 when the initial orbitor science instrument checkout of VO-2 occurred. This checkout revealed the health of the MAWD instrument following launch and 30 days in space. MAWD turned on without incident and the grating cam rotated from the launch stowed position to wavelength lock and stopped as expected. Internal calibrates which tell functionally how the heart of the instrument, the PbS channels, perform resulted in disclosure that the PbS responsivity was down by an average of 30 percent. All other aspects of the instrument were normal. In-depth analysis of the PbS data was started almost immediately. On October 20, 1976 VO-1 performed its initial science instrument checkout. It too was down in PbS responsivity by approximately 30 percent.

The next MAWD checkout was a month away so the data analysis was continued but hindered by the lack of computer software still in development. At the conclusion of the data analysis the noise figure of the instruments (Noise Equivalent Irradiance "NEIs") were intact as the noise had dropped by 25 percent. In short, the instrument's performance was not altered, only its operating point. The responsivity is discussed further in paragraphs 2b and 3a.

The MAWD instruments have gone through the primary mission with very few problems or special (unexpected) results. Table II-37 summarizes the operation cycles. Table II-38 lists the historical facts.

a. <u>Planet Radiance Calculations.</u> The most critical computation performed is the conversion of DN to radiance from the five PbS detector channels. Coupled with this calculation is a $\pm0.1^{\circ}$C detector temperature design limit between intensity calibrations (4.78 min). Observations coupled with non-propulsive maneuvers have temperature drift rates exceeding this $\pm0.1^{\circ}$C limit.

Table II-37. MAWD Operation Cycles

Operation	VO-1	VO-2
Turn-ons/Turn-offs	18	14
Observations	1,035	452
Orbits	137	85
Wavelength scans	54	26
Hours on	2,980	1,740
Intensity calibrations	40,000	22,000
Raster mirror steps	36,000,000	21,000,000
Turning fork cycles	1,200,000,000	670,000,000

Table II-38. MAWD Historical Facts

Event	Instrument	Date
Unlatch	VO-1	August 22, 1975
	VO-2	September 11, 1975
Radiator Plate Heater Off	VO-1/VO-2	October 8, 1975
MAWD Initial Turn-on	VO-2	October 16, 1975
	VO-1	October 20, 1975
Day Mars Detected	VO-1	June 4, 1976
	VO-2	July 23, 1976
First Wavelength Scan of Mars	VO-1	June 23, 1976
	VO-2	August 13, 1976
First Diffuser Plate Observation*	VO-1	July 24, 1976

*VO-2 diffuser blocked by the aft-bioshield

To accurately compute radiance, an interpolation was incorporated which uses the slope of detector responsivity as a function of detector temperature shifted by the average responsivity and average detector temperature for the data being processed (see Figure II-69). This interpolation accounts for day-to-day responsivity drifts and changes due to detector temperature. The two slopes meet at the detector thermal control heater-on point. This break point in the thermal control loop is discussed in paragraph 3a. The interpolation process is shown below.

$$RSi = \overline{RSi} + (\overline{Dett} - Dett)\ Mi$$

$$RADi = RSi\ (CDNGR_i)$$

$$RSi = \text{inverse detector responsivity (1/RVi)}$$

$$Dett = \text{detector temperature}$$

$$Mi = \text{Slope of RSi vs Dett}$$

$$RADi = \text{Radiance}$$

$$i = \text{1 thru 5 for PbS1 thru PbS5}$$
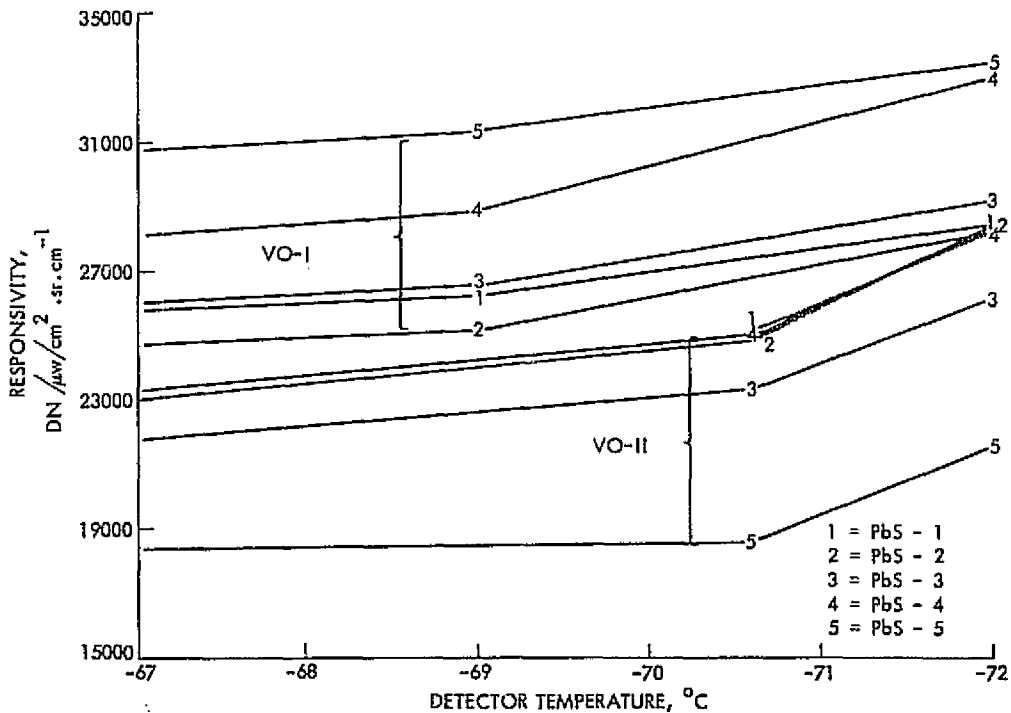
Figure II-69. MAWD Responsivity

b.   Responsivity Stability. During the primary mission, responsivity
was averaged on an orbit basis;   then the value used to compute radiance was
moved on the responsivity slope curve (Figure II-69). To display the stability
of the responsivity, its orbit average value at -70°C for VO-1 and -71°C for
VO-2 are plotted in Figures II-70 and II-71. The minimum shifts in responsi-
vities were 1.4 percent for PbS-1 of VO-1 and 1.0 percent for PbS of VO-2.
Maximum shifts in responsivity were 2.5 percent for PbS-3 of VO-1 and 1.9 percent
for PbS-1 of VO-2. There was no correlation expected or measured between instru-
ments or detectors as to responsivity changes. Also, the changes were small
relative to that allowed for in the design. The one-time drops of 30 percent in
responsivity which took place between the last calibration prior to shipment to
the Cape and the initial turn-ons were large. Subsequent small changes were less
than expected and required very little monitoring during the primary mission.
These small changes facilitated data reduction sufficiently enough to permit
reduction on an orbit-by-orbit basis.
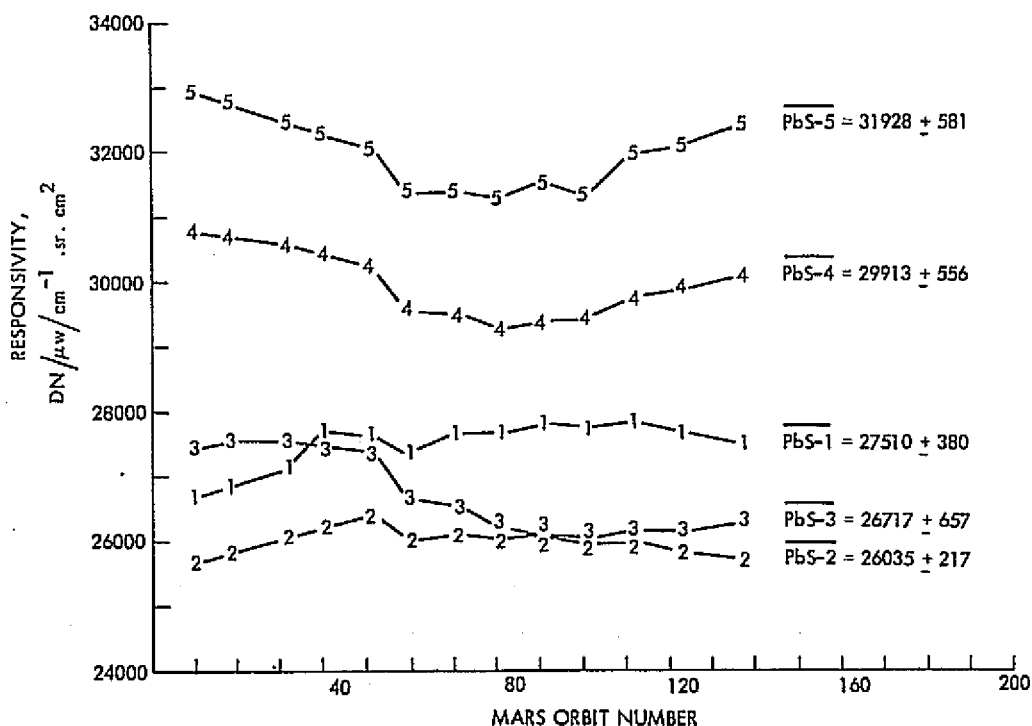
Figure II-70.   VO-1 MAWD Responsivity of the PbS Detectors at -70°C
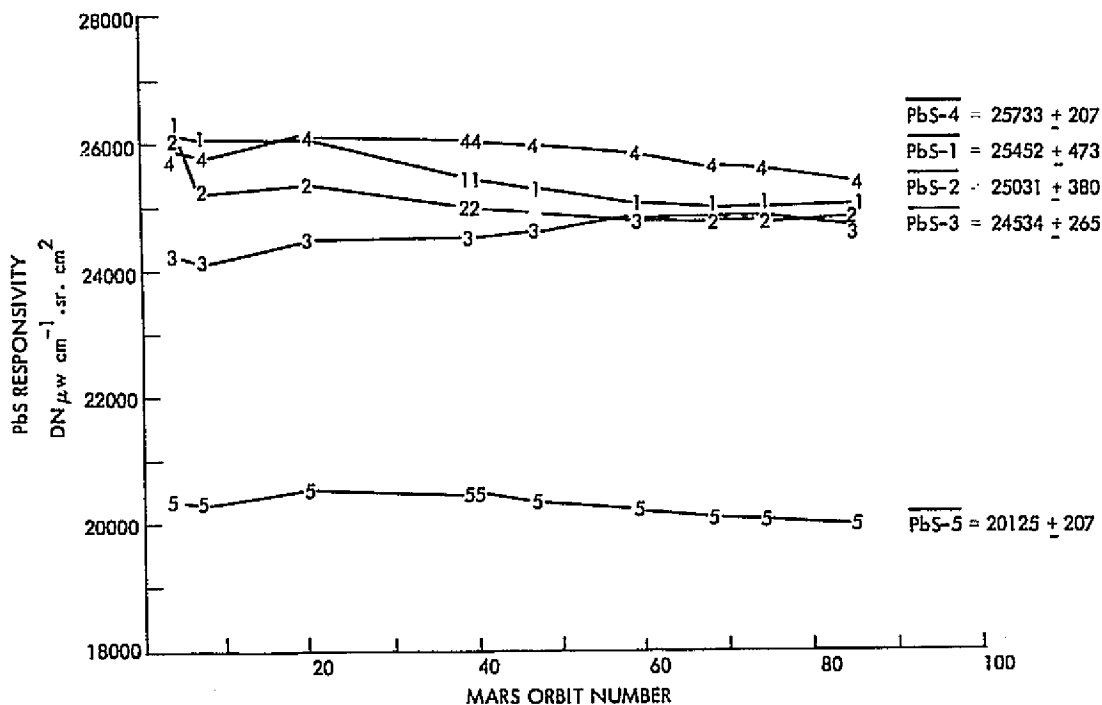
Figure II-71. VO-2 MAWD Responsivity of the PbS Detectors at -71°C

c.   Engineering Parameters. As an engineering instrument MAWD has
proven to be very stable and anomaly-free. The coefficients used to convert DN
to engineering units (EUs) have remained unchanged, and alarm limits have not
required adjustment throughout the primary mission. Table II-39 is a summary
of all MAWD engineering measurements and their deviations. Figures II-72 and
II-73 are plots of representative measurements obtained by MAWD while in orbit
about Mars.

3.   Anomalies

During the course of the primary mission the instruments have experienced
three anomalies. The first, low responsivity, occurred or was observed at the
initial science instrument checkouts; the second, monochromator heater servo,
occurred towards the end of cruise for VO-1; the third, false wavelength scans,
occurred first on Orbit 56 of VO-2.

Figure II-72.   VO-1 MAWD Measurements (1 of 2)

Figure II-72. VO-1 MAWD Measurements (2 of 2)

Figure II-73. VO-2 MAWD Measurements (1 of 2)

VO II MAWD ENGINEERING MEASUREMENTS
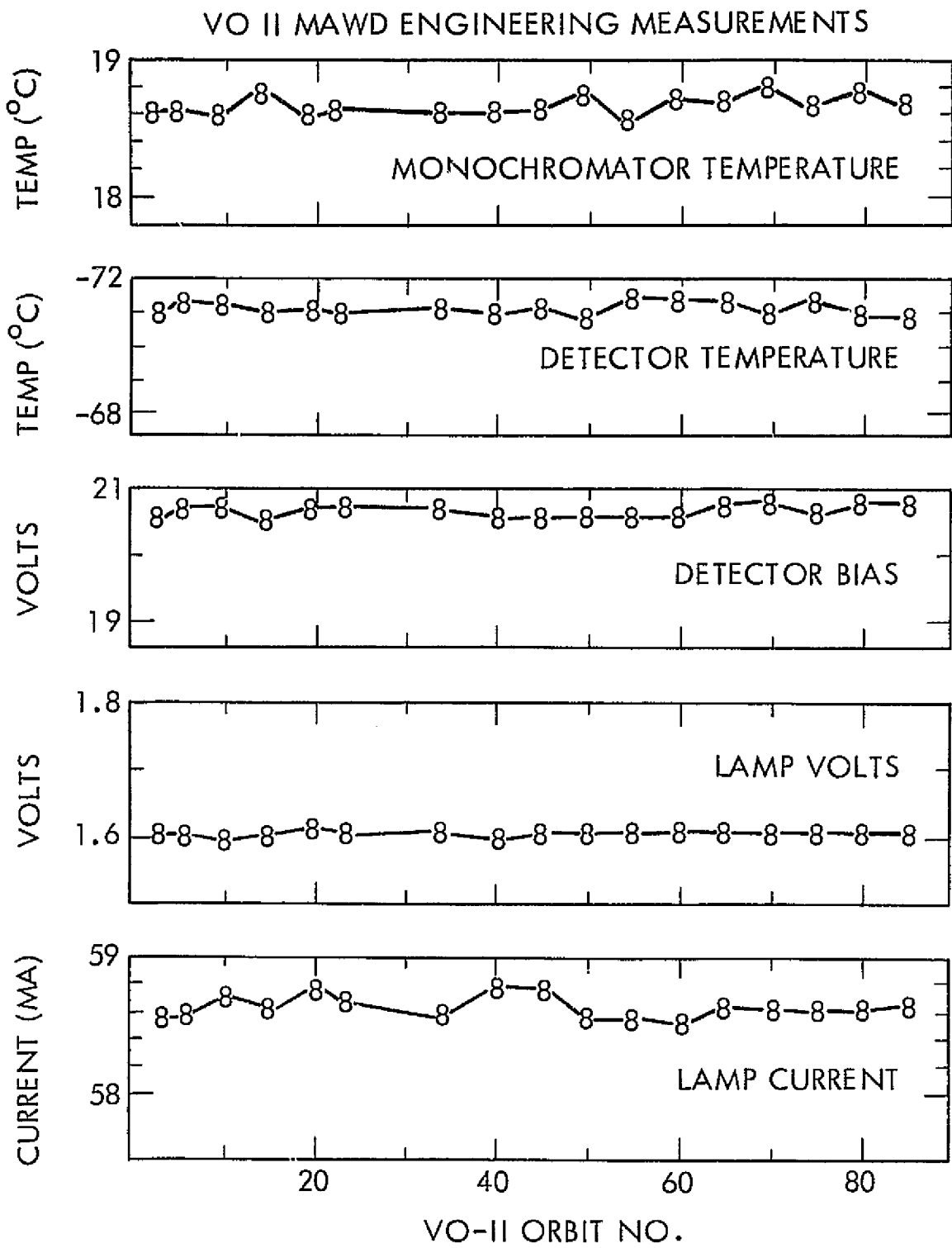
Figure II-73. VO-2 MAWD Measurements (2 of 2)

Table II-39. MAWD Engineering Measurement Values and Deltas

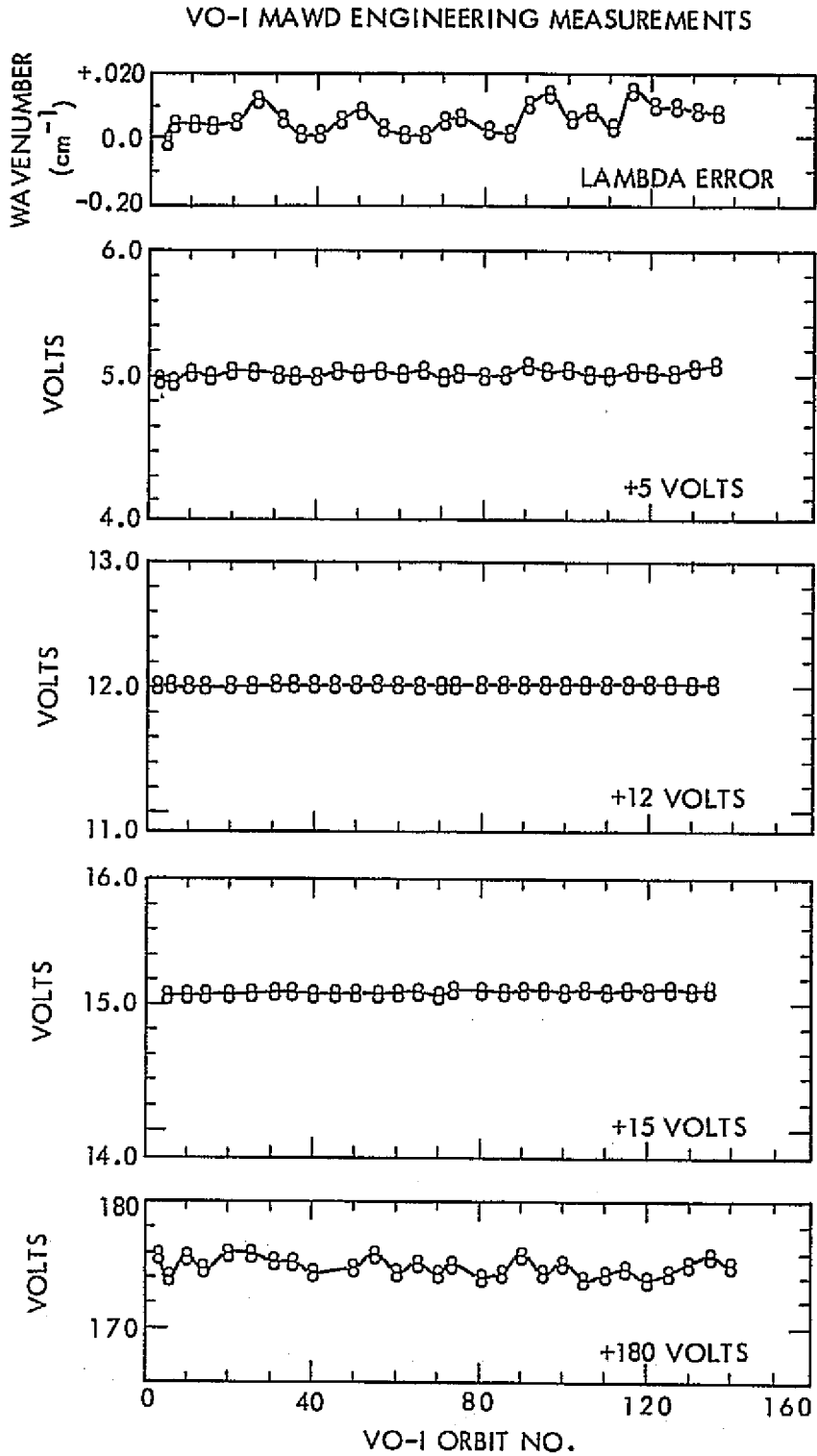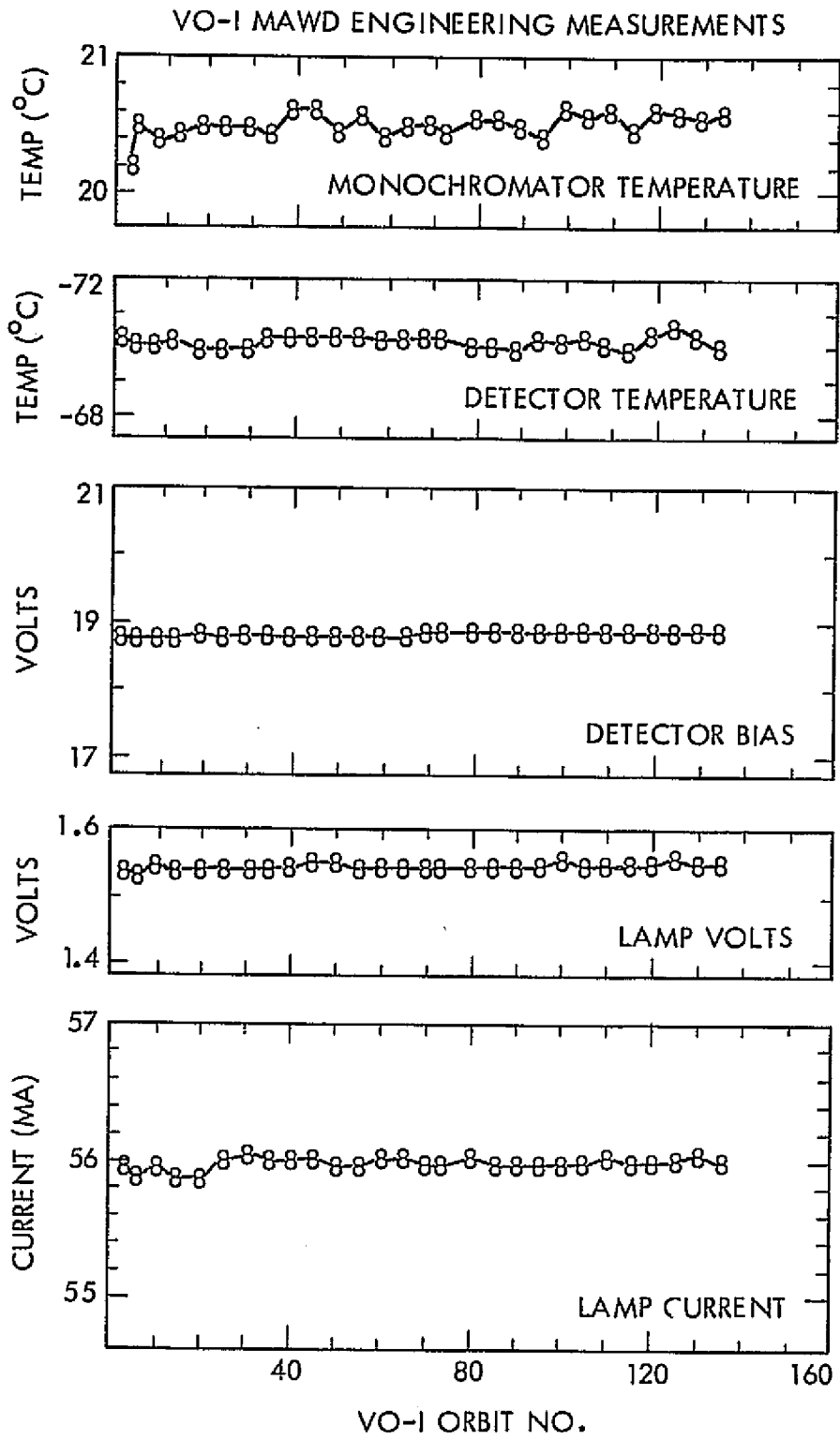| Channel		VO-1			VO-2		
No.	Title	AVG EU	Delta EU	Delta % of Data	AVG EU	Delta EU	Delta % of Data
E550	S/C H.T.	21.1°C	1.00°C	5	19.4°C	0.530°C	3
E551	S/C Rad P.T.	-86.0°C	13.3°C	15	-86.9°C	11.0°C	13
S551	λ Error	0.06 cm^{-1}	0.12 cm^{-1}	200	-0.060 cm^{-1}	0.010 cm^{-1}	17
S552	FOV Hi	31.5%	21.0%	21	50.3%	8.88%	9
S553	FOV Lo	68.8%	17.1%	17	61.4%	13.3%	13
S555	NEON I	4.94 ma	0.71 ma	14	4.94 ma	0.150 ma	3
S562	RAS POS 8	7.99 POS	0.09 POS	1	8.07 POS	0.120 POS	1
S563	A/PW Hi	100%	0.10%	0	100%	0.220%	0
S563	A/PW Lo	99.5%	1.05%	1	100%	0%	0
S564	Det. Temp.	-70.0°C	0.61°C	1	-71.2°C	0.630°C	1
S565	Head E. Temp.	14.7°C	1.94°C	13	15.0°C	0.970°C	6
S566	Bus E. Temp.	18.7°C	2.51°C	13	18.4°C	2.38°C	13
S567	Det. Bias	18.8 V	0.11 V	1	20.6 V	0.260 V	1
S568	Mono Temp.	20.4°C	0.32°C	2	18.7°C	0.270°C	1
S569	+30 Vdc	29.5 V	0.66 V	2	29.6 V	0.510 V	2
S570	+5 Vdc	4.99 V	0.10 V	2	5.07 V	0.100 V	2
S969	+12 Vdc	12.0 V	0.01 V	0	12.0 V	0.010 V	0
S970	-12 Vdc	-12.0 V	0.00 V	0	-11.9 V	0.00 V	0
S971	+6 Vdc	8.32 V	0.12 V	1	8.30 V	0.160 V	2
S972	+180 Vdc	175 V	2.53 V	1	174 V	2.99 V	2
S973	+15 Vdc	15.1 V	0.02 V	0	15.1 V	0.040 V	0
S974	-15 Vdc	-14.9 V	0.02 V	0	-15.1 V	0.020 V	0
S975	+17 Vdc	16.6 V	0.26 V	2	16.2 V	0.210 V	1
S976	-17 Vdc	-16.7 V	0.07 V	0	-16.6 V	0.070 V	0
S977	Lamp 4 V	1.44 V	0.01 V	1	1.47 V	0.00 V	0
S978	Lamp 4 I	54.8 ma	0.21 ma	0	59.1 ma	0.710 ma	1
S979	Lamp 3 V	1.61 V	0.03 V	2	1.72 V	0.010 V	1
S980	Lamp 3 I	55.0 ma	0.78 ma	1	58.4 ma	0.230 ma	0
S981	Lamp 2 V	1.55 V	0.03 V	2	1.67 V	0.00 V	0
S982	Lamp 2 I	57.14 ma	0.23 ma	0	61.9 ma	0.240 ma	0
S983	Lamp 1 V	1.59 V	0.01 V	1	1.56 V	0.010 V	1
S984	Lamp 1 I	56.9 ma	0.22 ma	0	55.5 ma	0.450 ma	1

a.   Low Responsivity. The initial science instrument checkouts revealed that the responsivity RVi of the PbS detectors, ability to convert photons to volts, were low by 26 to 49 percent. Both instruments were equally low. As a point of interest, the responsivity has remained very steady with only a deviation of 1 to 2.5 percent from the first checkout to the end of the primary mission.

The PbS responsivity drop cannot be explained, nor has it occurred on the PTO instrument residing at JPL in a constant vacuum. A possible hint, or related peculiarity, are the two-valued responsivity vs temperature curves (Figure II-69) whose break points occur at the heater-on temperature of each instrument. If by chance the thermal coupling between detectors and detector housing has changed such that the detectors are warmer, the low responsivities can be explained. A rough estimate of change, or temperature delta, required to drop the responsivity is $10^{\circ}C$ to $20^{\circ}C$. The PTO instrument has not experienced the two-valued responsivity vs detector temperature slopes now present with both in-flight instruments.

In spite of the low responsivity, the detector noise dropped an equivalent amount. This noise drop resulted in an instrument noise figure equal to the pre-launch NEI. With the NEI remaining unchanged, the science related performance has not degraded.

b.   Monochromator Heater Servo. The monochromator heater servo is an on/off radiative coupled blanket heater covering the three sides of the MAWD monochromator exposed to space. MAWD is also covered with the scan platform blanket. The heater servo maintains the temperature of the monochromator within $\pm 0.15^{\circ}C$. The set points are $20.4^{\circ}C$ for VO-1 and $18.7^{\circ}C$ for VO-2, resulting in VO-1 being $1.7^{\circ}C$ warmer than VO-2.

This extra heat load on VO-1 drove the heater fully on when VO-1 and Mars were the maximum distance from the Sun, a few days before VO-1's approach to Mars. Even at this extreme, VO-1's temperature only dropped $0.4^{\circ}C$. After the Lander and aft-bioshield separation, an auxiliary scan-platform heater was turned on which brought the servo back in range, with an on-time about equal to the

off-time. As related to MAWD's functioning, the change in monochromator temperature caused little difference. The only detectable change was in the Lambda Error which follows the monochromator temperature, and this caused only one grating step out of a possible 40.

c.   <u>False Wavelength Scans.</u> The most troublesome anomaly, which in fact is an idiosyncracy, was caused by the wire routing of signals between the scan platform and bay electronics of MAWD and VIS on VO-2. MAWD is susceptible to VIS camera turn-offs which can put MAWD into a wavelength scan just as if it was commanded to do so. A wavelength scan takes 13 minutes to complete and return to wavelength lock. During a scan, water amounts cannot be computed as the detectors are not at their proper wavelength position. If a scan occurs during an IR observation, the usefulness of the observation is lost. Following the first observed false scan on Orbit 56, the Orbiter Science Group (OSG) chose to extend VIS on-times whenever an observation could be disrupted. This resulted in VIS on-times increasing about one hr per day through the end of the primary mission.

4.   Conformance to Scientific Objectives

The scientific results, and their confirmation by other VO instruments, adequately verify that the scientific objectives have been met without implying that a higher noise figure would have been used to advantage.

Figure II-74 shows a typical raster plot from an observation at periapsis which is equivalent to the theoretical plot (Figure II-63). Alignment of MAWD's line-of-sight relative to the scan-platform "L" vector is within specification.

As discussed earlier, the noise figure remained constant even though the responsivity dropped roughly 30 percent. The NEI is approximately 8 $nW/cm^2.cm^{-1}.sr$ and the radiance from the planet is roughly 100 to 300 $nW/cm^2.cm^{-1}.sr$ with most of the data around the 100 nW value. To produce 1 percent radiance data, 5 rasters of data must be computer averaged at a radiance level of 100 $nW/cm^2.cm^{-1}.sr$. This technique of reducing uncertainly in the radiance is used very successfully. Some ground resolution can and is being recovered by averaging data from a given Mars latitude/longitude for up to 30 or more days.

MAWD IFOV LEVEL RASTER PLOT AT PERIAPSIS

VO-1 ORBIT 3
TIME FROM PERIAPSIS 1 MINUTE
MERCATOR PROJ SCALE 1 TO 500 THOUSAND
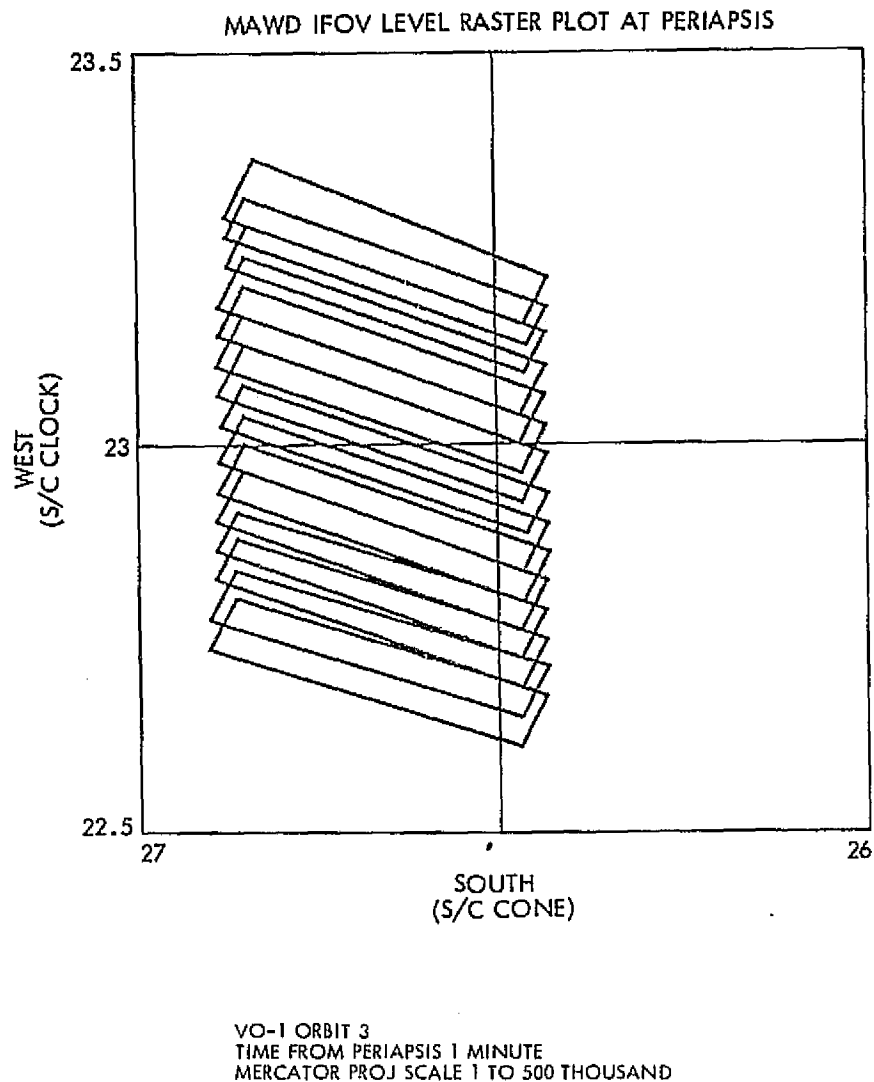
Figure II-74. MAWD IFOV Level Raster Plot at Periapsis

The diffuser plate has proven very valuable as an absolute radiance source to compare the Sun radiance against the intensity calibrator. An added plus (Figure II-75) is the Sun spectra at the resolution and wavelength of MAWD unobscured by an atmosphere. This Sun spectra is used to correct the Mars spectra (Figure II-75) inasmuch as MAWD uses the reflected Sun radiance and not Mars emitted radiance. Not being able to see the diffuser on VO-2 (blocked by the aft-bioshield) has prevented a cross correlation between instruments. This has hindered the absolute, but not the relative, radiance knowledge of Mars.
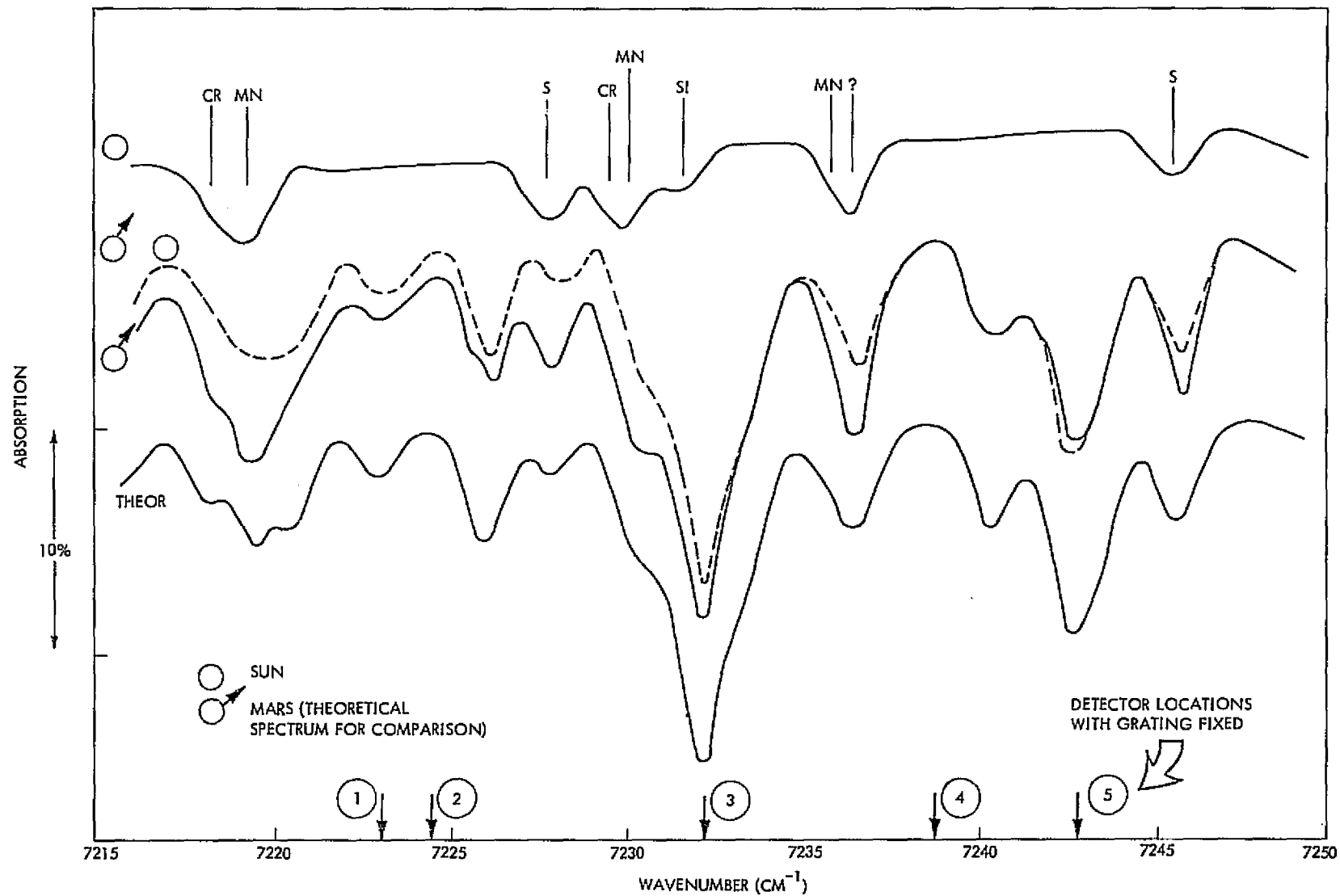
Figure II-75.   MAWD Spectra of Sun Using Diffuser Plate

D.   VISUAL IMAGING SUBSYSTEM

1.   Description

The VIS comprises two identical camera systems, each consisting of a telescope and camera head, (mounted on the Orbiter scan platform) and electronics assembly located in Bay 8 of the Orbiter (Figure II-76).

The pointing of the telescopes and the shutter times are offset, combining to produce a contiguous swath of pictures as the motion of the Orbiter traverses the fields-of-view across the surface of Mars.

VIS intensity information is obtained by reading out a vidicon photoconductor by raster scanning the electron beam. A continuous data stream is generated by reading out one camera while the other camera's photosensor is being erased and exposed. The intensity data are converted to digital form and transferred to the FDS where they are multiplexed with appropriate identification, synchronization, engineering data, and other science to form a composite data stream. This composite data stream is then recorded by the DSS on magnetic tape for subsequent playback to Earth at a rate commensurate with communications link performance.

  a.   Physical Parameters.

  (1)   Sensor: 38 mm Selenium Vidicon

         Electro-magnetic focus and deflection

         14.0 x 12.5 mm active target area

         42.2 lp/mm scan line density

  (2)   Optics: All spherical catadioptric cassegrain with Mangin primary.

         475 mm focal length

         f/3.5 geometric focal ratio

         T5.6 effective focal ratio

CAMERA HEAD "A" ASSEMBLY (2036 A1)

CAMERA HEAD "B" ASSEMBLY (2036 A2)

OPTICS ASSEMBLY

BUS ELECTRONICS "A" ASSEMBLY (2036 A3)

BUS ELECTRONICS "B" ASSEMBLY (2036 A4)

IMAGE SENSOR

FOCUS AND DEFLECTION COILS

LEGEND:

COMPARTMENT REFERENCE	LOCATION	FUNCTION
1	BOTTOM	SHUTTER & FILTER WHEEL OUTPUT ELECTRONICS
2	LEFT SIDE	DIGITAL SEQUENCING LOGIC
3	TOP FRONT	VIDEO AMPLIFIER CHAIN
4	TOP REAR	ANALOG TO DIGITAL CONVERTER
5	RIGHT SIDE	VIDICON ANALOG CONTROLS
6	REAR	VIDICON POWER SUPPLY
7A1	FRONT (A1)	SHUTTER ASSEMBLY
7A2	FRONT (A2)	FILTER WHEEL ASSEMBLY
8	BUS ELECTRONICS	LOW VOLTAGE POWER SUPPLY

Figure II-76. Visual Imaging Subsystem Configuration

(3)   Shutter: Mechanical focal plane, twin blade

0 to 2660 msec exposure range

(4)   Filter Wheel: Rotary six-position:

Blue

Minus Blue

Violet

Clear

Green

Red

(5)   Weight: 45 kilograms (total)

(6)   Power: 22.5 watts per camera

b.   Major Functional Elements. A simplified block diagram showing a single camera is shown in Figure II-77.

1)   Bus Electronics Assembly. Functions as power conditioner for the VIS. Accepts 2.4 kHz squarewave Orbiter power, and converts it to various voltages and currents needed throughout the VIS. Limits input current in the case of a VIS malfunction to protect other subsystems. Each camera has its own bus electronics assembly.

2)   Logic. Accepts timing signals and control words from the FDS and sequences the various VIS circuits accordingly. Stores and transmits the VIS digital status word (including filter position and camera S/N) to the FDS.

3)   Vidicon. Selenium photosurface, four grids, 4.48 s readout time, continuous (unchopped) beam.

4)   Sweep Circuits and Deflection Coil. Appropriate precision ramp currents are generated in the sweep circuits to drive the frame and line deflection coils. The sweep circuits accept timing and control signals from the logic.

Figure II-77. Visual Imaging Subsystem Simplified Block Diagram

5)   Focus Regulator and Focus Coil.   Current through the focus coil is regulated in the focus regulator so as to produce a focused electron beam at the vidicon target.

6)   Alignment Coil.   Provides a means to minimize beam landing error in the vidicon tube.   Accepts regulated currents from the alignment regulator in the bus electronics assembly.

7)   Vidicon Power Supply.   Generates the four grid-voltages necessary to accelerate and focus the vidicon electron beam.   The voltages are: G1, -70 to -10V; G2, 300V; G3, 1050V; and G4, 1250V.

8)   Cathode Switch and Blanking Circuit.   Accepts timing and controls from the logic and drives cathode to either blank, read, or erase voltages.

9)   Video Amplifier.   Accepts vidicon target current and converts it to an analog video voltage; output is 6V full scale, 150 kHz dB bandwidth.   The dc offset and gain are commandable by control signals generated in the logic from the control word.

10)   7-Bit Video A/DC.   Converts analog video from the video amplifier to digital data and transmits to the FDS; 2.112×10^{6} bps; 3.01×10^{5} samples/second.

11)   Filter Wheel, Drive, and Position Circuits.   Six spectral filters: blue, minus-blue, violet, clear, green, and red.   The violet filter also serves as protection from direct sunlight within the field of view during Orbiter maneuvers.   Position is read out by a set of LEDs and photo-sensors aligned with coded holes in the filter wheel.   The filter wheel position circuit transmits position code to logic circuitry, where it is subsequently transmitted to the FDS as part of a digital status word.   The filter wheel drive circuit steps the filter wheel upon command from the FDS (through the control word and the logic); maximum step rate is one step per 8.96-sec frame.

12)   Electro-Mechanical Shutter and Drive Circuit.   Resetting two-blade focal plane type provides the means of varying exposure to the vidicon.   Shutter drive circuits operate on timing generated in the logic from the control word.

13) <u>A/PW Signal Conditioner, Multiplexer, and Converter.</u> 16 engineering telemetry channels per camera, multiplexed to the input of a single A/PW converter; multiplexer accepts timing from the FDS and steps through all 16 channels in 4.48 sec. A/PW converter accepts timing from the FDS and converts the analog voltage at its input to a pulse with a width that is proportional to the input voltage level.

c. <u>Control Parameters.</u> The cameras operate in response to digital control words from the FDS which are set by ground command and specify the exposure duration, filter wheel stepping, light flood enable, amplifier gain state, and dc video offset. An exposure duration of zero can be specified when a picture is not to be played back. Zero exposure can also be used for the determination of sensor dark current and to prepare the sensor for low-residual imaging. The control word format is as follows:

Bit 1	Marker (Always logical one)
Bits 2-6	Exposure Duration (Bit 2 = MSB)
Bits 7-8	Filter Step (01, 10, 11 = Step; 00 = No Step)
Bit 9	Light Flood (1 = enable; 0 = inhibit)
Bit 10	Gain Control (1 = high; 0 = normal)
Bit 11	Video offset (1 = offset; 0 = no offset)

d. <u>Performance Parameters.</u> The VIS is operated synchronously with the Orbiter by timing signals received from the FDS. The format and data characteristics are:

Line Format:	1280 pixels (76 are retrace)
Frame Format:	1056 lines
Encoding:	7 bit/pixel
Total Data:	9 461 760 bits/frame
Frame Time:	4.48 sec
Data Rate:	2.112 mbps

2. Performance

a. Cruise Phase. VIS activities during the launch/cruise phase of the primary mission comprised instrument checkouts, photometric calibrations, and scan platform calibrations. The dates of these and the number of pictures imaged are tabulated in Table II-40.

1) Instrument Checkout. The purpose of these activities was to demonstrate that the Orbiter science instruments had survived the launch environment and were in good working order. For the VIS this was accomplished by imaging first a star field with each camera, then both Earth and a star field in each camera. All engineering, housekeeping, and status data were closely monitored and compared with pre-launch data. The real-time telemetry was correct and as expected in all instances. Processed pictures disclosed three anomalies: A pointing error for one Earth picture, saturated images of Earth, and veiling glare in the star field images during the Earth/star sequences. The saturation was caused by over-estimating the required exposure, due to poor knowledge of the photometric function at near 90 deg phase angle. It has been surmised that the veiling glare resulted from solar illumination of the interior of the telescope

Table II-40. VIS Activities During Cruise Phase

Activity	VO-1	VO-2	A/B Pix
Instrument Checkout			
Star/Star	13 Oct 75	9 Oct 75	1/1
Earth/Star	20 Oct 75	16 Oct 75	2/2
Photometric Calibration			
#1	23 Mar 76	16 Mar 76	29/29
#2A	1 May 76	21 May 76	46/0
#2B	8 May 76	25 May 76	0/46
Scan Platform Calibration			
#1	9 Feb 76	13 Feb 76	29/8
#2	12 Apr 76	15 Apr 76	16/8

sun-shade. This occurred due to the low cone angles (52.4 deg for VO-2) required to view the Earth at that time, and the effect was exacerbated by the long (2.66 sec) exposure required to permit detection of threshold magnitude stars. An additional picture pair was recorded without shuttering and with the scan platform slewing in both axes during their readout. No induced noise from this source was noted.

2)   Photometric Calibration. These sequences were designed to measure the responsivity and shading of the vidicons by imaging extended targets (Jupiter and Mars) in the center and corners of the photo-conductor through various color filters and at a number of different exposure levels. As before, all realtime telemetry was analyzed and the performance of all cameras was determined to be correct. Picture data indicated that some images intended to be in picture corners were missed due to pointing and limit cycle difficulties. The calibration data showed no significant deviations from pre-launch values and the minor variations noted were used to improve the video processing computer routines.

3)   Scan Platform Calibration. The intent of the scan platform calibration exercises was to determine the absolute pointing capability of the ARTC, in the presence of Orbiter attitude control motion, and to quantify any errors or offsets detected. To accomplish this, the VIS cameras were used to image selected star fields throughout the available cone/clock space (limited by the VLC during cruise). Additional information on camera-to-camera alignment and raster twist was obtained. Realtime telemetry indicated proper performance of all cameras during these sequences.

b.   MOI Phase. Events associated with the MOI phase involving the VIS were optical navigation and approach science.

1)   Optical Navigation. This activity began 33 days prior to MOI for VO-1. Initial pictures were images of Mars and adjacent star fields. These were taken using the A and B cameras alternately for Mars and star pictures. The "Star-Mars-Star" sequences were continued until MOI -3 days. At this time Mars satellite imagery was begun using the A camera. Operations for VO-2 were similarly conducted.

2)   <u>Approach Science.</u> Observations of Mars for scientific purposes commenced six days before MOI for VO-1. Imaging sequences were designed to view Mars at intervals of 15 deg longitude. The planet was viewed through violet, green, and red filters to determine the state of the Martian weather and to verify the exposure levels required. VO-2 operations were similar.

3)   <u>Results.</u> The MOI-related sequences accomplished the stated purposes of improving knowledge of Orbiter position for trajectory corrections and discerning the status of the Martian climate to support planning for landing of the VL.

Difficulties encountered in the course of these activities were sequence errors and some video saturation, predominately in the violet filter pictures. The sequence error problem originated in the FDS and resulted in control words from improper memory locations being issued to the VIS. The saturated video problem was caused by overexposure. This in turn was the result of unexpectedly bright scenes when viewed at short wavelengths near the limb of the planet. The exposure durations were successively decreased until correct, and improved, values for the photometric function in violet had been determined for use during orbital operations.

Throughout these events, all engineering, housekeeping and status data were examined and determined to be correct and as anticipated.

A summary of the pictures imaged is as follows:

	VO-1		VO-2	
	A	B	A	B
Optical Navigation	112	60	94	72
Approach Science	50	17	36	65

c.   <u>Orbital Phase.</u> VIS orbital operations began on June 22, 1976 with Rev. 3 certification observations of the A1 landing site from VO-1. Periapsis site surveys of all candidate areas were conducted daily, along with periodic high-altitude pictures through the red and violet filters to monitor weather and dust clouds over the landing sites. After VL-1 landing, the touchdown area was thoroughly mapped and sites for VL-2 further examined. At this time polar

surveys and mid-latitude mapping were initiated. Planetary mapping and observations of targets of interest, including Deimos and Phobos, were made throughout the primary mission. VIS operations were conducted almost daily near periapsis. Two additional scan platform calibrations were done early in the orbital phase.

On August 11, 1976, VO-2 VIS orbital operations were begun with scan platform and photometric calibrations. Subsequently, B site certification activities became the primary task. After VL-2 landing, the VO-2 VIS was used for planetary and satellite surveys and mapping in much the same way as the VO-1 cameras.

Whenever realtime high-rate telemetry was available during VIS operations, a careful scrutiny of the data was made. At no time were any deviations from commanded sequences noted, and all engineering, housekeeping, and status data were correct and as expected. Examination of processed pictures showed an artifact not present prior to MOI: a small circular blemish in the VO-1 B camera frames. This appears to be the shadow of a dust mote on the vidicon faceplate, probably dislodged from elsewhere and deposited there by vibration during the course of the MOI motor burn.

The pictures imaged during orbital operations are as follows:

	VO-1	VO-2
A Camera	2,365	1,516
B Camera	2,245	1,447

d.   Operating Statistics. Table II-41 summarizes the physical operations of the VIS cameras from launch through end of the primary missions. The counts include extra filter wheel steps and missed exposures due to incorrect control words being issued, and all ground commanded activities to correct errors or to adapt sequences (i.e., "safing" the filter wheels) in response to VO anomalies other than VIS.

e.   Engineering Measurements. 16 measurements from each VIS camera are made whenever the camera is operational. These data are imbedded in the flyback portion of each picture recorded as a part of the 1 kbps IR science stream.

Table II-41. VIS Camera Operations

Operation	VO-1		VO-2	
	VIS A S/N 7	VIS B S/N 4	VIS A S/N 8	VIS B S/N 6
Shutter (Cycles)				
Flight	2,649	2,417	1,769	1,678
Total	17,767	21,248	7,401	21,054
Filter Wheel (Steps)				
Flight	882	660	426	402
Total	3,338	1,929	1,321	1,662
Power (Cycles) Off-On-Off				
Flight	196	193	130	130
Operating Time (Hours)				
Flight	262.86	251.20	235.47	235.47
Total	693.30	719.62	718.50	616.00

Additionally, when high-rate data is available, these engineering (or "house-keeping") measurements are telemetered in real time. Analysis of these data comprises plotting of mode values of each measurement versus operating time and an examination of the range of variation. Some quantities measured are sensitive to VO bus voltage variations, others to the operating mode of the VIS at the time the sample was taken. Particular attention is paid to the vidicon cathode and filament currents as these are indicative of the health of the camera tube. The vidicon tube has a limited operating lifetime and is, historically, the "weakest line" in this type of television system.

Table II-42 lists the means of the DN mode values and ranges for all measurements. Long term trends have been established, and all levels are essentially the same as pre-launch values (adjusted for in-flight operating temperatures).

Table II-42. VIS Camera Measurements

Measurement	VO-1				VO-2			
	VIS-A S/N 7		VIS-B S/N 4		VIS-A S/N 8		VIS-B S/N 6	
	DN	Δ	DN	Δ	DN	Δ	DN	Δ
+50 VDC – Unreg.	412.3	7	414.3	7	414.6	7	409.0	6
+15 VDC – Reg.	341.2	1	344.0	1	341.4	2	342.8	2
+12 VDC – Unreg.	234.8	5	235.4	4	234.6	5	233.3	5
+5 VDC – Unreg.	428.2	9	431.3	7	427.4	7	425.5	7
−15 VDC – Reg.	−341.0	1	−340.8	2	−341.0	1	−342.1	2
−23 VDC – Reg.	−432.0	1	−425.6	2	−430.0	1	−431.0	1
Average Video*	2.8/39.6		2.0/25.9		2.9/30.3		2.1/32.4	
Input Current	289.0	3	281.7	2	287.4	3	276.8	3
Cathode Current	119.4	13	−91.0	7	121.4	5	225.7	7
Cathode Voltage	−216.0	1	−212.2	2	−217.0	2	−215.0	1
Filament Current	345.8	4	338.4	4	306.4	3	373.7	3
Frame Sweep	178.0	1	146.0	1	280.3	2	187.7	2
Line Sweep	87.0	1	167.4	2	106.3	2	53.0	2
Grid 3 Voltage	419.0	2	418.0	2	420.4	2	418.8	3
Focus Current	425.0	1	421.0	2	425.3	2	421.9	2
Digital Ladder	−210.0	1	−217.2	2	−210.0	2	−213.0	1

*The average video can have any value from −004 to +511 DN. Values shown are the means of the reading, without and with light flooding enabled and shuttering inhibited.

3.   Anomalies

During the primary mission, two anomalies occurred, or were noted, that were attributed to the VIS: the veiling glare seen during instrument checkout operations, and the circular blemish on all pictures from camera S/N 4 (VO-1, VIS-B).

a.   Veiling Glare.   This phenomenon was manifested as a series of concentric semi-circular areas of illumination superimposed on the star field images taken during the "Earth/star" phases of VIS instrument checkout. Preliminary theories suggested that the source was illumination of the baffles in the Sun-shade by the Earth (1.5 deg off-axis) or a reflection of sunlight from the +Y solar panel. Subsequent investigations during scan calibration #1 revealed that the effect was seen at low cone angles with any available clock angle and, therefore, must be attributable to direct solar illumination of the sunshade interior detectable only when using very long exposure times. This conclusion was given support by imaging star fields near the direction of Jupiter (at higher cone angles) and seeing no glare.

b.   Circular Blemish.   All post-MOI pictures from VIS S/N 4 show a small circular artifact in the image centered near line 597, pixel 554. The effect is caused by the shadow of a particle lodged on the vidicon faceplate, probably during the MOI propulsive maneuver(s). The appearance is that of a dark annulus of approximately 40 pixels I.D. and 60 pixels O.D. superimposed on the scene. The amplitude is ≈ -2 DN; thus, it is only apparent in highly contrast-enhanced pictures.

4.   Satisfaction of Mission Objectives

The overall performance of the VIS cameras throughout the primary mission was flawless. Although some imagary was lost or degraded due to various problems, that received was adequate to ensure complete satisfaction of all mission objectives for the VIS, both stated and hoped for.